NUMERICAL MODELING OF MACHINE-PRODUCT INTERACTIONS IN SOLID AND SEMI-SOLID MANURE HANDLING AND LAND APPLICATION

A Thesis Submitted to the College of Graduate Studies and Research
in Partial Fulfillment of the Requirements for the Degree of
Doctor of Philosophy
in the Department of Agricultural and Bioresource Engineering
University of Saskatchewan
Saskatoon

By

Hubert Landry

Permission to Use

In presenting this thesis in partial fulfilment of the requirements for a Doctor of Philosophy degree from the University of Saskatchewan, I agree that the Libraries of this University may make it freely available for inspection. I further agree that permission for copying of this thesis in any manner, in whole or in part, for scholarly purposes may be granted by the professors who supervised my thesis work or, in their absence, by the Head of the Department of Agricultural and Bioresource Engineering or the Dean of the College of Engineering. It is understood that any copying or publication or use of this thesis or parts thereof for financial gain shall not be allowed without my written permission. It is also understood that due recognition shall be given to me and to the University of Saskatchewan in any scholarly use which may be made of any material in my thesis. Requests for permission to copy or to make other use of material in this thesis in whole or part should be addressed to:

Head of the Department of Agricultural and Bioresource Engineering
University of Saskatchewan
Saskatoon, Saskatchewan S7N 5A9

Abstract

The general objective of the research effort reported in this thesis was to develop the knowledge required to optimize the design and operation of solid and semi-solid manure handling and land application equipment. Selected physical and rheological properties of manure products deemed to have an influence on the performances of manure handling and land application equipment were measured and general trends were identified among the measured properties. Relationships were also established between the measured properties and the type of manure as well as its total solids concentration. Field experiments were carried out to evaluate the effects of selected mechanical configurations, operating parameters and product properties on the discharge of manure spreaders. The influence of the type of conveying system (scraper conveyor and system of four augers) and the velocity at which it is operated, the geometry of the holding system and the position of a flow-control gate were all included in the analysis. The discharge rates of the machines as well as the specific energy required by the unloading operations were measured. A numerical modeling method called discrete element method (DEM) was used to create virtual manure, a numerical model of the real product. The measured physical and flow properties were used to develop and validate the virtual manure models. It was found that manure products could successfully be represented in a DE framework and that several parameters defining the contact constitutive model in the DEM had an influence on the behaviour of the virtual products. The DEM was then used to study machine-product interactions taking place in handling and land application equipment. Results from field experiments carried out using various land application equipment were used in the development and validation of the interaction models. The predicted flow rates and power requirements were in good agreement with measured data. The results obtained allowed for a better understanding of the flow of manure products in manure handling and land application equipment. It was found that the constitutive model used for the product influenced the results of the machine-product interactions models. A precision banded applicator under development at the University of Saskatchewan was also

modeled. The discharge rate of this equipment is influenced by a number of parameters. The predicted mass distribution across the width of the banded applicator was well correlated to the experimental results. The models developed in this thesis have the potential to become powerful engineering tools for the design of improved machines for the handling and land application of solid and semi-solid manure.

Acknowledgments

grandir. Je tiens à exprimer ma reconnaissance à messieurs François Thirion et Emmanuel Piron pour leur collaboration directe à cette thèse.

Thank you to everyone not mentioned but most importantly not forgotten.

Table of Contents

List of Tables

List of Figures

List of Symbols

Chapter 1

n	rheological behaviour index	[---]
K	consistency index	[Pa·s^n]
Φ_L	equilibrium sludge volume fraction	[---]
τ	shear stress	[Pa]
$\dot{\gamma}$	shear rate	[s^{-1}]
η_0	limiting viscosity	[Pa·s]
K", n"	rheological parameters	[Pa·s^n], [---]
M	mass matrix	[kg]
C	damping matrix	[kg/s]
S	stiffness matrix	[N/m]
ΔX	incremental displacement vector	[m]
ΔF	incremental force vector	[N]

Chapter 2

n	rheological behaviour index	[---]
K	consistency index	[Pa·s^n]
Φ_L	equilibrium sludge volume fraction	[---]
τ	shear stress	[Pa]
$\dot{\gamma}$	shear rate	[s^{-1}]
η_0	limiting viscosity	[Pa·s]
K", n"	rheological parameters	[Pa·s^n], [---]
S	shear rate	[s^{-1}]
ω	angular velocity	[rad/s]
R_c	radius of container	[m]
R_b	radius of spindle	[m]
F'	shear stress	[Pa]
M	torque	[N·m]

L	effective length [m]
Xgm'	modified geometric mean length [mm]
η_{app}	apparent viscosity [Pa·s]

Chapter 3

s_f	characteristic flow rate [kg/s]
n	number of samples [---]
m	number of samples during 30% of the unloading time [---]
x_i	flow rate at sample i [kg/s]
CV	coefficient of variation [%]
$E_{unloading}$	specific energy of the unloading operation [J/kg]
$t_{unloading}$	unloading time of the spreader [sec]
P(t)	power consumption of the floor conveyor as a function of time [kW]
M	mass of product unloaded [kg]

Chapter 4

K^n	normal secant stiffness [N/m]
F_i^n	total normal force [N]
U^n	total normal displacement [m]
k^s	shear tangent stiffness [N/m]
ΔF_i^s	increment of shear force [N]
ΔU_i^s	increment of shear displacement [m]
n_i	unit normal vector [---]
K	ratio of tangential (shear) stiffness to normal stiffness [---]
k_{t0}	initial tangential stiffness [N/m]
ν	Poisson's ratio [---]
G	shear modulus [MPa]
k	contact stiffness [N/m]
f	penetration factor [---]
v_0	estimated maximum velocity [m/s]
x_{max}	maximum anticipated overlap [m]

d	particle diameter [m]
m	mass of a particle [kg]
r	radius of contact area [m]
E	Young's modulus [MPa]
μ	friction coefficient [---]
θ_1	angle of the projection of the line joining the center of the first particle in a cluster and the origin of the global coordinate system with the x-axis in the x-y plane (spherical coordinates) [rad]
φ_1	angle of the line joining the center of the first particle in a cluster and the origin of the global coordinate system with respect to the z-axis (spherical coordinates) [rad]
θ_i	angle of the projection of the line joining the center of particle i and the origin of the local coordinate system with the x'-axis in the x'-y' plane (spherical coordinates) [rad]
φ_i	angle of the line joining the center of particle i and the origin of the local coordinate system with respect to the z'-axis (spherical coordinates) [rad]
φ_{min}	minimum value of angle φ (spherical coordinates) to maintain contact in a cluster [rad]
ρ_i	length of the line joining the center of particle i to the appropriate coordinate system [m]
r_i	radius of particle i [m]
ns_{cb}	normal strength of the contact bond [N]
ss_{cb}	shear strength of the contact bond [N]

Chapter 5

k_n	normal stiffness [N/m]
k_s	shear stiffness [N/m]
R_p	particle radius [m]
E	Young's modulus [MPa]
ν	Poisson's ratio [---]

G	shear modulus	[MPa]
τ	shear stress	[Pa]
$\dot{\gamma}$	shear rate	[s^{-1}]
s_f	characteristic flow rate	[kg/s]
n	number of samples	[---]
m	number of samples during 30% of the unloading time	[---]
x_i	flow rate at sample i	[kg/s]
$E_{unloading}$	specific energy of the unloading operation	[J/kg]
$t_{unloading}$	unloading time of the spreader	[sec]
P(t)	power consumption of the floor conveyor as a function of time	[kW]
M	mass of product unloaded	[m]
M_e	mass efficiency	[---]
H	height of the flow section	[m]
w	width of the flow section	[m]
v_c	velocity of the conveyor	[m/s]
ρ	bulk density of the product	[kg/m^3]
P_s	specific power	[---]
P	peak power	[kW]
L_c	length of the conveyor	[m]
g	acceleration due to gravity	[m/s^2]
v	velocity	[m/s]
L	length of trajectory	[m]
v_t	tangential velocity	[m/s]
ω	angular velocity	[rad/s]
v_r	radial velocity	[m/s]
R	disc radius	[m]
α	throw angle	[rad]

Chapter 6

w1_x1	x-axis coordinate of the first point of the first wall in the creation of an arc of a circle (to become a three-dimensional tube with apertures) [---]

w1_z1   z-axis coordinate of the first point of the first wall in the creation of an arc of a circle (to become a three-dimensional tube with apertures)   [---]

x0   x-coordinate of the center of the circle   [---]

z0   z-coordinate of the center of the circle   [---]

R   radius of the circle   [m]

α_o offset angle of the aperture   [rad]

α_a angle covered by the aperture   [rad]

Δx incremental displacement in the x-axis direction in the creation of an arc of a circle   [m]

Δz incremental displacement in the z-axis direction in the creation of an arc of a circle   [m]

$\Delta \alpha$ incremental angular displacement in the creation of an arc of a circle [rad]

w   length of the line segment in the creation of an arc of a circle   [m]

n   number of wall segments in the creation of an arc of a circle   [---]

x1   x-coordinate of the first point of a line segment   [---]

z1   z-coordinate of the first point of a line segment   [---]

x2   x-coordinate of the second point of a line segment   [---]

z2   z-coordinate of the second point of a line segment   [---]

Chapter 1

Introductory Material, General Literature Review and Objectives of the Thesis

1.1. Introduction

Animal production implies manure production. The main components of manure are feces, urine, bedding material and wasted feed and water. Other foreign materials may also become constituents of manure such as animal debris, wasted farm products, soil and cleaning water. In 1996, Canadian livestock operations produced 132 Tg of manure coming from beef cattle (51%), dairy cattle (19%), swine (16%), veal (7%), poultry and horses (3% each), and sheep (1%) (Statistics Canada, 2000). The expansion of livestock production in Canada will increase the amount of manure that will have to be managed in a sustainable fashion. Manure can be managed in different ways. One option is to recycle it in the animal production cycle as a feed ingredient, a practice not viewed favourably by many. Alternatively, manure can be recycled for crop production on or off-farm. It is also possible to recycle manure for non-agricultural uses or to discharge it to the environment. Usage of manure for crop production is the preferred management practice as it can become a readily available source of nutrients.

Land application of livestock manure can have both beneficial effects and drawbacks. It has an influence on the chemical and physical properties of the soil as well as on its microbial activity. It can become a source of nutrients and promote crop growth (Egrinya et al., 2001; Larney et al., 2000; Marinari et al, 2000). However, manure land application can have detrimental effects if the application rates are not properly

1

prescribed and controlled. It can be a major cause of deterioration of soil quality and a source of pollution of water bodies (Eghball, 2003; Young and Rainelli, 1991; Lea et al., 1982).

Optimal recycling of organic by-products through land application requires an appropriate understanding of the complex network of parameters that govern soils-crops-manures interactions. Also, one of the primary conditions required to make optimal use of livestock manure is the ability to control the rate at which the product is applied to the land. There is an unquestionable need to enhance the capacity to control the application rate on manure land application equipment, especially on machines designed to work with solid and semi-solid manure since none of the readily available machines performs adequately with respect to that criteria.

For technological solutions allowing for optimal manure land application operations to arise, fundamental questions must be addressed. A first step is to gain a good understanding of the products that are being handled. Then, the interactions between those products and the mechanical components of machine systems must be studied. The interactions taking place in manure handling and land application equipment involve the physical and flow properties of the product as well as the dynamics of the machinery elements. It is important to adopt a global approach in trying to improve the knowledge of the behaviour of manure products in handling and land application equipment. A need for improved technologies for the land application of solid and semi-solid organic fertilizers has been identified. To avoid cycles of designing-testing-modifying, a better knowledge of what is actually happening in land application machinery is required. This thesis proposes one approach to the problem: the numerical modeling of the machine-product interactions.

The general objective of this research effort was to develop the engineering knowledge required to optimize the design and operation of solid and semi-solid manure handling and land application equipment. Specifically, the objectives were to characterize manure products in terms of selected physical and rheological properties and then to

model the machine-product interactions taking place in land application equipment. The thesis is structured in a logical fashion going from the experimental work to the modeling effort. The determination of ranges of values for selected manure physical and flow properties is first presented. Secondly, the collection of validation data on spreading equipment is detailed. The numerical representation of manure products is then presented, followed by the development of models of machine-product interactions. This thesis is a collection of manuscripts written in a format suitable for publication in scientific journals. Before each manuscript, at the beginning of its corresponding chapter, a brief section indicates its relationship to the thesis in its entirety. This introductory chapter includes a general literature review. For completeness sakes, some information included in the general literature review is also included in the individual manuscripts. The candidate is the first author of all the manuscripts included in this thesis and unless otherwise specified, is the major contributor of the work presented. Chapters 2, 4 and 6 are co-authored by Drs. Claude Laguë and Martin Roberge who provided guidance and reviewed the manuscripts. Chapter 3 is co-authored by Mr. Emmanuel Piron of Cemagref, a French public research institution for agricultural engineering research, who participated to the data collection and analysis for the experiments that were carried out at Cemagref. Ms. Joy Agnew and Drs. Claude Laguë and Martin Roberge are also the co-authors of chapter 3. Ms. Agnew was involved in the experimental work reported in the manuscript while Drs. Laguë and Roberge provided guidance and reviewed the manuscript. Chapter 5 is co-authored by Mr. François Thirion of Cemagref, who carried out the experiments and data analysis related to computational fluid dynamics. Drs. Laguë and Roberge are also co-authors of chapter 5, as they provided input in the research and reviewed the manuscript. Chapters 2 and 3 have been published (*Landry, H., C. Laguë and M. Roberge. 2004. Physical and rheological properties of manure products. Applied Engineering in Agriculture 20(3):277-288* and *Landry, H., E. Piron, J.M. Agnew, C. Laguë and M. Roberge. 2005. Performances of conveying systems for manure spreaders and effects of hopper geometry on output flow. Applied Engineering in Agriculture 21(2):159-166*). The candidate is the major contributor of the research work presented in this thesis, and the collaborative work done at Cemagref led to the addition of complementary sections in chapters 3 and 5.

1.2. Definition of terms

This section is dedicated to the definition of the terminology used in this document. Other terms frequently used in the field of manure spreader evaluation are also presented.

Manure: the term *manure* is used as defined in ASAE S292.5 (ASAE, 2004). It represents the fecal and urinary excretion of livestock and poultry and can include other materials (bedding, feed, water, hair, feathers, etc.). Semi-solid manure has a solids content such that it will stack but has a lower profile than solid manure and seepage may collect around the outside. It can be pumped with positive displacement pumps or be handled with a front-end loader. Solid manure has a solids content such that it will stack with little or no seepage and is best handled with a front-end loader (ASAE, 2004).

Organic fertilizers: in addition to animal manures, several products are now being applied to agricultural land such as papermill residues, compost, municipal or industrial wastewater sludge and mixtures of different products. The term *organic by-product* encompasses all those products (manure is an agricultural organic by-product). When used for land application as a source of nutrients, organic by-products become organic fertilizers (vs mineral fertilizers).

Application rate: the quantity of manure that is applied to the land expressed in terms of mass per unit area (e.g. kg/m^2, tonne/ha).

Discharge rate: the quantity of manure that exits the application equipment expressed in terms of mass per unit time (e.g. kg/s, tonne/min).

Maximum application width: the maximum distance, measured perpendicularly to the travel direction of the application equipment, over which manure can be applied during a single pass of the equipment (e.g. m).

Effective application width: the distance, measured perpendicularly to the travel direction of the application equipment, between adjacent passes of the equipment required to obtain a uniform application rate; it is equal to the maximum application width minus any required overlap (e.g. m).

Longitudinal uniformity of application: the degree to which the application rate remains constant along the travel direction of the equipment; if the discharge rate varies, then the travel speed of the equipment needs to be modified accordingly in order to maintain a uniform application rate.

Transversal uniformity of application: the degree to which the application rate remains constant perpendicularly to the travel direction of the equipment; if the application rate varies across the maximum application width of the equipment, then it might be necessary to overlap adjacent passes of the equipment in order to maintain a uniform resulting application rate.

Characteristic flow rate: average flow rate calculated over a specified part of the unloading time of the machine (CEN, 2002).

Tolerance zone: interval of flow rates within -15% and +15% of the characteristic flow rate (CEN, 2002).

Stretch within the tolerance zone: percentage of the unloading time of the machine during which the instantaneous flow rates lie within the tolerance zone (CEN, 2002).

Longitudinal coefficient of variation: refers to the coefficient of variation of the mass distribution along the travel direction of the equipment. The longitudinal coefficient of variation is used to assess the longitudinal uniformity of application.

Transversal coefficient of variation: refers to the coefficient of variation of the mass distribution perpendicularly to the travel direction of the equipment. The transversal coefficient of variation is used to assess the transversal uniformity of application.

1.3. Operation of manure spreaders

The handling and land application of manures and solid organic fertilizers are the basic functions of manure spreaders. Typically, machines that are categorized as solid manure spreaders handle product having a dry matter content over 12% (Cemagref, 1997). Manure spreaders are generally semi-mounted trailers made of the following components: frame, hopper with floor conveyor, spreading devices (usually rotating mechanisms) and power transmission parts. They can also be truck-mounted, with the same working principles. The main characteristics differentiating manure spreaders are the type of spreading devices used, the location of the spreading devices (side or rear delivery) and the type of floor conveyor. Like any other agricultural machine, the design of manure spreaders requires sufficient knowledge of the interactions occurring between the machine components and the products handled.

The interactions between the machine and the product as well as the important product properties to be considered are dependent upon the type of manure spreader used. In this section of the first chapter, the functions and operation of the floor conveyor and spreading devices are studied. A description of different types of functional units found on commercial spreaders and an analysis of their interactions with the product is included. The interactions that the floor conveyor and the spreading mechanisms have with the product are also related to the relevant properties of the product. The discussion is focused on solid products.

1.3.1. Floor conveyor

1.3.1.1. Functions

The main function of the floor conveyor is to move the product toward the spreading mechanism. This main function implies that the floor conveyor will likely have to partially support the product. The velocity of the floor conveyor is a function of the desired application rate and is typically in the range of 0.03 to 5 m/s (Cemagref, 1997; Wilhoit et al., 1994; Ling and Wilhoit, 1999). The floor conveyor of a manure spreader can be mechanically driven by the tractor power take-off (PTO) or by the spreader support wheels. It can also be hydraulically driven, which allows for a better control of its velocity. The displacement direction of the floor conveyor is dictated by the type of spreader (rear vs. side delivery). The two main types of floor conveyor used on commercial manure spreaders are: (1) chain and slats or scraper conveyors and (2) augers. Belt conveyors are sometimes used on machines presented as universal spreader, i.e. machines supposedly capable of spreading various products, but won't be included in the analysis.

1.3.1.2. Scraper conveyor

(a) Description of the device

Scraper conveyors are made of two, three or four longitudinal chains linked by U-shaped or L-shaped steel bars. The longitudinal spacing of the bars usually varies between 200 and 400 mm (Cemagref, 1997). The floor of spreaders using this type of conveyor is generally covered with polyethylene or steel.

(b) Interactions

The desired action of the floor conveyor on the product is the movement of the product towards the spreading mechanism. Some adverse interactions may also be encountered. These undesirable interactions include adhesion of the product on the conveyor and hopper, product particles interfering with the conveyor mechanical drive system, loss of material and corrosion of the conveyor by the product.

(c) Important product properties

The physical properties of the product being conveyed must be known. Important properties include bulk density and porosity. The conveying system must be designed to sustain the forces generated when moving the product, and those forces are influenced by the weight of product in the machine. The design of the drive system of the conveyor is based on power requirements, which depend on the load on the conveyor. Other physical properties such as particle size and shape must be taken into account to ensure efficient conveying with minimal losses. The friction coefficient of the product on the conveyor will influence the extent of adhesion that can be expected. In this entire discussion on manure spreaders, it is implied that both the static and dynamic coefficients of friction are important. Adhesion of the product on the hopper walls will also affect the power requirements of the floor conveyor. The shearing properties (i.e. the angle of internal friction and the apparent cohesion) of the product will influence the power draw of the floor conveyor. Although the flow phenomenon occurring into the bulk of product is not well known in the case of solid manure land application, the internal cohesion and adhesion of the product are likely very relevant properties.

1.3.1.3. Augers

(a) Description of the device

The floor conveyor can be made of one or several augers placed longitudinally. A closed-bottom hopper is necessary for this type of conveyor to work properly. The rotating augers move the product towards the spreading mechanism. A commercially available line of spreaders features a third auger located above two discharge augers. The top auger runs in the direction opposite to the bottom two to avoid product build-up and bridging near the spreading mechanism. Augers have typically been used on sludge or semi-solid manure spreaders, but recently introduced equipment intended for a variety of organic fertilizers including solid manure also make use of discharge augers.

(b) Interactions

The beneficial and adverse interactions associated with the scraper conveyor (described in section 1.2.1.2.(b)) are also applicable to augers. However, the product is less likely to interfere with the drive system in the case of the auger. In fact, the drive system can be isolated from the product and particles are not likely to get to driving chains, stick to them and interfere with sprockets and other mechanical parts as it is the case for scraper conveyors. Excessive pulverization of the product may occur, particularly in a multiple-auger system. The size of the augers depends on the size of the clumps in the material to be conveyed. To handle manure without blocking problems, the diameter of the auger and the clearance between the flighting and trough must be selected based on the clump size.

(c) Important product properties

The same properties that affect the operation of scraper conveyors (presented in section 1.2.1.2.(c)) are also important in the interactions between an auger and the product. The shearing properties of the product should be more important with augers as shearing can occur in both a vertical and a horizontal plane in the volume of product.

1.3.1.4. "Pushing wall" conveying

(a) Description of the device

Another system exists to move the product towards the back of the spreader. This system consists of a moving panel, usually consisting of a hydraulic cylinder assembly, used to push the material towards the spreading mechanism. This system, illustrated in figure 1.1, is not widely used but is worth an analysis of the interactions.

(b) Interactions

Like the two other conveying systems, the desired action is the displacement of the product by the pushing panel system. The only adverse interaction is the adhesion of the product on the walls of the hopper and on the pushing surface.
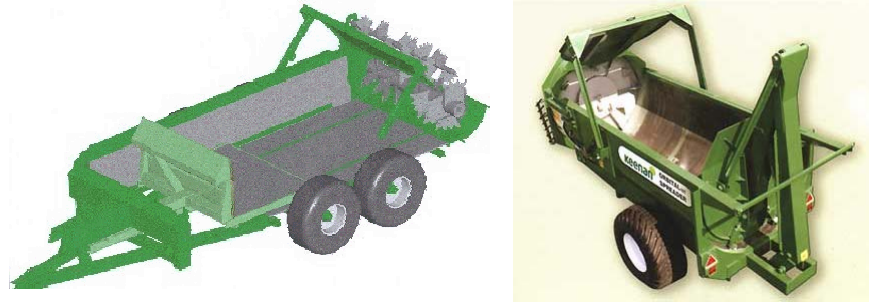
Figure 1.1.   Pushing wall principle on a rear-delivery spreader with horizontal beaters (left; source: http://www.pickrite.com; Hydra-Ram model illustrated) and a side-delivery turbine spreader (right; source: http://www.keenanservice.com).

(c) Important product properties

Friction coefficient and density are two important properties of the product that will determine the force required to push the product and thus the energy required to move the product to the spreading mechanism. The friction coefficient is directly related to both the beneficial and undesired interactions in this case. The movement and adhesion of the product are both influenced by the coefficient of friction.

1.3.2. Spreading mechanisms

1.3.2.1. Functions

The spreading mechanisms of manure spreaders are usually made of rotating devices having three main functions: (1) striking the product with impacts to cause it to crumble, (2) pulverizing the product, i.e. breaking it into smaller pieces to allow for a good throwing distance and an acceptable evenness of distribution and (3) projecting the product away from the spreader at an acceptable distance and with an acceptable evenness of distribution along the entire spreading width. The spreading uniformity in the direction of travel is also important.

Various spreading devices featured on commercial spreaders are presented. The tendency has long been to have one system fulfilling the three functions of the spreading mechanism. More recent designs have separated the hitting-pulverizing and

spreading functions by using two sub-systems. While this next section does not cover every machine available on the market, it explains the main spreading systems. Machines featuring various configurations are typically based on the same working principles and can be analyzed using the information presented.

1.3.2.2. Rear-delivery horizontal-axis beaters

(a) Description of the device

One to three horizontal-axis beaters rotating in the same direction form this spreading mechanism (fig. 1.2). The beaters can have different forms. They can be cylindrical with peripheral teeth, knives or blades. Another common form of beater is a helicoidal screw with peripheral blades.
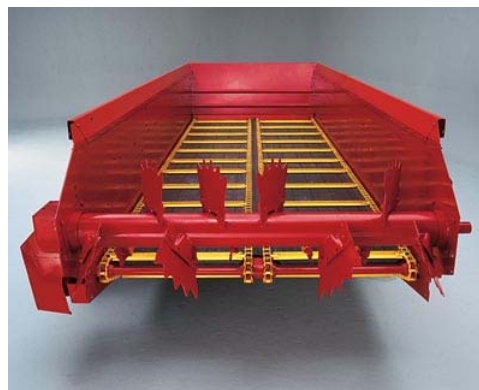
Figure 1.2. Single horizontal-axis beater on a manure spreader (source: http://www.newholland.com).

(b) Interactions

As mentioned in section 1.2.2.1., the beaters must strike the product that is pushed against them. They also must pulverize and throw the product in the field. Unwanted interactions include excessive pulverization that will impair the throwing capacity of the spreading mechanism and adhesion of the product on the beaters that can affect their pulverization and throwing capacities. With the beaters revolving in the same direction, important pulverization occurs when the product passes between two beaters.

(c) Important product properties

Mechanical properties are important in the analysis of the interactions between the beaters and the product. Shearing characteristics affect the way the product is stroked and pulverized. To a lesser extent, the compressibility of the product will influence how it is pulverized and thrown away from the machine. In fact, the product is pushed against the beaters by the movement of the floor conveyor. The compression is a function of the conveyor speed to beaters speed ratio. Compressibility may also affect the vertical homogeneity in the volume of product. If the product is highly compressible, an increase of density with depth can be expected. In a multiple-beaters configuration, the beater striking the lower part of the volume of product may be subjected to a higher loading. The porosity of the product is likely to influence its flow behaviour in terms of compressibility and compaction. Adhesion of the product on the beaters again depends on the friction coefficient. The aerodynamic properties of the product are also important to determine the working width of the spreader. The beaters must be designed (shape, size, rotational velocity) according to the shearing and impact resistance as well as the density of the product. The load supported (instantly) by the spreading mechanism is also a function of the density of the product.

1.3.2.3. Rear-delivery vertical-axis beaters

(a) Description of the device

The beaters themselves are similar to the ones described in section 1.2.2.2., except that they are placed vertically on the machine (fig.1.3). Two or four vertical-axis beaters can be used, depending on the type of spreader. The vertical-axis beaters revolve in opposite directions creating a wider spreading distribution.

Figure 1.3.   Manure spreader equipped with dual vertical-axis beaters and flow-control gate (source: http://www.ktwosales.co.uk).

(b) Interactions

The vertical-axis and horizontal-axis (section 1.2.2.2.) beaters have similar interactions with the product. Unequal loading along the length of the vertical beaters can be expected. As mentioned in section 1.2.2.2.(c), the lower blades may be subjected to a more important loading when compared to the blades located at the top of the beater if the product is compressible. As mentioned previously, the most important action of the machine on the product is the shearing action of the blades or knives of the beaters.

(c) Important product properties

Product properties mentioned in section 1.2.2.2.(c) are important in the analysis of the interactions between vertical-axis beaters and the product.

1.3.2.4. Side-delivery turbine

(a) Description of the device

A large diameter turbine having a longitudinal axis is placed at the front of the spreader (tractor end of the spreader). The product is spread by centrifugal force. An adjustable deflector covers the turbine and allows for the control of the spreading distance and pattern. The principle of the turbine spreader is illustrated in figure 1.4.

13
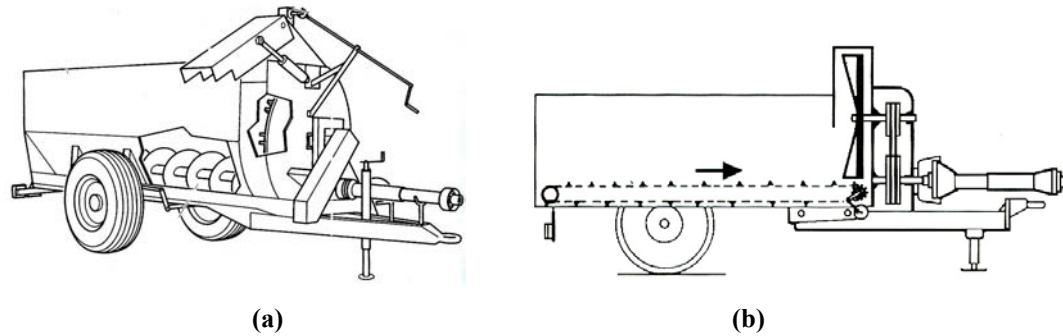
Figure 1.4. **Schematic representations of turbine spreaders with (a) auger and (b) scraper floor conveyors (adapted from Cemagref, 1997).**

(b) Interactions

The product is pushed against the turbine by the floor conveyor. The product is then picked up by the turbine, transported along the housing of the turbine and thrown out of the spreader via a deflector. The desired action is therefore throwing the product by centrifugal force. The product adhering on the turbine and on the deflector is an undesirable interaction. Depending on the design and/or adjustment of the turbine-deflector assembly, excessive pulverization may occur (depending on the angle at which the product is thrown on the deflector, it can slide on it or be excessively pulverized).

(c) Important product properties

The product has to be lifted. The density of the product is therefore an important property in this case, as it determines the weight of the product moved by each vane on the turbine. Like all the other spreading devices, the aerodynamic properties of the product become important once it has been thrown out of the spreader. Adhesion of the product is again influenced by the friction coefficient. As mentioned in the previous section, the impact resistance of the product can become an important property when it hits the deflector.

1.3.2.5. Rear-delivery centrifugal table

(a) Description of the device

The rear delivery centrifugal table is placed under a deflector, at the same height as the bottom of the hopper or lower. It features two or more spinning discs usually equipped with vanes. The discs can be horizontal or inclined. The table can be used in conjunction with horizontal-axis beaters. Such a system would represent an example of a machine that separates the striking-pulverizing and spreading functions. The functions of the beaters, when they are used, are to crumble and pulverize the product and to feed it to the table. The deflector is used to direct the pulverized product onto the spreading table. The material falling on the spinning discs is thrown by centrifugal force. The working principle of such a system is illustrated in figure 1.5. Spreaders featuring a centrifugal table are sometimes referred to as spinner-type spreaders. This type of spreading device is largely used for sludge application.
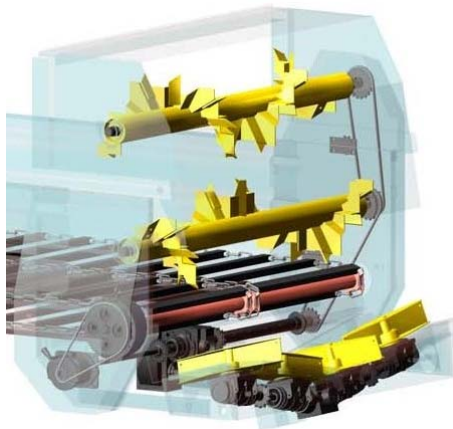
Figure 1.5.   Centrifugal table with three spinning disks and two horizontal beaters (source: http://www.agrostroj.cz)

(b) Interactions

The centrifugal table is similar to the turbine described in section 1.2.2.4. in the way of handling the product with the important difference of the table being horizontal (or slightly angled) as opposed to vertical. The centrifugal table is basically made of spinning horizontal discs that use centrifugal force to spread the product in the field. Unlike the turbine, the table does not need to pick up the product. The interactions, both beneficial and adverse, are the same as the ones describe in section 1.2.2.4.(b)

except that excessive pulverization is not likely to occur from only the action of the centrifugal table.

(c) Important product properties

The density of the product is important to determine the rotational velocity of the discs. The weight of the particles handled by the discs has to be considered to ensure proper product distribution. The friction coefficient must be taken into account to ensure efficient centrifugal throwing and to limit adhesion of the product on the surface of the discs. To a lesser extent, the product resistance to impact is a property that may be studied. In fact, on certain spreaders, the product is thrown on the deflector by the beaters and then directed to the table. There are then two possible points of impact. Excessive pulverization is not desirable and the impact resistance of the product may become an important property to be considered. The geometry, configuration and rotational velocity of the discs must also be selected according to the size and shape of the particles.

1.3.2.6. Side-delivery flails

(a) Description of the device

Spreaders using this mechanism have a longitudinal shaft with flails (fig. 1.6). The shaft rotates and moves vertically to progressively strike the volume of product that is thrown out of the spreader via an adjustable deflector. The application rate can be adjusted by changing the rotational and/or descent velocity of the shaft. It should be noted that this type of spreader does not feature a conveying system that displace the product towards the spreading mechanism.

(b) Interactions

The functions of the flails are to hit the volume of product, to break it into smaller clumps and to drag these clumps out of the spreader. Like other spreading mechanisms, the most important adverse interaction is the adhesion of the product. In this case, the product can stick to the flails and to the surface of the deflector. Excessive product

adhesion can also interfere with the movement of the chains on which the flails are mounted.
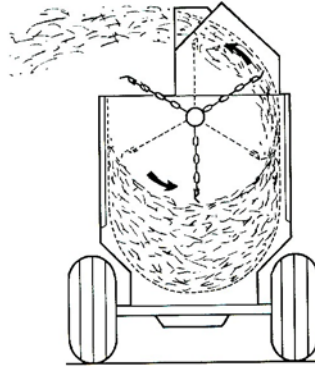
Figure 1.6.   Principle of the flail spreader (adapted from Cemagref, 1997).

(c) Important product properties

The product impact resistance and shearing characteristics are important properties that will have a great influence on the ability of the flails to break the product and to throw the clumps out of the spreader. The impact resistance of the product is important when the flails first hit it. Shear resistance then becomes important as the product is pealed off by the flails. The friction coefficient between manure particles plays a role in the movement of the product. The friction coefficient between the product and the machine components influences product adhesion, while breaking and dragging of the product by the flails is a function of impact resistance, shear resistance and internal cohesion. The density of the product will determine the ability of the flails to drag and lift the product in order to throw it out of the spreader. Once out of the spreader, the aerodynamic properties of the product are of first importance as they influence the throwing distance.

1.3.2.7. Flow control gate

(a) Description of the device

Flow control gates are not spreading mechanisms, but they are used to control the application rate. A flow control gate is placed between the volume of product and the spreading mechanism (fig. 1.3). Hydraulic cylinders are used to move the gate

17

vertically, the size of the opening being proportional to the application rate. It should be noted that the gate seen on figure 1.3 is more often used to control spillage during loading and transport. Gates that are designed and used as flow-control gates use the same principle.

(a) Interactions

The desired actions are to block part of the volume of product being pushed against the gate while allowing the remaining part to flow under. Adhesion of the product on the gate and bridging are adverse interactions.

(b) Important product properties

The friction coefficient and particle size distribution of the product are the most important properties to be taken into account.

1.3.3. Common issues

Basic product properties will influence many of the interactions previously described. As an example, moisture content has a great influence on friction coefficient. Moisture content will also influence how much pulverization of the product will occur. It is therefore very important to understand the relationships between the properties and also the impacts of the relevant properties on the interactions between the machine and the product. The type of product, its moisture content, the storage conditions and the method used to load the spreader are all parameters that will influence the properties of the product handled and spread by the machine. Some properties are intuitively assumed to have an influence on the performances of the mechanical systems used for manure handling and land application, properties like the static and dynamic coefficients of friction, as well as adhesion and cohesion, but it is not always clear how those properties intervene in the flow behaviours inside machines. The properties that affect the machine-product interactions are associated with product particles, but also with aggregates. It is important to notice that handling and spreading solid or semi-solid manure means dealing with particles and aggregates. As previously mentioned,

the aerodynamic properties of the product are important when analyzing what happens when the product is out of the spreader. This is true for all spreading mechanisms described in section 1.2.2. The spreading distance is a function of those properties. All parts of the spreader that are in contact with the product should be corrosion resistant. This introductory analysis highlighted how much the flow process in manure handling and land application is not well comprehended. Moreover, some of the properties deemed to be relevant to the flow process are linked together and values for these properties are not available (impact resistance, dynamic friction coefficient, adhesion, etc.).

The previous analysis was based on solid products. As the total solids concentration (TS) of manure products decreases, their behaviour evolves from granular to pseudoplastic. The transition zone between solid and liquid is not well known and the properties of the products in this zone are undefined. The properties deemed to have an influence on the machine-product interactions for the case of solid manure are also relevant when analyzing semi-solid products, although the properties describing the force-deformation relationships of the products must be adapted to reflect its state. Table 1.1 summarizes the analysis of manure spreaders.

Table 1.1. Summary of the analysis of the functional units featured on manure spreaders.

Mechanism	Desired interactions	Adverse interactions	Important product properties
All mechanisms		▸ Adhesion of the product ▸ Corrosion	▷ Friction coefficient
Scraper floor conveyor	Movement of the product	▸ Interference with drive mechanism ▸ Loss of material	▷ Density ▷ Volume ▷ Particles size and shape ▷ Angle of internal friction & cohesion
Screw-type floor conveyor	Movement of the product	▸ Excessive pulverization ▸ Bridging	▷ Density ▷ Volume ▷ Particles size and shape ▷ Angle of internal friction & cohesion
Hydraulic conveyor	Movement of the product		▷ Density
Rear-delivery horizontal-axis beaters	▸ Striking the product ▸ Product pulverization ▸ Product projection	▸ Excessive pulverization	▷ Angle of internal friction & cohesion ▷ Compressibility ▷ Aerodynamic properties
Rear-delivery vertical-axis beaters	▸ Striking the product ▸ Product pulverization ▸ Product projection	▸ Excessive pulverization	▷ Angle of internal friction & cohesion ▷ Compressibility ▷ Aerodynamic properties
Side-delivery turbine	Product projection	▸ Excessive pulverization	▷ Density ▷ Impact resistance ▷ Aerodynamic properties
Rear-delivery centrifugal table	Product projection		▷ Density ▷ Aerodynamic properties
Side-delivery flails	▸ Striking the product ▸ Product pulverization ▸ Product projection	▸ Excessive pulverization	▷ Impact resistance ▷ Angle of internal friction & cohesion ▷ Density ▷ Aerodynamic properties

1.4. Literature review

Several areas of the scientific literature are relevant to this study. First of all, previous research on manure properties needed to be investigated. Secondly, earlier work on the land application of manure and other products had to be considered. This research effort also included the numerical modeling of manure land application equipment. The representation of various products in the selected numerical modeling environment (discrete element method or DEM) was studied. Finally, other DEM studies have targeted the modeling of machine-product interactions and were included in the literature review.

1.4.1. Physical and rheological properties of manure and similar products

A large amount of information about manure can be found in the scientific literature. Results on the chemical composition of manures and their effects on soils and/or crops are readily available. Fewer research studies have targeted the physical and flow properties of manure products, and most of the published results are for liquid manure and slurry.

1.4.1.1. Manures and composts

Kumar et al. (1972) studied the flow properties of animal slurries. They found that the coaxial cylinder type viscometer was suitable for measuring the rheological properties of slurries. They concluded that the viscosity of dairy manure slurry decreased with an increase in dilution and an increase in temperature. Kumar et al. (1972) also noticed that the flow of slurry was Newtonian at solids contents below 5%. The addition of sawdust up to as much as 10% by weight of the amount of manure decreased the viscosity of a slurry having a total solids content up to approximately 9%.

Hashimoto and Chen (1976) attempted to identify a parameter that would mathematically describe the rheological properties of aerated and fresh dairy, poultry and swine slurries and that could be easily and precisely measured experimentally. They also described procedures to estimate the effect of rheological properties on pumping, mixing and aerating livestock slurries. The highest solids content Hashimoto and Chen (1976) worked with was swine slurry at 10.8% total solids. Their study showed that the rheological consistency index (K) and rheological behaviour index (n) of livestock slurries could be expressed in terms of the equilibrium sludge volume fraction (Φ_L), a measure of the ratio of sludge volume relative to the initial slurry volume, as:

$$K = b_1 \, \Phi_L^{b2} \qquad\qquad (1.1)$$
and
$$n = b_3 + b_4 \ln(\Phi_L) \qquad , \qquad (1.2)$$

where b_1 to b_4 are constants. Values of these constants were given for aerated and fresh dairy, poultry and swine slurries and were found to be dependent on the range of Φ_L. Relationships were also established to relate mixer power characteristics and pressure head loss in pipeline transport of slurries to the consistency index, the rheological behaviour index, the effective viscosity and generalized Reynolds number. Equations for the determination of the effective viscosity were given for the case of a non-Newtonian fluid flowing through a pipe and for the case of slurry mixing. A method of determining Φ_L was also presented. However, the equilibrium sludge volume fraction was never widely used in manure characterization. It is still possible to relate this approach to the work of Van Damme et al. (2002) on the rheology of pastes. They defined pastes as granular media lubricated by hydrodynamic or physical-chemical interactions and in which the presence of an interstitial fluid is expected to introduce two significant differences with respect to dry granular media. The first is the deceleration of the motion of the particle under a given force due to viscous drag and the second is the reduction of the inter-granular friction coefficient by lubrication. The effect of the solid volume fraction was observed on the evolution of the normal force

and yield stress in a shear experiment. Van Damme et al. (2002) observed a sharp
increase of normal force simultaneous to the onset flow only for solid volume fractions
above a critical value. They also noted that a yield stress was measurable before the
solid volume fraction reached that critical value, giving a threshold for the formation of
a weak gel. The parallel measurement of the yield stress and normal force in shear flow
allowed isolating a gel strength contribution to the yield stress and a frictional Coulomb
contribution typical of granular materials in jammed conditions. Van Damme et al.
(2002) suggested that the coexistence of these two aspects was a general feature of
pastes.

Chen (1986) later proposed a rheological model for manure slurries and applied this
model to experimental data of cattle manure slurry obtained using a rotational
viscometer. He concluded that cattle manure slurry showed negligible yield stress and
the Bingham Plastic, Herschel-Bulkley and Casson rheological models were not
applicable. The power law model could be used only for sieved slurries with TS below
4.5%. Chen (1986) also observed a curvilinear relationship of shear stress and shear
rate in the logarithmic plot for high TS slurries due to the existence of a limiting
viscosity. He proposed a rheological model for beef cattle manure slurry:

$$\tau = \eta_0\dot{\gamma} + K''\dot{\gamma}^{n''} \qquad , \qquad (1.3)$$

where τ is the shear stress, $\dot{\gamma}$ is the shear rate, η_0 is the limiting viscosity, and K'' and n''
are rheological parameters. Non-linear least square regression was used to fit the
proposed model to the experimental rheological data of slurries having TS above 4.5%.
The results showed that the proposed model fitted very well the experimental data with
correlation coefficients of 0.99 and above. The value of n'' for sieved slurries did not
vary with TS or temperature, having an average value of 0.307 with a standard
deviation of 0.054. Equations expressing η_0 and K'' in terms of TS and temperature
were also obtained. The values of η_0 and K'' were found to increase as TS increased
and to decrease as temperature increased.

Rheological consistency index, flow behaviour index, specific heat and thermal conductivity of beef cattle manure were determined by Chen (1982). Density was also measured for solid contents ranging from 1% to 99%. The results suggested that the density of manure increased as the total solids concentration increased for manure with less than 16% TS. This trend appeared to extend to solids concentrations of about 40%. The density decreased from 40% to 50% and for manure with TS higher than 50%, the bulk density dropped much below the liquid manure density. Rheological properties of manure were studied for TS ranging from 1% to 14%. Beef cattle slurries were described as non-Newtonian pseudoplastic fluids, the deviation from Newtonian behaviour increasing with TS.

Chen and Shetler (1983) studied the effect of temperature on the rheological properties of cattle manure slurry. Using a constant-temperature rotational viscometer, they investigated the effect of temperature on rheological properties of manure having total solids concentrations ranging from 2.5% to 19.3% at shear rates ranging from 20 to $200s^{-1}$ and temperatures ranging from 14°C to 64°C. This study confirmed previous findings that beef cattle manure slurry is non-Newtonian pseudoplastic and a power-law equation could be used in the range of shear rates of the study. The rheological behaviour index (n) was found to decrease exponentially with TS, but was not affected by temperature while the rheological consistency index (K), in general, increased as TS increased. The apparent viscosity of the slurry decreased exponentially as the temperature increased, and increased as TS increased. An equation relating the apparent viscosity to TS and to the absolute temperature was given.

Achkari-Begdouri and Goodrich (1992) studied the rheological properties of dairy cattle manure with total solids concentrations ranging from 2.5% to 12% at temperatures between 20°C and 60°C. The rheological properties studied included the consistency coefficient, the flow behaviour index and the apparent viscosity. Their results showed that in the ranges of total solids and temperatures of the study, dairy cattle manure behaved as a pseudoplastic fluid. Two equations based on the total solids content and the temperature, one expressing the consistency coefficient and the other to predict the

flow behaviour index, were proposed. The flow behaviour index was found to increase with the temperature while the consistency coefficient decreased as the temperature increased. The results of Achkari-Begdouri and Goodrich (1992) suggested that an increase in the total solids concentration induced an increase in the consistency coefficient and a decrease in the flow behaviour index.

It can be seen that the majority of the manure characterization studies have focused on liquid products. The general conclusion seems to be that manures are non-Newtonian pseudoplastic fluids, up to a total solids concentration of approximately 20%. It has also been suggested that below 5% TS, manures exhibit a Newtonian behaviour. The effects of the temperature and total solids concentration on the flow behaviour index and consistency coefficient are not consistent across the various research studies.

Glancey and Hoffman (1996) studied the physical properties of solid organic by-products. The measured properties were bulk density, moisture content, angle of repose, maximum clump size and static frictional characteristics. Ranges of values were given for each property. Glancey and Hoffman (1996) investigated trends in the measured properties to develop general guidelines for the design and analysis of material handling systems, transportation equipment and spreaders. They concluded that wet bulk density was dependent on moisture content for all the solid products evaluated and that knowledge of moisture content was therefore more important than the type or source of material. The static friction characteristics suggested that there was little practical difference between the different products. Another trend identified by Glancey and Hoffman (1996) indicated that all unscreened products contained large clumps. This presented potential design problems in developing conveying systems to handle unscreened materials.

Thirion et al. (1998) measured manure properties including normal stress, shear stress, bulk density, friction coefficient, straw content and dry matter content. The reported efforts were targeting the measurement of manure properties from a machinery testing and development viewpoint. Thirion et al. (1998) reported values of normal stress

between 0.14 and 1.60 MPa, as measured by a penetrometer. A vane shear apparatus was used to measure the shear stress that ranged from 3 to 50 kPa. They observed friction coefficients of about 0.84 for most tested samples. Thirion et al. (1998) included several comments on the heterogeneity of manure and the variability of its properties as well as the influence of the measurement method for bulk density on the results.

Agnew et al. (2003) used an air pycnometer to measure the air volume and density of compost. The free air space (FAS) and bulk density of manure compost, municipal solid waste compost, and mixtures of biosolids and amendment material were measured at various moisture content and compressive loads. The results indicated that the FAS decreased with loading and increasing moisture content while the wet bulk density increased with loading and increasing moisture content. A linear relationship was established between FAS and bulk density for all the materials tested under load. In light of the results obtained by Thirion et al. (1998) and the data presented in chapter 2 of this thesis, the pycnometer may very well be a suitable method for the determination of the bulk density of manure and other organic by-products. If conclusive results can be obtained for various products, the pycnometer could become an acceptable standard method to measure the bulk density.

1.4.1.2. Measurement methods for concrete

Because the amount of information on the properties of solid and semi-solid manure found in the scientific literature was limited, other products of similar consistency were considered. In a very complete article, Ferraris (1999) reviewed many test methods used for measuring the flow properties of concrete. The test methods reviewed were divided into two groups depending on the output of the tests based on the assumption that both the yield stress and the viscosity were required to correctly define the rheology of concrete. Among the one-factor tests described, the slump test consists of filling with concrete a truncated metal cone open at both ends and resting on a horizontal surface. The cone is then quickly lifted. The concrete will slump or move only if the

26

yield stress is exceeded and will stop when the stress is below the yield stress. Therefore, the slump test is related to the yield stress.

The penetrating rod test is based on the principle that the depth of penetration of an object depends on the yield stress of the concrete. The mass or the force applied on the penetrating object indicates if the applied stress exceeds the yield stress of the concrete.

The turning tube viscometer can be used to measure the viscosity of cement paste (concrete being a concentrated suspension of aggregates in cement paste). The viscometer consists of a tube that can be filled with the material to be tested. A ball is then dropped in the fluid and its velocity measured between two points. Potential problems can occur when using this test with concrete because the diameter of the ball should be significantly larger than that of the aggregates. Otherwise, the product cannot be considered to be a uniform medium in which the ball is freely falling.

The K-slump test gives a value related to the yield stress of the concrete. For this test, a probe is inserted in the concrete to be tested so that the collar floater is on the concrete surface. A portion of the concrete flows into the hollow center of the probe through the perforated exterior tube. A measuring rod placed inside the perforated tube measures how much concrete was able to flow into the probe. Again, a product having coarse aggregates may cause problems and the results of this test would only give an indication of the ability of the product to segregate.

The Ve-be time and remolding tests measure the capability of the concrete to change shape under vibration (frequency of 60 Hz; amplitude of 0.43 mm). In both tests, the concrete is placed in an open-ended truncated cone and the time it takes the concrete to remold itself into a cylinder under vibration, after the cone is lifted away, is measured giving a result related to the plastic viscosity of the concrete.

The LCL apparatus is also used to determine the time it takes to the concrete to remold into a new form. In this case, the amplitude and the frequency of vibration can be changed. The measurement given by this test is related to the plastic viscosity.

For the Fritsch test, the sample is placed in a container fitted with a vibrator. The time when the lid, which is resting on the concrete sample, is not descending anymore is measured. This test, done under vibration, yields a compaction factor for the tested concrete.

The flow cone test is done using a funnel with an orifice. The slope of the funnel wall is 6:1. The time required for a given amount of concrete to pass through the orifice is measured giving a value related to the viscosity.

Ferraris (1999) also presented two-factor tests. While these test results give two parameters, they don't necessarily allow for a direct calculation of the viscosity and yield stress. The factors measured are often indirectly related to the two fundamental parameters. The difficulty in designing tests that allow for the measurement of the two rheological parameters is due to the size of the coarse aggregates, the tendency of segregation and the time effects. The Tattersal two-point rheometer is the most widely known instrument for measuring the flow properties of concrete. The apparatus consists of a container filled with the concrete to be tested and an impeller. The torque required to rotate the impeller at different speeds is recorded. The yield stress and plastic viscosity are obtained on the linear graph of torque versus speed. Commercial versions of this equipment are available.

The Bertta apparatus allows the operator to calculate the viscosity and yield stress of concrete as a function of frequency. This equipment consists of two concentric cylinders. The outer cylinder rotates in an oscillatory mode with a frequency and amplitude selected by the operator. The torque induced by the movement is measured on the inner cylinder.

The BTRHEOM rheometer is a bucket with a serrated bottom and a rotating top wheel resting on the concrete. The shear stress distribution allows direct calculation of the viscosity and yield stress.

A modification of the slump cone test was developed to allow for the measurement of viscosity, the standard test being correlated to the yield stress only. The modification consists in measuring not only the final slump height but also the speed at which the concrete slumped. The yield stress and viscosity are then calculated using empirical equations.

Numerous tests and apparatuses exist to describe the rheology of concrete. Ferraris (1999) mentioned that it is hard to relate results obtained with different tests and emphasized that more research was required to better characterize the rheology of concrete.

1.4.1.3. Oils

DeKee et al. (1998) studied the rheological behaviour of Athabasca topped heavy oil. Crude oil and mixtures of crude oil with different additives were analyzed using three types of rheometer, namely, a cone and plate rheogoniometer, a concentric cylinder rheometer and a capillary viscometer. The results showed that the data obtained using the three different rheometers were in good agreement. The Newtonian or non-Newtonian behaviour of the product tested depended on its type and temperature. Observed non-Newtonian behaviour was successfully modeled by a simplified equation derived from a model proposed by DeKee and Chan Man Fong (1994).

The rheological behaviour of waxy oils is an important parameter in pipeline design and oil reservoir operations. The characteristics of these oils were found to be affected by temperature, shear rate and wax concentration. A mathematical correlation has been developed by Al-Farris et al. (1993) to describe the viscosity of waxy base oil as a function of shear rate, temperature and wax concentration. A rotational viscometer was

used to measure the rheological properties of the waxy oils at different temperatures and wax concentrations. The proposed correlation fitted the experimental data very well with a correlation coefficient of 95%.

1.4.1.4. Sludges and other organic by-products

The rheology and physico-chemistry of municipal sewage sludge have been the object of a doctoral thesis (Baudez, 2001). The rheological behaviour of sewage sludge was found to be viscoelastic linear under a critical value of shear stress and to follow the Hershel-Bulkley model beyond that critical value of shear stress. The effect of the storage period was highlighted. As the chemical composition of the sludge evolved during storage, the mechanical behaviour changed and the viscosity decreased with time. The slump test was used to establish the value of the critical shear stress, which defined the transition between the two rheological behaviours. Further work on the behaviour of sludge on spreading disks was conducted (Tabutot, 2004). Wolfe and Stowell (1999) found linear relationships between slump and solids content for apple sauce and sawdust, pizza sauce and sawdust, and dairy manure, water and sawdust mixtures over the solids content ranges of 18% to 24%, 12% to 20%, and 10% to 14%, respectively. The results presented by Wolfe and Stowell (1999) suggested that a simple slump test could be used to estimate the solids content of mixtures of manure and sawdust and eventually other non-Newtonian fluids.

Landry and Laguë (1999) studied physical properties of papermill residues. They measured bulk density, moisture content, angle of repose, friction coefficient over different materials and particle size distribution. Landry and Laguë (1999) concluded that while the values of the selected properties were relatively constant among samples that originated from the same papermill, there could also be large variations depending upon the specific origin of the products. Properties that were relatively constant for all samples were the angle of repose with an average value of 30º and the geometric mean length of the particles with an average of 7.5 mm.

1.4.2. Machine-product interactions

The influence of the properties of manure or other organic by-products on the performance of machines or components of machines has been studied, to some extent, for various applications. The development of land application machines has also led to the study of machine-product interactions.

1.4.2.1. Poultry litter spreading

Poultry litter is typically applied to agricultural fields using centrifugal-type (spinner-type) spreaders. These spreaders are similar to those used for broadcasting granular fertilizers and use horizontal spinning discs. Poultry litter is relatively non-homogeneous and light and thus difficult to spread uniformly. Poultry litter is characterized by fine material coming primarily from the manure, intermediate-size particles of bedding material, and larger clumps made of manure, feathers and bedding material. The most important part of the nutrients being in the manure, the nutrient value of the litter will vary with particle type. Particles of different sizes having different aerodynamic properties, non-uniform distribution of the nutrients across the spreader working width could be caused by variation in nutrient content with particle type. This hypothesis was tested by Wilhoit et al. (1993). Differences in particle size were found to be a major cause of segregation during spreading (Crowther, 1958; Hoffmeister et al., 1964). Centrifugal distributors have been analyzed theoretically in terms of fertilizer physical properties, particle trajectories and machine parameters (Patterson and Reece, 1962; Cunningham and Chao, 1967). Different machine parameters were tested to study their effect on distribution patterns (Reed and Wacker, 1968). Uniformity was strongly affected by spinner blade adjustment, point of delivery of the fertilizer onto the spinner and application rate. After evaluating the distribution characteristics of a centrifugal-type spreader broadcasting poultry litter based on both mass and nutrient concentrations, Wilhoit et al. (1993) concluded that most smaller particles (smaller than the openings of a no.12 screen) landed within a distance of 3.7 m of the center of the spreader while the larger particles were distributed more evenly out to a distance of 6.1 m. Wilhoit et al. (1993) also concluded that the nitrogen

concentration was relatively uniform between particle sizes while the carbon concentration tended to increase with increased particle size. However, the samples collected across the swath showed uniform concentrations for both nitrogen and carbon. This study by Wilhoit et al. (1993) showed the importance of the aerodynamic properties of the product to be spread. Even if no significant difference could be found in nutrient concentrations across the working width of the spreader, the segregation of particles during spreading due to differences in particles size could become a problem.

A study by Ling et al. (1996) had the objective of determining the influence of gate height and conveyor velocity settings on the performance of a spinner-type spreader broadcasting poultry litter. The performance of the spreader was evaluated in terms of uniformity of both material flow onto the spinners and material spread in the field. The pressure across a hydraulic spinner motor was used as a means of evaluating the variation of material flow falling onto the spinners. In field spreading tests, coefficients of variation were evaluated for simulated overlapping spread patterns across the swath at different combinations of gate openings and conveyor velocities. Ling et al. (1996) concluded that the variation of material flow onto the spinners decreased as the theoretical flow rates increased. They also observed that at a fixed conveyor velocity, the variation of material flow onto the spinners decreased as gate opening decreased. Moreover, at a fixed gate opening, the variation of material flow onto the spinners decreased as the conveyor velocity was reduced. Their observations of spread uniformity across the swath suggested that evenness decreased as the gate opening increased and it increased as the theoretical flow rate increased. Finally, no significant effects of gate opening and conveyor velocity on the spread uniformity in the direction of travel could be observed.

In an attempt to design a drop applicator for poultry litter, Wilhoit et al. (1994) had to consider machine-product interactions. The objective was to design a tractor-mounted applicator so the hopper capacity and configuration had to be selected based on load transfer considerations. The bulk density of the poultry litter can vary considerably depending on moisture content and a design value of 480 kg/m^3 was selected. The first

design featured gravity flow with agitation of the litter above an adjustable opening. The agitator was intended to keep the litter from bridging in the hopper and to help meter it through the opening. Preliminary tests showed, however, that this design was not appropriate. With larger gate openings, the litter would free flow with little or no metering effect from the agitator while when the gate was closed enough to restrict flow, litter clumps completely blocked the flow from the hopper. A different metering system was then needed. The drop applicator unit was modified by closing off the opening across the back of the hopper, opening up the bottom, and mounting a platform directly beneath that opening with a chain looped around the platform. The floor chain was powered hydraulically, the application rate being controlled by the output speed of the hydraulic motor. These modifications proved to be satisfactory at measuring poultry litter out of the hopper. Tests were then carried out to determine the effect of the depth of product in the hopper on the application rate, evaluate uniformity of litter application both across the swath and in the direction of machine travel and finally relate the application rate to the speed of the floor chain. The results showed that the application rate was not affected by the depth of litter in the hopper and that calibration was primarily volume-based and therefore dependent on chain speed. In that case, there was no significant effect of the depth in the hopper even for a compressible material. A different hopper design may have led to a relation between application rate and depth of product in the hopper. After adjustment of the chain system, the uniformity of application was good in this study, with the lowest coefficient of variation values of 11.8% and 16.0% for the uniformity in the direction of travel and across the swath, respectively.

1.4.2.2. Power requirements and evaluation of land application equipment

For most systems, the power requirements for spreading consist of conveyor power added to the power required by the spreading mechanism. The conveyor power requirement is a function of the type of product spread, flow rate and type of conveyor while the power required by the spinner-type spreading devices depends on velocity, configuration and type of power transmission. Ling and Wilhoit (1999) investigated the

power requirements of spinner-type spreaders broadcasting poultry litter and wood ash. The chain conveyor and the two spinners of the test spreader were driven separately by individual hydraulic motors. The products used in this study were poultry litter having an average moisture content of 22.2% and an average bulk density of 503 kg/m^3 and wood ash at 59.0% average moisture content and 517 kg/m^3 average bulk density. The power consumption of the spinner motor was estimated using the measured hydraulic pressure drop across one of the spinner motors and the measured spinner velocity. To estimate the power requirements of the conveyor system, formulas and design factors from the American Chain Association along with an analysis of the forces acting on a material flow block were used. The results showed that the power consumption of the hydraulically operated spinner system when spreading poultry litter increased as the spinner velocity and product flow rate increased. There was no significant difference in the power consumption of the spinner system for poultry litter and wood ash spreading, mainly because both materials had approximately the same bulk density at the testing conditions. The maximum power consumption of the spinner system was 10.4 kW (from the reported flow rate, the specific energy was 816.3 J/kg) for poultry litter and 10.2 kW (from the reported flow rate, the specific energy was 941.5 J/kg) for wood ash. The power consumption of the conveyor system was found to change with the depth of product inside the hopper, length of the hopper, gate height, gate width, hopper angle, specific weight of product, conveyor velocity, internal friction of the product and friction between the product and the hopper. From a sensitivity analysis, the factors significantly affecting the power consumption were found to be material depth, hopper length and gate opening while the least sensitive factors included gate height and hopper angle. The power consumption of the conveyor was smaller than that of the spinners. The conveyor power requirements increased as material flow rate increased and there was little difference between poultry litter and wood ash spreading. The conveyor power requirements and specific energy (calculated from the reported discharge rate) for poultry litter and wood ash spreading were very similar (maximum power requirement of 8.34 kW (specific energy of 654.6 J/kg) and 8.25 kW (specific energy of 629.9 J/kg), respectively) because the density and friction coefficient of the materials were similar.

Wilhoit and Ling (1996) also studied ash spreading in a forest environment. They observed that spreading uniformity was not satisfactory with coefficients of variation above 20%, even if less uniform spreading should be more acceptable when working with products like wood and fly ash. The nature of the products spread caused the uniformity results to be inconsistent from trial to trial. These products are not uniform in size or consistency. Ashes are especially prone to variations in physical consistency due to differences in moisture content, and these variations can have a major impact on spreading. A result of this study highlighting this fact is that the wood ash could not be spread at the slower conveyor velocity when having a moisture content of 49%, but could at a moisture content of 41%. Wood and fly ash were spread with reasonable uniformity at swath width up to about 12 m. The type of spreader used was a poultry litter spreader mounted on the back of a forwarder, a forest tractor used for carrying logs. Wilhoit and Ling (1996) concluded that important swath widths and good application rates should be possible with this type of spreader through optimization of products properties and spreader operating parameters.

Bulinski and Klonowski (1998) studied the power requirements of the working units of a manure spreader. The power requirements for the floor conveyor and the four vertical beaters were evaluated at four levels of hopper filling and four velocities of the floor conveyor. Their investigations showed that the power requirements for the studied spreader working units depended significantly on the floor conveyor velocity and the mass of manure in the hopper. Their results also showed considerable variation of loading on the spreader driving system. As could be expected, the density of manure was of first importance when analyzing the power requirements of the spreader.

The Swiss Federal Research Station for Agricultural Economics and Engineering (FAT) conducted a study to compare spreading devices (Bisang, 1987). The conclusions were to the effect that spreaders using horizontal-axis beaters had a working width of 2 to 3 m while vertical-axis beaters allowed for an effective spreading width of about 6 m. The precision of distribution was judged acceptable for most of the tested spreaders. Bisang (1987) observed that spreading mechanisms having one beater gave coarser

material and screw-type beaters led to smaller particles when compared to teethed beaters.

Frick et al. (2001) reported on the work conducted at FAT to study different spreading systems for feedlot manure and other organic by-products. Their study included seven commercial spreaders having different mechanical systems: (1) scraper conveyor and two horizontal beaters; (2) scraper conveyor and two horizontal beaters combined with four spinners; (3) scraper conveyor and two vertical beaters; (4) scraper conveyor and four vertical beaters; (5) scraper conveyor and side delivery multiple rotors; (6) belt conveyor and two spinners; (7) belt conveyor and two back spinners or front spreading auger with multiple drop tubes. Various organic by-products were used during the tests: (a) feedlot manure; (b) green wastes compost; (c) dehydrated wastewater sludge; (d) dried wastewater sludge, and (e) lime product resulting from sugar processing. Several parameters were studied during the spreading tests such as the transversal and longitudinal product distribution, extent of manure pulverization, power required for traction, power required by the spreading devices, power required by the floor conveyor, and finally the allowable load for each machine. The results for transversal product distribution highlighted the dependency of this parameter on the physical properties of the products and the type of spreading devices featured on the tested machines. The coefficients of variation were generally good. The spreader equipped with four vertical beaters performed better than the other machines with lower CVs for all products with the exception of the lime product. The longitudinal product distribution tests highlighted the typical poor performances of solid manure spreaders. The effect of a flow-control gate could be observed with lower values of CV when a gate was used. All the machines tested with manure generated acceptable pulverization, with the four vertical beaters and the side delivery rotors performing the best. With regard to the field operation of the spreaders, recommendations were included to the effect that a machine with a large volumetric capacity should be selected when spreading a product having a low bulk density. This selection would ensure that the targeted application rates can be reached without overly frequent loading of the spreader. The results suggested that the working width of a spreader should be selected

36

according to the desired spreading travel distance, the speed of operation and the targeted application rate. When considering the payload the machines are capable of carrying, Frick et al. (2001) noticed that with high density products, such as dehydrated wastewater sludge or lime product, the risk of overloading the spreader was increased. The situation was more critical for a machine having a high weight when empty or a low load bearing capacity. The power requirements of the spreaders were divided into three components: the tractive power, the power required by the floor conveyor and the power consumed by the spreading devices. The results obtained by Frick et al. (2001) indicated that the average power consumption was distributed 57% to the spreading devices, 38% for traction and 5% to the floor conveyor, which required 1.5 to 2.0 kW. The highest power requirements were for manure spreading. Spreaders featuring horizontal or vertical beaters demanded approximately 40 kW of power while the spreader with spinners and the side delivery machine required 60 kW. An additional 20 kW was deemed necessary for traction. The calculated tractive power for a tractor-spreader speed of 4 km/h ranged between 10 and 20 kW. The tractive power was found to be dependent upon the size of the tires of the spreader. The average tractive specific power was 4.2 kW/t for manure, 3.5 kW/t for compost, 2.8 kW/t for dehydrated wastewater sludge and 2.3 kW/t for the lime product. With bulk density values of 590, 690, 875 and 1035 kg/m^3 for manure, compost, dehydrated wastewater sludge and lime product respectively, there was an inverse linear relationship between the tractive specific power and the density.

Malgeryd and Wetterberg (1996) reported the efforts of the Swedish National Machinery Testing Institute and the Swedish Institute of Agricultural Engineering in order to provide the necessary knowledge of how the physical properties of manures and slurries affect the spreading performances of different machines. They highlighted the fact that there is a lack of general knowledge about which properties or parameters derived from physical properties are important in practice and how they should be measured. For manures that can be pumped, four parameters were considered to be important, namely, fluidity, separation tendency, risk of clogging and dry matter content. For manures that cannot be pumped, five parameters were considered

important: bulk density, stacking ability or consistency, comminuting resistance, heterogeneity and dry matter content. Methods were suggested to measure these properties and parameters. Testing methods were also proposed to evaluate manure spreaders. The results obtained by Malgeryd and Wetterberg (1996) suggested that there is no clear relationship between the active angle of repose and the dry matter content for non-pumpable manures and that bulk density and the active angle of repose are closely related to each other. The active angle of repose could be estimated from the bulk density, which is easier to measure. They concluded that bulk density and/or the active angle of repose affect important spreading parameters such as the steady flow and the optimum working width and that different spreader types are influenced in specific ways, depending on their mechanical configuration.

Picaud (2001) studied the relations between the properties of organic by-products and the performances of land application equipment. The measured properties were density, penetration resistance, dry matter content, and content in selected nutrients. The variability inherent to organic by-products as well as the limited number of data collected due to the heaviness of the experimental procedures were highlighted by Picaud (2001) as causes for the lack of clear relationships between the measured parameters. However, a trend could be identified between the resistance to penetration and the transversal coefficient of variation. Lower resistance to penetration yielded smaller coefficients of variation. Numerous comments were included on the lack of standardized procedure for manure characterization and on the difficulty of collecting a large amount of quality data when working with organic by-products and land application machines.

1.4.2.3. Design of spreaders

Laguë (1991) reported on the design and evaluation of a semi-solid dairy cattle manure land applicator. The objectives of the research study included the development of a machine capable of spreading as well as injecting semi-solid cattle manure at application rates of 100 t/ha at normal field operating speeds without using a pump.

One of the objectives was also to minimize the additional power required by the injection system. A trailer-mounted tank arrangement was proposed. In order to maintain a uniform flow rate of manure inside the injector hoses during unloading, the 15.3 m^3 tank was constructed so that its front end could be tilted during emptying. A vibrating distribution manifold was installed at the discharge end of the tank to collect the manure flowing out of the tank and to distribute it to the four injectors. The injection system was design so that the hoses connecting the manifold to the injectors were kept vertical when the system was operating. The injectors and injector hoses were removed and deflectors installed under the outlet openings of the manifold for surface spreading. Preliminary field tests indicated that excessive soil lifting was generated by the injectors. The flexible hoses were also found to be not rigid enough and partial or complete obstruction of the hoses sometimes occurred. Transversal uniformity tests were carried out and average application rates ranging from 112.7 to 264.7 t/ha were achieved during those tests. A significant decrease in the application rate as the tank was getting empty was observed. It was found difficult for the operator to tilt the tank in a continuous manner as it was emptied. The transversal distribution curves presented by Laguë (1991) demonstrated that more manure was flowing out of the middle two outlets. Values of the transversal coefficient of variation ranging from 63.5% to 74.4% were the consequence of the difference in flow rate at each outlet. Subsurface injection of manure into firm clay soil was found to require between 4.5 and 5.5 kW/injector of additional power compared to surface spreading.

Laguë et al. (1994) studied the possibility of using a wide-span boom to apply liquid manure onto growing crops. The boom featured a two-stage system to control the application rate. The volumetric flow rate controller could divide the incoming flow of manure and distribute it to six gravity distributors. The gravity distributors then divided the flow from the volumetric flow rate controller to six vertical hoses that were used to apply manure to the ground surface. The design characteristics of the flow rate controller and the rotational velocity of the controller were determinant factors of the accuracy of the entire system. This study reflects the importance of the physical and flow properties of the product in the design of the equipment.

Glancy and Adams (1996) designed an applicator for sidedressing row crops with solid organic by-products. First, a conveying system capable of metering and distributing material into bands was needed. Properties relevant to the land application of the products and conveyor design for the metering and delivery of poultry manure included moisture content, bulk density, angle of repose, maximum clump size and coefficient of friction of manure on different materials that could potentially be used in the fabrication of the spreader. For design purposes, maximum clump size and moisture content were identified as the physical properties of poultry manure that presented potential problems in raw manure conveying. Glancy and Adams (1996) concluded that pulverizing the manure on board the sidedress applicator to reduce the maximum clump size was required. The existing beaters of a manure spreader were used for this purpose. The first design of the sidedress applicator featured a single conveyor with drop tubes. After conducting tests to determine the flow rate through a drop hole as affected by hole size, conveying rate, conveyor rotational velocity and manure clump size, the single conveyor was proven not viable. The flow properties of the product did not allow for satisfactory metering and conveying using the single conveyor. The concept of the final design included the use of individual conveyors for each drop point. Using ranges of values provided by Glancey and Hoffman (1996), Glancy and Adams (1996) studied the effect of manure physical properties on conveyor size and power to drive the conveyors. They concluded that the required input power per unit length of each conveyor was most affected by the bulk density of manure. Using the calculated conveyor design parameters, an attachment for sidedressing 0.762 m-wide crop rows was designed and fabricated for the New Holland model 155 beater-type spreader. With this design, pulverized manure leaving the beaters was directed to a set of conveyors parallel to the direction of travel which conveyed then dropped the manure onto a second set of conveyors perpendicular to the direction of travel. The latter conveyors distributed and dropped material between the crop rows. Field testing showed that the sidedresser could apply manure between crop rows with fair uniformity. The coefficient of variation across the width of the applicator was 19% for an application rate of 27 kg N/ha and 15% for an application rate of 105 kg N/ha.

Khalilian et al. (2002) reported on the development of an injection system for municipal solid waste compost. The equipment was designed to apply compost under the seed row at sufficient depth to place it in the compacted subsoil layer. The platform for the equipment was a subsoiler to which a hopper was adapted. A drag chain was fitted in the hopper to move the compost. The flow of compost in the machine went from the hopper, under a vertical flow-control gate and fell by gravity in a transition section, where the product was funnelled in two drop tubes. The shanks of the equipment opened a slot into which the compost was dropped. Disks attached behind the drop tubes pulled back soil to close the slot. The application rate could be adjusted by modifying the velocity of the floor conveyor and the height of the flow-control gate. The actual application rates of the machine, in the range of 4 to 24 t/ha, were closely related to the targeted rates with an R^2-value of 0.985.

Pezzi and Rondelli (2002) developed and tested a prototype spreader for the land application of poultry manure. Their prototype featured a pentagonal hopper with a rotational mixer in the upper part and a discharge auger at the bottom. The auger conveyed the product to a circular outlet that could be opened or closed to meter the flow. A distribution system, made of two four-bladed spinners and adjustable for longitudinal position, was located under the outlet. An adjustable shield was installed on the support of the spinners allowing the machine to perform either broadcast or banded application. The objective of the testing program was to find the proper mechanical adjustments to land apply poultry manure with different levels of moisture content and composting. The tested products had moisture content values ranging from 29% to 48%, bulk densities from 220 to 443 kg/m^3 and static coefficient of friction on unpainted steel between 0.63 and 0.91. The particle size distribution of the samples was also measured. Pezzi and Rondelli (2002) concluded that the adjustment of the spinner velocity modified the distribution pattern, with an increase of the velocity improving the throwing width and effective spreading width. The point of delivery of the product on the spinners also had an influence on the distribution pattern, but did not affect the throwing width. For banded application, the best results were obtained when the point of delivery coincided with the center of the spinners whereas better broadcasting results

41

happened when the point of delivery was moved far from the center. The influence of the size of the particles on the performance of the spreader was highlighted. Without clearly drawing conclusions to this effect, Pezzi and Rondelli (2002) underlined the effect of the static coefficient of friction and bulk density of the products on the quality of distribution.

In an effort to provide farmers with a valid machine to land apply farm yard manure (FYM) and compost, Balsari et al. (2002) developed a spreader featuring two interchangeable spreading devices and a system for the automatic control of the application rate. The spreading units were attached at the back of the large-capacity hopper (13.7 m^3). Two vertical beaters were used for FYM spreading while compost land application was achieved by two horizontal beaters feeding two spinning discs via a deflector. The spreader also featured a moving panel attached to a chain conveyor to move the volume of product as a unit towards the spreading devices. The application rate was controlled using the signals from load cells placed between the frame and sub-frame of the machine combined with the information on the speed of travel provided by a velocity sensor. The system controlled the velocity of the hydraulically driven conveyor to match the desired application rate. Tests were performed using dairy cattle manure with bedding, having a density of about 620 kg/m^3 and 25% TS. The compost used during the experiments had 45% TS and a particle size of 12 mm. The transversal evenness of distribution was found to be acceptable for both the compost and FYM spreading systems, with coefficient of variation below 30% for working widths up to 13 m. The application rate control system was capable of adjusting the speed of the floor conveyor with a lag time of approximately 10 s.

1.4.3. Modeling the flow of manure and other organic by-products

The flow of manure and other organic by-products has been the object of very few published modeling research efforts. To an extent that depends upon the total solids concentration (TS) of the product, manure handling and land application systems

involve a flow of granular material. In order to develop solid and semi-solid manure land application machinery that will be more efficient in terms of power consumption as well as longitudinal and transversal uniformity of application, an enhanced understanding of the interactions between the products and the functional systems of the machines is required. The volume of manure being handled by a machine cannot be treated as a bulk phenomenon if one wants to gain a better understanding of the dynamic flow of the product. Models that incorporate particle-scale parameters to capture the dependency of the behaviour of a discontinuous medium on the arrangement and physical properties of individual particles are therefore required. The discrete element method is an explicit numerical method of modeling the dynamic behaviour of assemblies of distinct objects. It makes use of contact mechanics between particles in an assembly and between particles and enclosing surfaces to model the dynamics of assemblies of particles (Kremmer and Favier, 2000; Cundall, 1988). In the DEM, the governing equations are a set of equilibrium equations for resultant forces and moments at the centers of particles. The resultant forces and moments emerge from contact forces, body forces, inertia forces and damping forces. The original DEM (Cundall, 1971) had the following assumptions:

1. the particles are circular rigid bodies,
2. the contact points between particles occur over an infinitesimally small area,
3. the particles are allowed to overlap slightly at the contact points,
4. the magnitude of the overlap is linearly related to the contact force, unless slip or separation occurs between particles and
5. the slip condition between particles is given by the Mohr-Coulomb law.

The set of governing equations in DEM can be expressed in matrix form as:

$$M\Delta\ddot{X} + C\Delta\dot{X} + S\Delta X = \Delta F \quad , \qquad (1.4)$$

where M is the mass matrix, C the damping matrix, S the stiffness matrix, ΔX is the incremental displacement vector which includes incremental rotations, and ΔF is the incremental force vector which includes incremental moments. To get a step-by-step solution, equation 1.4 should be converted into a set of algebraic equations in terms of a

finite difference operation (Oda and Iwashita, 1999). Detailed information of the implementation of the method in the computer code PFC^{3D} (Itasca Consulting Group Inc., Minneapolis, Minnesota, USA) that was used in this study can be found in the software documentation (Itasca, 2003).

The amount of research publications involving the DEM is overwhelming. The two major areas of interest are applications of the DEM and development of the method. Some overlap will sometimes occur where particular applications of DEM lead to advancements in the numerical method, but the literature generally offers publications focusing on either modeling a particular engineering application or on improving the method. From the DEM enhancement viewpoint, three main areas of research can be identified: (a) general shaped particles representation, (b) boundaries and rigid body dynamics representation and (d) contact-force-friction models implementation.

1.4.3.1. Particle shape representation

If the general DEM can handle deformable polyhedral blocks, many codes make use of circular or spherical particles (Cundall, 1988; Itasca, 1999). Spherical elements have the major advantage of computational simplicity. However, particle rotation is constrained only by friction forces coming from contacting particles. It has been stated that the representation of particle shape is among the critical physical models that will influence the DEM simulation accuracy (Favier et al., 1999). Many efforts have therefore been devoted to representing irregular particles in DEM. The key is to model the real particle shapes as closely as possible while maintaining reasonable efficiency in contact detection and computation time. The use of elliptical elements was introduced by Ting et al. (1993) to represent particles with an aspect ratio greater than one. The extension to 3D using ellipsoids is described by Lin and Ng (1995). Elliptical elements have the drawback of difficult contact detection. Ning et al. (1997) joined a large number of spheres in the objective of studying the impact breakage of lactose agglomerates. Adhesion was applied between spheres using different models for normal contact stiffness and tangential behaviour. Two-dimensional clusters made of

three circles having the same diameter arranged in a triangular pattern were used by Jensen et al. (1999) to model granular media. The results of simulations of a two-dimensional shear test on clustered and non-clustered particles suggested the shear strength of the assembly is increased by clustering, due to reduced particle rotation. Ni et al. (2000) also used clustered particles made of two spheres of different diameter to simulate sand in their model of the direct shear test. They observed higher peak and residual bulk friction angle for clustered particles when compared to single spheres.

It is also possible to use mathematical functions to represent smooth irregular shaped particles. One or more superquadrics, which can be defined as three-dimensional parametric objects, can be used to generate a wide range of shapes (Barr, 1981; Williams and Pentland, 1989). Contact detection becomes a matter of finding the intersection of the two functions, but the non-linearity of the equations makes this step almost impractical computationally. The use of a discrete function representation (DFR) was proposed by Williams and O'Conner (1995) to enable the use of shapes derived from superquadrics. The proposed method consisted of the discretization of the body's boundary using a certain density of nodes. Contact detection was done by using the node coordinates in a function derived from the superquadric. The application of DFR was later extended to three-dimensional particles by Hogue (1998). The two major drawbacks of using the DFR approach included the approximation of the surface by lines or triangular plates and the use of an average rather than the true contact normal that is usually calculated due to the lack of coincidence of nodes on contacting bodies.

Favier et al. (1999) proposed a method of generating and modeling contacts between three-dimensional axi-symmetrical particles made of overlapping spheres. The spheres of arbitrary size had their centers fixed in position relative to each other along the major axis of symmetry of the particle. Contact detection and calculation of force-deformation as well as particle movement were performed using standard DE techniques modified to take into account the behaviour of each single sphere with that of the multi-element particle to which it belongs. The efficiency of this particle-

generation method comes from the computational speed and accuracy of contact detection for spheres.

1.4.3.2. Boundary conditions

Modeling engineering systems requires a precise representation of boundary conditions. This is especially important when modeling systems in which the particle dynamics are affected by the geometry and mechanical behaviour of the boundary (Kremmer and Favier, 2001a). The geometrical representation of the boundary and the modeling of the boundary kinematics are the two important aspects when incorporating moving boundaries in the DEM (Kremmer and Favier, 2001b). Until recently, DE models did not include the dynamics of the spatial physical boundaries. Efforts were invested more in developing and validating models of the dynamics of particles to particles contacts. Techniques for representing boundaries in the DEM framework have received little attention in the literature. Two main types of boundaries can be found in publications on DEM: periodic and physical. Periodic boundaries allow a particle to pass across one side of the problem domain and automatically reappear on the opposite boundary in the same position and with the same initial velocity as the original particle. They avoid the need for contact detection. Periodic boundaries have been used by Jensen et al. (1999) in order to increase computing efficiency as well as remove any deleterious boundary effects in their shearing test of assemblies of clustered and non-clustered particles. The application of periodic boundaries requires the choice of initial particle dynamic conditions and often assumes homogeneity of behaviour with respect to at least one dimension (Kremmer and Favier, 2001a). Periodic boundaries are sometimes combined with physical boundaries to model a domain representing a small section of a larger system. Kei-ich et al. (1998) modeled the motion of toners and carriers particles in screw feeders using periodic boundaries in the axial direction and a physical helical boundary. Hopkins and Tuhkuri (1999) also used periodic boundaries to simulate channels without edge friction in their simulation of the compression of a floating layer of circular ice floes confined within a rectangular channel.

The geometrical representation of physical boundaries in the DEM can be done using either discredited or continuous formulations. Physical boundaries can be represented by fixing some of the discrete elements at particular locations in the assembly, and the inter-particle contact detection algorithms can be used. Other boundary representation methods such as line segments for simple boundaries and polygonal or superquadric objects for more complex shapes have been used, but the contact detection scheme, when explicitly stated, still present efficiency or accuracy issues. Screw conveyors were modeled by Shimizu and Cundall (2001) using a commercial DEM code (PFC^{3D}). The parametric approach developed to model the machine components is presented. Local and global coordinate systems were used for both boundary representation and contact detection. The simulation results were in good agreement with previous work and empirical equations for both horizontal and vertical screw conveyors.

In a two-part paper series, Kremmer and Favier (2001a and 2001b) proposed a method for representing boundaries in discrete element modeling. In their so-called finite wall method (Kremmer and Favier, 2001a), the boundary surfaces were modeled using a discretized triangular mesh made of planar triangular wall elements, each of them having its position, orientation and radius of curvature with respect to the global and element reference frame described by a set of parameters. The detection scheme developed for contact between spherical elements and wall elements employed the reboxing and linked list method common to many DE codes.

Quasi-kinematic boundary motion can be modeled by applying a defined velocity to the boundary surface. Another form of quasi-kinematic motion is modeled using variable gravitational fields (e.g. an alternating gravity vector can model a harmonic motion). The most recent codes allow the modeling of fully kinematic motion of boundary objects. A method for representing fully kinematic boundaries of arbitrary shape in two or three-dimensional DE models is presented by Kremmer and Favier (2001b). Using the finite wall method to represent the boundary objects (Kremmer and Favier, 2001a), the boundary kinematics were included by repositioning and reorienting the wall element groups. The motion of the boundaries could be pre-defined or dynamically

47

calculated translational and rotational accelerations and velocities could be applied, or a combination of the two. The method enables the boundary wall elements to move independently or to react to loading from the assembly of particles. This method deepens DE analysis that can be coupled with finite element (FE) analysis.

1.4.3.3. DE modeling of engineering applications

The development of contact-force-friction models typically comes from efforts targeting the modeling of particular engineering problems. The DEM has been utilized to model a very broad range of applications. The compression of floating ice fields has been modeled by Hopkins and Tuhkuri (1999). They measured the forces exerted by the ice on a vertical pusher plate moving at a constant velocity and developed a DE model capable of predicting those forces. Their conclusions suggested some dependency between failure behaviour and the floes properties as well as the boundary conditions. Hopkins (1997) also studied onshore ice pile-up using DE models. The physical experiments and the DE models consisted of an inclined ramp pushed against a long stationary strip of intact floating ice. The measured parameters included forces on the ramp, total expended energy and potential energy increase of the ice as it is piled on the ramp. Differences between the results of the physical experiments and simulations were attributed to the two-dimensionality of the model. While the predicted ridge-building forces were an underestimation of the measured forces, the model predicted the ratio of work to potential energy with good accuracy.

Rong et al. (1995a; 1995b) developed a two-dimensional DE model to study the flow of bulk solids in bins. They compared the observed flow of hollow cylindrical particles during gravity emptying of a parallel wall bin with the simulated DE flow. The model predictions were in good agreement with the experimental data on displacement and trajectories of selected particles for different sample sizes, surface roughness, outlet widths and outlet location. The simulations also allowed getting some insights into the development of shear bands, the effect of flow corrective inserts and flow patterns at a microscopic level. By studying gravity flow of particles through a vertical tube

containing a static mixer element using a distinct element model, Gyenis et al. (1999) concluded that the use of such a numerical tool not only allowed to correlate the flow regimes observed experimentally, but also revealed some features of gas-solids two-phase flows in tubes that cannot be measured by experiments.

Cleary (1998) used a DE model to simulate the filling process of two different mechanical configurations of dragline buckets. With the bucket motion dynamically responding to the balance of forces applied to it, the simulated fill times, spoil profiles and flows were consistent with available observations. The bucket designs implemented in the model could be compared in terms of filling pattern and drag coefficient. The motion and stability of the buckets were also found to be dependent upon the size distribution of the particles and their density. Cleary (1998) concluded that such DE models, enabling the prediction of drag coefficient, final spoil volume, surface wear rates and distribution, could become tools to optimize bucket design.

Using a commercial DEM code (PFC^{3D}), Ni el al. (2000) modeled the direct shear test to study the effects of the micro-properties of granular material on its shear behaviour. The investigated parameters were the shape factor of clustered particles, number of particles in the sample, inter-particles friction angle and normal stress. Some of the conclusions reflected the effect of particle shape on the behaviour of the granular sample.

Kaneko et al. (2000) attempted to develop a three-dimensional DEM code to simulate particle motion in a vertical helical ribbon agitator. Particle circulation time in the agitator and horizontal velocity distribution in the core region predicted by the model were in good agreement with those obtained by experiments. Some information was derived from the simulations for data that are difficult to obtain experimentally. Kaneko et al. (2000) demonstrated that the distance between the blade top and the bed surface is the most important parameter to attain good mixing.

Djordjevic (2003) used the DEM to study the power consumption of a tumbling mill as a function of the height of the lifters. It was found that the power draw of the mill and the mode of energy consumption were significantly affected by the height of the lifter. The proportion of power consumed as friction increased with decreasing lifter height, leaving less power for high intensity comminution caused by impacts. The influence of the friction coefficient of the material was observed and a value of 0.1 was suggested as the effective coefficient of friction for a real mill.

Djordjevic et al. (2003) studied horizontal and vertical shaft impact crushers using the DEM. The distribution of collision energies obtained via DEM simulations was converted to a product size distribution using impact breakage test data. Experimental results were used to validate the DEM simulation results. An investigation of the effects of the machine design and operational conditions on velocity and energy distribution of collision inside the milling chamber was then carried out. The results indicated that the DEM can be used to model the particle flow behaviour, energy utilisation and product size in the impact crushers.

1.4.3.4. Selection of input parameters for DEM models

A challenge common to the vast majority of research studies involving the DEM is the choice of appropriate input parameters. It is often difficult to choose a set of properties that will make the behaviour of the virtual material similar to that of the physical material. A code like PFC synthesizes macro-scale material behaviour from the interactions of micro-scale components and the input properties of the microscopic constituents are usually unknown. The responses that characterize the relevant behaviours must first be determined and then the appropriate microproperties must be selected by means of a calibration process (Itasca, 2003). In the calibration process, the responses of the virtual material are compared directly to the relevant measured responses of the intended physical material. This calibration procedure can target laboratory and field-scale events, depending upon the application of the model. In PFC, the model parameters generally cannot be related directly to a set of relevant material

properties because the behaviour of the PFC model is also affected by particle size and packing arrangement. The relation between the numerical model parameters and commonly measured material properties is only known *a priori* for certain simple packing arrangements. For the general case of arbitrary packing and size distribution, the relation is found by means of the calibration process in which a particular instance of a PFC model is used to simulate a set of material tests. The numerical model parameters are then chosen to reproduce the relevant material properties as measured in such tests. Although the behaviour of the PFC model is found to resemble that of the physical material, in general, the PFC particle is not associated with an elementary constituent of the physical material. The assembly of bonded particles is a valid microstructural model in its own right and should not be confused with the microstructure of the physical material (Itasca, 2003). The discussion presented by Oreskes et al. (1994) suggested that it is impossible to fully verify and validate any numerical model of a natural system. Numerical models are representation of physical systems that are useful for corroborating hypotheses, elucidating discrepancies in other models, performing sensitivity analyses, supporting design decisions and guiding further study (Itasca, 2003). When the predictions of numerical models agree with observations and measured data on the physical system, the likelihood that the models are correct increases and generally warrants acceptance.

In their simulation of the squeeze molding process of green sand, Maeda et al. (2003) included the soft shell and hard core characteristics of the material by taking into account their respective stiffnesses. The stiffness of the soft shell was determined by the free falling simulation result and the stiffness of the hard-core was determined from the compaction simulation results. Maeda et al. (2003) concluded that the simulated sequential sand compacting behaviour was reasonably correspondent to the experimental one.

Mishra and Murty (2001) discussed the importance of selecting appropriate parameters for realistic DEM simulations of ball mills. They mentioned that DEM modeling can only be successful if the parameters of the models are determined correctly. These

51

parameters not only influence the critical time step used in the simulations, but they also affect the accuracy of the quantitative results. Mishra and Murty (2001) stressed the fact that the issue of parameter selection is not properly addressed in the literature and that it is important to seek a compromise between numerical accuracy and computational cost. They developed a three-dimensional DEM code to compare the performance of various contact models to simulate the ball mill system. Experimental data on drop ball tests showed that the deformation behaviour of the contact is non-linear. The non-linear contact model parameters were determined by matching the model response with the experimental data. The non-linear model performed well in terms of predicting the energy dissipated during collisions, but was computationally demanding due to the high value of the associated contact stiffness parameter. A linearization method was applied to the model to circumvent the problem resulting in a stiffness value two orders of magnitude lower. Simulations were run to compare the linear, equivalent linear and non-linear models. All three models predicted the peak power within 5%, but the utilization of low values for the contact stiffness led to excessive amounts of deformation and to improper predictions of the peak force.

Di Renzo and Di Maio (2004) compared three mechanical models for the simulation of elastic frictional collisions. The results of the simulations were microscopically compared to analytical solutions and macroscopically to experimental results. The first model was a linear model based on a Hooke-type relation. The second model was a non-linear model based on Hertz theory in the normal direction and on the no-slip solution of the theory developed by Mindlin and Deresiewicz (1953) for the tangential direction. Finally, a non-linear model with hysteresis based on the complete theory of Hertz and Mindlin and Deresiewicz (1953) for elastic frictional collisions was included. The macroscopic comparison showed that the agreement of the linear model was good, indicating that no significant improvements can be attained using the Hertz&Mindlin-Deresiewicz model with no-slip (H-MDns) or the Hertz&Mindlin-Deresiewicz model (H-MD). The evolution of the normal and tangential forces, velocities and displacements predicted by the three models during a collision was compared to an analytical solution developed by Maw et al. (1976). In these comparisons, the H-MD

model was closer to the analytical solution. The H-MDns model was deemed worse than the linear model with regard to these results. The precision of the linear model was however dependent upon precise evaluation of its input parameters. The non-linearity and micro-slip effects were deemed important if deeper analyses of the motion of granular materials or of systems that are sensitive to the actual force or displacement are performed. In these cases, more accurate models such as the H-MD model should be addressed.

Masson and Martinez (2000) studied the flow from a rectangular silo for different values of particle mechanical parameters in DEM simulations. The DEM wall pressures at the end of the filling were in agreement with experimental and macroscopic numerical results obtained by FEM. The analytical and FEM results provided a validation of the DE simulations for their capacity to reproduce a quasi-static stress field at the filling stage that is qualitatively and quantitatively consistent with classical macroscopic results. The friction coefficient and contact stiffness appeared to have an important influence in the contact network connectivity, macroscopic porosity, stress anisotropy within the granular material and the magnitude and heterogeneity of wall pressure. These particle microscopic parameters also had an influence on the flow kinematics and stresses during discharge.

In their simulations of concrete, Puri and Uomoto (2002) used rheological properties to define the parameters to be used in DE models. In DEM modeling of fresh concrete, it was determined that the Bingham model with two rheological parameters, namely the yield stress and plastic viscosity, could be used. Puri and Uomoto (2002) underlined the fact that for quantitative DEM simulations, one of the greatest challenges was how to select DEM parameters. To define the mortar DEM parameters, they attempted to connect the simulation with the rheology of fresh concrete. Due to computational considerations, fine aggregate particles could not be considered as distinct elements and had to be considered with mortar. The interaction between fine aggregate and cement paste could not be considered. Each distinct element comprised an inner gravel core surrounded by a mortar layer. A simple two-phase model was proposed and a set of

springs, dashpot, and cohesion (for mortar) were used separately for mortar and gravel. Puri and Uomoto (2002) concluded that the yield value was related to stiffness and cohesion while viscosity was related to the dashpot parameter. The slump was controlled by the yield stress, while the rate of slumping was influenced by viscosity. The model was used to assess the performances of pneumatically applied concrete or shotcrete. Equations were proposed to link the mix proportion characteristics of the concrete to the DEM input parameters. The results indicated that some minimum yield stress had to be present in the concrete for it to attach to the target wall. A higher yield stress value reduced rebound losses, but over a critical value, rebound losses increased due to poor compaction. Puri and Uomoto (2002) concluded that fresh concrete with a high yield stress value, but pumpable, and a viscosity sufficient to enable good flow was a good material for shotcrete.

Tripodi et al. (1992) reviewed several constitutive models for cohesive particulate materials. They included constitutive models based on both microscopic concepts and continuum principles. The criteria used to analyze the models were time dependency, path dependence and physically representative parameters. Numerous comments were included to the effect that for several models, no explanation is provided as how to determine the input parameters. A parallel between soils and other agricultural products was made. References are cited where sand models were used for wheat (Zhang et al., 1986; Li et al., 1990), results for wheat, sugar and lentils were in a form consistent with sands and clays (Feda, 1982), and sugar and flour showed trends similar to clays (Kamath et al., 1991). Tripodi et al. (1992) concluded that based on their evaluation criteria, three candidate models could be considered. The modified Cam-clay model (Desai and Siriwardane, 1984) was deemed a candidate because it was the foundation for numerous other models and its parameters have clear physical representations. The elastoplastic model of Adachi and Oka (1982) was also selected as it was the most complete critical state model and had the potential to be very versatile and accurate in predicting the load-deformation behaviour of powders. The final model selected was the endochronic model (based on thermodynamic theory instead of plasticity) developed by Krizek et al. (1978), because of its fundamental soundness and flexibility.

Oida et al. (1998) studied the effect of several input parameters on the results of their simulation of soil deformation and reaction under a track shoe using the DEM. They tried different combinations of stiffness and specific gravity values. They also investigated the effect of the number of particles and their friction coefficient on the simulation results. Oida et al. (1998) observed that the simulated soil deformation approached the actual deformation pattern as the stiffness in the model increased. The simulated soil reaction force also increased as the stiffness and the specific gravity increased. An influence of the ratio of stiffness to specific gravity on the stability of the simulation was observed. Oida et al. (1998) concluded that there was no significant difference among the results obtained for the various numbers of elements tested. The soil reaction force was dependant upon the coefficient of friction while the soil deformation did not seem to be affected by that parameter. Oida et al. (1998) finally concluded that an increase in stiffness and specific gravity allowed the simulated reaction force to be the same as the force measured in a soil bin.

1.5. Current state of the research on solid and semi-solid manure land application

From what can be observed and from contacts developed with research scientists in Europe and North America, the work currently done on the land application of solid organic by-products, from a machinery perspective, seems to be focusing on (1) ways to improve the evenness of transversal and longitudinal product distribution, (2) specialized equipment to accommodate specific products and (3) the flow of organic by-products in land application equipment and how it is influenced by the operating parameters and geometrical characteristics of the machines. The first category has seen the development of systems aimed at controlling the discharge rate of the spreader. Thirion et al. (1998) of Cemagref developed a weighing platform as part of a flow regulation system. Using the mass measured by a platform cut-out from the floor at the back of the spreader, the speed of the floor conveyor could be adjusted according to the desired application rate. In the UK, researchers at Silsoe Research Institute developed a control system that uses the torque measured at the beater of a side delivery spreader

(SRI, 1998). The system controlled engine speed, forward speed and spreader variables to match the user-specified application rate. A torque-based system has also been developed at the Swedish Institute of Agricultural and Environmental Engineering (JTI). Rodhe (1999) reported on the development of a spreader with a movable front wall and a system that controlled the speed of the moving floor based on the torque measured at the beaters. Recent developments of manure land application technology were also the results of efforts aimed at developing spreaders for specific products. The machines developed by Pezzi and Rondelli (2002) for poultry manure and by Khalilian et al. (2002) for the injection of municipal solid wastes are good examples. The study of the flow of organic by-products in land application equipment is among the research priorities identified by Cemagref. They highlighted the need for an improved understanding of the machine-product interactions, in particular the flow inside the hopper and the role of the beaters. The concepts related to variable spreading in a precision agriculture framework and the associated sensors and information systems have also been targeted as future research priorities. The assessment and reduction of the environmental impacts of spreading operations are always considered important in land application research. The research at JTI has also focused on the measurement of manure properties that are influencing handling and land application operations (Malgeryd and Wetterberg, 1996) and on the development and evaluation of systems to better control the application rates on manure spreaders. Future research needs at JTI, described by Rodhe (1999), include the study of factors controlling solid manure composition, nutrient availability and long term efficiency of the nutrient cycle in solid manure management systems. From a machinery perspective, their objectives comprise high precision spreading with optimized plant nutrient utilization and reduced wheel damage to the crops.

The work reported in this thesis is very much relevant to the identified research needs in terms of developing an enhanced understanding of the flow of organic fertilizers in land application equipment. It is also prevalent to the development of machines capable of "precision spreading". There also seems to be a shift towards alternate application modes for solid manure (e.g. banded application, sub-surface injection) and the

advances presented here are certainly the basis of future machinery design and development. This work should be considered bearing in mind the ultimate objective of developing virtual prototypes to allow for comprehensive research on the machine-product interactions taking place in manure handling and land application equipment. The literature review demonstrated that: (1) the properties of solid and semi-solid manure products are not well known, (2) an enhanced understanding of how manure products behave in relation to machinery components and systems is required, and (3) numerical modeling is a very worthwhile means of providing tools to better design and operate manure land application equipment.

1.6. Objectives of the thesis

The general objective of the work reported herein is to develop the engineering knowledge required to optimize the design and operation of solid and semi-solid manure handling and land application equipment. The specific objectives of the thesis are:

1. to select, design and construct the measuring apparatuses required to meet objective 2,
2. to measure selected physical and rheological properties of manure products,
3. to develop relationships between the measured properties,
4. to develop models of manure products in the DEM code PFC^{3D},
5. to model selected manure handling and land application functional units, using PFC^{3D} and
6. to validate selected models developed to meet objective 5 using field-scale manure spreaders.

1.7. References

Achkari-Begdouri,A. and P.R. Goodrich. 1992. Rheological properties of Moroccan dairy cattle manure. Bioresource Technology, 40(2): 149-156.

Adachi, T. and F. Oka. 1982. Constitutive equations for normally consolidated clay based on elasto-viscoplasticity. Soils and Foundations, 22(4): 57-70.

Agnew, J.M., J.J. Leonard, J. Feddes, and Y. Feng. 2003. A modified air pycnometer for compost air volume and density determination. Canadian Biosystems Engineering, 45(6): 27-35.

Al-Fariss, T.F., L.K. Jang, H.O. Ozbelge and N.M. Ghasem. 1993. A new correlation for the viscosity of waxy oils. Journal of Petroleum Science & Engineering, 9(2): 139-144.

ASAE Standards, 2004. S292.5. Uniform Terminology for Rural Waste Management. St. Joseph, Mich.: ASAE.

Balsari, P., G. Airoldi and F. Gioelli. 2002. An innovative FYM and compost spreader. ASAE Paper No. 021190, St. Joseph, Mich.: ASAE.

Barr, A.H. 1981. Superquadrics and angle-preserving transformations. IEEE Computer Graphics and Animation, 1: 11-23.

Baudez, J.C. 2001. Rhéologie et phisico-chimie des boues résiduaires pâteuses pour l'étude du stockage et de l'épandage. Unpublished Doctoral Thesis. École national du génie rural, des eaux et des forêts.

Bisang, M. 1987. Epandeuses de fumier: comparaison de differents dispositifs d'épandage. *Technique Agricole*, Switzerland. 1987, 49(3), 8pp.; Rapports FAT No. 300.

Bulinski, J and J. Klonowski. 1998. Analysis of power requirement for manure spreader working units. Annals of Warsaw Agricultural University, No. 33, 27-32.

Cemagref, 1997. Les materiels de fertilisation et traitement des cultures. Technologies de l'agriculture. Collection FORMAGRI. Volume 4/5, 1re édition. Cemagref-Dicova, Lavoisier-TEC et DOC, ITCF, FNCUMA. 343 pages.

CEN. 2002. European Standard EN 13080: Agricultural machinery – Manure spreaders – Environmental protection – Requirements and test methods. CEN, European Committee for Standardization.

Chen, Y.R. 1982. Engineering properties of beef cattle manure. ASAE Paper No.824085, St. Joseph, Mich.: ASAE.

Chen, Y.R. 1986. Rheological properties of sieved beef-cattle manure slurry: rheological model and effects of temperature and solids concentration. Agricultural Wastes, 15(1):17-33.

Chen, Y.R. and E.L. Shetler. 1983. Temperature effect on rheological properties of cattle manure slurry. Journal of Testing and Evaluation, 11(6): 360-364.

Cleary, P.W. 1998. The filling of dragline buckets. Mathematical Engineering in Industry, 7(1): 1-24.

Crowther, A.J. 1958. The distribution of particles by a spinning disc. Journal of Agricultural Engineering Research, 3(4): 288.

Cundall, P.A. 1971. A computer model for simulating progressive large scale movements in blocky rock systems. Proceedings of the Symposium of the International Society for Rock Mechanics, Vol. 1, Paper No. II-8.

Cundall, P.A. 1988. Formulation of a three-dimensional distinct element model – Part I. A scheme to detect and represent contacts in a system composed of many polyhedral blocks. International Journal of Rock Mechanics, 25(3): 107-116.

Cunningham, F.M. and E.Y.S. Chao. 1967. Design relationships for centrifugal fertilizer distributors. Transactions of the ASAE, 10(1): 91-95.

De Kee, D. and C.F. Chan Man Fong. 1994. Rheological properties of structured fluids. Polymer Engineering and Science, 34: 438-445.

De Kee, D., E.Chornet and W.Zhang. 1998. Viscous and yield stress properties of Athabasca topped heavy oil. Canadian Journal of Chemical Engineering, 76(4): 816-820.

Desai, C.H. and H.J. Siriwardane. 1984. Constitutive laws for engineering materials with emphasis on geological materials. Englewood Cliffs, New Jersey, Prentice-Hall.

Di Renzo, A. and F.P. Di Maio. 2004. Comparison of contact-forces models for the simulation of collisions in DEM-based granular flow codes. Chemical Engineering Science 59: 525-541.

Djordjevic, N. 2003. Discrete element modeling of the influence of lifters on power draw of tumbling mills. Minerals Engineering, 16: 331-336.

Djordjevic, N., F.N. Shi and R.D. Morisson. 2003. Applying discrete element modeling to vertical and horizontal shaft impact crushers. Minerals Engineering, 16: 983-991.

Eghball, B. 2003. Leaching of phosphorus fractions following manure or compost application. Communications in Soil Science and Plant Analysis, 34(19-20): 2803-2815.

Egrinya, E.A., S. Yamamoto and T. Honna. 2001. Rice growth and nutrient uptake as affected by livestock manure in four Japanese soils. Journal of Plant Nutrition, 24(2): 333-343.

Favier, J.F., M.H. Abbaspour-Fard, M. Kremmer and A.O. Raji. 1999. Shape representation of axi-symmetrical, non-spherical particles in discrete element simulation using multi-element model particles. Engineering Computations, 16(4): 467-480.

Feda, J. 1982. Mechanics of particulate materials – the principles. Amsterdam, The Netherlands, Elsevier, 1982.

Ferraris, C.F. 1999. Measurement of the rheological properties of high performance concrete: State of the art report. Journal of Research of the National Institute of Standards and Technology, 104(5): 461-478.

Frick, R., J. Heusser and M. Shick. 2001. Technique d'épandage des engrais à base de déchets et de fumier de stabulation libre : Qualité du travail et adéquation de différents systèmes d'épandage. Rapport FAT No. 560.

Glancey, J.L. and R.K. Adams. 1996. Applicator for sidedressing row crops with solid wastes. Transactions of the ASAE, 39(3): 829-835.

Glancey, J.L. and S.C. Hoffman. 1996. Physical properties of solid waste materials. Applied Engineering in Agriculture, 12(4): 441-446.

Gyenis, J. Zs Ulbert, J. Szépvölgyi, and Y. Tsuji. Discrete particle simulation of flow regimes in bulk solids mixing and conveying. Powder Technology, 104(3): 248-257.

Hart, R., P.A. Cundall and J. Lemos. 1988. Formulation of a three-dimensional distinct element model – Part II. Mechanical calculations for motion and interaction of a system composed of many polyhedral blocks. International Journal of Rock Mechanics, 25(3): 117-125.

Hashimoto, A.G. and Y.R. Chen. 1976. Rheology of livestock waste slurries. Transactions of the ASAE, 19(5): 930-934.

Hoffmeister, G., S.C. Watkins and J. Siveburg. 1964. Bulk blending of fertilizer material: Effect of size, shape, and density on segregation. Journal of Agriculture and Food Chemistry, 12(1): 64-69.

Hogue, C. 1998. Shape representation and contact detection for discrete element simulations of arbitrary geometries. Engineering Computation, 15(3): 374-390.

Hopkins, M.A. 1997. Onshore ice pile-up: a comparison between experiments and simulations. Cold Regions Science and Technology, 26(3): 205-214.

Hopkins, M.A. and J. Tuhkuri. 1999. Compression of floating ice fields. Journal of Geophysical Research, 104(C7): 15815-15825.

Itasca, 1999. PFC3D User's Manual, Version 2.1., Itasca Consulting Group Inc., Minneapolis, Minn.., 55415 USA.

Itasca, 2003. PFC3D User's Manual, Version 3.0.., Itasca Consulting Group Inc., Minneapolis, Minn.., 55415 USA.

Jensen, R.P., P.J. Bosscher, M.E. Plesha and T.B. Edil. 1999. DEM simulation of granular media-structure interface: effects of surface roughness and particle shape. International Journal for Numerical and Analytical Methods in Geomechanics, 23(6): 531-547.

Kamath, S., V.M. Puri, H.B. Manbeck and R. Hogg. 1991. Measurement of flow properties of bulk solids using four testers. ASAE Paper No. 91-4517, St. Joseph, Mich.: ASAE.

Kaneko, Y., T. Shiojima and M. Horio. 2000. Numerical analysis of particle mixing characteristics in a single helical ribbon agitator using DEM simulations. Powder Technology, 108: 55-64.

Kei-ich, T. 1998. Particle Motion in Screw Feeder Simulated by Discrete Element Method. International Conference on Digital Printing Technologies, 1998, p 429-431.

Khalilian, A., R.E. Williamson, M.J. Sullivan, J.D. Mueller and F.J. Wolak. 2002. Injected and broadcast application of composted municipal solid waste in cotton. Applied Engineering in Agriculture, 18(1): 17-22.

Kremmer, M. and J.F. Favier. 2000. Coupling discrete element and rigid body dynamics. ASAE Paper No. 003077, St. Joseph, Mich.: ASAE.

Kremmer, M. and J.F. Favier. 2001a. A method for representing boundaries in discrete element modeling – Part I: Geometry and contact detection. International Journal for Numerical Methods in Engineering, 51: 1407-1421.

Kremmer, M. and J.F. Favier. 2001b. A method for representing boundaries in discrete element modeling – Part II: Kinematics. International Journal for Numerical Methods in Engineering, 51: 1423-1436.

Krizek, R.J., A.M. Ansal and Z.P. Bazant. 1978. Constitutive equation for cyclic behavior of cohesive soils. Proceedings of the ASCE Geotechnical Engineering Division, Special Conference Earthquake Engineering and Soil Dynamics I: 557-558.

Kumar, M., H.D. Bartlett and N.N. Mohsenin. 1972. Flow properties of animal waste slurries. Transactions of the ASAE, 15(4): 718-722.

Laguë, C. 1991. Design of a Semi-Liquid Dairy Cattle Manure Spreader/Injector. Applied Engineering in Agriculture, 7 (6): 655-660.

Laguë, C., P.M. Roy, L. Chénard and R. Lagacé. 1994. Wide-span boom for band-spreading of liquid manure. Applied Engineering in Agriculture, 10(6): 759-763.

Landry, H. and C. Laguë. 1999. Selected properties of papermill residues. ASAE Paper No. 996058, St. Joseph, Mich.: ASAE.

Larney, F.J., H.H. Janzen, B.M. Olson and C.W. Lindwall. 2000. Soil quality and productivity responses to simulated erosion and restorative amendments. Canadian Journal of Soil Science, 80(3): 515-522.

Lea, J.W., D.A. Gibbs and N.G. Lawrance. 1982. Morphological changes in brown earth soil in response to application of pig slurry. Journal of Agricultural Science, 98: 325-330.

Li, Y., V.M. Puri and H.B. Manbeck. 1990. Elastic-viscoplastic cyclic constitutive model parameter determination and evaluation for wheat en masse. Transactions of the ASAE, 33(6): 1984-1995.

Lin, X. and T.T. Ng. 1995. Short communication, contact detection algorithms for three dimensional ellipsoid in discrete element modeling. International Journal for Numerical Methods in Geomechanics, 19: 653-659.

Ling, Q. and J.H. Wilhoit. 1999. Power requirements of spinner-type spreaders broadcasting poultry litter and wood ash. Applied Engineering in Agriculture, 15(5): 405-409.

Ling, Q., J.H. Wilhoit and L.J. Kutz. 1996. Effect of material metering on the performance of a spinner-type spreader broadcasting poultry litter. New trends in farm machinery development and agriculture, 41-49, Society of Automotive Engineers, Warrendale, PA

Maeda, Y., Y. Maruoka, H. Makino and H. Nomura. 2003. Squeeze molding simulation using the distinct element method considering green sand properties. Journal of Materials Processing Technology, 135: 172-178.

Malgeryd, J. and C. Wetterberg. 1996. Physical properties of solid and liquid manures and their effects on the performance of spreading machines. Journal of Agricultural Engineering Research, 64: 289-298.

Marinari, S., G. Masciandaro, B. Ceccanti and S. Grego. 2000. Influence of organic and mineral fertilizers on soil biological and physical properties. Bioresource Technology, 72(1): 9-17.

Masson, S. and J. Martinez. 2000. Effect of particle mechanical properties on silo flow and stresses from distinct element simulations. Powder Technology, 109: 164-178.

Maw, N., J.R. Barber and J.N. Fawcett. 1976. The oblique impact of elastic spheres. Wear 38, 101-114.

Mindlin, R.D. and H. Deresiewicz. 1953. Elastic spheres in contact under varying oblique forces. Journal of Applied Mechanics, 20: 327-344.

Mishra, B.K. and C.V.R. Murty. 2001. On the determination of contact parameters for realistic DEM simulations of ball mills. Powder Technology, 115: 290-297.

Ni, Q., W. Powrie, X. Zhang and R. Harkness. 2000. Effect of particles properties on soil behaviour: 3-D numerical modeling of shearbox tests. Geotechnical special publication, 96: 58-70.

Ning, Z., R.Boerefijn, M. Ghadiri and C. Thornthon. 1997. Distinct element simulation of impact breakage of lactose agglomerates. Advanced Powder Technology, 8(1): 15-37.

Norman, H.A., H.M. Hanna, T.L. Richard and G.R. Quick. 2002. Distribution patterns of solid manure spreaders. ASAE Paper No. 021099, St. Joseph, Mich.: ASAE.

Oda, M. and K. Iwashita. 1999. *Mechanics of Granular Materials: An Introduction*. Rotterdam: A.A. Balkema.

Oida, A., H. Schwanghart, S. Ohkubo and M. Yamazaki. 1998. Simulation of soil deformation and reaction under a track shoe by distinct element method. Actual

Tasks in Agricultural Engineering, 26th International Symposium on Agricultural Engineering, Opatija, Croatia, 3-6 February 1998, 167-176.

Oreskes, N., K. Shrader-Frechette and K. Belitz. 1994. Verification, validation, and confirmation of numerical models in the earth sciences. Science, 263(5147): 641-646.

Patterson, D.E. and A.R. Reece. 1962. The theory of the centrifugal distributor. I: Motion on the disc, near-center feed. Journal of Agricultural Engineering Research, 7(3): 232-240.

Pezzi, F. and V. Rondelli. 2002. Evaluation of a prototype spreader in the distribution of poultry manure. Applied Engineering in Agriculture, 18(3): 285-291.

Picaud, D. 2001. Importance des caractéristiques des fumiers sur les performances d'épandage. Unpublished report. École Nationale d'Ingénieurs des Travaux Agricoles, Clermont-Ferrand, France.

Puri, U.C. and T. Uomoto. 2002. Characterization of distinct element modeling parameters for fresh concrete and its application in shotcrete simulations. Journal of Materials in Civil Engineering, 14(2): 137-144.

Reed, W.B. and E. Wacker. 1968. Determination of the distribution pattern of dry fertilizer applicators. ASAE Paper No. 68-606. St. Joseph, Mich.: ASAE.

Rhode Lena. 1999. Advancements on the technologies for inputs distribution: the case of manure. Review paper - Club of Bologna - November 14 1999.

Rong, G.H., S.C. Negi and J.C. Jofriet. 1995a. Simulation of flow behavior of bulk solids in bins. Part 1: Model development and validation. Journal of Agricultural Engineering Research, 62: 247-256.

Rong, G.H., S.C. Negi and J.C. Jofriet. 1995b. Simulation of flow behavior of bulk solids in bins. Part 2: Shear bands, flow corrective inserts and velocity profiles. Journal of Agricultural Engineering Research, 62: 257-269.

Shimizu, Y. and P.A. Cundall. 2001. Three-dimensional DEM simulations of bulk handling by screw conveyors. Journal of Engineering Mechanics, 127(9): 864-872.

Silsoe Research Institute (SRI). 1998. Improved precision of manure application. Final Project Report. Silsoe Research Institute, Bedford, UK.

Statistics Canada. 2000. A Geographical Profile of Manure Production in Canada. Ottawa, ON: Statistics Canada (Publication no. 16F0025XIB).

Tabuteau, H., J.C. Baudez, F. Bertrand and P. Coussot. 2004. Mechanical characteristics and origin of wall slip in pasty biosolids. Rheologica Acta, 43 : 168 − 174.

Thirion F., F. Chabot and D. Andeler. 1998. Determination of physical characteristics of animal manure. *Proceedings of RAMIRAN 98* (8th International Conference on Management Strategies for Organic Waste Use in Agriculture) Rennes France, p. 457 −469.

Ting, J.M., M. Khwaja, L. Meachum and J.D. Rowell. 1993. An ellipse based discrete element model for granular materials. International Journal for Numerical and Analytical Methods in Geomechanics, 17: 603-23.

Tripodi, M.A., V.M. Puri, H.B. Manbeck and G.L. Messing. 1992. Constitutive models for cohesive particulate materials. Journal of Agricultural Engineering Research, 53: 1-21.

Van Damme, H., S. Mansoutre, P. Colombet, C. Lesaffre and D. Picart. 2002. Pysique de la matière en grains – Physics of granular media. Pastes : lubricated and cohesive granular media. C.R. Physique 3 : 229-238.

Wilhoit, J.H. and Q. Ling. 1996. Spreader performance evaluation for forest land application of wood and fly ash. Journal of Environmental Quality, 25: 945-950.

Wilhoit, J.H., J.S. Bannon, R.R. Duffield and Q. Ling. 1994. Development and evaluation of a drop applicator for poultry litter. Transactions of the ASAE, 10(6): 777-782.

Wilhoit, J.H., C.W. Wood, K.H. Yoo and M.Y. Minkara. 1993. Evaluation of spreader distribution patterns for poultry litter. Transactions of the ASAE, 9(4): 359-363.

Williams, J.R. and A.P. Pentland. 1989. Superquadrics and model dynamics for discrete elements in concurrent design. First US Conference on the Discrete Element Method, Golden, Colorado.

Williams, J.R. and R. O'Conner. 1995. A linear complexity intersection algorithm for DEM simulations of arbitrary geometries. Engineering Computations, 12: 185-201.

Wolfe, K. and R. Stowell. 1999. Slump tests can predict the solids content of dairy manure and similar non-newtonian fluids. ASAE Paper No. 994098. St. Joseph, Mich.: ASAE.

Young, M.D. and P. Rainelli. 1991. Intensive livestock production in France and its effects on water quality in Brittany. Towards sustainable agricultural development: 115-146.

Zhang, Q., V.M. Puri and H.B. Manbeck. 1986. Determination of elastoplastic constitutive parameters for wheat en masse. Transactions of the ASAE, 29(6): 1739-1746.

Chapter 2

Physical and Rheological Properties of Manure Products

2.1. Significance

The literature review clearly demonstrated that the properties of the products that are being spread have an influence on the performance of land application machines. Therefore, any effort targeting improved machinery devices to better handle and land apply solid and semi-solid manure must take into account those properties. From the literature review, it was also possible to observe the lack of a comprehensive database of manure properties. Several authors have studied such properties, especially in the liquid manure range. Because the information on the properties of manure products was deemed insufficient, the first step of the research reported herein was to develop a database of physical and rheological properties of a broad range of products in the semi-solid and solid ranges. The following manuscript details this first step. It corresponds to objectives 1, 2 and 3 of the thesis. The content of this chapter was submitted and accepted for publication on March 3, 2003 and November 10, 2003, respectively (*Landry, H., C. Laguë and M. Roberge. 2004. Physical and rheological properties of manure products. Applied Engineering in Agriculture 20(3):277-288*). The candidate carried out the experimental work and data analysis presented in this chapter. The writing of the manuscript was also done by the candidate while the co-authors, Drs. Laguë and Roberge, reviewed it. A peer-reviewing process was involved in the publication of the manuscript. Three reviewers submitted comments prior to the acceptation of the manuscript. The

reviewers recognized the original work presented in the manuscript and its importance to the understanding of manure properties and to the design of handling and land application equipment. Besides minor editorial suggestions, the reviewers asked for precisions regarding the manure samples (if they contained bedding materials, their original total solids concentration, handling/storage practices, etc.), the experimental methods and the effect of the sample preparation method on the validity of the results. The reviewers' comments were addressed by including additional information in the manuscript. Because the work presented in this chapter was published before the submission of the thesis, the content of the published article slightly differs from the following material. The manuscript in its published format is included in Appendix A.

2.2. Abstract

Selected physical and rheological properties deemed to influence the performance of handling and land application equipment were quantified for different types of manure at different levels of total solids concentration (TS) ranging from 10% to 50% on a wet mass basis. The selected properties included total solids concentration, bulk density, particle size distribution, friction characteristics and shearing behaviour and were measured for dairy cattle, sheep, poultry and pig manure. The bulk density of all manure products was found to increase with TS and the values for poultry and pig manure were not significantly different at the tested TS levels. The measured density values were in close agreement with ASAE D384. The proposed modified geometric mean length of the particles was found to significantly increase as TS became smaller. The static friction coefficients of all manure types with the exception of pig manure on the different surface materials (plywood, plastic, steel (bare and painted)) did not exhibit large differences and a single linear equation was suggested to predict the static friction coefficient as a function of TS. Animal manures were described as pseudoplastic fluids and the consistency coefficients were found to decrease as TS increased for all manure types. The apparent viscosity of the tested manure products was well correlated to TS. The implications of the property results obtained in this study as well as future research are discussed.

2.3. Introduction

Proper recycling of animal manure is of paramount importance to increase the sustainability and social acceptance of intensive livestock production. As the environmental and agronomic requirements for effective and safe land application of manure products become more prescriptive, equipment used in manure management systems are subjected to higher performance expectations. Solid and semi-solid manure products represent potential alternatives to reduce some of the environmental and societal problems that may be associated with liquid manure management. Commercial equipment designed to handle and land apply solid and semi-solid manure do exhibit large coefficients of variation for both transversal and longitudinal product distribution (Thirion and Chabot, 2003; Frick et al., 2001; Wilhoit et al., 1993; Bisang, 1987). Appropriate knowledge of the physical and flow properties of the products to be handled is fundamental to the design and operation of efficient systems.

2.4. Literature review

Published research results are readily available in the area of manure chemical properties. Much fewer journal articles have targeted the physical and flow properties of manure products and most of the manure characterization efforts have focused on liquid manure and slurry.

Kumar et al. (1972) studied the flow properties of animal slurries. They found that the coaxial cylinder type viscometer was suitable for measuring the rheological properties of slurries. They concluded that the viscosity of dairy manure slurry decreased with an increase in dilution and an increase in temperature. Kumar et al. (1972) also noticed that the flow of slurry was Newtonian at solids contents below 5%. The addition of sawdust up to as much as 10% by weight of the amount of manure decreased the viscosity of a slurry having a total solids content up to approximately 9%.

Hashimoto and Chen (1976) attempted to identify a parameter that would mathematically describe the rheological properties of aerated and fresh dairy, poultry

and swine slurries and that could be easily and precisely measured experimentally. They also described procedures to estimate the effect of rheological properties on pumping, mixing and aerating livestock slurries. The highest solids content Hashimoto and Chen (1976) worked with was swine slurry having 10.8% total solids. Their study showed that the rheological consistency index (K) and rheological behaviour index (n) of livestock slurries could be expressed in terms of the equilibrium sludge volume fraction (Φ_L) as:

$$K = b_1 \, \Phi_L^{b2} \qquad\qquad (2.1)$$
and
$$n = b_3 + b_4 \ln(\Phi_L) \qquad , \qquad (2.2)$$

where b_1 to b_4 are constants. Values of these constants were given for aerated and fresh dairy, poultry and swine slurries and were found to be dependent on the range of Φ_L. Relationships were also established to relate mixer power characteristics and pressure head loss in pipeline transport of slurries to the consistency index, the rheological behaviour index, the effective viscosity and generalized Reynolds number. Equations for the determination of the effective viscosity were given for the case of a non-Newtonian fluid flowing through a pipe and for the case of slurry mixing. A method of determining Φ_L was also presented, but to the authors' knowledge, the equilibrium sludge volume fraction has never been widely used in manure characterization.

Rheological consistency index, flow behaviour index, specific heat and thermal conductivity of beef cattle manure were determined by Chen (1982). Density was also measured for solid contents ranging from 1% to 99%. The results suggested that the density of manure increased as the total solids concentration increased for manure with less than 16% TS. This trend appeared to extend to solids concentrations of about 40%. The density decreased from 40% to 50% and for manure with TS higher than 50%, the bulk density dropped much below the liquid manure density. Rheological properties of manure were studied for TS ranging from 1% to 14%. Beef cattle slurries were

described as non-Newtonian pseudoplastic fluids, the deviation from Newtonian behaviour increasing with TS.

Using a constant-temperature rotational viscometer, Chen and Shetler (1983) investigated the effect of temperature on the rheological properties of cattle manure having total solids concentrations ranging from 2.5% to 19.3%. The experimental shear rates ranged from 20 to 200 s^{-1} and temperatures varied from 14ºC to 64ºC. This study confirmed previous findings that beef cattle manure slurry is a non-Newtonian pseudoplastic fluid and a power-law equation could be used in this range of shear rates. The rheological behaviour index (n) was found to decrease exponentially with TS, but was not affected by temperature while the rheological consistency index (K), in general, increased as TS increased. The apparent viscosity of the slurry decreased exponentially as temperature increased, and increased as TS increased. An equation relating the apparent viscosity to TS and to the absolute temperature was given.

Chen (1986) later proposed a rheological model for manure slurries and applied this model to experimental data of cattle manure slurry obtained using a rotational viscometer. He found that cattle manure slurry showed negligible yield stress and that the Bingham Plastic, Herschel-Bulkley and Casson rheological models were not applicable. The power law model could be used only for sieved slurries with TS below 4.5%. Chen (1986) also observed a curvilinear relationship of shear stress and shear rate in the logarithmic plot for high TS slurries due to the existence of a limiting viscosity. He proposed the following rheological model for beef cattle manure slurry:

$$\tau = \eta_0 \dot{\gamma} + K'' \dot{\gamma}^{n''} \qquad , \qquad (2.3)$$

where τ is the shear stress, $\dot{\gamma}$ is the shear rate, η_0 is the limiting viscosity and K'' and n'' are rheological parameters. Non-linear least square regression was used to fit the proposed model to the experimental rheological data for slurries having TS above 4.5%. The results showed that the proposed model was well correlated to the experimental data. The value of n'' for sieved slurries did not vary with TS or temperature, having an

average value of 0.307 with a standard deviation of 0.054. Equations expressing η_0 and K" in terms of TS and temperature were also obtained. The values of η_0 and K" were found to increase as TS increased and to decrease as temperature increased.

Achkari-Begdouri and Goodrich (1992) studied the rheological properties of dairy cattle manure with total solids concentrations ranging from 2.5% to 12% at temperatures between 20°C and 60°C. The results showed that in the ranges of total solids and temperature of the study, dairy cattle manure behaved as a pseudoplastic fluid. Two equations based on the total solids content and the temperature, one expressing the consistency coefficient and the other to predict the flow behaviour index, were proposed. The flow behaviour index was found to increase with the temperature while the consistency coefficient decreased as the temperature increased. The results of Achkari-Begdouri and Goodrich (1992) suggested that an increase in the total solids concentration induced an increase in the consistency coefficient and a decrease in the flow behaviour index.

Solid and semi-solid manures have not been studied as much as liquid manure and slurry in terms of physical properties. A few studies have mentioned the effect of manure properties on the performance of various mechanisms. In their study of spreader distribution patterns for poultry litter, Wilhoit et al. (1993) made observations on the effect of particle size on spreading distances. They concluded that large particles were distributed more evenly and on a larger width when compared to smaller particles that landed closer to the spreader. Wilhoit et al. (1994) also observed the effects of particle size distribution while developing a drop applicator for poultry litter. They concluded that their gravity flow-metering system was not appropriate due to the presence of clumps blocking the flow of material from the hopper. Observations were made by Wilhoit and Ling (1996) to the effect that the nature of wood and fly ash caused the spreading uniformity to be inconsistent from trial to trial. In their design of an applicator for sidedressing row crops with solid organic by-products, Glancey and Adams (1996) identified maximum clump size and moisture content as the physical properties presenting potential problems in raw manure conveying.

Glancey and Hoffman (1996) measured physical properties of poultry manure and compost under different management practices. They investigated trends in the measured properties to develop general guidelines for the design and analysis of material handling systems, transportation equipment and spreaders. Glancey and Hoffman (1996) concluded that wet bulk density was dependent on moisture content for all the solid products evaluated and that knowledge of moisture content was therefore more important than the type or source of material. The static friction characteristics suggested that there was little practical difference between the different products. Another trend identified by Glancey and Hoffman (1996) indicated that all unscreened products contained large clumps. This presented potential design problems in developing conveying systems to handle unscreened products.

Agnew et al. (2003) used an air pycnometer to measure the air volume and density of compost. The free air space (FAS) and bulk density of manure compost, municipal solid waste compost, and mixtures of biosolids and amendment materials were measured at various moisture contents and compressive loads. The results indicated that the FAS decreased with loading and increasing moisture content while the wet bulk density increased with loading and increasing moisture content. A linear relationship was established between FAS and bulk density for all the materials tested under load.

Malgeryd and Wetterberg (1996) reported the efforts of the Swedish National Machinery Testing Institute and the Swedish Institute of Agricultural Engineering to provide the necessary knowledge of how the physical properties of manures and slurries affect the spreading performances of different machines. They highlighted the fact that there is a lack of general knowledge about which properties or parameters derived from physical properties are important in practice and how they should be measured. For manures that can be pumped, four parameters were considered significant, namely, fluidity, separation tendency, risk of clogging and dry matter content. For manures that cannot be pumped, five parameters were deemed important: bulk density, stacking ability or consistency, comminuting resistance, heterogeneity and dry matter content. Methods were suggested for measuring those parameters. The results suggested that

there is no clear relationship between the active angle of repose and the dry matter content for non-pumpable manures and that bulk density and the active angle of repose are closely related to each other. The active angle of repose could be estimated from the bulk density, which is easier to measure.

Thirion et al. (1998) experienced difficulties in trying to implement the test methods outlined by Malgeryd and Wetterberg (1996). Thirion et al. (1998) reported manure properties including normal stress, shear stress, bulk density, friction coefficient, straw content and dry matter content. They included numerous comments on the difficulty of obtaining reliable results and proposed a method for obtaining a numerical value of manure heterogeneity.

Landry and Laguë (1999) studied selected physical properties of papermill residues. They measured bulk density, moisture content, angle of repose, friction coefficient on different materials and particle size distribution. They concluded that while the values of the selected properties were relatively constant among samples that originated from the same papermill, there could also be large variations depending upon the specific origin of the products.

The literature review clearly demonstrates the variability that exists in manure properties and the lack of widely accepted and used methods to measure those physical and rheological properties. More data are required to highlight general trends and to develop design guidelines for manure handling and land application equipment.

2.5. Objective

The objective of the work reported herein was to measure selected physical and rheological properties of different types of manure products at different levels of total solids concentration with an emphasis on the solid and semi-solid ranges.

2.6. Materials and methods

Based on the review of previous work, the properties that were deemed having the most influence on the performances of manure handling and land application equipment were identified as: (a) total solids concentration, (b) bulk density, (c) particle size distribution, (d) friction characteristics and (e) shearing properties. Four types of manure were investigated: (1) dairy cattle, (2) sheep, (3) poultry and (4) pig. Manure samples were collected from the facilities on the University of Saskatchewan farm (Saskatoon, Saskatchewan, CANADA). The dairy, pig and poultry (laying hens) barns all featured scrapers to move the manure out of the buildings. The dairy and poultry barns are scraped twice a day and the manure goes directly into underground pits. The pig manure is stored in a room at the end of the barn and that room is periodically emptied. Fresh samples were collected after scraping, just before the manure entered the pits. In the case of sheep manure, the samples were collected from outside pens and contained a large proportion of straw. A small amount of chopped straw was used in the free stall barn where the dairy cattle manure samples were collected. No bedding material was used in the pig and poultry barns. With the objective of characterizing the manure products in the state they would be when handled and/or land applied, the samples were not submitted to any treatment (e.g. separation, screening, etc.) prior to testing. Several large samples (approximately 170 L per sample) were collected for each type of manure to avoid using the same material more than once. In order to reach the targeted total solids concentrations, the raw samples were either dried outside or diluted with water. Based on the initial and targeted total solids concentrations, the amount of water to add was estimated by weighing the samples. The TS of the large samples was measured daily during the preparation phase. The majority of the tested samples went through one wetting or drying cycle, two wetting phases were sometimes necessary to reach the desired TS level. The samples were stored and handled in 170-L barrels and were tested as soon as the targeted TS level was reached. Using a large sample that had reached a targeted TS level, all property measurements were replicated on four sub-samples taken from the large sample, including an additional set of measurements for the total solids concentration.

2.6.1. Total solids concentration

The total solids (TS) concentration of the manure products was determined by drying the samples (350 g on average) in an oven at 103ºC for 24 hours (ASAE, 2002a). TS was the ratio of oven-dry weight to wet weight and was expressed as a percentage.

2.6.2. Bulk density

The bulk density of manure products was measured in an uncompacted state by weighing large containers of known volume filled with manure according to the procedure described by Glancey and Hoffman (1996). A weighing apparatus was designed and built to accommodate large samples (i.e. 170-L barrels). The apparatus was made of a platform supported by two load cells (2224 N capacity; ±1.11 N non-linearity; ±0.67 N hysteresis; Interface, 7401 E Butherus Drive, Scottsdale, Arizona 85260, USA) and allowed for easy placement of the barrels (fig. 2.1). The load cells with the data acquisition system were calibrated using a universal testing machine (Model 1011; Instron Corporation Headquarters, 100 Royall Street, Canton, Massachusetts, 02021, USA). All the test apparatuses that required calibration featured load cells (weighing apparatus, shearbox and large-scale viscometer), and the universal testing machine was used. Observations were made by Thirion et al. (1998) and Frick et al. (2001) to the effect that density values are affected by the measurement method. The chosen method consisted of manually handling the samples to create a consistent state of compaction for the entire test series. Once the open-top barrels were filled to the desired level, they were agitated by rocking the barrels twice approximately 25º from side to side to compact and level the material.

Figure 2.1. Weighing apparatus used for the determination of the bulk density of manure samples.

2.6.3. Particle size distribution

A modified soil sieves shaker and a screen set (fig. 2.2) were used to determine the particle size distribution of the manure samples using a procedure adapted from ASAE S424.1 (ASAE Standards, 2002b). The size openings of the screen set used in this study were 25.4, 16.4, 8.7, 5.2 and 1.2 mm. The samples were placed on the top screen (25.4 mm openings), shaken for 90 seconds and the manure retained on each screen was weighed on a laboratory scale. The standard method uses the amount of material retained on the 5 screens and in the pan to calculate the geometric mean length. The proposed method presented in section 2.7.1 uses the screen with 16.4-mm openings as the largest for the calculation of the modified geometric mean length.

Figure 2.2. Modified soil sieves shaker and screen set used to measure the particle size distribution of manure samples.

2.6.4. Friction characteristics

The values of the static friction coefficient of manure products on different surface materials were measured using the inclined plane method (Mohsenin, 1986). Four different surfaces, representative of possible candidate materials for the construction of manure handling and land application equipment, were selected: steel (bare and painted), plastic (PVC) and plywood. An inclined plane apparatus was designed and built to measure the static coefficients of friction of manure products (fig. 2.3). The apparatus featured an electric motor giving an average angular inclination velocity of 0.007 rad/s over the 0 to $\pi/2$ radians range. For the static coefficient of friction experiments, the samples were placed and held in a fiberglass ring having a diameter of 300 mm and a height of 30 mm. The angle of repose of manure products was also measured according to the method described by Henderson et al. (1997) using an apparatus made of a cylinder that could be lifted from a base plane to let the sample flow out of it and form a pile. The radius of the pile was measured at four different locations 90 degrees apart on the base plane. The height of the pile was also measured and the angle of repose was calculated as the arctangent of the ratio of the height to the average radius. Approximately 10 to 15 L of manure were used for each angle of repose measurement.

Figure 2.3. Tilting plane apparatus used to measure the static coefficient of friction of manure samples.

2.6.5. Shearing properties

Depending on the total solids concentration of the product that was tested, three different apparatuses were used to characterize the relation between shear stress and shear rate: the shearbox apparatus (Wykeham Ferrance Engineering Ltd. model no. 25301, Slough, England), a laboratory rotational viscometer (DV-III+ Digital Rheometer, Brookfield, 11 Commerce Boulevard, Middleboro, Massachusetts 02346, USA) and a large-scale rotational viscometer. The large-scale viscometer was designed and built to accommodate the 170-L barrels that were used in the study. It was also introduced to compare the results obtained with small and very large samples (0.5 L-samples were used with the laboratory viscometer compared to approximately 85 L-samples for the large-scale unit). The large-scale viscometer is illustrated in figure 2.4. The barrel was rotated through the 90-degree gearbox and the torque calculated from the force measured via a load cell located between a fixed back plate and a rigid member attached to the free-wheeling spindle shaft. The rotational velocities varied from 0.3 to 100 rpm and 3 to 100 rpm for the laboratory and large-scale viscometer, respectively. The shear rate and shear stress were calculated using equations 2.4 and 2.5, respectively:

$$S = \frac{2\omega R_c^2 R_b^2}{R_b^2 \left(R_c^2 - R_b^2\right)} \qquad \text{and} \qquad (2.4)$$

$$F' = \frac{M}{2\pi R_b^2 L} \qquad , \qquad (2.5)$$

where S : shear rate [s^{-1}],

    ω : angular velocity of spindle (lab) or container (large) [rad/sec],

    R_c : radius of container [m],

    R_b : radius of spindle [m],

    F' : shear stress [Pa],

    M : torque input by instrument [N·m] and

    L : effective length of spindle [m].

The appropriate values of R_c, R_b, and L were obtained from the Brookfield documentation in the case of the laboratory viscometer. For the large viscometer, the integration of the apparatus parameters into equation 2.4 gave a shear rate, in s^{-1}, equal to 0.239 times the rotational velocity of the barrel in revolutions per minute. The immersion depth of the spindle was used as the effective length for the large unit. Four normal loads were used for the direct shear tests (7.0, 22.5, 38.1 and 70.7 kPa) and the rate of shear was constant at 1.2 mm/min. The standard procedure ASTM D3080-98 (ASTM, 1998) was followed.
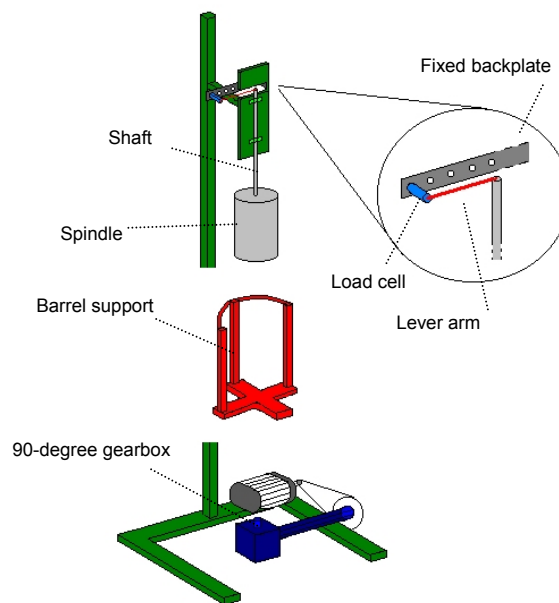
Figure 2.4. Schematic representation of the large-scale viscometer.

2.7. Results and discussion

Table 2.1 summarizes the results obtained for the total solids concentration of the tested animal manures. It can be seen that some of the tested samples exhibited variability, as assessed by the values of standard deviation. However, the ANOVA performed on the TS results indicated that the measured TS values were statistically similar enough to proceed to comparisons between the different products based on the target TS level. The original total solids concentrations of the dairy cattle, sheep and pig manure samples were approximately 15%, 30% and 25%, respectively. For the poultry manure

samples, two different initial levels of TS were observed (12% and 18% approximately) depending on the amount of water that got into the manure from leaking drinkers. Samples with a TS level corresponding to a target value were tested as is.

Table 2.1.   Average total solids concentration for the manure products evaluated.

Target TS level	Measured TS (%)			
(%)	Dairy cattle	Sheep	Poultry	Pig
50	47.8[a] **ab**[b]	53.0 **a**	47.3 **b**	48.0 **ab**
	(3.1) [c]	(3.1)	(1.9)	(1.7)
40	44.4 **a**	41.5 **a**	41.5 **a**	41.7 **a**
	(4.7)	(4.9)	(0.9)	(5.2)
30	33.5 **a**	30.7 **a**	34.5 **a**	32.0 **a**
	(1.6)	(1.9)	(0.6)	(4.5)
20	23.4 **a**	18.4 **a**	21.2 **a**	22.8 **a**
	(1.7)	(2.5)	(4.2)	(0.2)
15	14.2 **ab**	13.8 **a**	14.5 **ab**	14.8 **b**
	(0.4)	(0.1)	(0.6)	(0.04)
10	8.9 **a**	10.4 **b**	10.3 **b**	10.7 **b**
	(0.2)	(0.3)	(0.3)	(0.6)

[a]   Average value based on the four sub-samples;
[b]   Values within each TS level row not followed by the same letter are significantly different as determined by Fisher's LSD test at the 1% level;
[c]   Standard deviation based on the four sub-samples.

2.7.1. Solid manure products

Solid manure products can be compared on the basis of the properties presented in table 2.2. As it can be seen from the bulk density results included in table 2.2, poultry and pig manure were similar, while dairy cattle and sheep manure showed significant differences at most TS levels. Using the density values obtained at the appropriate TS level, the results were very similar to those outlined in ASAE D384.1 (ASAE, 2002c). According to the ASAE standard, the density in kg/m^3 of fresh manure is: 990 for dairy cattle (14.0%TS) and swine (13.1%TS), 1000 for sheep (27.5%TS), and 997 for layer hens (25.0%TS). Using the TS level closest to the ASAE standard, the comparisons (ASAE vs current study) of density values in kg/m^3 become: dairy cattle (990 vs 973); sheep (1000 vs 521); layer hens (997 vs 1028) and swine (990 vs 1026). The only major difference was in sheep manure. This difference was due to the presence of a

large proportion of straw in the sheep manure that was used in this study. The densities of all manure products were expected to become stable near the liquid density as TS becomes small.

Relationships between density and total solids concentration were obtained and are presented in figures 2.5 and 2.6. The following equations were obtained by polynomial regression analysis, using third order models and forcing the density at 0% TS to be 1000 (the density is in kg/m^3). Extra available data sets (not presented in table 2.2 but included in figures 2.5 and 2.6) were utilized to establish the relationships with more accuracy. The regression analysis revealed that all parameters of the third order polynomials were statistically significant. An analysis of the results published by Chen (1982) suggested that the relationship between the density of beef cattle manure and its total solids concentration followed a trend similar to those identified in this study. The relationship for poultry and pig manure was

$$Density = -0.0235 \ TS^3 + 1.189 \ TS^2 - 11.185 \ TS + 1000 \qquad R^2 = 0.83 \qquad , \qquad (2.6)$$

for dairy cattle manure was

$$Density = 0.0367 \ TS^3 - 2.377 \ TS^2 + 14.571 \ TS + 1000 \qquad R^2 = 0.93 \qquad and \qquad (2.7)$$

for sheep manure was

$$Density = 0.0086 \ TS^3 - 0.873 \ TS^2 + 8.899 \ TS + 1000 \qquad R^2 = 0.91 \qquad . \qquad (2.8)$$

Equations 2.6, 2.7 and 2.8 can be used to obtain a reasonable approximation of the bulk density of poultry and pig, dairy cattle and sheep manure, respectively, within the ranges of total solids concentrations of this study. It can be seen on figures 2.5 and 2.6 that some density measurements yielded high values, up to 260 kg/m^3 greater than the density of water (1000 kg/m^3). Although density values above 1000 kg/m^3 were also reported by Chen (1982), a bias induced by the initial compression state of the load cells on the weighing apparatus as well as vibration during measurements are potential sources of experimental errors that must be taken into account when assessing the

accuracy of the density measurements. The use of S-type load cells on the weighing
apparatus was justified by availability and simplicity but does not represent the optimal
choice for such an application. Nevertheless, the density results were comparable to
other published values.

Table 2.2. Density, static coefficients of friction and angle of repose for the solid manure products evaluated.

Target TS level (%)	Manure type	Measured and calculated properties					
		Density (kg/m³)	Static coefficient of friction (dimensionless)				Angle of repose (°)
			Plywood	Plastic	Painted steel	Bare steel	
50	Dairy cattle	238.4 [a] **a** [b]	0.88 **a**	0.93 **a**	0.90 **a**	0.80 **a**	n.a. [d]
		(20.1) [c]	(0.042)	(0.0082)	(0.026)	(0.0050)	
	Sheep	332.3 **b**	0.73 **b**	0.79 **b**	0.68 **b**	0.66 **b**	32.2 **a**
		(20.3)	(0.051)	(0.048)	(0.029)	(0.028)	(1.3)
	Poultry	607.5 **c**	0.82 **a**	0.88 **a**	0.89 **a**	0.79 **a**	36.1 **a**
		(75.3)	(0.013)	(0.022)	(0.017)	(0.018)	(5.3)
	Pig	552.5 **c**	0.83 **a**	0.86 **ab**	0.84 **a**	0.89 **c**	30.1 **a**
		(18.1)	(0.029)	(0.052)	(0.042)	(0.045)	(2.2)
40	Dairy cattle	198.6 **a**	0.88 **a**	0.88 **a**	0.82 **a**	0.79 **a**	n.a
		(7.9)	(0.065)	(0.029)	(0.031)	(0.021)	
	Sheep	556.9 **b**	0.81 **a**	0.86 **a**	0.83 **a**	0.83 **a**	48.0 **a**
		(52.1)	(0.057)	(0.056)	(0.021)	(0.022)	(6.8)
	Poultry	884.7 **c**	0.90 **a**	0.83 **a**	0.89 **a**	0.86 **a**	40.3 **a**
		(117.2)	(0.047)	(0.051)	(0.039)	(0.030)	(2.9)
	Pig	948.7 **c**	6.4 **b**	2.3 **b**	2.3 **b**	1.5 **b**	n.a
		(30)	(0.94)	(0.43)	(0.80)	(0.22)	
30	Dairy cattle	267.1 **a**	0.91 **a**	1.0 **a**	1.0 **a**	0.95 **a**	n.a
		(6.6)	(0.051)	(0.052)	(0.027)	(0.036)	
	Sheep	520.8 **b**	0.92 **a**	0.93 **a**	0.96 **a**	0.91 **a**	33.8
		(34.9)	(0.088)	(0.021)	(0.019)	(0.055)	(0.9)
	Poultry	1028.2 **c**	3.4 **b**	0.87 **a**	1.1 **a**	1.0 **a**	n.a.
		(45.5)	(0.38)	(0.062)	(0.078)	(0.20)	
	Pig	1140.9 **c**	7.8 **c**	0.95 **a**	1.0 **a**	0.80 **a**	n.a
		(112.3)	(0.49)	(0.12)	(0.17)	(0.080)	
20	Dairy cattle	411.0 **a**	1.0	1.2	1.1	1.1	n.a
		(32.1)	(0.070)	(0.030)	(0.10)	(0.03)	
	Sheep	1051.2 **b**					
		(60.2)					
	Poultry	1091.8 **b**	These samples were not solid enough to measure the static coefficient of friction, the geometric mean length and the angle of repose				
		(63.9)					
	Pig	1090.0 **b**					
		(77.3)					

[a]   Average value based on the four sub-samples;
[b]   Values within each TS level row and property column not followed by the same letter are significantly different
       as determined by Fisher's LSD test at the 1% level;
[c]   Standard deviation based on the four sub-samples;
[d]   Data not available.
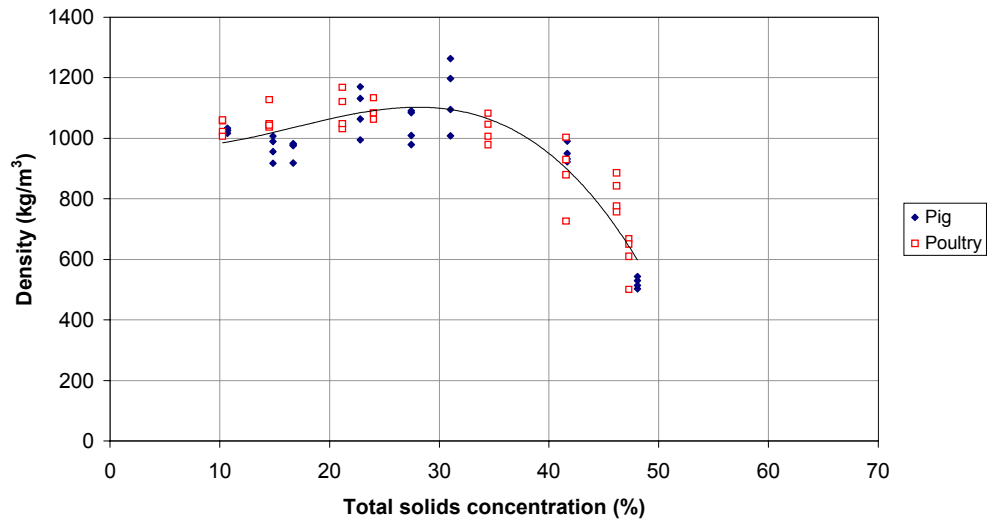
Figure 2.5. Bulk density values for poultry and pig manure and regression curve.
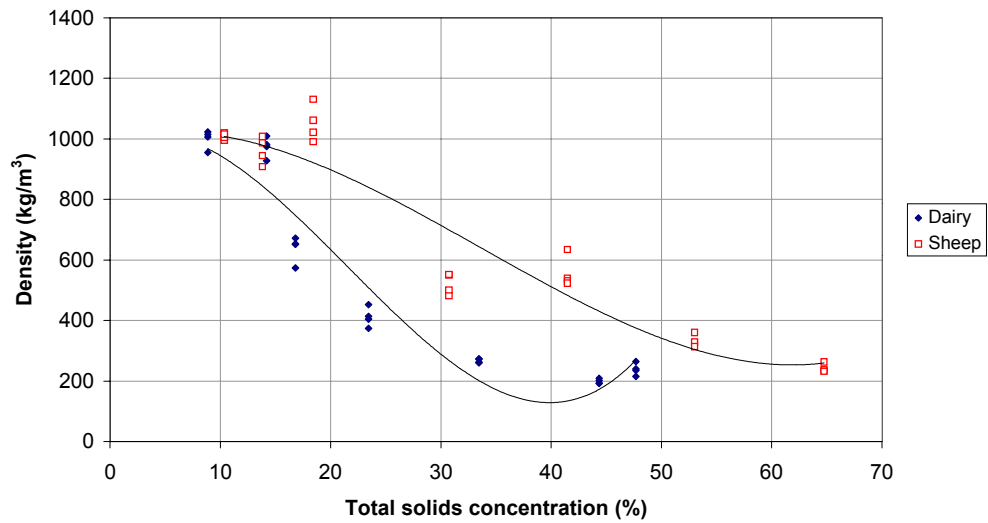
Figure 2.6. Bulk density values for dairy cattle and sheep manure and respective regression curves.

Modified geometric mean lengths (Xgm') are presented in table 2.3. Large clumps were observed on the top screen (25.4 mm openings) yielding an overestimation of the particles' geometric mean length, as calculated according to ASAE S424.1 (ASAE Standards, 2002b). The calculations were then adapted using 16.4 mm as the largest size opening to obtain the modified value (Xgm'). Observations were made on the size of the clumps collected on the top screen. Their largest dimension was generally

between 30 and 50 mm, but large 100-150 mm clumps were also observed, as mentioned by Glancey and Hoffman (1996). These clumps will affect the conveying behaviour of the products, but it becomes difficult to predict how without prior knowledge of their mechanical strength. The data included in table 2.3 allow seeing the effect of total solids concentration on the characteristic dimensions of the particles for each manure type. It can be seen that as the total solids concentration decreased, or as the manure products became wetter, the modified geometric mean length became significantly higher. This was due to the increased aggregation ability of the animal manures as the proportion of water in the manure increased. Table 2.3 is presented to show the results of the statistical analysis. Figure 2.7 allows for the visualization of the relationship between the modified geometric mean length and the total solids concentration. The data of table 2.3 indicate there was no significant difference in the overall average modified geometric mean length of poultry and pig manure. Also, the difference between dairy cattle manure and sheep manure in terms of modified geometric mean length was not very important, as suggested by the values of table 2.3. Predictive equations 2.9 and 2.10 for the modified geometric mean length of dairy cattle and sheep manure as well as for poultry and pig manure were obtained (figure 2.7). The relationship for dairy cattle and sheep manure was

$$Xgm' \text{ [mm]} = 16.107 - 0.159 \text{ TS} \qquad R^2 = 0.83 \qquad \text{and} \qquad (2.9)$$

the predictive equation for poultry and pig manure was

$$Xgm' \text{ [mm]} = 31.855 - 0.425 \text{ TS} \qquad R^2 = 0.84 \qquad . \qquad (2.10)$$

Table 2.3. Average modified geometric mean length and standard deviation for dairy cattle, sheep, poultry and pig manure.

	Average TS (%)	Average Xgm' [a] (mm)	Standard-deviation (mm)
Dairy cattle (**a** [b])	16.8	14.0 **a**	1.7
	23.4	12.6 **ab**	0.3
	33.5	11.2 **bc**	0.5
	44.4	9.6 **c**	1.3
	47.7	9.5 **c**	1.1
Sheep (**b**)	18.4	11.6 **a**	0.3
	30.7	11.1 **a**	0.8
	41.5	10.1 **b**	0.3
	53.0	6.5 **c**	0.1
	64.8	5.4 **d**	0.5
Poultry (**c**)	34.5	18.9 **a**	1.0
	41.5	14.2 **b**	0.4
	46.2	13.4 **b**	0.5
	47.3	10.9 **c**	0.4
Pig (**c**)	27.4	18.6 **a**	1.0
	31.0	19.7 **a**	0.3
	41.7	12.6 **b**	0.0
	44.5	11.3 **b**	0.2
	48.1	12.0 **b**	1.0

[a]   Modified geometric mean length;
[b]   Values within each manure type group (rows) and manure type column not followed by the same letter are significantly different as determined by Fisher's LSD test at the 1% level.
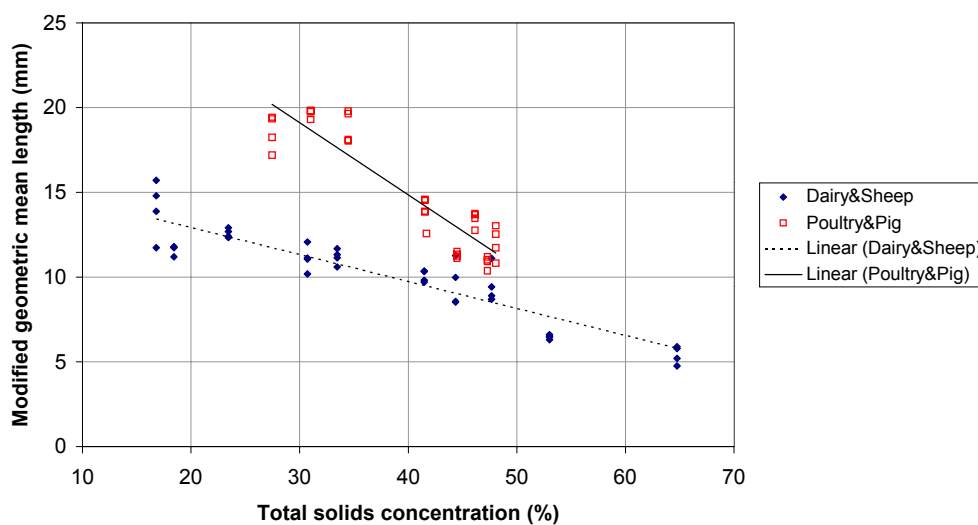
Figure 2.7. Modified geometric mean length of dairy cattle, sheep, poultry and pig manure as a function of total solids concentration (data of table 2.3).

The results obtained for the static friction coefficient indicated that while the experimental results exhibited some variability, similar values of friction coefficient were also present in the database. The large values of static coefficient of friction for pig manure could not be explained. More measurements would be required to see if pig manure really exhibits such large friction coefficients or if the values obtained were marginal. When all the coefficient of friction data were analyzed together, no significant differences were found between materials except for plywood which had significantly higher coefficients of friction. It was observed during the experiments that some products had a different behaviour on the inclined plane when they had a paste-like consistency or when seepage occurred. The tested poultry and pig manures exhibited a paste-like consistency at TS between 20% and 30%. It is difficult to define the limits of the solid or liquid states because small TS increments have not been studied in the suspected transition zone. The dairy cattle and sheep manure samples did not seem to have a solid to liquid transition zone as defined as the poultry and pig manure samples. The coefficient of friction results were further analyzed without the results obtained for these particular cases when seepage occurred or when the product had a paste-like consistency. The resulting linear regression equation was (figure 2.8):

Static friction coefficient = 1.340 – 0.0114 TS, $\qquad$ $R^2 = 0.71.$ $\qquad$ (2.11)

Equation 2.11 can be used to predict the static friction coefficient of the tested manure products on the selected surface materials (plywood, plastic, painted and bare steel). For the design and analysis of handling and land application systems, the choice of appropriate safety factors should compensate for the lack of fit of the equation. More data would be required to deepen the observations made on the friction behaviour of pasty products. The coefficients of friction measured in this study are consistent with those reported by Glancey and Hoffman (1996) and with their conclusion that there is little practical difference between the coefficients measured on the various surfaces and for the manure products tested.
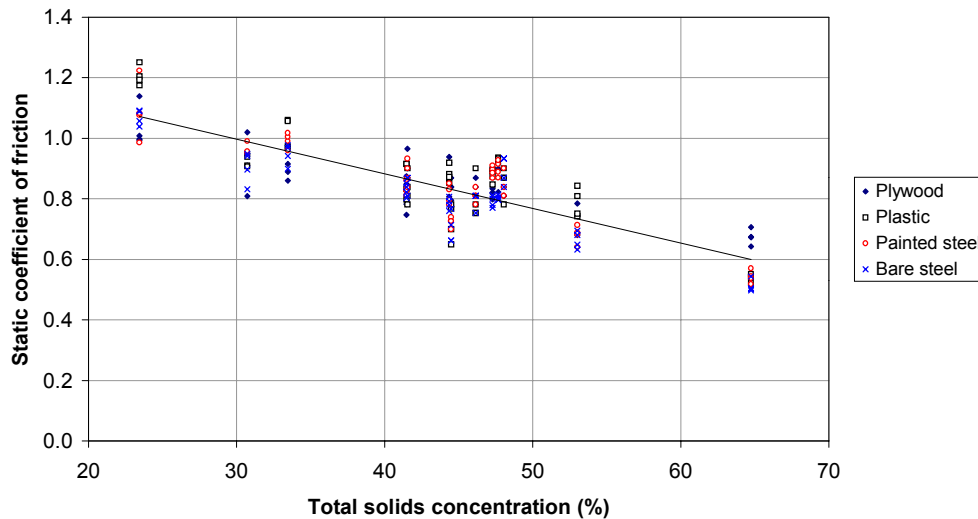
Figure 2.8. **Static coefficient of friction of dairy cattle, sheep, poultry and pig manure as a function of total solids concentration. All data points are included to highlight that there is little practical difference between the measured static coefficients of friction over the different surface materials and that a single predictive equation can be used.**

The angle of repose results included in table 2.2 demonstrate that there was no significant difference between the angles measured for all manure types at a given level of total solids concentration. The missing data for this property were due to problems encountered with the apparatus. Some products would also keep the shape of the cylinder they were confined in after it had been lifted from the base plane. However, the results indicate there was little practical difference between the angle of repose values of the tested animal manures. The average of all angle of repose measurements was 38°, which was in agreement with what was presented by Glancey and Hoffman (1996) (average of 37°) and also close to the values reported by Moysey and Hiltz (1985) for commercial fertilizers that had angles of repose between 33° and 36°. The average value of the current study is greater than what was measured by Landry and Laguë (1999) for papermill residues (average of 30°).

The results obtained for the direct shear test were highly variable, as revealed by the large values of standard deviation presented in table 2.4. General trends could not be observed for the angle of internal friction or the apparent cohesion. The direct shear tests were carried out using a 190.5 x 101.6 x 63.5 mm box and the samples were not

screened prior to the experiments. The large aggregates present in most of the tested samples may have been responsible for the inconclusive results, although observations made while testing samples free of large clumps did not show major differences in the recorded data. The direct shear test was difficult to carry out due to the clumpy and heterogeneous nature of manure products. A larger split box could be used to attempt investigating the shearing behaviour of manure products with the aggregates. Another option would be to carry out the test on screened samples. Other tests should also be explored as they may be more suitable to characterize the shear stress – shear rate behaviour of organic by-products.

Table 2.4.   Angle of internal friction and apparent cohesion for the manure products tested.

	Average TS	Angle of internal friction (°)		Cohesion (kPa)	
	(%)	Average	Standard deviation	Average	Standard deviation
Dairy cattle	16.8	36.3 a [a]	3.1	3.0 a	0.7
	23.4	35.6 a	1.1	2.8 a	1.0
	33.5	37.3 ab	1.5	2.1 a	1.4
	44.4	37.6 ab	0.8	3.7 a	0.4
	47.7	40.7 b	1.0	3.1 a	0.9
Sheep	18.4	26.5 a	1.0	7.2 a	1.5
	30.7	23.9 a	0.4	7.4 a	0.9
	41.5	25.9 a	0.8	7.5 a	0.1
	53.0	38.3 b	3.3	1.7 b	1.9
Poultry	34.5	12.4 a	0.2	7.3 a	0.6
	41.5	28.1 b	0.8	11.9 b	0.3
	47.3	22.4 c	3.7	12.0 b	1.2
Pig	31.0	19.2 a	4.0	0.5 a	0.9
	41.7	9.2 b	2.4	9.3 b	0.8
	48.1	24.2 a	1.7	15.6 c	1.4

[a]   Values within each manure type row and property column not followed by the same letter are significantly different as determined by Fisher's LSD test at the 1% level

2.7.2. Liquid and semi-solid products

For manure products that could not be submitted to the direct shear test and for which static friction coefficients were irrelevant, the focus was on the density and on the shear stress – shear strain behaviour as determined by rotational viscometry. The tested manure products generally displayed a decreasing viscosity with an increasing shear rate, which corresponds to the typical behaviour of non-Newtonian pseudoplasic fluids.

It was found that the power law could be used to describe the relation between shear stress and shear rate for the tested products:

$$\tau = K \dot{\gamma}^{\,n} \qquad , \qquad (2.12)$$

where τ is the shear stress, K the consistency coefficient, $\dot{\gamma}$ the shear rate and n the flow behaviour index, could be used to describe the relation between shear stress and shear rate for the tested products. The values of the consistency coefficient K and of the flow behaviour index n are presented in table 2.5 for both the laboratory and the large-scale viscometers. The density results have been previously discussed and included in predictive equations 2.6, 2.7 and 2.8. Comparisons between the results obtained using the large-scale viscometer and the laboratory unit showed there was in most cases no significant difference between the two apparatuses, for both the consistency coefficient K and the flow behaviour index n. The high variability of the results obtained using the large-scale viscometer, with an average coefficient of variation of 20% for all groups of measured data, combined with the discriminant statistical test used, is one factor explaining the similarities between the two viscometers. Results obtained using the laboratory viscometer also exhibited variability, but this could be expected when very small quantities, to fill a 600-mL beaker, are taken from large 150-L samples. To reduce the variability of the results obtained with the large-scale viscometer, two issues must be addressed. The mechanical vibration coming from the motor and the gearbox were substantial and should be damped or reduced to ensure the torque measured is mainly related to the shearing of the fluid. Also, the sensitivity of the torque-measuring load cell should be increased by using a combination of smaller capacity (the load cell used had a capacity of 222 N) and variable lever arm length. More conclusive results might be obtained with an improved large-scale viscometer.

Many similarities between products having the same level of total solids were detected by the statistical analysis. The rather large standard deviations are partly responsible for those conclusions. Figures 2.9, 2.10 and 2.11 allow for a visual appreciation of the shear stress – shear strain relationships for animal manures. They also illustrate the

effect of TS on the consistency coefficient and on the flow behaviour index for the various types of manure tested. It should be noted that these charts were plotted using the average experimental values of K and n to calculate the shear stress at the minimum and maximum shear rate values. Results from other studies (Achkari-Begdouir and Goodrich, 1992; Chen and Hashimoto, 1976; Kumar et al., 1972) have been included, using the same plotting method, to illustrate the similarities and differences among results obtained for manure products originating from very similar sources.

Table 2.5. Bulk density, consistency coefficient (K) and flow behaviour index (n) for the animal manure products tested [a].

Total solids concentration (%)	Manure type	Density (kg/m³)	Lab viscometer K (Pa·sⁿ)	Lab viscometer n (--)	Large viscometer K (Pa·sⁿ)	Large viscometer n (--)	Shear rate range (s⁻¹) Lab	Shear rate range (s⁻¹) Large
20	Dairy cattle	411.0 [b] a [c] (32.1) [d]	n.a.	n.a.	n.a.	n.a.	n.a.	n.a.
	Sheep	1051.2 b (60.2)	n.a.	n.a.	n.a.	n.a.	n.a.	n.a.
	Poultry	1091.8 b (63.9)	9.9 a (1.4)	0.43 a (0.078)	35.4 a (2.7)	0.29 a (0.083)	[0.07 - 22.10]	[0.64 - 24.14]
	Pig	1090.0 b (77.3)	41.1 b (4.7)	0.34 a (0.018)	56.8 a (14.8)	0.35 a (0.074)	[0.08 - 25.38]	[0.24 - 23.90]
15	Dairy cattle	973.0 a (33.9)	22.9 a (8.3)	0.41 a (0.042)	31.3 a (7.2)	0.30 a (0.12)	[0.07 - 21.61]	[0.61 - 24.37]
	Sheep	961.5 a (44.8)	26.9 a (11.5)	0.36 a (0.076)	19.4 a (8.4)	0.29 a (0.035)	[0.07 - 22.07]	[0.70 - 23.90]
	Poultry	1063.6 b (42.4)	1.7 b (0.06)	0.41 a (0.012)	2.4 b (0.3)	0.38 a (0.018)	[0.07 – 22.00]	[0.80 - 23.90]
	Pig	967.7 a (39.5)	3.4 b (0.2)	0.42 a (0.0058)	2.4 b (0.3)	0.38 a (0.018)	[0.07 – 22.00]	[0.96 - 23.90]
10	Dairy cattle	999.6 a (30.7)	2.6 a (0.3)	0.42 a (0.026)	5.3 a (2.1)	0.11 a (0.10)	[0.07 – 22.00]	[0.90 - 23.90]
	Sheep	1008.3 a (11.1)	3.7 b (0.5)	0.42 a (0.029)	2.7 a (0.9)	0.33 b (0.084)	[0.07 – 22.00]	[0.90 - 23.90]
	Poultry	1036.5 a (26.6)	1.2 c (0.07)	0.37 a (0.022)	8.9 b (2.3)	0.29 ab (0.11)	[0.12 - 30.79]	[0.96 - 24.14]
	Pig	1025.7 a (7.1)	1.0 c (0.04)	0.55 b (0.018)	2.2 a (0.8)	0.21 ab (0.041)	[0.12 - 38.75]	[0.90 - 23.90]

[a] For the viscometry tests, the temperature of the manure samples was between 17ºC and 24ºC;
[b] Average value based on the four sub-samples;
[c] Values within each total solids concentration level row and property column not followed by the same letter are significantly different as determined by Fisher's LSD test at the 1% level (a T-test was used when only two means were available);
[d] Standard deviation based on the four sub-samples.
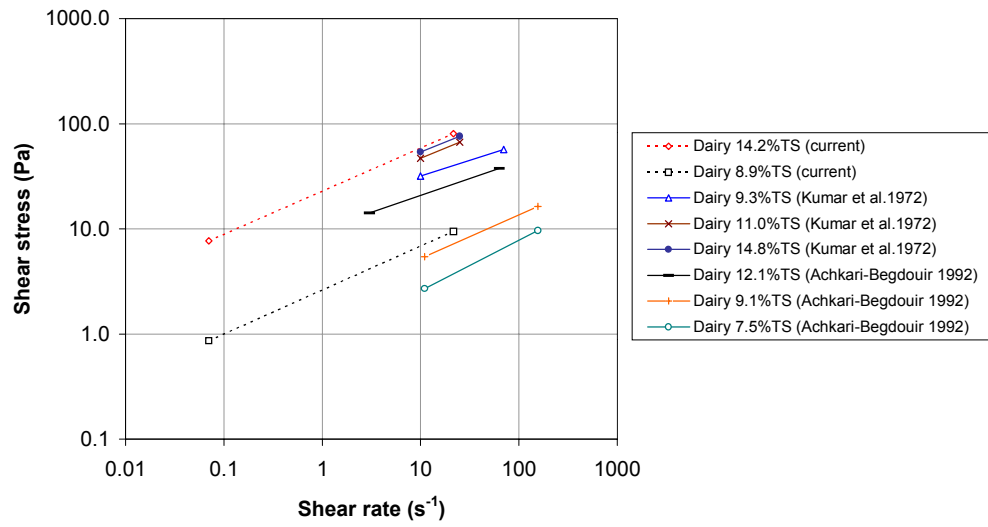
Figure 2.9. Shear stress – shear rate curves for dairy cattle manure (current study and other published results).
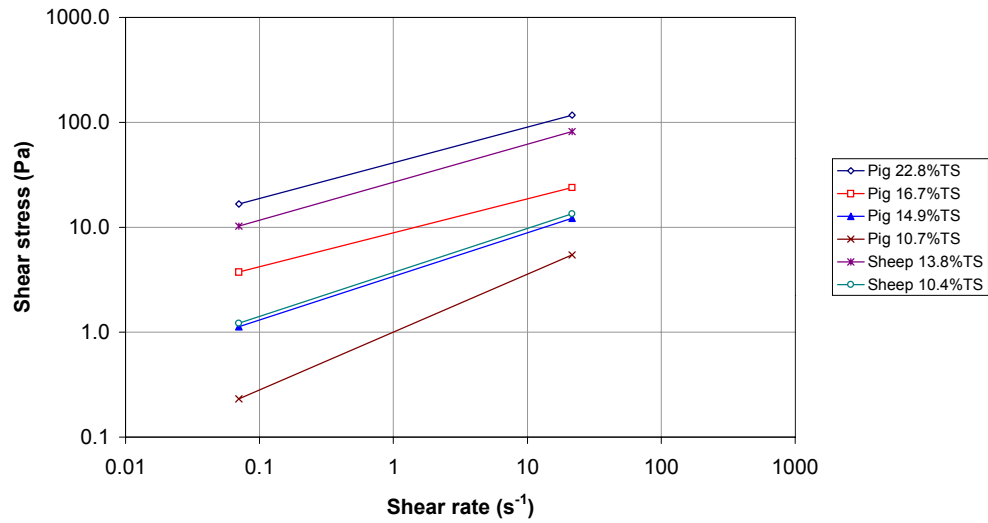
Figure 2.10. Shear stress – shear rate curves for sheep and pig manure.
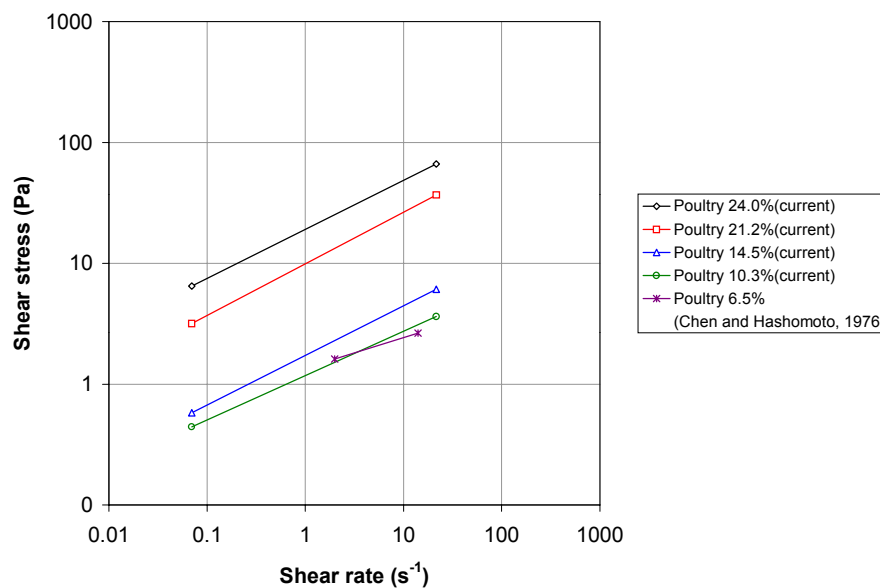
Figure 2.11.   Shear stress – shear rate curves for poultry manure (current study and other published results).

If the viscometry results are further analyzed to evaluate the effect of total solids concentration on the consistency coefficient and flow behaviour index using the results obtained with the laboratory viscometer, it can be seen that the value of K became significantly larger with an increase in TS (table 2.6). The values of n however were not significantly different at various levels of total solids concentration except for pig manure for which the value of the flow behaviour index was significantly higher for lower values of TS. This is consistent with the conclusions of Chen and Shetler (1983), but the relationship was not generalized enough to make this observation a conclusion. These observations can also be visualized on figures 2.9, 2.10 and 2.11. Even though limited data were available, a relationship was identified between the consistency coefficient and the total solids concentration for poultry and pig manure. Similar relationships could be established using data obtained by Chen and Shetler (1983). Equations 2.13 and 2.14 can be used to predict the consistency coefficient for poultry and pig manure, respectively within the ranges of total solids concentration (10% to 25%), temperature (17ºC to 24ºC) and shear rate (approximately 0.07 to 30 s^{-1}) of this study (where K is in Pa·s^n). The equation for poultry manure was

$$K = 0.139 \text{ TS}^2 - 3.525 \text{ TS} + 22.930 \qquad R^2 = 0.95 \qquad \text{and} \qquad (2.13)$$

the relationship for pig manure was

$$K = 0.334 \text{ TS}^2 - 7.867 \text{ TS} + 46.907 \qquad R^2 = 0.98 \qquad . \qquad (2.14)$$

Table 2.6. Consistency coefficient (K) and flow behaviour index (n) obtained using the laboratory viscometer.

	Total solids concentration	Laboratory viscometer	
		K	n
	(%)	(Pa·s[n])	(--)
Dairy cattle	14.2	22.9 [a] **a** [b]	0.41 **a**
		(8.3) [c]	(0.042)
	8.9	2.6 **b**	0.42 **a**
		(0.3)	(0.026)
Sheep	13.8	26.9 **a**	0.36 **a**
		(11.5)	(0.076)
	10.4	3.7 **b**	0.42 **a**
		(0.5)	(0.029)
Poultry	24.0	19.1 **a**	0.40 **a**
		(3.5)	(0.071)
	21.2	9.9 **b**	0.43 **a**
		(1.4)	(0.078)
	14.5	1.7 **c**	0.41 **a**
		(0.06)	(0.012)
	10.3	1.2 **c**	0.37 **a**
		(0.07)	(0.022)
Pig	22.8	41.1 **a**	0.34 **a**
		(4.7)	(0.018)
	16.7	8.9 **b**	0.32 **a**
		(0.9)	(0.036)
	14.9	3.4 **c**	0.42 **b**
		(0.2)	(0.0058)
	10.7	1.0 **c**	0.55 **c**
		(0.04)	(0.018)

[a]   Average value based on the four sub-samples;
[b]   Values within each manure type row and property column not followed by the same letter are significantly different as determined by Fisher's LSD test at the 1% level (a T-test was used when only two means were available);
[c]   Standard deviation based on the four sub-samples.

To obtain a parameter that may be more useful for design purposes, it was possible to calculate the apparent viscosity (η_{app}) using equation 2.15 (Chen and Shetler, 1983):

$$\eta_{app} = K \, S^{(n-1)} \quad . \qquad (2.15)$$

Plotting the apparent viscosity at a shear rate of 10 s^{-1} against the total solids concentration on a log-log chart gave predictive equations 2.16, 2.17 and 2.18 (where η_{app} is in Pa·s). The relationship for dairy cattle manure was

$$\eta_{app} = 4E\text{-}05 \ TS^{\,4.4671} \qquad R^2 = 0.95 \qquad , \qquad (2.16)$$

the equation for poultry manure was

$$\eta_{app} = 6E\text{-}05 \ TS^{\,3.4721} \qquad R^2 = 0.94 \qquad and \qquad (2.17)$$

the relation for pig manure was

$$\eta_{app} = 4E\text{-}06 \ TS^{\,4.6432} \qquad R^2 = 0.95 \qquad . \qquad (2.18)$$

The observed relationships between the apparent viscosity and the total solids concentration were in agreement with the relationship obtained by Chen and Shetler (1983). An analysis of the results obtained by several authors (Achkari-Begdouir and Goodrich, 1992; Chen and Shetler, 1983; Chen, 1982; Chen and Hashimoto, 1976; Kumar et al., 1972) have demonstrated the heterogeneity of viscometry results highlighting the fact that the focus should be on determining ranges of acceptable values for manure properties. These results also allowed seeing that data obtained at several different times and locations still showed similarities. The results of this study also suggested that processing animal manures to produce more homogeneous products in terms of physical and rheological properties may be the only effective way of making handling and land application equipment more efficient in terms of power requirement and uniformity of distribution. With the wide range of animal diets, management practices and climates that can affect the properties of animal manures combined with differences between animal herds as well as between individual animals, it is very difficult to design and operate machines with the objective of obtaining optimal performances. However, ranges of values for manure physical and rheological properties, such as the ones obtained in this study, should be the basis of any machinery design or optimization effort. Along with the judgment of the designing engineers, the knowledge base developed in the literature and in this study should allow for improved

design and operation of manure handling and land application equipment, within the limits imposed by the inherent variability in the properties of animal manures.

2.8. Conclusions

Physical and flow properties of manure products were measured over a wide range of total solids concentration. Based on the results obtained, the major findings were:

- the density of dairy cattle, poultry and pig manure was in agreement with ASAE D384.1 and other published results. Predictive equations based on total solids concentration were obtained.

- A method was proposed to calculate a modified value of the geometric mean length obtained by screening. Significantly larger modified geometric mean lengths were observed as the total solids concentration of the products decreased.

- Static friction coefficients were measured on different surface materials. For design purposes, the observation of similar values for most of the manure products over the majority of the tested surfaces led to a unique equation to predict the static friction coefficient as a function of total solids concentration.

- The animal manures studied were found to be non-Newtonian pseudoplastic fluids and the power law could be used to relate shear stress and shear rate. The value of the consistency coefficient was found to increase with the total solids concentration. The apparent viscosity was found to be well correlated to TS for dairy cattle, poultry and pig manure.

- For the design and analysis of manure handling and land application systems, the ranges of values presented can be used with proper care. Poultry and pig manure generally exhibited similar behaviours while dairy cattle and sheep

manure showed similarities, though not as strong as the former pair due to the straw content of the tested sheep manure. The density values and friction characteristics of manure products were found to be consistent with other published results. The shear stress – shear strain relationships seemed however to be study-specific, but published values still showed similarities.

2.9. Recommendations

The lack of standard methods to measure the physical and rheological properties of organic by-products made the characterization of manure products more challenging. Some methods have successfully been used in this study and by other authors. For example, the oven method used to determine total solids concentration of the samples poses no difficulties. The inclined plane method is also a relatively simple means of measuring the static coefficient of friction. Other methods have proven to be more difficult to implement in a manure testing program. The results for the angle of repose, obtained using a rather simple apparatus, were not consistent. The screening method presented in this study gave good results when the calculations were based on the bottom five screens of the six-screen set. It was, however, very labour-intensive to screen adhesive manure products. The results must also be interpreted with care as the calculated characteristic dimension can become a measure of the aggregation ability of the tested sample. The change in particle size distribution from one TS level to another also included the effect of the mechanical disturbances induced by the sample preparation. Different screening approaches should be suggested to enhance the potential information that such tests can yield. Innovative tests such as the triaxial test, the slump test, non-rotational viscometry or a test to measure the dynamic coefficient of friction should also be attempted. The pycnometer method used by Agnew et al. (2003) to measure the density of compost gave good results and would certainly be worth trying with other organic by-products. These new tests could deepen the knowledge of the engineering properties of manure products, potentially leading to improved ways of handling and land-applying those products.

2.10. Acknowledgements

2.11. References

ASAE Standards, 2002a. S385.2. Moisture Measurement – Forages. St. Joseph, Mich.: ASAE.

ASAE Standards, 2002b. S424.1. Method of Determining and Expressing Particle Size of Chopped Forage Materials by Screening. St. Joseph, Mich.: ASAE.

ASAE Standards, 2002c. D384.1. Manure Production and Characteristics. St. Joseph, Mich.: ASAE.

ASTM 1998. Annual Book of ASTM Standards. D3080-98. Standard Test Method for Direct Shear Test of Soils Under Consolidated Drained Conditions. West Conshohocken, Penn.: ASTM.

Achkari-Begdouri,A.and P.R. Goodrich. 1992. Rheological properties of Moroccan dairy cattle manure. *Bioresource Technology*, 40(2): 149-156.

Agnew, J.M., J.J. Leonard, J. Feddes, and Y. Feng. 2003. A modified air pycnometer for compost air volume and density determination. *Canadian Biosystems Engineering* 45(6): 27-35.

Bisang, M. 1987. Epandeuses de fumier: comparaison de differents dispositifs d'épandage. *Technique Agricole*, Switzerland. 1987, 49(3), 8 pp.; Rapports FAT No. 300.

Chen, Y.R. 1986. Rheological properties of sieved beef-cattle manure slurry: rheological model and effects of temperature and solids concentration. *Agricultural Wastes*, 15(1):17-33.

Chen, Y.R. 1982. Engineering properties of beef cattle manure. ASAE Paper No. 824085. St. Joseph, Mich.: ASAE.

Chen, Y.R., and A.G. Hashimoto. 1976. Rheological properties of aerated poultry waste slurries. *Transactions of the ASAE* 19(1): 128-133.

Chen, Y.R. and E.L. Shetler. 1983. Temperature effect on rheological properties of cattle manure slurry. *Journal of Testing and Evaluation*, 11(6): 360-364.

Frick, R., J. Heusser and M. Shick. 2001. Technique d'épandage des engrais à base de déchets et de fumier de stabulation libre : Qualité du travail et adéquation de différents systèmes d'épandage. Rapport FAT No. 560.

Glancey, J.L. and R.K. Adams. 1996. Applicator for sidedressing row crops with solid wastes. *Trans. ASAE* 39(3): 829-835.

Glancey, J.L. and S.C. Hoffman. 1996. Physical properties of solid waste materials. *Applied Eng. Agric.* 12(4): 411-446.

Hashimoto, A.G. and Y.R. Chen. 1976. Rheology of livestock waste slurries. *Trans. ASAE* 19(5): 930-934.

Henderson, S.M., R.L. Perry and J.H. Young. 1997. Agricultural process engineering. St. Joseph, Mich.: ASAE.

Kumar, M., H.D. Bartlett and N.N. Mohsenin. 1972. Flow properties of animal waste slurries. *Trans. ASAE* 15(4): 718-722.

Landry, H. and C. Laguë. 1999. Selected properties of papermill residues. ASAE Paper No. 996058. St. Joseph, Mich.: ASAE.

Ling, Q. and J.H. Wilhoit. 1999. Power requirements of spinner-type spreaders broadcasting poultry litter and wood ash. *Applied Eng. Agric.* 15(5): 405-409.

Malgeryd, J. and C. Wetterberg. 1996. Physical properties of solid and liquid manures and their effects on the performance of spreading machines. *J. Agric. Eng. Res.*, 64(4):289-298.

Mohsenin, N.N. 1986. *Physical Properties of Plant and Animal Materials*, 2nd ed. New York, NY : Gordon and Breach.

Moysey, E.B., and S. Hiltz. 1985. Friction properties of fertilizers. Canadian Agricultural Engineering 27(2): 79-84.

Reed, W.B. and E. Wacker. 1968. Determination of the distribution pattern of dry fertilizer applicators. ASAE Paper No. 68606. St. Joseph, Mich.: ASAE.

Thirion, F. and C. Chabot. 2003. Épandage des boues résiduaires et effluents organiques: Matériels et pratiques. Cemagref Éditions. Paris, France.

Thirion F., F. Chabot and D. Andeler. 1998. Determination of physical characteristics of animal manure. *Proceedings of RAMIRAN 98* (8th International Conference on Management Strategies for Organic Waste Use in Agriculture) Rennes, France, pp. 457 –469.

Wilhoit, J.H. and Q. Ling. 1996. Spreader performance evaluation for forest land application of wood and fly ash. *Journal of Environmental Quality*, 25(5): 945-950.

Wilhoit, J.H., J.S. Bannon, R.R. Duffield and Q. Ling. 1994. Development and evaluation of a drop applicator for poultry litter. *Applied Eng. Agric.* 10(6): 777-782.

Wilhoit, J.H., C.W. Wood, K.H. Yoo and M.Y. Minkara. 1993. Evaluation of spreader distribution patterns for poultry litter. *Trans. ASAE* 9(4): 359-363.

Chapter 3

Performances of Conveying Systems for Manure Spreaders and Effects of Hopper Geometry on Output Flow

3.1.   Significance

In order to obtain data to develop and validate models of the machine-product interactions taking place in handling and land application equipment, experiments were carried out. Starting with the fact that very little information is available on the flow behaviours of organic fertilizers in such machines, experiments were carried out to study different conveying systems as well as the effect of selected operating parameters. This chapter corresponds to objective 6 of the thesis. A condensed version of this manuscript has been published as a *Technical Note* in *Applied Engineering in Agriculture* (*Landry, H., E. Piron, J.M. Agnew, C. Laguë and M. Roberge. 2005. Performances of conveying systems for manure spreaders and effects of hopper geometry on output flow. Applied Engineering in Agriculture 21(2):159-166*). The candidate conducted the major part of the data collection and analysis presented in the manuscript. Mr. Emmanuel Piron of Cemagref provided the information included in sections 3.6.2 and 3.8.2 and part of the material presented in sections 3.2 and 3.9. Ms. Joy Agnew of the University of Saskatchewan participated in the collection of the data presented in section 3.8.1.1. The writing of the manuscript was done by the candidate and Drs. Laguë and Roberge reviewed it. The article was peer-reviewed. The comments of the three reviewers were

to the effect that some experiments could not be replicated and that the conclusions drawn from these experiments should be clearly identified.

3.2.   Abstract

The objectives of the work reported herein were to evaluate the performances of different conveying systems for manure spreaders and to study the effect of the geometry of the holding system on material flow. Experiments were carried out at the University of Saskatchewan (Canada) and at Cemagref (France). A prototype spreader was evaluated with both a scraper conveyor and a system of four augers. The specific energy required to unload the machine with the 4-auger system was found to be higher than with the scraper conveyor, with average values for all experimental runs of 184 J/kg and 73 J/kg, respectively. A 3-factor factorial design was used to study the effect of the vertical position of a flow-control gate, the velocity of the conveying system and the inclination angle of the sidewalls, for both conveying systems. The specific energy for both conveying systems was found to be significantly affected by the position of the gate. The characteristic flow rate, as defined in European Standard EN 13080, was influenced by all three factors in the case of the scraper conveyor. The position of the gate, the velocity of the conveyor and the interaction between these two factors were found to be significantly affecting the characteristic flow rate of the 4-auger system. The output flow of three commercial manure spreaders having similar functional units but different hopper geometries was studied. The stretch within the tolerance zone was found to increase when the length and width of the hopper were increased. The longitudinal coefficient of variation was found to decrease when the length of the hopper was increased. The same effect was observed when increasing the width of the hopper and when reducing its height. The physical properties of the products spread were deemed to have an influence on the response of the evaluation criteria to changes in hopper geometry. Cohesive products were found to improve the discharge flow in terms of the stretch within the tolerance zone, the longitudinal coefficient of variation and the actual to theoretical unloading time ratio.

3.3. Introduction

For many years, modern agriculture has relied on mineral fertilizers to maintain and improve the fertility of highly productive soils. Mineral fertilizers present definite advantages over organic fertilizers such as concentrated and controlled fertilizing value. Because of this, organic fertilizers in general, and livestock manure in particular, have gradually grown to be considered waste products of which must be disposed. As a result, low cost, simplicity and large capacity now constitute the most important criteria for the design of land application equipment for livestock manure, while controlled application rate and uniform distribution are not considered to be a priority.

That situation is rapidly evolving as more severe environmental regulations now bring a different perspective on the usage of organic fertilizers. Their fertilizing value is now more appreciated and efforts are being invested to better utilize organic by-products in agriculture. As a result, land application equipment for livestock manure and other organic by-products need to better accommodate a broad range of products having variable physical and rheological properties. As for mineral fertilizers, the appropriate control of the application rate is critically important for optimizing the agronomic and environmental benefits associated to the application of manure or other organic by-products to agricultural land.

Optimal design of the manure holding and conveying systems on land application equipment constitutes a critical step in controlling material discharge and thus application rate. These systems need to be designed or selected on the basis of the physical and flow properties of the materials to be handled. Sludge spreaders are typically equipped with one or several discharge augers while solid manure spreaders generally feature scraper conveyors. The geometry of the manure holding system, or hopper, is defined by the required machine capacity and other design constraints. To improve the performances of solid and semi-solid manure land application equipment, an enhanced understanding of material flow within such machines is required. The role of the conveying system must therefore be examined in greater detail in terms of power requirements as well as the qualitative and quantitative characteristics of the induced

flow. The effect of the geometry of the holding system on the output flow must also be investigated in more depth.

3.4.   Objectives

The general objective of the research work reported herein was to investigate the effects of different holding and conveying systems for solid and semi-solid manure spreaders on material discharge rate and energy requirements. The specific objectives were to:

- investigate the performances of two types of conveying systems (scraper conveyor and system of 4 augers) in terms of specific energy and discharge rate as affected by the velocity at which these conveying systems are operated, the position of a vertical flow-control gate and the inclination of the sidewalls of the manure holding system,

- examine the effect of the position of a flow-control gate on the specific energy and discharge rate for different types of organic by-products and

- study the longitudinal uniformity of product distribution obtainable with commercial manure spreaders having different hopper geometries and used to spread organic by-products exhibiting various physical properties.

3.5.   Literature review

Bulinski and Klonowski (1998) studied the effect of floor conveyor velocity and hopper loading on the overall power requirements of a solid manure spreader. They measured power ranging from 2.03 to 25.67 kW for manure loads and conveyor velocities ranging from 0 to 60.35 kN and 5 to 33 mm/s, respectively. The manure used in the study had an average bulk density of 824 kg/m^3. Bulinski and Klonowski (1998) concluded that both the velocity of the floor conveyor and the amount of manure in the hopper significantly affected the power requirements.

Ling and Wilhoit (1999) investigated the power requirements of spinner-type spreaders broadcasting poultry litter (moisture content of 22.2% and bulk density of 503 kg/m^3) and wood ash (moisture content of 59.0% and bulk density of 517 kg/m^3). The power consumption of the spinner motor was estimated using the measured hydraulic pressure drop across one of the motors and the measured spinner speed. To estimate the power requirements of the conveyor system, formulas and design factors from the American Chain Association along with an analysis of the forces acting on a material flow block were used. The results showed that the power consumption of the hydraulically operated spinner system when spreading poultry litter increased as the spinner speed and flow rate increased. There was no significant difference in the power consumption for poultry litter and wood ash spreading, mainly because both products had approximately the same bulk density at the testing conditions. The maximum power consumption of the spinner system was 10.4 kW (from the reported flow rate, the specific energy was 816.3 J/kg) for poultry litter and 10.2 kW (from the reported flow rate, the specific energy was 941.5 J/kg) for wood ash. The power consumption of the conveyor system was found to change with the depth of product inside the hopper, length of the hopper, gate height, gate width, hopper angle, specific weight of product, conveyor velocity, internal friction of the product and friction between the product and the hopper. From a sensitivity analysis, the factors significantly affecting the power consumption were found to be material depth, hopper length and gate opening while the least sensitive factors included gate height and hopper angle. The power consumption of the conveyor was smaller than that of the spinners. The conveyor power requirements increased as material flow rate increased and there was little difference between poultry litter and wood ash spreading. The conveyor power requirements and specific energy (calculated from the reported discharge rate) for poultry litter and wood ash spreading were very similar (maximum power requirement of 8.34 kW (specific energy of 654.6 J/kg) and 8.25 kW (specific energy of 629.9 J/kg), respectively) because the density and friction coefficient of the materials were similar.

Ling et al. (1996) also investigated the influence of the height of the flow-control gate and the velocity of the floor conveyor on the performance of a spinner-type spreader broadcasting poultry manure. They obtained longitudinal distributions with coefficients of variation between 9% and 41%. Ling et al. (1996) concluded that there were no significant effects of gate opening and conveyor velocity on the longitudinal uniformity of application of the material.

Weil and Higgins (1975) conducted tests on helicoid and ribbon screw conveyors to determine which sewage sludge physical properties and which screw conveyor operational variables were most closely correlated to the total power requirements and the mass flow rate for the conveyors. The wet basis solids contents of the sludge used were 9%, 12% and 15% and the sludge samples were submitted to the slump test as well as viscometry and density measurements. The results indicated that solids content and viscosity were highly correlated with slump and could therefore be substituted in the predictive equations for power and mass flow rate. Weil and Higgins (1975) concluded that the screw conveyor rotational velocity and one sludge physical property were sufficient to adequately describe the power requirements of the conveyors. The proposed mathematical model for the mass flow rate required the inclination angle of the conveyor in addition to its rotational velocity and one property of the sludge.

3.6. Materials and methods

Experimental work associated with the first specific objective was completed at the University of Saskatchewan (Canada). Experiments to meet the second specific objective were carried out at the Montoldre station of Cemagref (France). The assessment of the effects of hopper geometry, which corresponded to the third specific objective, was also completed at Cemagref.

3.6.1. Conveying systems

A prototype land applicator built from a commercial manure spreader (New Idea, model 362) was used in the part of the study completed at the University of Saskatchewan. Two different types of conveyor could be fitted in the prototype: a scraper conveyor and a system of four augers. Both conveying systems were PTO-driven. A hydraulically actuated vertical gate was added at the discharge end of the spreader to better control the flow. The sidewalls of the spreader were extended vertically to increase the volume of the hopper and were mounted on hinges that allowed control of their inclination for the study of the effects of hopper geometry. The sidewalls were hinged at the top and their lower extremities were located just above the conveying systems. Later development of the prototype spreader included the addition of a transverse auger for banded application. The prototype featured four load cells (two beam-type units made of two load cells each; model ML-100BC; 44.5 kN capacity; Massload Technologies, Saskatoon, CANADA) placed between the hopper and the main frame for continuous mass measurement of the machine and determination of the mass flow rate. The torque at the power take-off was measured using a torque transducer (Lebow Associates, model 1248H, 20 000 in-lbs capacity, Troy Michigan) and a magnetic velocity sensor was used to measure the rotational velocity of the PTO shaft. A schematic of the 4-auger system is presented in figure 3.1. Table 3.1 presents the characteristics of the prototype land applicator.
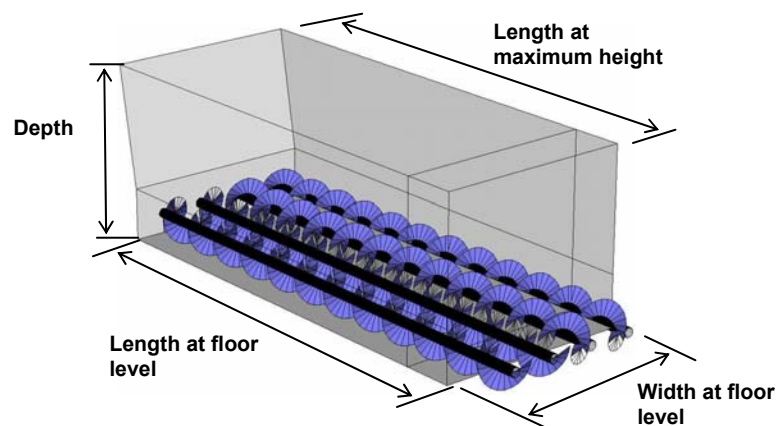
Figure 3.1. **Schematic representation of the 4-auger conveying system (discharge at the right-hand side).**

Table 3.1. Characteristics of the prototype land applicator and of the two conveying systems.

Length at the floor level (m)	3.31
Length at maximum height (m)	3.67
Maximum width at the floor level (m)	1.31
Width at maximum height (m)	1.31
Depth (m)	1.33
Volume (m^3)	6.04
Cross-sectional area (m^2)	1.74
Floor area (m^2)	4.34
Slat interval (mm)	413
Slat height (mm)	38
Auger diameter (mm)	305
Auger flighting pitch (mm)	305
Auger spacing (mm)	324

Experiments were carried out with two types of conveying systems (scraper and system of 4 augers) to evaluate the effect of the discharge conveyor linear velocity (19 and 38 mm/s for the scraper conveyor; 471 and 840 mm/s for the 4-auger system), gate vertical opening (bottom of the gate 0.56 and 1.28 m from the bottom of the hopper) and angle of the sidewalls (0 and 10° from vertical) on power requirements and mass flow rate. The velocity values for the floor conveyors were selected to cover the broadest allowable range for the two systems.

The experiments were carried out using beef feedlot manure that had been stored in swaths for about five months and that had an average total solids concentration (TS) of 57.0% ± 2.8% on a wet mass basis. The manure contained chopped straw and presented large clumps. Enough material was available to run three replications of all treatment combinations in a complete factorial design for each of the conveying systems (three 2-level factors (conveyor velocity, gate height and sidewalls angle)). During the field experiments, the tractor-land applicator system was moving forward at speeds ranging between 1.5 and 3.0 km/h to prevent manure accumulation behind the machine.

An additional series of experiments was carried out at Cemagref to study the effects of the vertical position of the flow-control gate on the discharge rate and power consumption of the scraper conveying system for different organic by-products. The vertical beaters of a commercial manure spreader (corresponding to the machine featuring a narrow, short hopper in the geometry experiments, summarized in table 3.3) were removed, and stationary unloading trials were run. The mass of the tractor-spreader system was continuously recorded by six truck-type scales (50 kN capacity per

scale; Captels, Saint-Mathieu de Tréviers, France). The power requirements of the hydraulically driven floor conveyor were measured by means of a flow meter (270 l/min capacity; Hydrotechnik, London, UK) and a pressure transducer (400 bars capacity; Bourdon-Haenni Ltd, Aldershot, UK). Three different products were used for these experiments and are presented in table 3.2 (three replications of the properties measurements were performed).

Table 3.2. Products used to study the effect of the vertical position of the flow-control gate on the discharge rate and power consumption of the scraper conveying system at Cemagref.

Product description	Total solids concentration (%)		Bulk density (kg/m³)	
	Average	Standard-deviation	Average	Standard-deviation
(1) Feedlot manure with straw stored in the field for approximately 1 year	28.1	11.0	720.9	44.2
(2) Compost of product (1)	29.3	1.0	810.7	23.4
(3) Product (2) after several passes into the spreader and an outside drying period of approximately 3 weeks; designated as dry compost	59.0	0.6	612.0	6.9

3.6.2. Hopper geometry

Three commercial manure spreaders were used in this part of the study. The machines were selected according to the similarity of their spreading system (dual vertical beaters), floor conveyor (hydraulically driven scraper conveyor) and the differences in the geometry of their hopper. Table 3.3 summarizes the characteristics of the machines. A schematic representation of the spreaders is included in figure 3.2. Static spreading tests were carried out and the mass of the tractor-spreader system was continuously recorded by truck-type scales. To obtain the velocity of the floor conveyor, a magnetic displacement sensor was also installed on the floor conveyor of every spreader during the experiments.
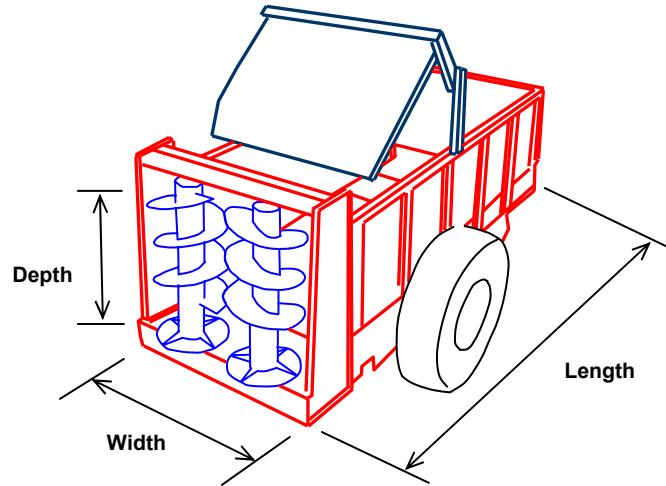
Figure 3.2. Schematic of the spreaders used to study the effect of the hopper geometry.

Table 3.3. Characteristics of the three spreaders used to study the effect of the hopper geometry.

	Narrow hopper		Wide hopper
	Short hopper	Long hopper	Long hopper
Length (m)	3.57	5.85	4.45
Width at the floor level (m)	1.43	1.42	1.94
Width at maximum height (m)	1.63	1.97	1.94
Depth (m)	1.30	1.30	1.15
Volume (m^3)	6.15	10.00	9.50
Cross-section (m^2)	1.74	2.14	2.22
Floor area (m^2)	3.70	7.83	8.61
Angle of the beaters (vs floor) (deg)	75	75	75
Gate	Yes	Yes	No
Slat interval (mm)	425	453	490
Beaters diameter (mm)	690	860	980
Beaters velocity (rpm)	360	380	353

Three different products were used in the hopper geometry experiments and are presented in table 3.4. The first two products (manure and compost) were the same as in the study of the effect of the position of the gate (table 3.2). A more substantial analysis of the products properties was performed for this part of the study. However, no replications of the properties measurements could be performed due to the limited amounts of products available.

Table 3.4. **Products used to study the effect of the geometry of the spreader hopper on the longitudinal uniformity of product distribution and energy requirements.**

Product description	Total solids concentration (%)	Bulk density (kg/m³)	Static friction coefficient on steel[1]	Angle of internal friction[2] (deg)	Apparent cohesion[2] (kPa)
(1) Feedlot manure with straw	28.1	720.9	0.73	19.3	23.0
(2) Compost of product (1)	29.3	810.7	0.63	17.1	7.8
(3) Co-compost of green wastes mixed with fermentable domestic wastes	66.5	1085.0	0.65	42.0	8.8

[1] Measured by the inclined plane method (Mohsenin, 1986);
[2] Determined by the direct shear test.

The global homogeneity was evaluated using an automatic penetrometry method developed at Cemagref (Piron, 2003). The method was developed as a non-destructive means of measuring the consistency and homogeneity of organic by-products stored in swaths. It consists of taking a number of penetrometer readings side by side in the swaths to produce a spatial representation of the measured pressures. The length of the apparatus is 1.2 m and the distance between adjacent readings can be specified by the user (4 cm to 6 cm typically separate adjacent descents giving between 20 and 25 readings). The results can then be analyzed graphically or statistically. Using a data set, the average pressure and its standard deviation can be calculated and used to determine a consistency index as well as a homogeneity index. Those indices allowed for objective comparisons to be made among different products. The measured homogeneity increased from manure to compost and then to co-compost. The calculated heterogeneity indices were 1.11, 0.92 and 0.70 for manure, compost and co-compost, respectively. The feedlot manure was characterized by large clumps structured by intermeshing straw and these clumps were compacted to various degrees, creating a heterogeneous product. At the other end of the spectrum, the co-compost had a fairly well defined and constant particle size and had less internal structure.

3.7. Data analysis

The basis for the analysis of all series of experiments was European Standard EN 13080 (CEN, 2002). The mass was recorded at a frequency of 2 Hz and instant flow rates were calculated for every pair of recorded values of mass. The flow rate results were

then filtered using a fifth order low-pass filter (infinite impulse response filter; Butterworth type; cut-off frequency of 0.0667 Hz). Figures 3.3 and 3.4 illustrate typical mass flow rate and power requirement curves, respectively. A representative plot used for the analysis of the longitudinal distribution obtained with a manure spreader according to Standard EN 13080 is presented in figure 3.5. Several parameters can be calculated from the flow curve. The first parameter used to compare the conveying systems was the characteristic flow rate as outlined in European Standard EN 13080 (CEN, 2002). The characteristic flow rate can be calculated using equation (3.1):

$$s_f = \max_{j=1}^{n-m+1} \left[\frac{1}{m} \sum_{i=j}^{j+m-1} x_i \right] \quad , \quad (3.1)$$

where

s_f = characteristic flow rate (kg/s),

n = number of samples during unloading,

m = number of samples during 30% of the unloading time (m=0.3·n) and

x_i = flow rate at sample i (kg/s).

This parameter is used to assess the amount of material coming out of the spreader as a function of its operating parameters. The characteristic flow rate basically corresponds to the highest average flow rate occurring during 30 percent of the unloading time of the spreader. From the characteristic flow rate, it is possible to define the tolerance zone, which corresponds to the interval of flow rates between -15% and +15% of the characteristic flow rate (fig. 3.5). It is also possible to calculate the stretch within the tolerance zone, corresponding to the percentage of the unloading time during which the momentary flow rates lie within the tolerance zone. The longitudinal coefficient of variation (CV) is calculated based on the average flow rate and its standard deviation. It is used to evaluate the variability of the flow rate during the unloading of the machine. Another comparison criterion makes use of the power data to calculate the specific energy required by the conveying systems during the unloading operation. The specific energy is calculated using equation (3.2):

$$E_{unloading} = \frac{\int_0^{t_{unloading}} P(t)dt}{M} \quad , \qquad (3.2)$$

where

$E_{unloading}$ = specific energy of the unloading operation (J/kg),

$t_{unloading}$ = unloading time of the spreader (s),

$P(t)$ = power consumption of the floor conveyor as a function of time (W) and

M = mass of product unloaded (kg).

The specific energy values allowed for comparisons to be made between the different sets of operating parameters independently of the initial mass of product present in the machine at the beginning of the experiments.
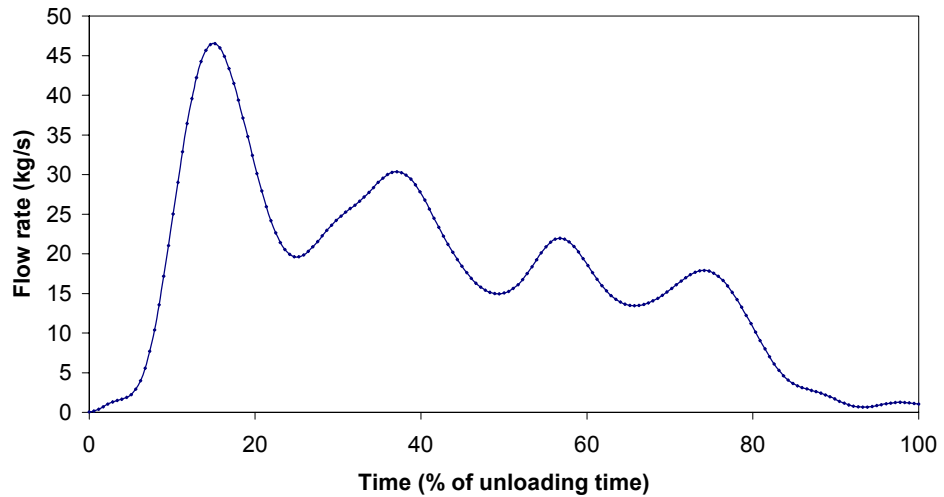
Figure 3.3. **Mass flow rate as a function of time (test carried out at the University of Saskatchewan with the 4-auger system operated at 839.5 mm/s and with the bottom of the gate 0.56 m above the spreader floor).**
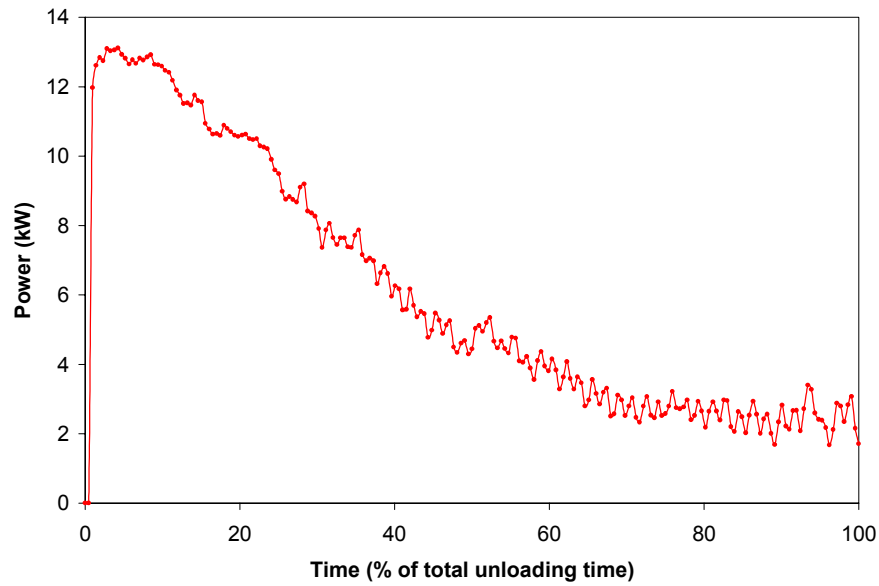
Figure 3.4.   Power requirements of the floor conveyor as a function of time (test carried out at the University of Saskatchewan with the 4-auger system operated at 839.5 mm/s and with the bottom of the gate 1.28 m above the spreader floor).
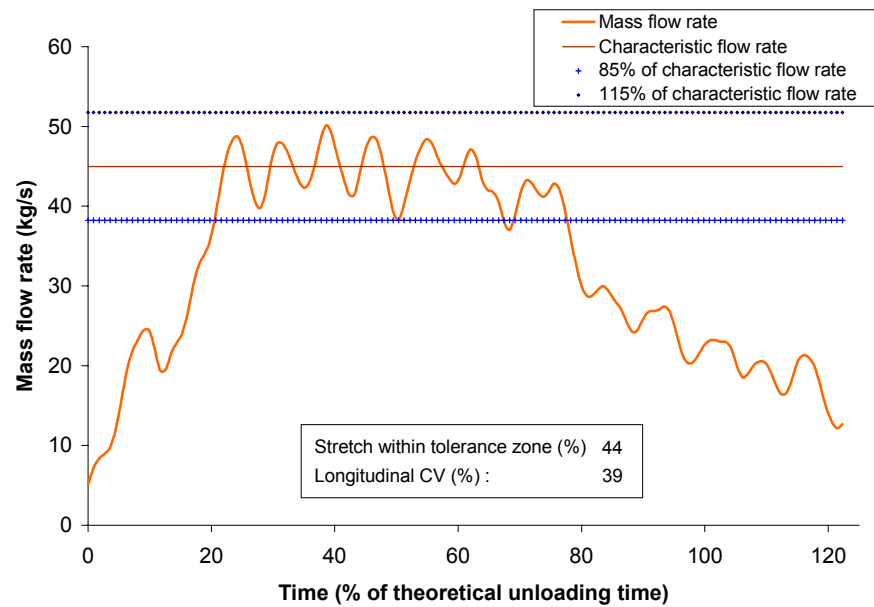
Figure 3.5.   Longitudinal distribution curve (static spreading trial carried out at Cemagref with the machine having a narrow and long hopper; with compost).

112

3.8. Results and discussion

3.8.1. Conveying systems

3.8.1.1. Effects of flow-control gate and sidewall inclination (scraper and auger conveying systems)

Figures 3.6 and 3.7 summarize the results obtained for the power requirements of the conveying systems as well as their characteristic flow rate, for the experiments carried out at the University of Saskatchewan with beef feedlot manure. The experimental results for both the specific energy and characteristic flow rate were analyzed using least squares regression estimations. The results of the statistical analysis indicated a significant effect of the gate opening on the specific energy for both conveying systems at the 5% level. The characteristic flow rate of the scraper conveyor was significantly affected by the gate, the velocity of the conveyor and the inclination angle of the sidewalls. In the case of the characteristic flow rate of the 4-auger system, the significant factors were the gate, the velocity of the conveyor and the interaction between these two parameters.

The 4-auger system required significantly more energy to move the mass of manure out of the spreader when compared to the scraper conveyor. As expected, the usage of a flow-control gate had a significant effect on the power required to unload the spreader, as reflected by the values of specific energy. The effect of the gate was significant for both conveying systems.
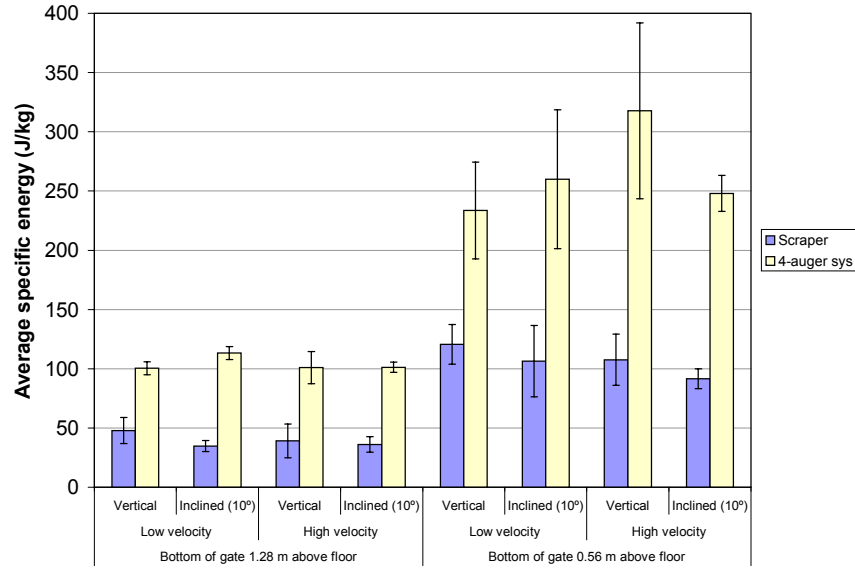
Figure 3.6.   Specific energy required by the conveying systems for the unloading of the spreader as a function of the operating parameters (the error bars correspond to the standard deviation; vertical and inclined at 10º refer to the sidewalls; the low velocity corresponds to 19 mm/s and 471 mm/s for the scraper conveyor and the system of 4 augers, respectively; the high velocity corresponds to 38 mm/s and 840 mm/s for the scraper conveyor and the system of 4 augers, respectively).
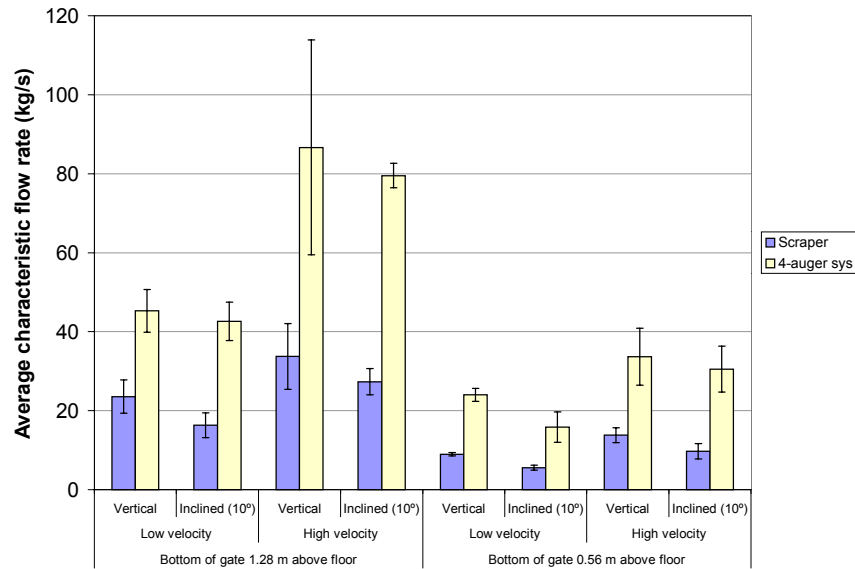
Figure 3.7.   Characteristic flow rate obtained for the unloading of the spreader as a function of the operating parameters (the error bars correspond to the standard deviation; vertical and inclined at 10º refer to the sidewalls; the low velocity corresponds to 19 mm/s and 471 mm/s for the scraper conveyor and the system of 4 augers, respectively; the high velocity corresponds to 38 mm/s and 840 mm/s for the scraper conveyor and the system of 4 augers, respectively).

114

The analysis of the characteristic flow rate is more complex. A qualitative analysis based on a number of field and laboratory observations is included in the next section. It should be understood that European Standard EN 13080 (CEN, 2002) is intended for the analysis of the results of spreading tests, as defined by the standard. This study targeted the evaluation of conveying systems and hopper geometries and, as a result, did not correspond entirely to the tests and test conditions described in the standard. Nevertheless, the machines produced flows that were dependent upon their operational parameters, and these flows can be characterized using the criteria included in European Standard EN 13080 (CEN, 2002). The standard becomes a tool to analyze with consistency the results obtained during the field experiments. In this case where the focus was on the unloading of the hopper by the conveying system, the characteristic flow rate gives a numerical value to describe the discharge flow rate curves. The statistical analysis suggested that the gate vertical position, the velocity of the conveyor and the angle of the sidewalls all influenced the characteristic flow rate obtained when the scraper conveyor was used. As one would expect, the characteristic flow rate was higher when the gate was at its high position and when the conveyor was operated at the high velocity setting. For the angle of the sidewalls, the reduction of the flow section resulting from the inclination of the side walls caused the characteristic flow rate to become significantly smaller when compared to the results obtained with vertical sidewalls. The flow section when the bottom of the gate was at 0.56 m above the bottom of the hopper and the sidewalls were vertical, including the cross-section of the conveyors themselves, was 0.73 m^2. When the bottom of the gate was at 1.28 m above the spreader floor, this cross-section increased to 1.68 m^2. With the sidewalls inclined 10º from vertical and the bottom of the gate 0.56 m above the bottom of the hopper, the cross-section of the opening was 0.53 m^2 and 0.54 m^2 for the scraper conveyor and the 4-auger system, respectively. Raising the bottom of the gate to 1.28 m above the bottom of the hopper increased the flow section to 1.37 m^2 and 1.38 m^2 for the scraper and 4-auger conveying system, respectively. No clear relationships could be established between the reduction in flow section and the decrease in flow rate, except for the scraper conveyor operated at 38 mm/s. For the case of the gate at 1.28 m above the bottom of the hopper, the reduction in flow section of 18.5% caused by the

115

inclination of the sidewalls resulted in a reduction of 18.9% of the flow rate. When the gate was 0.56 m above the bottom of the hopper, a reduction of 27.4% in flow section resulted in a reduction of 29.6% in flow rate.

The results obtained with the 4-auger system indicated significant effects of the gate vertical position and conveyor velocity. The statistical analysis also highlighted the interaction of conveyor velocity and gate opening. At the high velocity setting, the effect of the vertical position of the gate on the characteristic flow rate became more important. The 4-auger system featured 2 augers with left-hand flighting next to 2 right-hand augers. This promoted the flow of product towards the center of the spreader, making the effect of the angle of the sidewalls less significant, as indicated by the results of the statistical analysis.

Based on the operating parameters of the spreader, it was possible to calculate the theoretical flow rate of the machine assuming there is no shearing in, or crumbling of, the volume of product, i.e. the manure moves as a block. A density value of approximately 300 kg/m^3 was obtained by dividing the average mass of product spread during the experiments by the volume of the hopper. This density value was used along with the linear velocity of the conveying systems and the flow section to calculate the theoretical flow rates. The actual flow rates were always inferior to the theoretical flow rate, indicating the bulk of manure is not ideal and includes crumbling and shearing effects.

3.8.1.2. Effects of flow-control gate (scraper conveying system)

Figures 3.8 and 3.9 summarize the results obtained at Cemagref for the specific energy and characteristic flow rate as a function of the vertical position of the flow-control gate for different organic by-products. The experiments were not performed with manure at the lowest gate height due to magnitude of the force that would be transmitted to the gate. Also, the available amounts of products did not allow for replications of the experiments to be carried out. The results obtained confirmed the effect of the flow-

control gate concluded from previous experiments (section 3.8.1.1). As the gate was lowered, the energy required to unload the spreader increased and the characteristic flow rate decreased for all products. When looking in greater detail at the values of the characteristic flow rate, one can observe that a reduction of approximately 42% of the flow section (the gate was moved down from 1300 mm to 750 mm) induced a reduction of 51%, 46% and 41% in the characteristic flow rate of manure, compost and dry compost, respectively. When the flow section was further reduced by approximately 31% (the gate was further lowered from 750 mm to 515 mm), the characteristic flow rate decreased by 32% for both compost and dry compost.
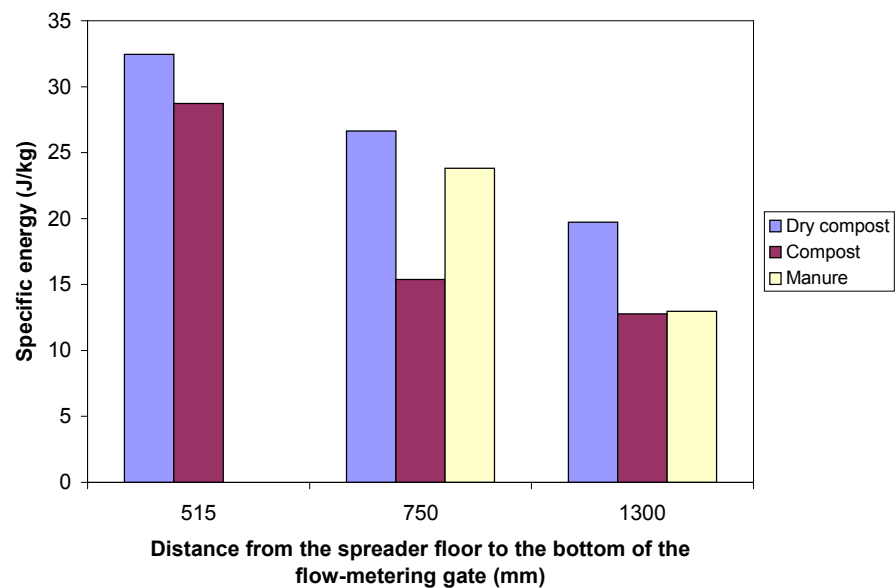
Figure 3.8.   Specific energy required by the scraper conveyor to unload the spreader as a function of the vertical position of the flow-control gate for three different products. Results from a single experimental run.

117
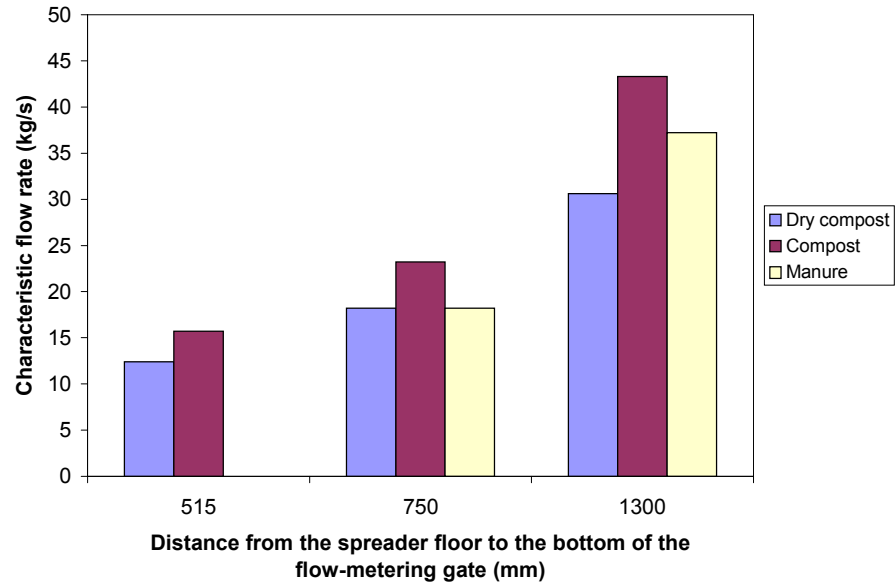
Figure 3.9. Characteristic flow rate obtained for the unloading of the spreader as a function of the vertical position of the flow-control gate for three different products. Results from a single experimental run.

3.8.1.3. Qualitative analysis

During the experiments, several observations were made that can now be related to the measured data. With the gate fully open or close to fully open, the volume of product would somewhat move as a unit until it reached the end of the spreader and crumbled on the ground. With the gate lowered, the flow of manure was much more even with less crumbling. This translated in a clear smoothing effect on the flow rate curves. The theoretical unloading time was calculated based on the theoretical flow rate and hopper volume. The differences between the actual and theoretical unloading times were consistently higher for the 4-auger system, for all the experimental runs, when compared to the scraper conveyor. The actual times were also consistently higher than the theoretical times for that conveying system (the actual unloading time was 153% of the theoretical time on average), indicating a greater shearing of the product since the crumbling phenomenon was observed to be comparable to what occurred with the scraper conveyor. This can in turn be related to the higher energy requirement of the 4-auger system. It was also observed that the product was, to a certain degree, processed by the augers, especially when the gate was low. The analysis of the action of both conveyors in terms of their active surface area and the consequent magnitude of

118

shearing force confirms the observations made and the data measured during field experiments. In the absence of the spreading systems, the stretch within the tolerance zone and longitudinal coefficient of variation were not analyzed in detail for the experiments targeting the performances of the conveying systems.

3.8.2. Hopper geometry

Three phases can be identified on the discharge flow curves (fig 3.5): (1) a phase of increasing flow rate, associated to the "loading" of the beaters, having a length proportional to the distance between the gate and the beaters; (2) an intermediate "constant" flow rate phase; (3) a phase of decreasing flow rate that lasts until the end of the unloading of the spreader. A visual analysis of the flow rate curves revealed that a product with less internal structure, indicated by a small value of cohesion, produced a shorter constant flow rate phase, and a longer phase of decreasing flow rate. This observation was independent of the hopper geometry. Also, the more heterogeneous the product, the noisier the flow rate curve was.

Figures 3.10, 3.11 and 3.12 summarize the results obtained for the hopper geometry experiments. The amount of compost available did not allow for the experiments with the machine featuring a wide and long hopper to be carried out. Therefore no data could be collected for that machine-product combination. Some effects of the hopper geometry on the evaluation criteria, namely stretch within the tolerance zone, longitudinal coefficient of variation and unloading time, can be observed from the values presented in these three figures. An increase in hopper length translated in higher values of stretch within the tolerance zone, resulting in less variation of the application rate in the field. The same effect was observed with an increase in hopper width. The longitudinal coefficient of variation decreased as the hopper went from narrow and short to narrow and long. It was further reduced when using a wide and long hopper. The actual unloading time, expressed as a percentage of the theoretical unloading time, consistently decreased when going from a short to a long hopper, with the exception of the product having the smallest cohesion (co-compost). With the

hopper height being equivalent, the crumbling of the volume of product at the beater-end of the machine happened over an equivalent longitudinal distance, regardless of the width of the machine. Also, the longer the unloading time, which increased with the hopper length, the smaller the ratio of the time required to evacuated the crumbled product to the total unloading time was. This attenuation of the effect of the crumbling events on the total unloading time made it closer to the theoretical unloading time. This explains the lower ratios of actual to theoretical unloading time observed when using a longer machine.

A mechanical parameter inherent to the spreader that can explain the improvement in the evaluation criteria for the wider machine is the absence of a gate. A more even loading of the spreading system (beaters) was observed for the spreader not fitted with a gate, favouring the even flow rate phase of the longitudinal distribution curve, which in turn benefited the stretch within the tolerance zone and the longitudinal coefficient of variation. Since the depth of the machines tested did not vary significantly, the effect of that parameter was studied by conducting spreading trials with the narrow and short hopper half-full. The results were very much affected by the depth of the hopper with values of stretch within the tolerance zone twice as large on average as the values obtained with the hopper full. The longitudinal coefficient of variation also decreased with the hopper depth. Crumbling events of lesser importance at both ends of the spreader, associated with an inferior depth of product in the machine, contributed to improve the duration of the even flow rate phase. With the total unloading time only slightly affected by the reduction of hopper depth, this effect translated into better results in terms of stretch within the tolerance zone and longitudinal coefficient of variation.

The effects of the hopper geometry on the flow coming out of the machines are not independent from the characteristics of the product spread. Highly cohesive products allowed for higher values of stretch within the tolerance zone when compared to non-cohesive products (fig. 3.10). The greater duration of the decreasing flow rate phase at the end of the unloading process in the case of products with low cohesion values was

detrimental to this criterion. Non-cohesive products crumbled, regularly or by intermittent crumbling events, while more cohesive products moved as a block. As a result, the durations of the increasing and decreasing flow rate phases were inferior for cohesive products. This translated into less variation in the flow rate and better values of stretch within the tolerance zone. The longitudinal coefficient of variation and unloading time, expressed as a proportion of the theoretical unloading time, were always greater when spreading non-cohesive products as compared to more cohesive products. The non-cohesive products exhibited a more homogenous particle size distribution, resulting in less instant variations of the flow rate.
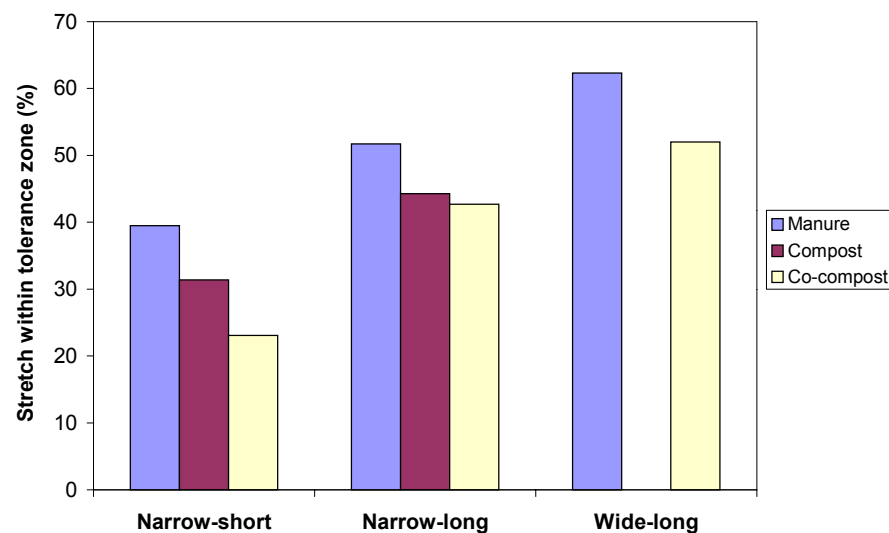
Figure 3.10.   Effect of hopper geometry and product type on the stretch within the tolerance zone. Results from a single experimental run.
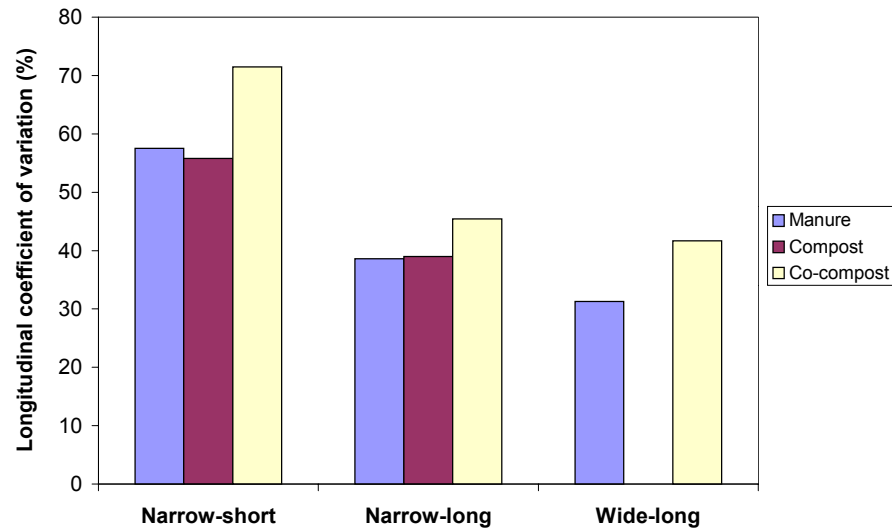
Figure 3.11. Effect of hopper geometry and product type on the longitudinal coefficient of variation. Results from a single experimental run.
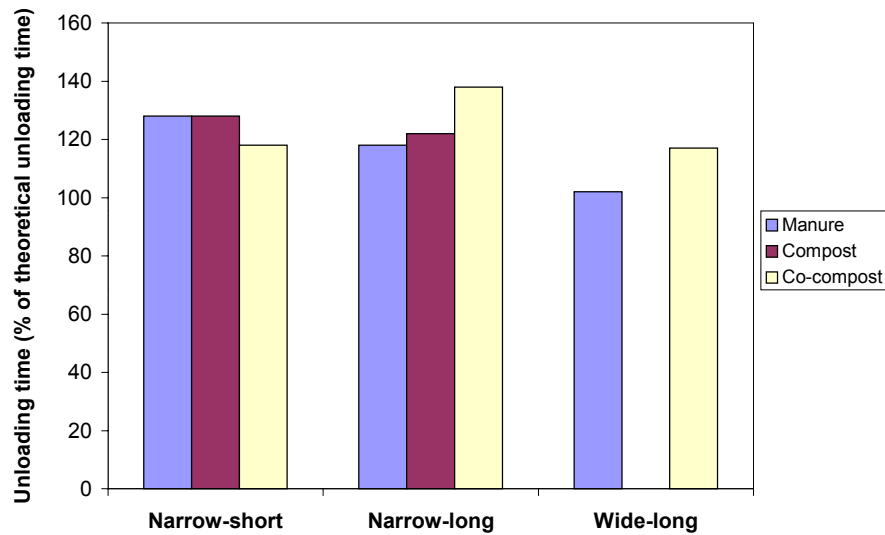
Figure 3.12. Effect of hopper geometry and product type on the unloading time expressed as a percentage of the theoretical unloading time. Results from a single experimental run.

When comparing the results obtained from the experiments aimed at evaluating the performances of the conveying systems to those yielded by the hopper geometry tests, it was observed that the spreading devices had a regulating effect on the flow. The values of the coefficient of variation were somewhat higher when the spreading devices were

removed. The values of stretch within the tolerance zone were rather low since the crumbling events were not attenuated by the spreading devices. The 4-auger system seemed to perform better than the scraper conveyor, with an average value of longitudinal CV of 58% compared to 75% for all the experimental runs. This can again be related to the shearing and "processing" action of the augers on the product.

Using the data collected for the second specific objective, the coefficient of variation of the longitudinal distribution can be studied and related to the results obtained from the hopper geometry experiments. The results obtained at Cemagref highlighted an important effect of the gate on the longitudinal coefficient of variation (table 3.5). The longitudinal CV obtained when unloading dry compost with fine homogeneous particles was the most affected by the vertical position of the gate. This is consistent with the observation made on the behaviour of cohesive and non-cohesive products, and on the smoothing effect of the gate on the flow curves.

Table 3.5. Longitudinal coefficient of variation as a function of the vertical position of the gate and of the product spread (experiments carried out at Cemagref with the spreader featuring a narrow and short hopper, without beaters).

Distance from the spreader floor to the bottom of the gate (mm)	Longitudinal coefficient of variation (%)		
	Manure	Compost	Dry compost
1300	70.5	82.1	60.8
750	51.1	43.6	35.6
515	n.a.[1]	41.8	24.0

[1] Data not available

3.9. Conclusions

Experiments were carried out to gain an enhanced understanding of the flow of organic by-products in land application equipment. The focus was on the conveying and holding systems. The performances of two types of conveying systems for manure spreaders have been investigated. The results indicated that:

- the 4-auger system designed at the University of Saskatchewan required more energy to unload manure out of the spreader, when compared to the scraper conveyor.

123

- The specific energy requirements of both the scraper conveyor and the 4-auger system were significantly affected by the vertical position of the flow-control gate.

- The characteristic flow rate obtained with the scraper conveyor was significantly affected by the position of the gate, the velocity of the conveyor and the angle of the sidewalls.

- The characteristic flow rate produced by the 4-auger system was significantly influenced by the position of the gate and the velocity of the augers. There was also a significant effect of the interaction between gate position and conveyor velocity.

3.9.1. Observations

Experiments similar to those carried out to study conveying systems were performed using a manure spreader of larger capacity featuring a similar scraper conveyor. The results from single runs indicated a relation between the vertical position of the gate and the specific energy and the characteristic flow rate for three different products. A relationship was also observed between the reduction in the flow section and the reduction of the characteristic flow rate for manure, compost and dry compost.

The effect of the geometry of the spreader holding system was studied. The main observations were:

- the stretch within the tolerance zone, which corresponds to the percentage of the unloading time during which the momentary flow rates lie within plus or minus 15% of the characteristic flow rate, was observed to increase with an increase in the length and the width of the hopper.

- The mass flow rate longitudinal coefficient of variation was observed to decrease when the length of the hopper was increased. The same effect was observed when increasing the width of the hopper and when reducing its depth.

- The physical properties of the product spread had an influence on the flow curves. Cohesive products generated better values for the stretch within the tolerance zone, the longitudinal coefficient of variation and the unloading time expressed as a percentage of the theoretical unloading time.

The amount of engineering data related to the design and operation of land application equipment for solid organic fertilizers is very limited. Research studies focusing on such data have to face very heavy experimental setups. It is therefore extremely important to disseminate the research results so the scientific community can build on the acquired knowledge. The results of the research reported herein allowed for a better understanding of the flow of organic fertilizers in land application equipment and of the roles of the conveying and holding systems. They include numerical values of specific energy and mass flow rates in relation to the operating parameters of the machine and the properties of the product spread.

3.10. Acknowledgements

3.11. References

Bulinski, J and J. Klonowski. 1998. Analysis of power requirement for manure spreader working units. Annals of Warsaw Agricultural University, No. 33, 27-32.

CEN. 2002. European Standard EN 13080: Agricultural machinery – Manure spreaders – Environmental protection – Requirements and test methods. CEN, European Committee for Standardization.

Ling, Q. and J.H. Wilhoit. 1999. Power requirements of spinner-type spreaders broadcasting poultry litter and wood ash. Applied Engineering in Agriculture, 15(5): 405-409.

Ling, Q., J.H. Wilhoit and L.J. Kutz. 1996. Effect of material metering on the performance of a spinner-type spreader broadcasting poultry litter. New trends in farm machinery development and agriculture, 41-49, Society of Automotive Engineers, Warrendale, PA.

Chapter 4

Discrete Element Representation of Manure Products

4.1. Significance

The application of the discrete element method to manure handling poses the challenge of selecting the properties of the virtual material to create a representative model of the physical material. As discussed in the literature review presented in chapter 1, a calibration procedure must be applied to determine those properties. It would seem reasonable to think that defining how manure products are modeled should be the very first step of the research work presented in this thesis. However, as the modeling method was adapted and applied to manure products, advancements in numerical manure models had to be tested and validated using machine-product interaction models. This created an iterative and parallel approach rather than a linear progression from manure models to interaction models. This chapter, which corresponds to objective 4, details how manure products are modeled in PFC^{3D}.

4.2. Abstract

To develop models of the machine-product interactions taking place in land application equipment, models of manure products must be developed and validated. Several parameters must be defined to appropriately represent organic by-products in the discrete element method framework. The work reported herein was aimed at

127

determining the properties of the virtual product that would allow mimicking the behaviour of manure in the DEM software PFC^{3D}. A code was developed to generate a user-defined particle size distribution, as would be measured by screening, to fill the domain under investigation. The output of the code was very close to the user specifications with errors on the number of particles and on their size averaging 0.53% and 0.33%, respectively. A procedure was also developed to create clusters of particles randomly oriented and located within the modeled domain. The cluster-generation code was tested for clusters made of up to six particles, but could be expanded to include more particles. A calibration procedure based on a virtual direct shear test was developed to define the properties of the resulting virtual manure. A sensitivity analysis was performed to study the influence of parameters defining the linear and Hertz-Mindlin contact constitutive models. The simulations were based on experimental results obtained for pig manure at a total solids concentration of 48%. The results showed that numerous parameters have an influence on the behaviour of the virtual product in the direct shear test. Implementing the measured particle size distribution for pig manure at 48% TS, a friction coefficient of 0.8 and a Young's modulus value of 0.3 MPa allowed reaching an angle of internal friction of 27.4º and an apparent cohesion value of 25.1 kPa that favourably compared to the 24.5º and 16.5 kPa values measured experimentally.

4.3. Introduction

Land application is known to be a beneficial method of recycling agricultural by-products. However, uncontrolled application of organic fertilizers can become an environmental hazard. The machinery that is used to handle and land apply organic fertilizers needs to be improved to better control the application rates and distribute the product more evenly to the cropped land.

The flow behaviours of organic fertilizers in handling and land application machines are not well comprehended. As a result, the possible improvements on these types of equipment are very limited as they largely depend upon an adequate understanding of

the machine-product interactions taking place in such machines. With the ever increasing availability of computational resources, numerical modeling is becoming very popular and has been identified as a means of getting important insights into the flow of manure in handling and land application machinery, insights that would be very difficult to obtain experimentally. The Discrete Element Method (DEM) constitutes one promising numerical method for the modeling of manure products and that of machine-manure interactions.

In the DEM, the trajectory of each constituent particle in an assembly is calculated based on all the forces acting on it and by integrating Newton's second law of motion along with the kinematic equation for position and orientation. This modeling method has been successfully applied to many applications involving the flow of granular materials. The objective of the work reported herein was to develop models of manures in the DEM code PFC^{3D} (Itasca Consulting Group Inc., Minneapolis, USA).

4.4.   Literature review

A challenge common to the vast majority of research studies involving the DEM is the choice of appropriate input parameters. It is often difficult to choose a set of properties that will make the behaviour of the virtual material similar to that of the physical material. A code like PFC synthesizes macro-scale material behaviour from the interactions of micro-scale components and the input properties of the microscopic constituents are usually unknown. The responses that characterize the relevant behaviours must first be determined and then the appropriate microproperties must be selected by means of a calibration process (Itasca, 2003). In the calibration process, the responses of the virtual material are compared directly to the relevant measured responses of the intended physical material. This calibration procedure can target laboratory and field-scale events, depending upon the application of the model. In PFC, the model parameters generally cannot be related directly to a set of relevant material properties because the behaviour of the PFC model is also affected by particle size and packing arrangement. The relation between the numerical model parameters and

commonly measured material properties is only known *a priori* for certain simple packing arrangements. For the general case of arbitrary packing and size distribution, the relation is found by means of the calibration process in which a particular instance of a PFC model is used to simulate a set of material tests. The numerical model parameters are then chosen to reproduce the relevant material properties as measured in such tests. Although the behaviour of the PFC model is found to resemble that of the physical material, in general, the PFC particle is not associated with an elementary constituent of the physical material. The assembly of bonded particles is a valid microstructural model in its own right and should not be confused with the microstructure of the physical material (Itasca, 2003).

The discussion presented by Oreskes et al. (1994) suggested that it is impossible to fully verify and validate any numerical model of a natural system. Numerical models are representation of physical systems that are useful for corroborating hypotheses, elucidating discrepancies in other models, performing sensitivity analyses, supporting design decisions and guiding further study (Itasca, 2003). When the predictions of numerical models agree with observations and measured data on the physical system, the likelihood that the models are correct increases and generally warrants acceptance.

Mishra and Murty (2001) discussed the importance of selecting appropriate parameters for realistic DEM simulations of ball mills. They mentioned that DEM modeling can only be successful if the parameters of the models are determined correctly. These parameters not only influence the critical time step used in the simulations, but they affect the accuracy of the quantitative results. Mishra and Murty (2001) stressed the fact that the issue of parameter selection is not properly addressed in the literature and that it is important to seek a compromise between numerical accuracy and computational cost. They developed a three-dimensional DEM code to compare the performance of various contact models to simulate the ball mill system. Experimental data on drop ball tests showed that the deformation behaviour of the contact is non-linear. The non-linear contact model parameters were determined by matching the model response with the experimental data. The non-linear model performed well in

terms of predicting the energy dissipated during collisions, but was computationally demanding due to the high value of the associated contact stiffness parameter. A linearization method was applied to the model to circumvent the problem resulting in a stiffness value two orders of magnitude lower. Simulations were run to compare the linear, equivalent linear and non-linear models. All three models predicted the peak power within 5%, but the utilization of low values for the contact stiffness led to excessive amounts of deformation and to improper predictions of the peak force.

Di Renzo and Di Maio (2004) compared three mechanical models for the simulation of elastic frictional collisions. The results of the simulations were microscopically compared to analytical solutions and macroscopically to experimental results. The first model was a linear model based on a Hooke-type relation. The second model was a non-linear model based on Hertz theory in the normal direction and on the no-slip solution of the theory developed by Mindlin and Deresiewicz (1953) for the tangential direction. Finally, a non-linear model with hysteresis based on the complete theory of Hertz and Mindlin and Deresiewicz (1953) for elastic frictional collisions was included. The macroscopic comparison showed that the agreement of the linear model was good, indicating that no significant improvements can be attained using the Hertz&Mindlin-Deresiewicz model with no-slip (H-MDns) or the Hertz&Mindlin-Deresiewicz model (H-MD). The evolution of the normal and tangential forces, velocities and displacements predicted by the three models during a collision was compared to an analytical solution developed by Maw et al. (1976). In these comparisons, the H-MD model was closer to the analytical solution. The H-MDns model was deemed worse than the linear model with regard to these results. The precision of the linear model was however dependent upon precise evaluation of its input parameters. The non-linearity and micro-slip effects were deemed important if deeper analyses of the motion of granular materials or of systems that are sensitive to the actual force or displacement are performed. Di Renzo and Di Maio (2004) recommended that, in these cases, more accurate models such as the H-MD model should be addressed.

Masson and Martinez (2000) studied the flow from a rectangular silo for different values of particle mechanical parameters in DEM simulations. The DEM wall pressures at the end of the filling were in agreement with experimental and macroscopic numerical results obtained by FEM. The analytical and FEM results provided a validation of the DE simulations for their capacity to reproduce a quasi-static stress field at the filling stage that is qualitatively and quantitatively consistent with classical macroscopic results. The friction coefficient and contact stiffness appeared to have an important influence in the contact network connectivity, macroscopic porosity, stress anisotropy within the granular material and the magnitude and heterogeneity of wall pressure. These particle microscopic parameters also had an influence on the flow kinematics and stresses during discharge.

Tripodi et al. (1992) reviewed several constitutive models for cohesive particulate materials. They included constitutive models based on both microscopic concepts and continuum principles. The criteria used to analyze the models were time dependency, path dependence and physically representative parameters. Numerous comments were included to the effect that for several models, no explanation is provided as how to determine the input parameters. A parallel between soils and other agricultural products was made. References are cited where sand models were used for wheat (Zhang et al., 1986; Li et al., 1990), results for wheat, sugar and lentils were in a form consistent with sands and clays (Feda, 1982), and sugar and flour showed trends similar to clays (Kamath et al., 1991). Tripodi et al. (1992) concluded that based on their evaluation criteria, three candidate models could be considered. The modified Cam-clay model (Desai and Siriwardane, 1984) was deemed a candidate because it was the foundation for numerous other models and its parameters have clear physical representations. The elastoplastic model of Adachi and Oka (1982) was also selected as it was the most complete critical state model and had the potential to be very versatile and accurate in predicting the load-deformation behaviour of powders. The final model selected was the endochronic model (based on thermodynamic theory instead of plasticity) developed by Krizek et al. (1978), because of its fundamental soundness and flexibility.

Oida et al. (1998) studied the effect of several input parameters on the results of their simulation of soil deformation and reaction under a track shoe using the DEM. They tried different combinations of stiffness and specific gravity values. They also investigated the effect of the number of particles and of the friction coefficient on the simulation results. Oida et al. (1998) observed that the simulated soil deformation approached the actual deformation pattern as the stiffness in the model increased. The simulated soil reaction force also increased as the stiffness and the specific gravity increased. An influence of the ratio of stiffness to specific gravity on the stability of the simulation was observed. Oida et al. (1998) concluded that there was no significant difference among the results obtained for the various numbers of elements tested. The soil reaction force was dependant upon the coefficient of friction while the soil deformation did not seem to be affected by that parameter. Oida et al. (1998) finally concluded that an increase in stiffness and specific gravity allowed the simulated reaction force to be the same as the force measured in a soil bin.

4.5. Modeling approach

This section first details the contact-constitutive model at the particle level. Background information on how PFC^{3D} encompasses the constitutive model and on relationships between selected input parameters is given. The approach developed to implement some macroscopic aspects of organic by-products in the models is then presented. The last part of the section dedicated to the modeling approach explains the virtual testing environment, which is the backbone of the calibration procedure referred to in the previous sections.

4.5.1. Input parameters

4.5.1.1. Contact model

As mentioned, the objective of this work is to determine how manures can be modeled in PFC^{3D} (version 3.0). In turn, the manures models will be used to study machine-product interactions in handling and land application equipment using the same DEM

code. It is then important to model the behaviour of manure products on a macroscopic scale. In PFC^{3D}, the overall constitutive behaviour of a material is replicated by associating a constitutive model with each contact.   The constitutive model acting at a contact consists in a stiffness model, a slip model and a bonding model (Itasca, 2003).

The contact stiffnesses relate the contact forces and relative displacements in the normal and shear directions. The normal stiffness (K^n) is a secant (symbolized by a capital letter) stiffness since it links the total normal force (F_i^n) to the total normal displacement (U^n) (eq. 4.1.), while the shear stiffness (k^s) is a tangent stiffness (symbolized by a small case letter) as it relates the increment of shear force (ΔF_i^s) to the increment of shear displacement (ΔU_i^s) (eq. 4.2.). The relationships are

$$F_i^n = K^n\, U^n\, n_i \qquad \text{and} \qquad (4.1)$$
$$\Delta F_i^s = -k^s \Delta U_i^s \qquad , \qquad (4.2)$$

where n_i is the unit normal vector to the contact plane. PFC^{3D} gives the user the choice of two built-in contact-stiffness models: a linear model and a simplified Hertz-Mindlin model.

4.5.1.1.1. Linear contact model

The linear contact model in PFC^{3D} is defined by the normal and shear stiffnesses k_n and k_s of the two entities in contact. The contact stiffnesses for the linear contact model are computed assuming that the stiffnesses of the two contacting entities act in series (equations 4.3 and 4.4):

$$K^n = \frac{k_n^A k_n^B}{k_n^A + k_n^B} \qquad \text{and} \qquad (4.3)$$

$$k^s = \frac{k_s^A k_s^B}{k_s^A + k_s^B} \qquad , \qquad (4.4)$$

where the superscripts A and B refer to the two entities in contact. The choice of the stiffnesses values is somewhat critical and complex. Di Renzo and Di Maio (2004) highlighted the fact that the method for the evaluation of the parameters in the linear

model has received very little attention in the literature. They proposed a method to calculate the ratio (K) of initial tangential stiffness (k_{t0}) to normal stiffness (k_n) based on the mechanical properties of the material (equation 4.5):

$$K = \frac{k_{to}}{k_n} = \frac{\dfrac{(1-v_i)}{G_i} + \dfrac{(1-v_j)}{G_j}}{\dfrac{(1-0.5v_i)}{G_i} + \dfrac{(1-0.5v_j)}{Gj}} \quad , \qquad (4.5)$$

where indices i and j refer to the first and second entity in contact, v is the Poisson's ratio (dimensionless) and G the shear modulus (MPa). It is suggested that k_n be determined based on the non-linear force-displacement relations and k_s calculated from the ratio K. The suggested method of obtaining k_n is by taking the derivative of the forces with respect to the corresponding displacements, calculated at a certain normal displacement. Di Renzo and Di Maio (2004) suggested that the common practice of choosing equal stiffnesses in the normal and tangential directions may influence the performance of the model. In their simulation of squeeze molding of green sand, Maeda et al. (2003) used a stiffness in the tangential direction that was 0.2 times the stiffness in the normal direction according to the law of Mindlin and Deresiewicz (1953).

Mishra and Murty (2001) outlined that it is quite common to limit the maximum anticipated overlap x_{max} to a small fraction of the particle diameter d and define the contact stiffness as:

$$k=(f^2 \, m \, v_0^2)/d^2 \qquad , \qquad\qquad (4.6)$$

where m is the mass of the particle, v_0 is an estimated maximum velocity of any particle in the system and f is the penetration factor defined by d/x_{max}. Mishra and Murty (2001) also suggested that the contact stiffness for the case of two spheres of the same material

and size could be determined based on the Young's modulus (E), the Poisson's ration
(v) and the radius of the contact area (r):

$$k = \frac{E\sqrt{2r}}{3(1-v^2)} \quad .$$ (4.7)

Both equation 4.6 and 4.7 require detailed knowledge of the contact or the system,
whether it is the radius of the contact area or the anticipated maximum velocity of the
particles. They become somewhat useless when attempting to model products having
undefined behaviours or for which the properties are not well known. It has also been
suggested (Itasca, 2003) that the stiffnesses be determined using the following equation:

$$k_n = k_s = 4\, E\, R_p \, ,$$ (4.8)

where R_p is the radius of the particle.

4.5.1.1.2. Hertz-Mindlin model

The simplified Hertz-Mindlin model included in PFC^{3D} is a non-linear contact model
defined by the shear modulus (G) and the Poisson's ratio (v). The Hertz-Mindlin model
is not defined for spheres that are in tension and thus is not compatible with contact
bonding. For ball-ball interactions, the elastic properties are taken to be the mean
values. For ball-wall interactions, the wall is assumed to be rigid and the elastic
properties of the ball are used. For the Hertz-Mindlin contact model, the shear modulus
can be calculated from the Young's modulus and Poisson's ratio using equation 4.9:

$$G = E / (2(1+v)) \quad .$$ (4.9)

The contact normal secant stiffness is given by

$$K^n = \left(\frac{2\langle G\rangle \sqrt{2\tilde{R}}}{3(1-\langle v\rangle)} \right)\sqrt{U^n} \quad ,$$ (4.10)

and the contact shear tangent stiffness is given by

$$k^s = \left(\frac{2\left(\langle G \rangle^2 3(1-\langle \upsilon \rangle)\tilde{R}\right)^{1/3}}{2-\langle \nu \rangle} \right) |F_i^n|^{1/3} \qquad . \qquad (4.11)$$

where U^n is the sphere overlap and $|F_i^n|$ is the magnitude of the normal contact force. The multipliers in equations 4.10 and 4.11 are a function of the geometric and material properties of the two entities in contact as described in equation 4.12, 4.13 and 4.14:

$$\tilde{R} = \begin{cases} \dfrac{2R^A R^B}{R^A + R^B} & \text{for ball} - \text{to} - \text{ball contact} \\[2em] R^{ball} & \text{for ball} - \text{to} - \text{wall contact} \end{cases} , \qquad (4.12)$$

$$\langle G \rangle = \begin{cases} \dfrac{1}{2}\left(G^A + G^B\right) & \text{for ball} - \text{to} - \text{ball contact} \\[2em] G^{ball} & \text{for ball} - \text{to} - \text{wall contact} \end{cases} \qquad \text{and} \qquad (4.13)$$

$$\langle \nu \rangle = \begin{cases} \dfrac{1}{2}\left(v^A + v^B\right) & \text{for ball} - \text{to} - \text{ball contact} \\[2em] v^{ball} & \text{for ball} - \text{to} - \text{wall contact} \end{cases} \qquad . \qquad (4.14)$$

4.5.1.2. Slip model

The slip model offers no normal strength in tension and allows slip to take place if the shear force exceeds the maximum allowable shear force. The slip model is defined by the friction coefficient (μ) at the contact.

4.5.1.3. Bonding

In PFC^{3D}, it is possible for particles to be bonded at contacts by two bonding models: the contact-bond model and the parallel-bond model. The contact bond acts only at the

contact point while the parallel-bond can be envisioned as the addition of a virtual cement-like material between the two balls in contact. The contact bond can only transmit a force while the parallel bond can transmit both a force and a moment. Both bonding models can be active at the same time but the existence of a contact bond voids the slip model, since these last two models define the behaviour at the contact point. Both types of bond can be broken if their strengths are exceeded.

The contact bond is modeled as a pair of elastic springs with constant normal and shear stiffnesses acting at the contact point and specified shear and tensile normal strengths. When a contact bond is present, the shear contact force is limited by the shear contact bond strength, as opposed to being limited by the maximum allowable force based on the friction coefficient of the slip model. When the magnitude of the tensile normal contact force becomes equal or greater than the normal contact bond strength, the bond breaks and both the normal and shear contact forces are set to zero. If the shear contact force equals or surpasses the shear contact bond strength, then the bond breaks but the contact forces are not altered unless the shear force exceeds the friction limit.

The parallel bonds create an elastic interaction between the bonded particles that acts in parallel with the slip or contact-bond models. They can transmit both forces and moments between particles and thus can contribute to the resultant force and moment experienced by the two bonded particles. The parallel bonds can be seen as a set of elastic springs with constant normal and shear stiffnesses uniformly distributed over a circular disc lying on the contact plane. A force and a moment can develop within the bond material due to relative motion at the contact. This force and moment act on the two bonded particles and can be related to maximum normal and shear stresses acting within the bond material at the periphery of the bond. The parallel bond will break if either of these maximum stresses surpasses its corresponding bond strength.

4.5.1.4. Input parameters for manure products

The first parameters that need to be determined are the normal and tangential stiffnesses. Published values for the Young's modulus and Poisson's ratio of manures are not available. Values were derived from soils properties. Bardet (1997) reported ranges of values for the Young's modulus and Poisson's ratio of various soil types. The values of Young's modulus vary greatly from 0.4 to 1440 MPa while typical Poisson's ratio values for soils range from 0.1 to 0.5.

Using values of 2.0 MPa for the Young's modulus and 0.25 for the Poisson's ratio, equation 4.8 yields a k_n value of 4.0e4 N/m for a particle having a diameter of 5 mm. Starting with this stiffness value of 4.0e4 N/m, equation 4.6 requires a radius of the contact area of 0.71 mm. Two 5-mm diameter spheres would have to overlap each others by 0.1 mm to create that contact area and for equation 4.6 to yield a stiffness value of 4.0e4 N/m. This appears to be a considerable overlap. Values of normal stiffness used by other authors for soil varied from 1e3 to 50e3 N/m (Oida et al., 1998), 0.9e10 to 1.8e10 N/m (Kato et al., 2000) and 1e3 N/m (Shikanai and Ueno, 2002; Tanaka et al., 2000).

In this work, equation 4.8 is used to calculate the stiffness in the normal direction as a function of the radius of the particle and its Young's modulus. Equation 4.5 is used to calculate the ratio of shear to normal stiffness based on the Poisson's ratio. The shear stiffness is then calculated from the normal stiffness and the stiffness ratio. The radii of the particles as well as two of their mechanical properties are therefore utilized to calculate the normal and shear stiffness.

4.5.2. Macroscopic representation

4.5.2.1. Particle size distribution

The flow of organic fertilizers in handling and land application machinery at a macroscopic level will be influenced by the size of the particles (or aggregates). The influence of the size of the particles on the behaviour of various granular products has

been demonstrated in DEM studies (e.g. Ni et al., 2000; Cleary, 1998; Hopkins and Tuhkuri, 1999). A procedure has been developed to enable the implementation of user-defined particle size distributions in PFC's assemblies of particles. The code is based on the results presented in chapter 2 for the particle size distribution of manure samples obtained by a screening method. It offers the possibility to generate an assembly of particles with up to 6 size classes.

4.5.2.2. Clusters

Clustered-particles were implemented to model the clumpy and brittle nature of organic fertilizers. Figure 4.1 presents three- and six-sphere clusters. In the cluster-generation code, spherical coordinates are used to create the clusters. The mathematical relations presented in this section are derived for a three-sphere cluster. The radii of the spherical elements composing the cluster are first defined. The first sphere of the cluster is created at a random distance from the global coordinate origin (X-Y-Z system in figure 4.2) within a user-defined range. The angles φ_1 and θ_1 are also randomly selected in the range $[0, 2\pi]$ (or any user-defined range). The second and third spheres are defined with respect to a coordinate system having its origin at the center of the first sphere (X'-Y'-Z' system in figure 4.2). To ensure the spheres composing the cluster are in contact two by two without overlapping (overlapping at the creation stage would generate artificial repulsive forces), mathematical relations were derived to calculate the possible ranges for the angles defining the second and third spheres (φ_2, φ_3 and θ_3). The angle θ_2 can take any value in the range $[0, 2\pi]$. A range is then calculated for φ_2 based on the radii of sphere #1 and #2 (r_1 and r_2, respectively) to ensure contact is maintained. The range for φ_2 is defined as $[\varphi_{min}, (\pi - \varphi_{min})]$. Angle φ_3 has to be determined based on the value of φ_2 and must be within a certain range to maintain contact between sphere #2 and sphere #3. The maximum possible difference between φ_2 and φ_3 happens when $\theta_2 = \theta_3$ and the value φ_3 can take depends on θ_2 and θ_3. Since θ_3 can be calculated based on the value of φ_2 and φ_3, the angle φ_3 is taken in the same interval as φ_2 to avoid an iterative calculation of the angles (that would not have any spatial distribution advantage). Equation 4.15 is derived from geometric relations between lines

connecting the spheres radii (see figure 4.2) and is used to calculate the limiting angle (φ_{min}):

$$\varphi_{min} = \begin{cases} \left| \dfrac{\pi}{2} + \varphi_{lim} \right| & \text{for } \varphi_{lim} < 0 \\[3mm] \dfrac{\pi}{2} - \varphi_{lim} & \text{for } \varphi_{lim} \geq 0 \end{cases} \quad , \tag{4.15}$$

where

$$\varphi_{limit} = a\tan(x_\varphi, y_\varphi) \quad , \tag{4.16}$$

$$x_\varphi = 2\left(\frac{x_n}{x_d} \right) \quad , \tag{4.17}$$

$$y_\varphi = \frac{\sqrt{y_{n1} y_{n2}}}{y_d} \quad , \tag{4.18}$$

$$x_n = \sqrt{-\left[-3r_3^2 - 2r_2 r_3 + r_2^2 - 8r_3 r_1 - 4r_1^2 + (4r_3^2 + 8r_3 r_1 + 4r_1^2)\sin((\pi\sin^2)) \right] r_2 r_3} \quad , \tag{4.19}$$

$$x_d = y_{n1} = y_d = -3r_3^2 - 2r_2 r_3 + r_2^2 - 8r_3 r_1 - 4r_1^2 + (4r_3^2 + 8r_3 r_1 + 4r_1^2)\sin((\pi/4)^2) \quad \text{and} \tag{4.20}$$

$$y_{n2} = -4r_1^2 + -8r_3 r_1 + r_2^2 + 2r_2 r_3 - 3r_3^2 + (8r_3 r_1 + 4r_1^2 + 4r_3^2) \, \sin((\pi/4)^2) \quad . \tag{4.21}$$

It would be possible to derive relationships to make the cluster generation algorithm more flexible using iterative calculation, but the level of randomization yielded by equations 4.15 to 4.21 was judged sufficient. The example was given for clusters composed of three spheres, but the same method can be used to create clusters made of several spheres (the theoretical limit depending upon the radii of the spheres). The algorithm used to create the first three spheres (indices 1, 2 and 3) is just repeated with incremented indices. For example, to create sphere #4, the parameters for spheres 1, 3

and 4 are used (1,4 and 5 to create sphere #5 and so on). The cluster creation is done either clockwise or counter-clockwise. A random number generator is used to randomize the direction of creation.
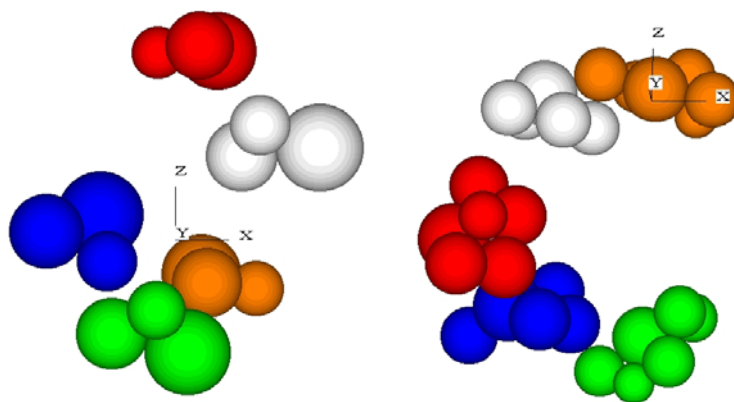
Figure 4.1. Examples of three- and six-sphere clusters (radii 0.8, 1.0 and 1.2 units).
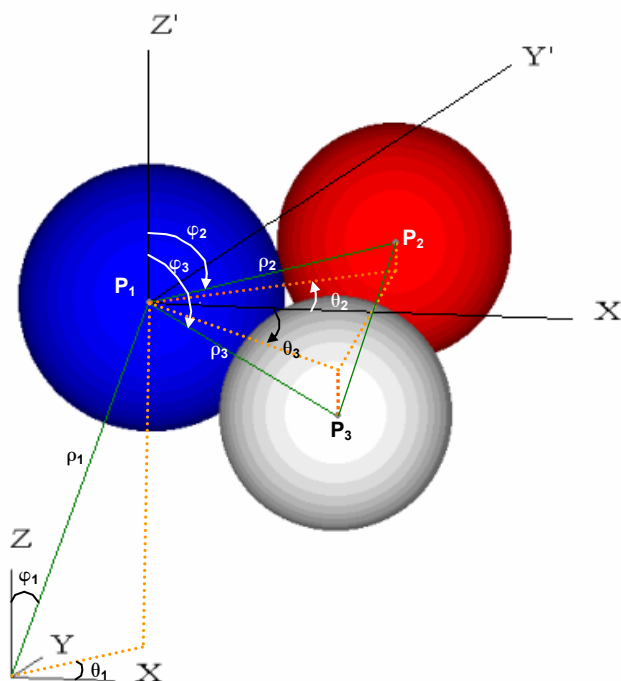
Figure 4.2. Geometry of a three-sphere cluster.

4.5.3. Virtual testing environment

The direct shear test and the triaxial test are the experimental procedures that are often used to characterize the constitutive relationships for physical materials. For this reason, it is also to the results of these two tests that the DEM parameters are generally related. A virtual direct shear test was implemented in PFC^{3D} to carry out the calibration procedure that allows defining the properties of the virtual product that will make its behaviour similar to that of real manure. A shearbox apparatus was implemented in PFC^{3D} and the normal loading stress was applied via a platen made of several small particles grouped in a clump (figure 4.3). The clump logic imbedded in PFC^{3D} allows for the creation of slaved particles acting as a rigid body. The normal loads were applied to the samples and shearing was initiated after the samples had reach equilibrium, i.e. the maximum unbalanced force is small compared to the maximum contact force in the model.

(a)

(b)
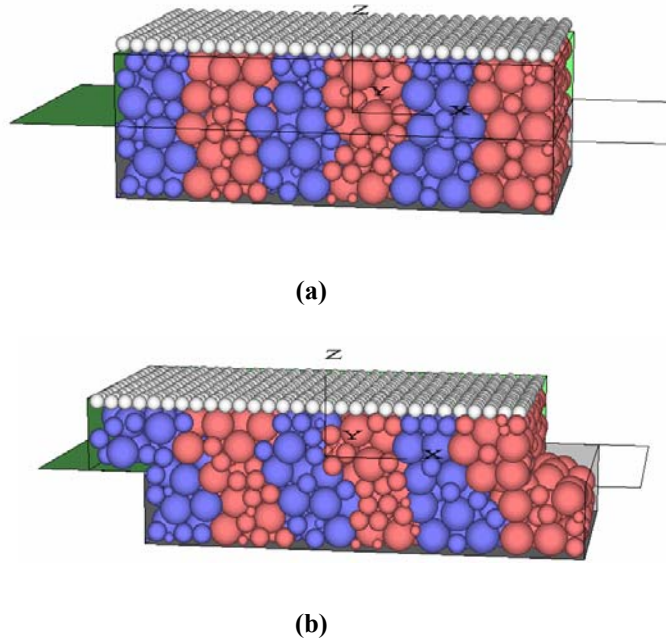
Figure 4.3.   Numerical direct shear test: (a) initial and (b) final state.

Several numerical direct shear tests were carried out to perform a sensitivity analysis for the various parameters defining the constitutive models. Figure 4.4 illustrates a typical shear force vs horizontal displacement curve produced during a simulation. The shape

of the curve in figure 4.4 is in agreement with experimental results typically obtained with the direct shear test.
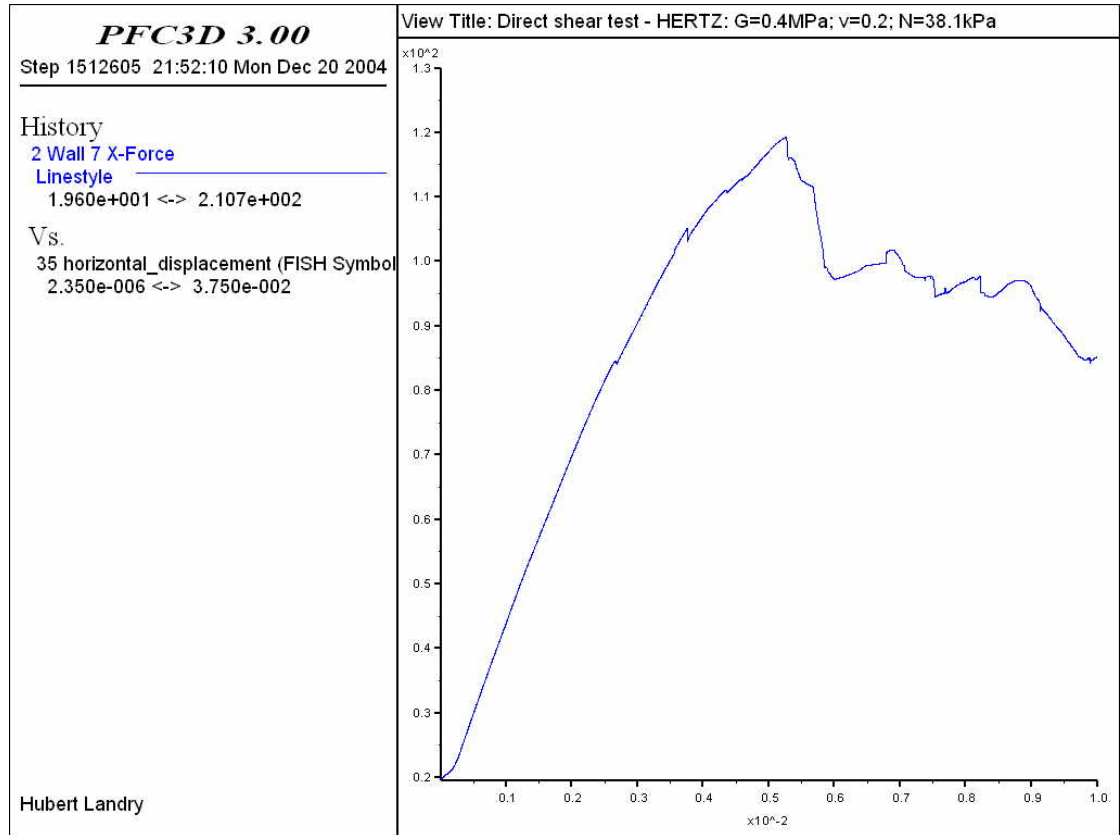
Figure 4.4. Screenshot of the results produced by PFC³ᴰ for the direct shear test. The shear force vs horizontal displacement curve is illustrated (Hertz-Mindlin contact model, G=0.4 MPa, *ν*=0.2, normal applied load is 38.1 kPa).

4.6. Results and discussion

4.6.1. Macroscopic representation

The particle size distribution code was tested to ensure that it produces an assembly of particles that respects the user specifications. Table 4.1 presents the results obtained for an assembly of particles with sizes ranging from 0.82 to 30.00 mm and with various percentages in each of the 6 classes. The results included in table 4.1 clearly

144

demonstrate the ability of the code to produce an assembly of particles based on a user-defined particle size distribution.

Table 4.1. Results obtained with the particle size distribution code.

Size class	Input		Output		Errors	
	Number of balls	GML[1]	Number of balls	GML	Number of balls	GML
	(% of total)	(mm)	(% of total)	(mm)	(%)	(%)
1	17.70	30.00	17.64	29.90	0.32	0.33
2	16.80	20.40	16.75	20.33	0.29	0.33
3	39.40	11.90	39.36	11.86	0.09	0.33
4	9.80	6.70	9.75	6.68	0.56	0.33
5	13.90	2.50	13.89	2.49	0.11	0.33
6 (pan)	2.40	0.82	2.36	0.82	1.80	0.33

[1]Geometric mean length (ASAE Standards, 2002)

4.6.2. Linear contact model

The linear model was mostly studied. A sensitivity analysis was performed based on pig manure at a total solids concentration of 48%. The measured properties of this product are presented in table 4.2 (re. chapter 2). This product was selected because the largest proportion of its particles is in the first two size classes meaning it could be modeled using a reasonable number of spheres. It also gave good results during the laboratory direct shear tests, with small standard-deviation values for the angle of internal friction and apparent cohesion. Most virtual direct shear tests were carried out with 7.0, 15.0, 22.5 and 38.1 kPa as the normal stress values, with some simulations having 70.7 kPa as the highest normal stress.

Table 4.2. Measured properties of the basic product used to develop numerical manure models (pig manure at 48% total solids).

Particle size distribution		Average bulk density	Average static friction coefficient	Average internal friction angle	Average apparent cohesion
GML (mm)	Proportion of mass (%)	(kg/m^3)	(---)	(deg)	(kPa)
20.4	37.0				
11.9	50.0				
6.7	10.0	522.5	0.86	24.5	16.5
2.5	3.0				
0.8	0.0				

Several properties are linked together, as presented in section 4.5.1. To conduct the sensitivity analysis, care had to be taken to isolate as much as possible each parameter. The first parameter that was investigated is the Young's modulus. The Young's

modulus is used to calculate the normal stiffness (equation 4.8). In studying the effect of the Young's modulus, the normal stiffness was calculated based on its value, and a fixed value of 0.86 was used for K, the ratio of shear to normal stiffness. The ball-ball and ball-wall friction coefficient was set at 0.5 and the particle size distribution presented in table 4.2 was implemented. The results obtained for the direct shear test at different values of Young's modulus are presented in figure 4.5.
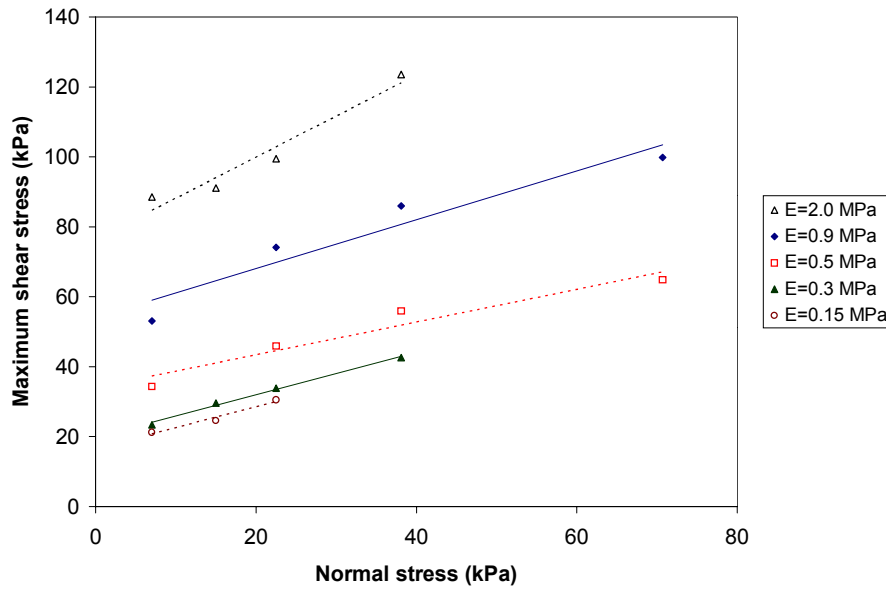
Figure 4.5. Maximum shear stress as a function of normal stress for different values of the Young's modulus (k_n calculated with eq. 4.8; k_s calculated using the ratio K; K=0.86; μ=0.50).

The results presented in figure 4.5 indicate that the Young's modulus mostly influenced the apparent cohesion. There also seemed to be an increasing effect on the angle of internal friction as the value of the Young's modulus increased. It should be kept in mind that the value of the normal and shear stiffness are dependent upon the value of the Young's modulus (equation 4.8). The tensile elastic modulus, or Young's modulus, is related to the force that is necessary to elongate a material. In the present case, the value of the Young's modulus influenced the model through the normal (and shear) stiffness; the higher the Young's modulus, the stiffer the particles. The results indicated that an increase in the particles stiffness translated into an increase in the apparent cohesion.

Since the stiffnesses are major parameters in DEM models, the influence of the ratio of shear to normal stiffness was studied. The value of the Young's modulus was set at 0.3 MPa and the friction coefficient was 0.5 for all contacts. The particle size distribution of table 4.2 was again used in this analysis. The results are presented in figure 4.6.
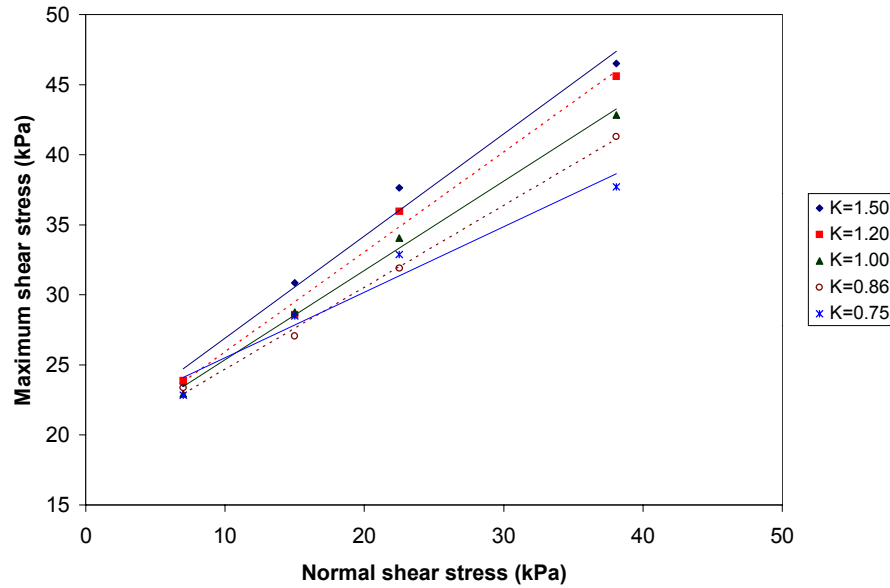
Figure 4.6. Maximum shear stress as a function of normal stress for different values of the ratio of normal to shear stiffness (E=0.3MPa; k_n calculated with eq. 4.8; k_s calculated using the ratio K; μ=0.50).

This time, it is clear that the ratio of shear to normal stiffness determined the angle of internal friction, with little effect on the apparent cohesion. As the shear stiffness increased, more force was required to shear the sample. At the particle level, the shear contact force is computed based on the relative shear-displacement. The elastic shear force at the contact is incrementally increased based on the shear-displacement at each timestep. The increase in the angle of internal friction was proportional to the increase of the ratio K, according to a second order relation in the range of K included in the analysis.

Another important parameter is the friction coefficient at a contact, as it defines the slip model. The next parameter that was studied for its influence on the simulations results was therefore the friction coefficient. The results obtained are presented in figure 4.7.

147
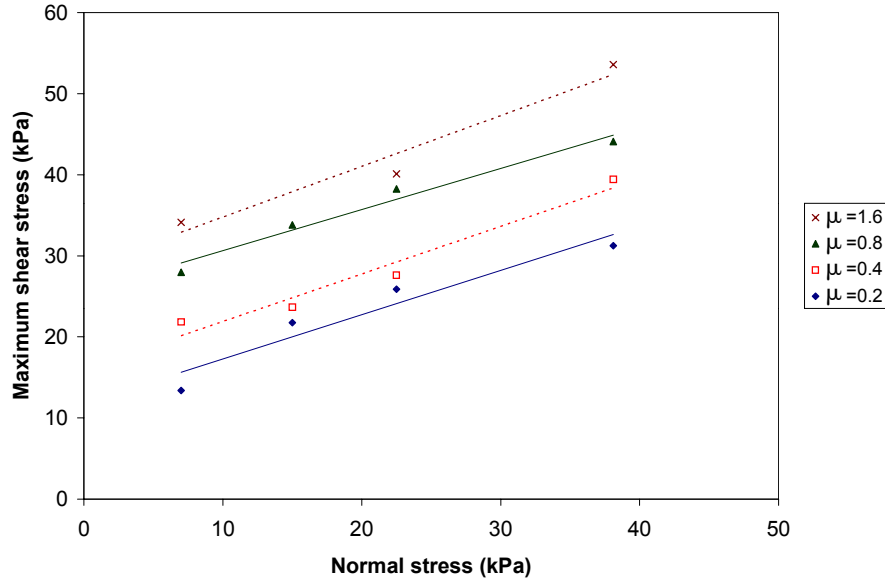
Figure 4.7. Maximum shear stress as a function of normal stress for different values of static coefficient of friction (E=0.3MPa; k_n calculated with eq. 4.8; k_s calculated using the ratio K; K=0.86).

The results included in figure 4.7 suggest that the static coefficient of friction is mostly related to the apparent cohesion, as demonstrated by the parallel lines. The increase in the apparent cohesion was proportional to the change in the friction coefficient.

Contact bonds have been identified as a potential means of modeling the adhesion and cohesion that can be observed in manures. Contact bonding was implemented in the whole assembly of particles and different values of the normal (ns_{cb}) and shear strength (ss_{cb}) of the bonds were studied. The results are presented in figure 4.8. The contact bonds influenced the apparent cohesion of the product, as indicated by the results in figure 4.8. The simulation allowed seeing that the bonds located near the shear plane would fail during the test and that some bonds would stay intact at the periphery of the box. When a contact bond is active, it precludes the slip model defined by the friction coefficient. Since the contact bonds were failing in some regions of the model, a change in the friction coefficient would have an effect on the results of the direct shear test for a bonded assembly of particles.

148
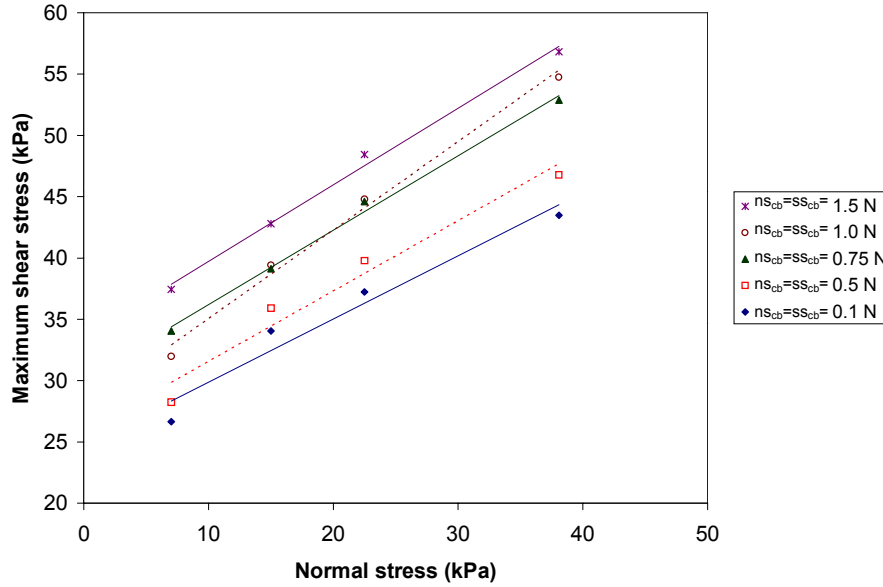
Figure 4.8.   Maximum shear stress as a function of normal stress for different values of contact bond strength (normal and shear strength are equal; E=0.3MPa; k_n calculated with eq. 4.8; k_s calculated using the ratio K; K=0.86; μ=0.80).

The clustered particles presented in section 4.5.2.2 were tested for their influence on the results of the direct shear test. Contact bonds were used to join the four particles included in each cluster and the strength of the bonds was varied. The results are presented in figure 4.9. The strength of the clusters seemed to be mostly affecting the apparent cohesion of the sample as shown in figure 4.9. It was observed that the clusters failed according to their strength and to the normal stress applied to the sample. At a strength value of 0.25 N, very few clusters were intact at the end of the shearing for a value of normal stress of 7.0 kPa. At the other end of the range, clusters with a strength value of 3.0 N were not broken by the shearing of the sample even at the normal stress level of 38.1 kPa. The strength values between 0.25 and 3.0 N showed a similar trend with the clusters being increasingly affected as their strength value was reduced and the normal stress on the sample increased.

Setting the friction coefficient at 0.8 and using a value of 0.3 MPa for the Young's modulus yielded an internal friction angle of 27.4º and an apparent cohesion of 25.1 kPa, values that can be favourably compared to the results obtained experimentally

149

(table 4.2). It is now obvious that several parameters of the linear model can have an influence on the results of the simulated direct shear test.
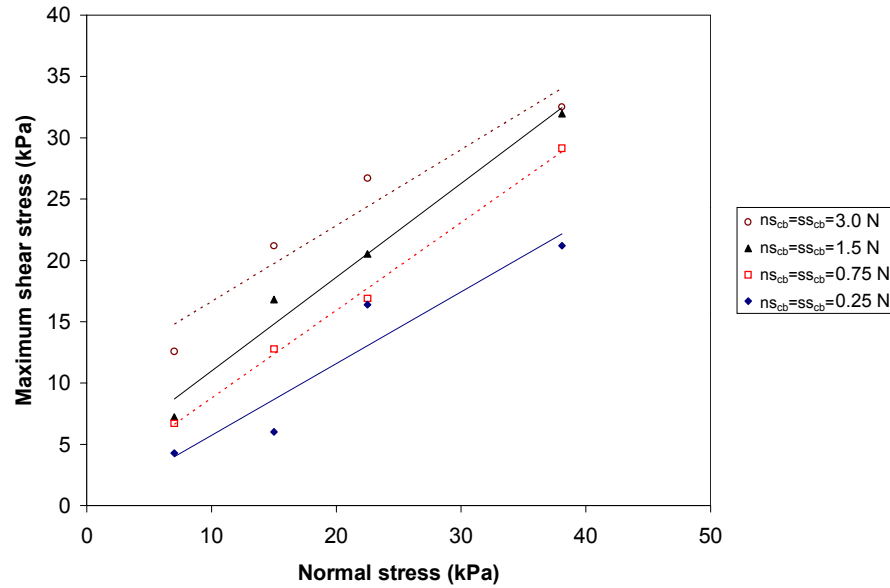
Figure 4.9.   Maximum shear stress as a function of normal stress for different values of contact bond strength in 4-particle clusters (normal and shear strength are equal; E=0.3MPa; k_n calculated with eq. 4.8; k_s calculated using the ratio K; K=0.86; μ=0.50).

4.6.3. Hertz-Mindlin contact model

The effects of the shear modulus and Poisson's ratio were studied for the simplified Hertz-Mindlin contact model. This contact constitutive model is mostly appropriate when modeling assemblies having no bonds, experiencing small-strain conditions and exclusively compressive stresses (Itasca, 2003). The simplified Hertz-Mindlin model is therefore of limited interested when attempting to model organic fertilizers. Figure 4.10 includes the results obtained for the direct shear test at different levels of shear modulus. The results indicated that both the apparent cohesion and the angle of internal friction were affected by the shear modulus. This observation is consistent with the results obtained for the effect of the Young's modulus of the linear model. Since the shear modulus and the Young's modulus are mathematically related (eq. 4.9), it was expected that the two parameters would have a similar influence. Figure 4.11 presents the results of the sensitivity analysis of the Poisson's ratio. It appears that this

150

parameter had very little influence on the results of the direct shear test. Table 4.3 includes the regression parameters for all the simulations.
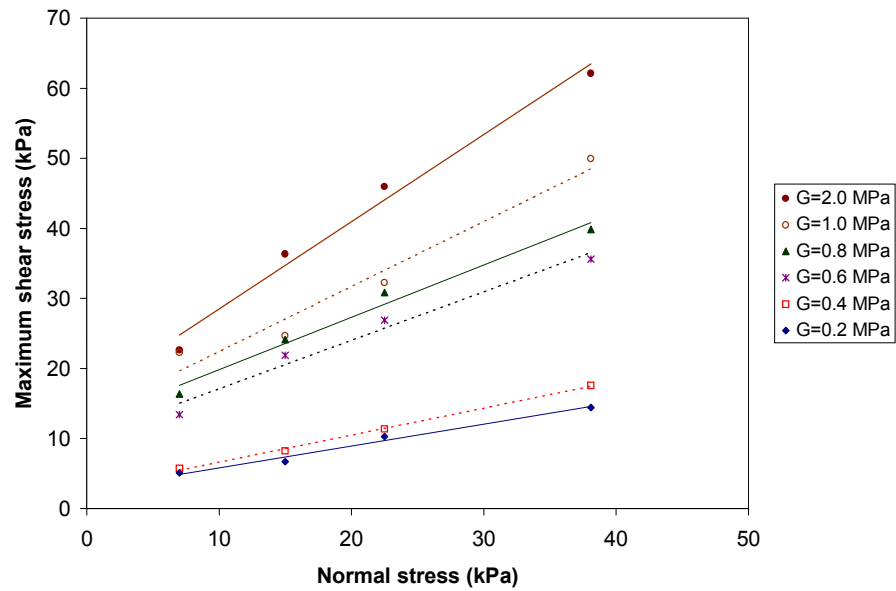
Figure 4.10. **Maximum shear stress as a function of normal stress for different values of shear modulus**
(ν=0.35; μ=0.50).
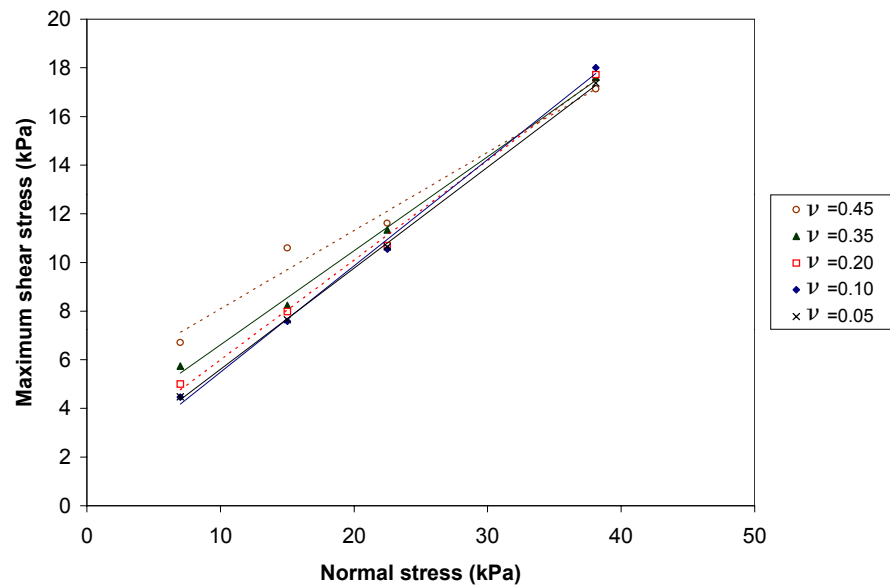
Figure 4.11. **Maximum shear stress as a function of normal stress for different values of Poisson's ratio**
(G=0.4 MPa; μ=0.50).

Table 4.3. Summary of the sensitivity analysis on the parameters defining the linear and Hertz-Mindlin contact models.

Contact Model	E (MPa)	G (MPa)	ν (---)	μ (---)	k_n (N/m)	k_s (N/m)	K (---)	Contact bonds strength (N)	Regression equation[a]	R^2 (---)
Linear	2.0	n.a.[b]	n.a.	0.5	from eq. 4.8	from value of K	0.86	n.a	y = 1.2x + 76.4	0.95
	0.9								y = 0.70x + 54.1	0.92
	0.5								y = 0.47x + 34.0	0.94
	0.3								y = 0.61x + 19.8	0.99
	0.15								y = 0.60x + 16.5	0.97
	0.3	n.a.	n.a.	0.5	from eq. 4.8	from value of K	1.50	n.a	y = 0.73x + 19.6	0.98
							1.20		y = 0.71x + 18.8	0.99
							1.00		y = 0.64x + 19.0	1.00
							0.86		y = 0.58x + 18.8	1.00
							0.75		y = 0.47x + 20.8	0.96
	0.3	n.a.	n.a.	1.6	from eq. 4.8	from value of K	0.86	n.a	y = 0.63x + 28.5	0.95
				0.8					y = 0.51x + 25.6	0.97
				0.4					y = 0.59x + 16.0	0.96
				0.2					y = 0.55x + 11.8	0.92
	0.3	n.a.	n.a.	0.8	from eq. 4.8	from value of K	0.86	1.5 [c]	y = 0.62x + 33.5	0.99
								1.0	y = 0.72x + 27.8	0.99
								0.75	y = 0.61x + 30.1	1.00
								0.5	y = 0.57x + 25.8	0.96
								0.1	y = 0.52x + 24.7	0.95
	0.3	n.a.	n.a.	0.5	from eq. 4.8	from value of K	0.86	3.0 [d]	y = 0.62x + 10.5	0.93
								1.5	y = 0.76x + 3.3	0.98
								0.75	y = 0.71x + 1.6	1.00
								0.25	y = 0.58x - 0.11	0.90
Hertz-Mindlin	n.a	2.0	0.35	0.5	n.a.	n.a.	n.a.	n.a.	y = 1.25x + 16.1	0.98
		1.0							y = 0.93x + 13.1	0.96
		0.8							y = 0.75x + 12.4	0.98
		0.6							y = 0.69x + 10.2	0.97
		0.4							y = 0.39x + 2.7	1.00
		0.2							y = 0.31x + 2.7	0.98
	n.a	0.4	0.45	0.5	n.a.	n.a.	n.a.	n.a.	y = 0.32x + 4.9	0.98
			0.35						y = 0.39x + 2.7	1.00
			0.2						y = 0.41x + 1.9	1.00
			0.1						y = 0.44x + 1.1	1.00
			0.05						y = 0.42x + 1.46	1.00

[a] in the regression equations, y corresponds to the maximum shear stress and x represents the normal stress;
[b] not applicable;
[c] bonds applied to the whole assembly of particles;
[d] bonds linking the clustered particles

It has been shown that the parameters defining the contact constitutive models influenced the results of the direct shear test in different ways. Several parameters could not be included in the analysis. As an example, using different values for the normal and shear strength of contact bonds would likely influence the outcome of the simulations. A broader range of values for the parameters that have been studied would also deepen the analysis. The interactions of all the parameters defining the contact constitutive models should also be analyzed to enhance our understanding of the manure models. The particles used in this study are evidently not the basic elements

making up manure. The question remains as to what level of breakdown into the structure of the product studied will yield the best results. The number and size of the particles would likely influence the results of the simulations. Many of the simulations carried out for the sensitivity analysis were based on different initial samples. Therefore, the initial packing of the assemblies of particles did not prevent the establishment of relationships. Although several questions are left unanswered, the work reported here demonstrated that it was possible to generate a virtual product that mimics the behaviour of manure.

4.7. Conclusions

Methods have been developed to implement manure models in the discrete element code PFC^{3D}. A procedure to create user-defined particle size distributions was presented. From the input-output comparison for a test run, it was demonstrated that the procedure generated very small errors for the number and characteristic dimension of the particle for each size class (average relative error of 0.53% and 0.33%, respectively) over a wide range of particle diameters (0.82 to 30.0 mm). Clustered particles were also introduced to better model the brittle and clumpy nature of organic fertilizers. The mathematical relations used to generate randomly oriented and located three-sphere clusters were presented. Parameters defining the linear and simplified Hertz-Mindlin constitutive models were studied. For the linear model, it was shown that the ratio of shear to normal stiffness had a major influence on the angle of internal friction as determined by the virtual direct shear test. To a lesser extent, the Young's modulus was also observed to have an influence on the angle of internal friction. The Young's modulus, friction coefficient, normal and shear strength of the contact bonds as well as normal and shear strength of the contact bonds linking the clustered particles all influenced the apparent cohesion. In the case of the Hertz-Mindlin model, the shear modulus affected both the apparent cohesion and the angle of internal friction while the Poisson's ratio had little influence on those parameters. The methods presented have the potential to be extended to any type of solid organic by-products.

4.8. References

Adachi, T. and F. Oka. 1982. Constitutive equations for normally consolidated clay based on elasto-viscoplasticity. Soils and Foundations, 22(4): 57-70.

ASAE Standards, 2002. S424.1. Method of Determining and Expressing Particle Size of Chopped Forage Materials by Screening. St. Joseph, Mich.: ASAE.

Bardet, J.P. 1997. Experimental soil mechanics. Upper Saddle River, NJ : Prentice Hall.

Cleary, P.W. 1998. The filling of dragline buckets. Mathematical Engineering in Industry, 7(1): 1-24.

Desai, C.H. and H.J. Siriwardane. 1984. Constitutive laws for engineering materials with emphasis on geological materials. Englewood Cliffs, New Jersey, Prentice-Hall.

Di Renzo, A. and F.P. Di Maio. 2004. Comparison of contact-force models for the simulation of collisions in DEM-based granular flow codes. Chemical Engineering Science, 59: 525-541.

Feda, J. 1982. Mechanics of particulate materials – the principles. Amsterdam, The Netherlands, Elsevier, 1982.

Hopkins, M.A. and J. Tuhkuri. 1999. Compression of floating ice fields. Journal of Geophysical Research, 104(C7): 15815-15825.

Itasca, 2003. PFC3D User's Manual, Version 3.0.., Itasca Consulting Group Inc., Minneapolis, Minn.., 55415 USA.

Kamath, S., V.M. Puri, H.B. Manbeck and R. Hogg. 1991. Measurement of flow properties of bulk solids using four testers. ASAE Paper No. 91-4517, St. Joseph, Mich.: ASAE.

Kato, S., S. Yamamoto, S. Nonami, H. Rahardjo, D.G. Toll and E.C. Leong. 2000. Study of the influence of adhesion force on deformation and strength of unsaturated soil by DEM analysis. Unsaturated soils for Asia, Proceedings of the Asian Conference on Unsaturated Soils, UNSAT Asia 2000, Singapore: 113-118.

Krizek, R.J., A.M. Ansal and Z.P. Bazant. 1978. Constitutive equation for cyclic behavior of cohesive soils. Proceedings of the ASCE Geotechnical Engineering Division, Special Conference Earthquake Engineering and Soil Dynamics I: 557-558.

Li, Y., V.M. Puri and H.B. Manbeck. 1990. Elastic-viscoplastic cyclic constitutive model parameter determination and evaluation for wheat en masse. Transactions of the ASAE, 33(6): 1984-1995.

Masson, S. and J. Martinez. 2000. Effect of particle mechanical properties on silo flow and stresses from distinct element simulations. Powder Technology, 109: 164-178.

Maw, N., J.R. Barber and J.N. Fawcett. 1976. The oblique impact of elastic spheres. Wear 38, 101-114.

Maeda, Y., Y. Maruoka, H. Makino and H. Nomura. 2003. Squeeze molding simulation using the distinct element method considering green sand properties. Journal of Materials Processing Technology, 135: 172-178.

Mindlin, R.D. and H. Deresiewicz. 1953. Elastic spheres in contact under varying oblique forces. Journal of Applied Mechanics, 20: 327-344.

Mishra, B.K. and C.V.R. Murty. 2001. On the determination of contact parameters for realistic DEM simulations of ball mills. Powder Technology, 115: 290-297.

Ni, Q., W. Powrie, X. Zhang and R. Harkness. 2000. Effect of particles properties on soil behaviour: 3-D numerical modeling of shearbox tests. Geotechnical special publication, 96: 58-70.

Oida, A., H. Schwanghart, S. Ohkubo and M. Yamazaki. 1998. Simulation of soil deformation and reaction under a track shoe by distinct element method. Actual Tasks in Agricultural Engineering, 26th International Symposium on Agricultural Engineering, Opatija, Croatia, 3-6 February 1998, 167-176.

Oreskes, N., K. Shrader-Frechette and K. Belitz. 1994. Verification, validation, and confirmation of numerical models in the earth sciences. Science, 263: 641-646.

Shikanai, T. and M. Ueno. 2002. Simulation of soil resistance at plate penetration by the distinct element method. ASAE Paper No. 023046. St. Joseph, Mich.: ASAE.

Tanaka, H., M. Momozu, A. Oida and M. Yamazaki. 2000. Simulation of soil deformation and resistance at bar penetration by the Distinct Element Method. Journal of Terramechanics, 37: 41-56.

Tripodi, M.A., V.M. Puri, H.B. Manbeck and G.L. Messing. 1992. Constitutive models for cohesive particulate materials. Journal of Agricultural Engineering Research, 53: 1-21

Zhang, Q., V.M. Puri and H.B. Manbeck. 1986. Determination of elastoplastic constitutive parameters for wheat en masse. Transactions of the ASAE, 29(6): 1739-1746.

Chapter 5

Numerical Modeling of the Flow of Organic Fertilizers in Land Application Equipment

5.1.   Significance

Having studied the physical and flow properties of manure products, the next step is to investigate how the products behave and interact with mechanical systems in "machinery situations". Numerical modeling was deemed a valuable method to attempt gaining an enhanced understanding of the flow of organic fertilizers in handling and land application equipment. The discrete element method was targeted in particular, as this modeling technique is capable of simulating the flow of unbonded (granular) or bonded materials. As part of his research program, the candidate spent several months at Cemagref. Mr. François Thirion of Cemagref had done some work on the modeling of sludge flow in land application equipment using computational fluid dynamics (CFD) and it was decided that a publication giving an introduction to the application of numerical modeling to spreading problems should be the objective of the collaborative work. The unique fact that the co-authors had done some work with products at both ends of the consistency spectrum and with two different modeling methods (computational fluid dynamics and discrete element method) was an incentive to prepare an introductory paper that would discuss the modeling approaches along with their challenges and limitations with regard to land application problems. This chapter partially fulfills objectives 4 and 5 of the thesis. Mr. Thirion contributed sections 5.5.2, 5.6.2, 5.7.2 and 5.8.2. The writing of the manuscript was done by the candidate.

5.2. Abstract

Numerical modeling using the Discrete Element Method (DEM) and Computational Fluid Dynamics (CFD) was applied to the flow of organic fertilizers in land application equipment. The DEM was used to simulate the flow of compost while CFD was applied to sludge spreading. A full manure spreader with dual vertical beaters was modeled using the DEM. The simulated product distributions and power requirements were consistent with published results for that type of machine. Two types of composts were modeled in simulations aimed at studying the effect of a flow-control gate on the discharge flow and energy requirements of the discharge conveyor. The first product was a dry, homogenous sand-like material, while the second had a lower total solids concentration (29.3% compared to 59.0% on a wet mass basis) and a higher density (810.7 kg/m^3 compared to 612.0 kg/m^3). Both products were modeled by assemblies of particles having radii normally distributed between 2.5 and 10 mm. The Young's modulus, from which the particles stiffness values were calculated, was set to 20 MPa and 0.3 MPa for the dry compost and compost, respectively. Contact bonds were implemented in the compost model. Dimensionless parameters were developed to allow for comparisons to be made between the scaled simulations and the experimental results obtained with a full size spreader. Two gate height settings were studied for the two types of composts. Simulated results for the discharge flow in the open gate configuration were in good agreement with measured data. The effect of the gate on the power requirements of the discharge conveyor were replicated by the models. Fracture behaviours observed during field experiments were also replicated by the model. Two Hershel-Bulkley rheological models were used to simulate fluid pasty sludge and plastic pasty sludge using CFD. Field experiments were carried out with a sludge spreader to measure the discharge rate of the spreader for the two types of sludge included in the study. The simulated flow rate curves closely replicated the experimental ones, for both sludge types. The simulated streamlines during the unloading of the spreader were also well correlated to observations made during field experiments. The flow of sludge on a spinning disc was studied using high-speed photography and a scaled spreader physical model. It was found that the viscosity of the sludge influenced the spreading pattern. The flow of sludge on the disc was also numerically simulated with CFD. The

simulated and measured residence time of the sludge on the disc were influenced by the viscosity of the sludge and were in close agreement.

5.3. Introduction

Manure and other organic by-products can be land applied and recycled by soil-crop systems, where they become a valuable source of nutrients and also enhance the soil physical structure (Egrinya et al., 2001; Larney et al., 2000; Marinari et al, 2000). However, uncontrolled applications of organic fertilizers can become a form of diffuse pollution causing the contamination of groundwater and watercourses. To ensure the sustainability of intensive livestock production and agriculture in general, land application operations must be as accurate and even as possible. Readily available equipment designed to handle and land apply solid and semi-solid organic fertilizers do not have efficient application rate control systems and exhibit uneven longitudinal and transversal product distribution (Thirion and Chabot, 2003; Frick et al., 2001; SRI, 1998).

The primary condition required to obtain an even distribution of the product on the soil surface is to achieve a steady discharge rate from the holding system of the land application machine. The flow of product inside the holding system or hopper is mainly influenced by the physical and flow properties of the product, the hopper geometry and the design of the conveying system. Due to the variability of these three parameters and the large volumes of products involved, experimental studies of the performances of spreaders are difficult to carry out. Information can be obtained from comprehensive performance tests which are occasionally conducted to assess the compliance of manufactured spreaders with laws and regulations. However, these studies are not rigorous enough as unsatisfactory results are usually not published. As a result, the knowledge of the flow behaviours of organic fertilizers in land application equipment as well as the machine-product interactions is very sparse and empirical. Therefore, it can hardly contribute to the design of innovative high-performance systems or to the optimization of the operational parameters of available machines.

Numerical modeling is an effective way of simulating various processes. It represents an easily adaptable method that can be substituted to heavy experimental procedures. It also allows getting some useful insights into the flow behaviours inside machines, information that would otherwise be very hard to obtain experimentally. With the ever-increasing power of personal computers, numerical modeling techniques are becoming very popular. To enhance our understanding of the behaviours of organic fertilizers in land application equipment, it seems very worthwhile to attempt applying these numerical modeling methods. This introductory paper illustrates the utilization of two numerical modeling methods in the field of organic fertilizer land application. The discrete element method (DEM) was used to study the flow of solid compost while computational fluid dynamics (CFD) has been selected to simulate sludge flow. The structure of this paper is intended to present the two methods in parallel so each major section is divided into two sub-sections: one for the DEM and the other for CFD.

5.4. Objective

The objective of the work reported herein was to model the flow of organic fertilizers in land application equipment and to validate the models against various parameters measured during field experiments using commercial spreaders. This study was carried out to assess the possibility of using numerical modeling as a tool to optimize the design and operation of handling and land application machinery for organic fertilizers.

5.5. Literature review

5.5.1. Discrete Element Method

The DEM was introduced by Cundall (1971). Since then, the method has been used to model a very broad range of engineering applications involving the flow of various materials or products. The filling of dragline buckets (Cleary, 1998), crushing and grinding in tumbling mills (Djordjevic, 2003), vehicle-soil interactions (Horner et al., 2001), squeeze moulding of green sand (Maeda et al., 2003), the compression of

159

floating ice fields (Hopkins and Tuhkuri, 1999) and the flow of bulk solids in bins (Rong et al., 1995a; 1995b) are just a few examples of engineering problems that have been successfully modeled using the DEM. Numerous journal articles report on the efforts invested in developing and evaluating the discrete element method. A complete description of the DEM can be found in the two-part paper of Cundall (1988) and Hart et al. (1988). Some of the most recent developments have involved the representation of non-spherical particles (Favier et al., 1999) and of fully kinematic boundaries (Kremmer and Favier, 2000; 2001a; 2001b). Many studies have included the development of a code specific to the application being modeled. As a result, the amount of information on models developed using commercial DE codes is limited. Moreover, the field of numerical modeling is evolving very fast making it a real challenge to build on previous knowledge. However, the amount of published results based on commercial discrete element codes seems to increase as the sophistication of such codes is improving and as computational resources become more readily available.

5.5.2. Computational Fluid Dynamics

The early beginnings of CFD occurred in the 1960's, particularly at Los Alamos National Laboratory where the world's largest computer resources were available. Its utilization in the industry expanded significantly in the 1990's. CFD is now commonly used for design purposes in a wide range of domains such as automotive, aerospace and turbo machinery where it largely contributes to the design of new machines or the optimization of existing systems. Its expansion has been favoured by the introduction of software packages that link CFD and CAD (computer assisted design), enabling the simultaneous development of flow studies and stress-strain analyses. CFD has been used to model various applications such as the climate in greenhouses (Reichrath and Davies, 2002), the airflow in animal rooms (Bjerg et al., 2001) and spraying processes (Tsay et al., 2002a and 2002b). Information on diverse applications can also be obtained through the proceedings of user group meetings organized by the main commercial CFD code developers. In the field of liquid manure and wastewater, CFD has been used to analyze tank agitation (Börjesson and Fahlgren, 2001) and calculate

pipe dimensions and pump requirements (Chilton et al., 1996). Commercial CFD codes are more widely used than DEM codes.

5.6. Theoretical background and models parameters

5.6.1. Discrete Element Method

The commercial code PFC^{3D} (version 3.0, Itasca Consulting Group Inc., Minneapolis, Minnesota, USA) was used in this study. With this code, the models are composed of distinct particles that can move independently from one another and that interact only at contacts or interfaces between the particles. If the particles are assumed to be rigid and the contact behaviour is described using a soft contact approach, then the mechanical behaviour of the system of particles can be described in terms of the movement of each particle and the inter-particle forces acting at each contact points (Itasca, 1999 and 2003). More complex system can be modeled by allowing bonding of particles at points of contact. The soft-contact approach implies overlapping of the rigid particles at contact points. The magnitude of the overlap is related to the contact force via the force-displacement law. The physical boundaries of the models are represented by walls. Balls and walls interact with one another via the forces that arise at contacts. Basically, the contact forces and displacements of a stressed assembly of particles are determined by monitoring the movements of individual particles. Specified wall and particle motion and/or body forces cause disturbances that are propagated through the particle system resulting in movements in the assembly. Each calculation step comprises the application of the laws of motion to the particles, a force-displacement law to each contact and constant updating of wall position (Cundall and Strack, 1979). A thorough discussion of the theoretical background of PFC^{3D} can be found in the software documentation (Itasca, 2003). PFC^{3D} models the material behaviour based on the geometry and properties of the micro-components that make up the material. To model products for which the micro-properties are not known like it is the case for manures and composts, it is necessary to use inverse modeling where properties are assumed and the results compared with the desired response of the real product. To

161

model composts in PFC^{3D}, a set of the properties included in the description of the virtual product must be derived from known compost rheological and physical properties. This is a very challenging issue that is not discussed in detail in this chapter (see chapter 4). Rather, simple models were developed based on selected measured properties for the two types of composts used in the study (re. table 5.1): (1) composted feedlot manure stored in the field for one year and mechanically turned twice (designated as compost); (2) compost no.1 after several passes into a spreader equipped with dual vertical beaters and an outside drying period of approximately three weeks (designated as dry compost). These products were selected because of their relatively uniform particle sizing and good homogeneity, which allowed for parallels to be made between the preliminary DE models.

Table 5.1. Measured properties of the two types of compost used in the study.

	Compost	Dry compost
Total solids concentration (%)	29.3 ± 1.0	59.0 ± 0.6
Density (kg/m³)	810.7 ± 23.4	612.0 ± 6.9
Static friction coefficient over steel (dimensionless)	0.63	0.60

Stiffnesses used in the models presented were calculated using equations 5.1 and 5.2. The equation giving the normal stiffness was

$$k_n = 4R_p E \quad , \tag{5.1}$$

where k_n = normal stiffness (N/m),

R_p = Particle radius (m) and

E = Young's modulus (Pa).

The shear stiffness was calculated using

$$K = \frac{k_s}{k_n} = \frac{\dfrac{(1-v_i)}{G_i} + \dfrac{(1-v_j)}{G_j}}{\dfrac{(1-0.5v_i)}{G_i} + \dfrac{(1-0.5v_j)}{Gj}} \quad , \tag{5.2}$$

where indices i and j refer to the first and second entity in contact, k_s is the shear stiffness (N/m); ν is the Poisson's ratio (dimensionless) and G the shear modulus (Pa). The shear modulus is related to the Young's modulus and Poisson's ratio by equation 5.3:

$$G = E / (2 (1+\nu)) \qquad . \qquad\qquad (5.3)$$

Young's modulus values derived from soil properties were used. Compost can be compared to organic soils and a value of 0.3 MPa was used for the Young's modulus (Bardet, 1997). A value of 20 MPa was used in the case of dry compost that was compared to sand (Bardet, 1997). A fixed value of 0.25 was used for the Poisson's ratio. From the observation of the physical characteristics of both products, it was decided that contact bonds would be used to model the behaviour of compost while the dry compost would remain unbonded. When a contact bond is present, the shear contact force is limited by the shear contact bond strength, as opposed to being limited by the maximum allowable force based on the friction coefficient of the slip model. When the magnitude of the tensile normal contact force becomes equal or greater than the normal contact bond strength, the bond breaks and both the normal and shear contact forces are set to zero. If the shear contact force equals or surpasses the shear contact bond strength, then the bond breaks but the contact forces are not altered unless the shear force exceeds the friction limit (Itasca, 2003). The default normal particle size distribution of PFC^{3D} was used with minimum and maximum radius values that would be realistic while maintaining reasonable computation time for the simulations. Table 5.2 summarizes the input parameters of the models.

Table 5.2. **Input parameters of the DE models**

	Dry compost	Compost
Range of particles radii (mm)	2.5 - 10	2.5 – 10
Friction coefficient (---)	0.6	0.6
Poisson's ratio (---)	0.25	0.25
Young's modulus (MPa)	20	0.3
Bulk density (kg/m^3)	507	748
Bonds normal and shear strength (N)	---	0.5

5.6.2. Computational Fluid Dynamics

CFD is a numerical modeling method based on solving the partial differential equations (continuity, momentum and energy) that govern the flow inside a specific continuous domain. In this way, the volume filled by the fluid is spatially divided into small cells defined by a grid. For each cell, the primary variables (density, pressure, velocities and temperature) are solved as a function of time. For these applications the liquid is considered to flow at steady state, where density, pressure and velocities can be defined for each cell of the grid. In the case of the flow inside a spreader, the volume filled with fluid will decrease as the machine is emptied. This type of flow is known as a free surface flow described by a specific model called volume of fluid (Hirt and Nichols, 1981). In these conditions, the modeling approach is to use a multi-phase model. The two phases (air and sludge) are stratified and separated by a clear interface. Each cell is entirely filled by one of the two phases, except for cells at the interface. The free surface can be identified during post processing by displaying the volume fraction contour of one fluid phase. Successful applications of this modeling approach include the flow of rivers (Ma et al., 2002) and that of industrial fluids (Courbebaisse and Garcia, 2002).

From the perspective of fluid mechanics, a product is basically considered as fluid when no tangential stress is observed in a stationary volume. Based on this criterion, semi-solid manure or sludge could not be considered as fluid. However, this definition has been extended to products exhibiting a yield stress. These particular fluids will only flow after a sufficient load has been applied. Rheological measurements have been applied to pasty sewage sludge used for land application (Baudez, 2001). Specific measuring procedures have been designed for determining the rheological behaviour of this type of product: initial preshear, roughened surfaces, large gap measurements, flow curve and yield value calculations. The results showed that the flow curves approximately followed a Herschel-Bulkley model. This non-Newtonian model can be implemented in the selected CFD code CFX (version 4.4, ANSYS Europe Ltd., Oxfordshire, UK). Two types of pasty sludge were selected for the study: the fluid pasty sludge (can be pumped with high-performance volumetric pumps) and the plastic

pasty sludge (can be stacked in a 60 cm height heap with a rough surface). These two different types of pasty sewage sludge can be represented, for CFD simulations, by two Hershel-Bulkley rheological models. The rheological models are presented in table 5.3 where τ is the shear stress in Pa and $\dot{\gamma}$ the shear rate in s^{-1}.

Table 5.3. Rheological models used to describe fluid and plastic pasty sludge.

Sludge type	Rheological model
Fluid pasty sludge	$\tau = 20 + 10 \ \dot{\gamma}^{0.30}$
Plastic pasty sludge	$\tau = 300 + 150 \ \dot{\gamma}^{0.20}$

Because of the high viscosity values exhibited by these products (1 to 200 Pa-s), an assumption of laminar flow was made. In the CFD model, the physical boundaries of the domain are represented by walls. For a sludge spreader, the bottom wall of the hopper is the discharge conveyor which in this case was modeled by a constant velocity wall along with a no slip condition at its interface with the fluid. Sludge spreaders are usually equipped with discharge augers, but including that type of discharge conveyor in the model would have considerably increased the complexity of the geometry definition. It was assumed for this model that a wall in translation and a no slip condition would have an effect similar to that of a screw conveyor. The flow of product on the spinning discs used to spread the sludge on the ground was also modeled and, in this instance, the model and the experimental equipment had the same geometry.

5.7. Material and methods

5.7.1. Compost spreading

Experiments were carried out to study the effect of the vertical position of the flow-control gate on the discharge rate and power consumption of the discharge conveyor of a manure spreader for different organic fertilizers. Using a commercial manure spreader (Miro Heywang Saturne), stationary unloading trials were performed with and without the spreading devices (dual vertical beaters). The mass of the tractor-spreader system was continuously recorded by six truck-type scales (50 kN capacity per scale;

Captels, Saint-Mathieu de Tréviers, France). The power requirement of the hydraulically driven scraper conveyor was measured by means of a flow meter (270 l/min capacity; Hydrotechnik, London, UK) and a pressure transducer (400 bars capacity; Bourdon-Haenni Ltd, Aldershot, UK). The recommendations of European Standard EN 13080 (CEN, 2002) were followed for the field experiments and data analysis. The characteristic flow rate can be calculated using equation (5.4):

$$s_f = \max_{j=1}^{n-m+1} \left[\frac{1}{m} \sum_{i=j}^{j+m-1} x_i \right] \qquad , \qquad (5.4)$$

where s_f = characteristic flow rate (kg/s),

   n = number of samples during unloading,

   m = number of samples during 30% of the unloading time ($m=0.3 \cdot n$) and

   x_i = flow rate at sample i (kg/s).

This parameter was used to assess the amount of material discharged by the spreader as a function of its operating parameters. The characteristic flow rate basically corresponds to the highest average flow rate occurring during 30 percent of the unloading time of the spreader. Another evaluation criterion makes use of the power data to calculate the specific energy required by the conveying system during the unloading operation. The specific energy is calculated using equation (5.5):

$$E_{unloading} = \frac{\int_0^{t_{unloading}} P(t)dt}{M} \qquad , \qquad (5.5)$$

where $E_{unloading}$ = specific energy of the unloading operation (J/kg),

   $t_{unloading}$ = unloading time of the spreader (s),

   $P(t)$ = power consumption of the floor conveyor as a function of time (W) and

   M = mass of product unloaded (kg).

The characteristic flow rate and the specific energy were calculated for the experimental and simulated unloading operations and comparisons were made between those parameters to assess the performance of the discrete element machine-product interactions models.

5.7.2. Sludge spreading

Jointly with CFD simulations, experiments were carried out with a Hill 15-2000 spreader (LK Verkstad, 590 62 Linhem Sweden). This spreader featured a V-shaped hopper with two augers to move the sludge towards the rear outlet. The size of the outlet could be adjusted to control the discharge rate. Measurements were carried out according to European Standard EN 13080 (CEN, 2002) which defines the procedure for the measurement of manure spreaders longitudinal distribution. The sludge discharge rate was measured by continuously recording the weight of the tractor-spreader system.

The sludge flow was also studied on the spinning discs, by means of an experimental apparatus. A scaled experimental spreader (1/5 scale) was designed and built for this purpose. The sludge delivered by the auger fell on a single disc fitted with two vanes. For practical reasons, this apparatus was mainly used with suspensions of kaolin exhibiting a viscosity similar to that of pasty sewage sludge. High-speed video recordings were taken as the experimental scaled spreader was operated. Photographs of the flow from the disc were taken with an aperture time of 1/500 second. The spreading pattern was visually analyzed and transversal distribution measured according to standard procedure EN 13080 (CEN, 2002).

5.8. Results and discussion

5.8.1. Compost spreading & DEM models

This section first presents the preliminary models that were developed of a full solid manure spreader with dual vertical beaters. The main simulations targeting different operating parameters for the two types of composts are then presented with detailed comparisons with experimental results.

Figure 5.1 illustrates the DE model of the spreader equipped with two vertical beaters. The objective of this preliminary spreader model was to assess the ability of this numerical approach to effectively simulate spreading operations. The simulation parameters are presented in table 5.4. Figures 5.2, 5.3 and 5.4 illustrate the ground distribution of the compost particles at the end of the simulated static unloading operation. These ground distributions were obtained by using a post-processing procedure that divides the spreading area into cells and calculates the mass of product in each cell. Figure 5.2 presents an overall view of the ground distribution. Figure 5.3 allows for a better visualization of the spreading width. Both figure 5.2 and 5.3 were created from a grid made of 1 m x 1m cells. Figure 5.4 illustrates the ground distribution with a finer grid with 0.5 m x 0.5 m cells. The ground distribution remains the same, but the finer grid highlights the irregularities in the manure distribution. Figure 5.5 presents a cross section of the ground distribution of figure 5.4. It can be seen that the simulated effective spreading width was approximately 4 to 8 meters which was in good agreement with the typical spreading width of this type of equipment (Cemagref, 1997; Frick et al., 2001).

Table 5.4.   Parameters used for the simulation of the static unloading of the spreader.

Spreader parameters	Spreader length (mm)	3,580
	Spreader width (mm)	1,460
	Spreader height (mm)	1,000
	Conveyor slats height (mm)	160
	Inter-slat distance (mm)	425
	Conveyor linear velocity (mm/s)	30
	Beaters diameter (mm)	690
	Beaters rotational velocity (rpm)	360
	Spreader speed (km/h)	5.0
Compost parameters	Bulk density (kg/m^3)	612
	Static coefficient of friction	0.6
	Particle diameter (mm)	85
	Normal and shear stiffness (N/m)	5.1e4
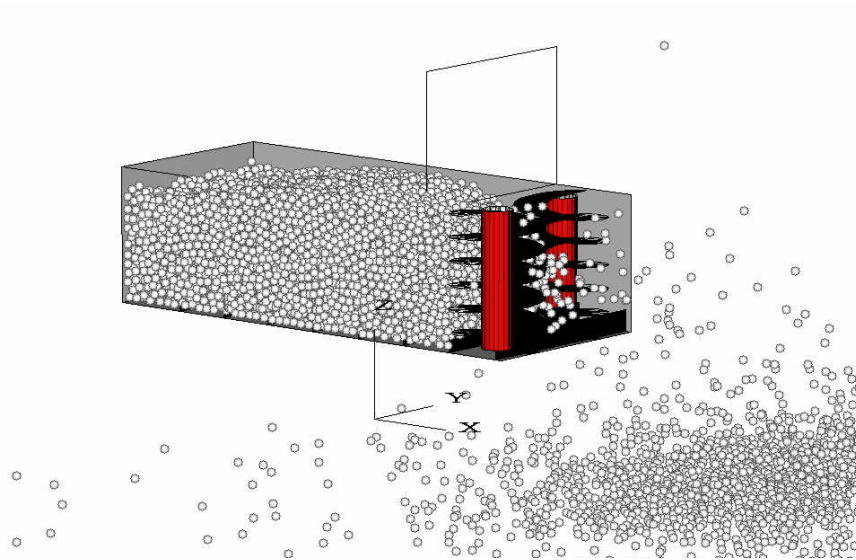
Figure 5.1.   Numerical simulation of the discharge of a manure spreader with two vertical beaters using the discrete element method.

Figure 5.2.   Surface plot of the ground distribution of compost particles after the simulated static spreading operation (each data point used to generate the surface represent the total mass in a 1m x 1m cell).

Figure 5.3.   Transversal view of the surface plot of the ground distribution of compost particles after the simulated static spreading operation (each data point used to generate the surface represent the total mass in a 1m x 1m cell).

170

Figure 5.4.   Surface plot of the ground distribution of compost particles after the simulated static spreading operation highlighting the irregularities (each data point used to generate the surface represent the total mass in a 0.5 m x 0.5 m cell).
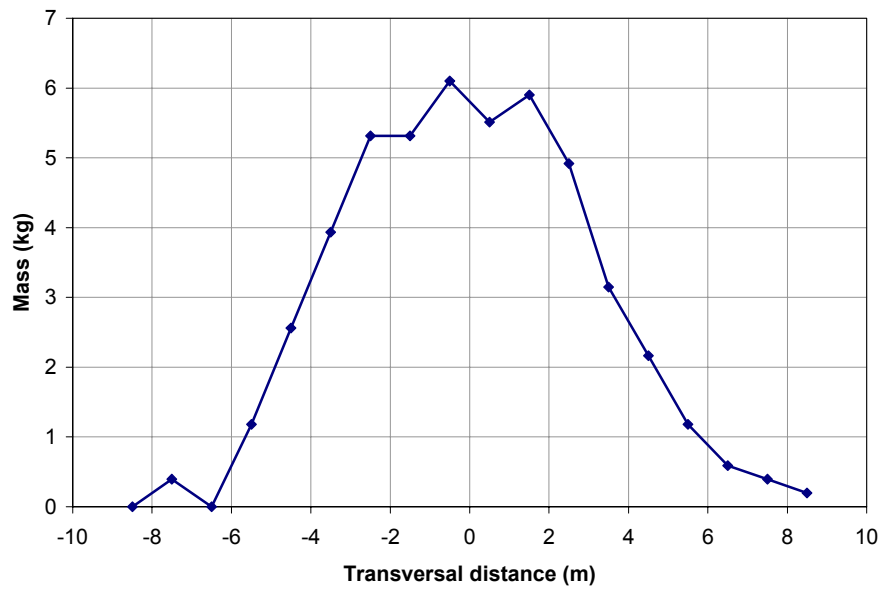
Figure 5.5.   Simulated transversal mass distribution at a longitudinal distance of 1.25 m for the static unloading operation.

A second simulation of the complete spreader was performed. This time 3 sizes of particles were used and the spreader was moving at a speed of 7.5 km/h. The parameters for the second simulation are presented in table 5.5. Figures 5.6 and 5.7 illustrate the ground distribution for the moving spreader simulation, with 1.1 m x 1.2 m (longitudinal dimension x transversal dimension) cells. It can be seen on figure 5.7 that while some particles were thrown at considerable distances from the spreader, the effective spreading width was quite limited. Figure 5.8 illustrates the irregularities in the ground distribution both longitudinally and transversally. The longitudinal distribution was consistent with what can typically be obtained when spreading homogenous granular products. It should be noted that for simplicity purposes, vertical beaters were modeled whereas in reality, the beaters are typically inclined towards the tractor-end of the machine at an angle of approximately 15º from the vertical. Spiral walls have also been used to model the beaters, without including the peripheral teeth or blades that are present on most commercial machines.

Table 5.5. **Parameters used for the simulation of the unloading of the moving spreader.**

Spreader parameters	Spreader length (mm)	3,580
	Spreader width (mm)	1,460
	Spreader height (mm)	1,000
	Conveyor slats height (mm)	80
	Inter-slat distance (mm)	425
	Conveyor linear velocity (mm/s)	30
	Beaters diameter (mm)	690
	Beaters rotational velocity (rpm)	360
	Spreader speed (km/h)	5.0
Compost parameters	Particles density (kg/m^3)	1300
	Bulk density (kg/m^3)	650
	Static coefficient of friction	0.6
	Particle diameter (mm) and proportion of total number (%)	74.4 - 30 59.5 - 40 49.6 - 30
	Young's modulus (MPa)	0.3
	Poisson's ratio (---)	0.25
	Normal stiffness (N/m)	from eq. 5.1
	Shear stiffness (N/m)	from eq. 5.2

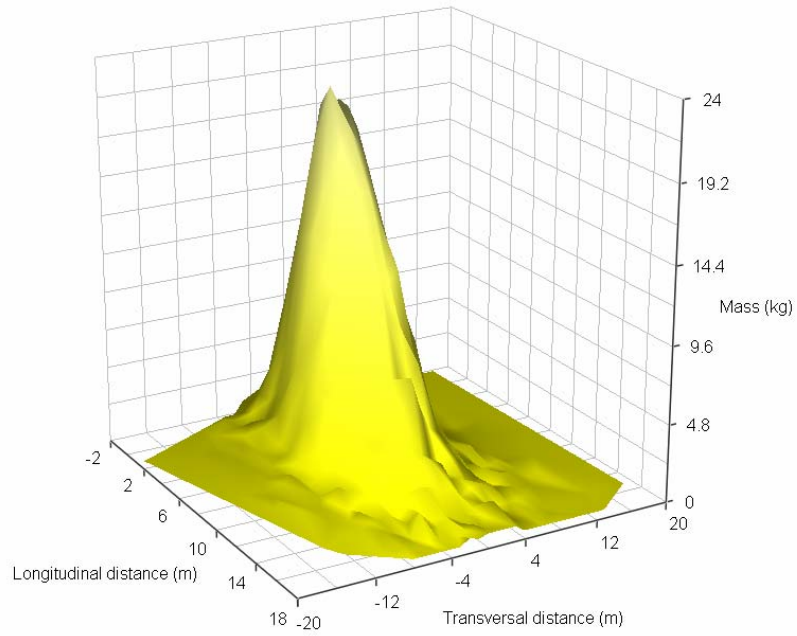**Figure 5.6.   Surface plot of the ground distribution of compost particles after the simulated spreading operation (each data point used to generate the surface represent the total mass in a 1.1 m x 1.2 m cell).**
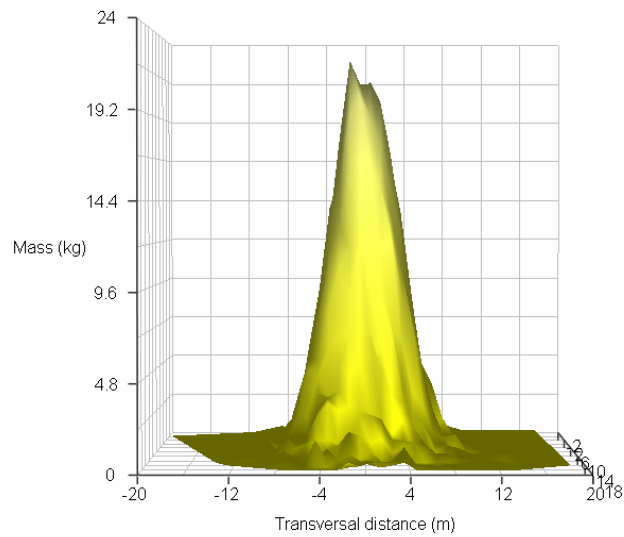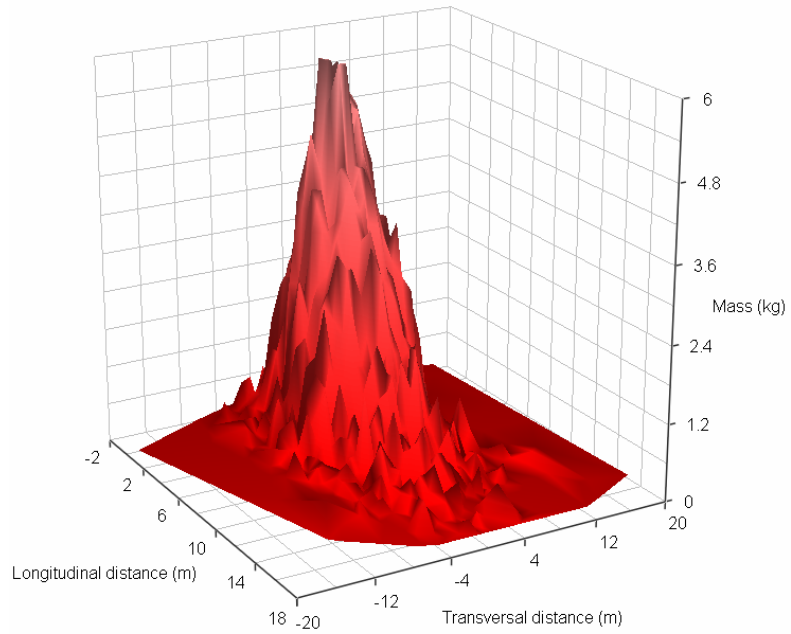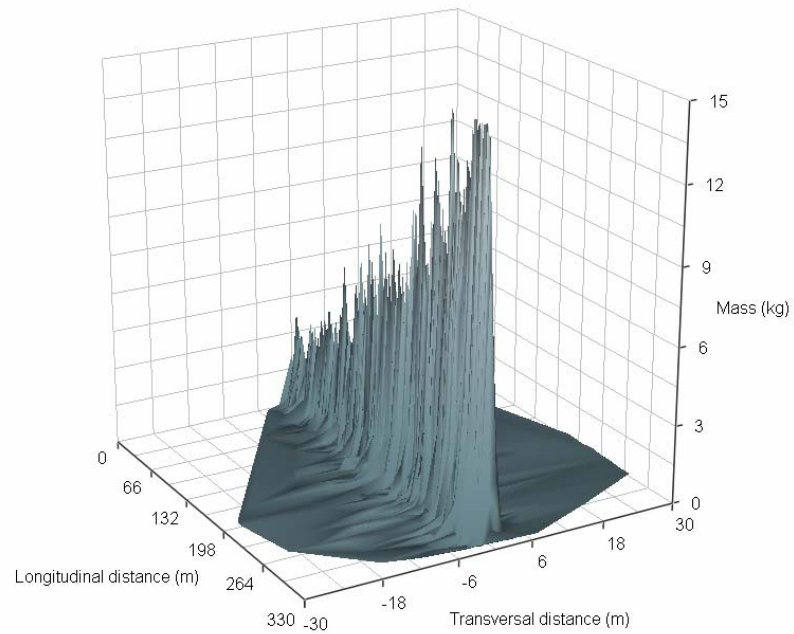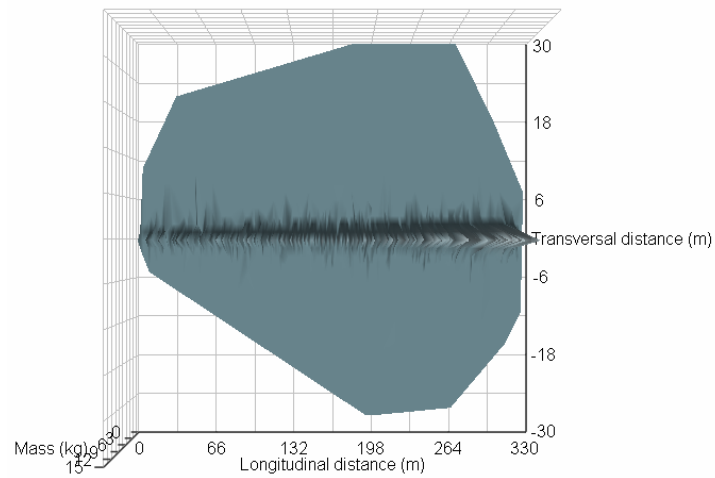

Figure 5.7.   Top view of the surface plot of the ground distribution of compost particles after the simulated spreading operation (each data point used to generate the surface represent the total mass in a 1.1 m x 1.2 m cell).
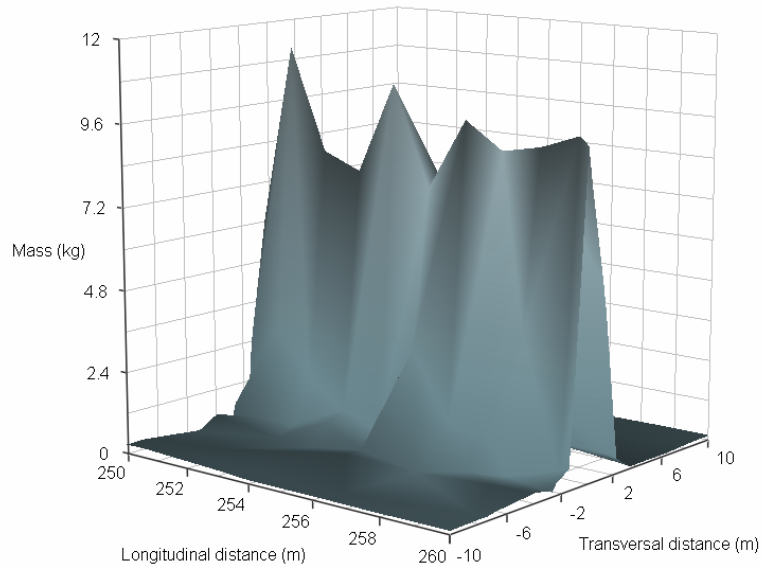
Figure 5.8. Section (10-m long by 20-m wide) of the surface plot of the ground distribution of compost particles after the simulated spreading operation highlighting the uneven longitudinal and transversal distribution (each data point used to generate the surface represent the total mass in a 1.1 m x 1.2 m cell).

The results obtained for these simulations were favourably compared to results published by Frick et al. (2001), who reported power values of approximately 19 kW and 1 kW for the mechanical (beaters) and hydraulic (conveyor) power requirements, respectively. The spreader that they used featured dual vertical beaters and had a capacity similar to that of the spreader included in the simulation. The product spread by Frick et al. (2001) was dehydrated sewage sludge (32% TS; 875 kg/m^3) and the application rate was 12 t/ha. The simulation results for an application rate of approximately 12 t/ha indicated that the power requirements were 13.1 kW and 0.2 kW for the beaters and discharge conveyor, respectively. The static unloading simulation indicated power requirements of 18.9 kW for the beaters and 0.4 kW for the conveyor. Even though the simulations were not aimed at replicating the experiments published by Frick et al. (2001) and the products spread were different, this comparison clearly demonstrates the potential of the method with simulated power values that are very close to the typical values measured experimentally.

Extensive simulations were also run for the unloading of the spreader without the spreading devices and with the conveyor operated at 0.03 m/s. A scale mode (1/5 scale)

174

of the spreader described in table 5.5 was implemented in PFC^{3D}. The two types of compost described in table 5.2 were generated in the model spreader and the effect of the flow-control gate was investigated. Dimensionless relationships were established to allow for comparisons to be made between the experimental full-scale spreader and the simulated scaled machine. To study the characteristic flow rate, the mass efficiency was defined as:

$$M_e = S_f / (H \; w \; v_c \; \rho) \quad , \qquad (5.6)$$

where M_e = mass efficiency (dimensionless),

S_f = characteristic flow rate (kg/s),

H = height of the flow section (distance between the bottom of the gate and the bottom of the hopper) (m),

w = width of the flow section (m),

v_c = velocity of the conveyor (m/s) and

ρ = bulk density of the product (kg/m^3).

The power data were made dimensionless using equation 5.7:

$$P_s = (P/L_c) / S_f \; g \qquad , \qquad (5.7)$$

where P_s = specific power (dimensionless),

P = peak power (W),

L_c = length of the conveyor (m) and

g = acceleration due to gravity (m/s^2).

Figure 5.9 illustrates how the simulated results compared to the measured data. The detailed results are included in table 5.6. Different scales are used for the measured and simulated results in figure 5.9 to allow for the visualization of how the trends were replicated by the model. The same approach was used in figures 5.15 and 5.16.
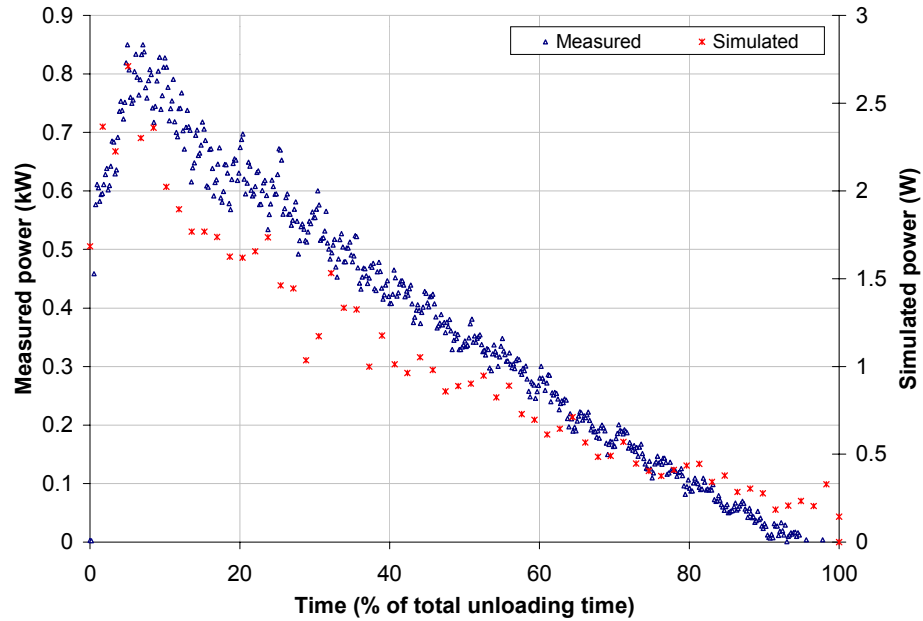
Figure 5.9.   Simulated and measured power at the conveyor (dry compost; bottom of gate 515 mm above the bottom of the hopper).

Table 5.6.   Mass efficiency and specific power for the two gate positions and two organic fertilizers included in the study.

			Measured	**Simulated**
Dry compost	Mass efficiency	Gate open	1.21	1.22
		Gate low[a]	1.02	2.84
	Specific power	Gate open	0.87	0.26
		Gate low[a]	2.27	0.32
Compost	Mass efficiency	Gate open	1.22	0.92
		Gate low[a]	0.90	1.65
	Specific power	Gate open	0.62	0.54
		Gate low[a]	1.79	0.69

[a]Bottom of gate 515 mm above the bottom of the hopper.

Looking at the results for dry compost in more detail reveals that the simulated and measured mass efficiency were virtually the same in the case of the gate fully open. The values of approximately 1.2 indicate that the actual flow rate was larger than the theoretical value. The most probable cause for this ratio is the gravity flow that would occur with the gate fully open. When the gate was in its low position, the measured mass efficiency was very close to unity, meaning that the actual flow rate was very close to the theoretical value. In the simulated case, the mass efficiency increases to 2.84 when the gate is lowered. Even though the actual characteristic flow rate did decrease from the simulated open gate scenario to the simulated closed gate setting

176

(1.30 kg/s compared to 1.26 kg/s), the difference was too small to make the mass efficiency comparable to the measured value. This high value of mass efficiency seems to indicate that the effect of the gate on the flow rate was not well replicated by the model. This would suggest that the gravity flow phenomenon was still very present in the simulation despite lowering the gate. The action of the conveyor might have been altered by the scaling used in the model. The ratio of particle dimension to slat height should be investigated in more detail to highlight its influence on the accuracy of the model predictions. Both the measured and simulated specific power values showed an increase when the gate was lowered. The effect was however much less significant in the simulated case.

The results for compost showed similar trends. The simulated mass efficiency exhibited the opposite tendency when compared to the measured values. Again, the results of the simulations showed an increase in flow rate when the gate was raised to fully open, but the absolute difference in flow rate did not allow for the mass efficiency to become the same as the measured value. The specific power indicated an effect of the flow-control gate, but the magnitude of this effect was attenuated in the simulated case.

Figures 5.10 and 5.11 present the values of characteristic flow rate (eq. 5.4) and specific energy (eq. 5.5) obtained for dry compost experimentally and by simulation, respectively. Figures 5.12 and 5.13 include the values of characteristic flow rate and specific energy obtained for compost experimentally and by simulation, respectively. Figures 5.10 to 5.13 allow visualizing the trends of the two parameters without resorting to the dimensional analysis. Figures 5.10 and 5.12 illustrate that the flow-control gate positioned 515 mm above the bottom of the hopper resulted in an increase in specific energy and a diminution of the characteristic flow rate when compared to the results obtained with the gate fully open, for both products. The models were capable of replicating the gate effects, but not proportionally. The results included in table 5.6 and figures 5.10 to 5.13 demonstrated that the models are capable of predicting the effects of the flow-control gate for products exhibiting different properties, but that the models

177

are perfectible. Refinements of the compost models have the potential to increase the accuracy of the interactions models. The effect of scaling the models should be investigated in more depth by carrying out simulations at different scales.

Figure 5.10.   Measured characteristic flow rate and specific energy for dry compost.

Figure 5.11.   Simulated characteristic flow rate and specific energy for dry compost.
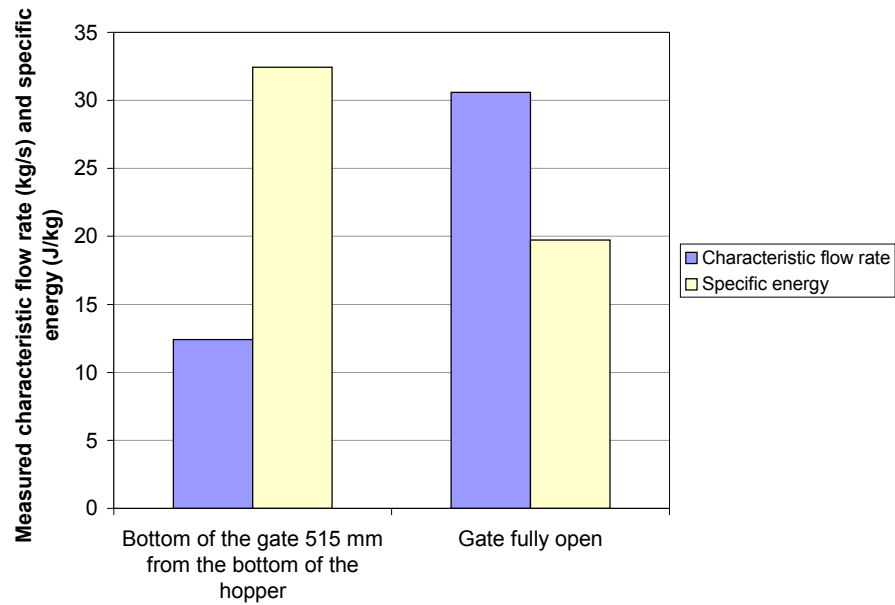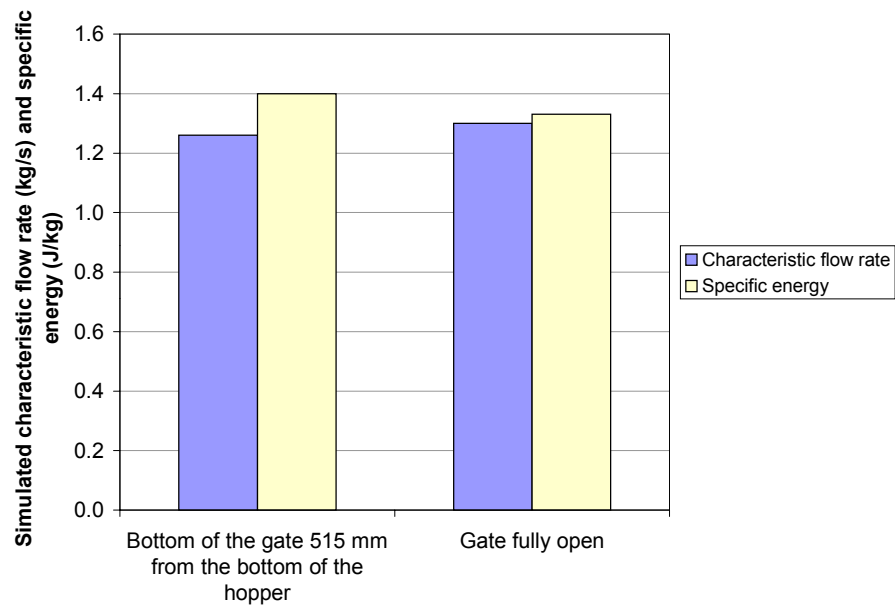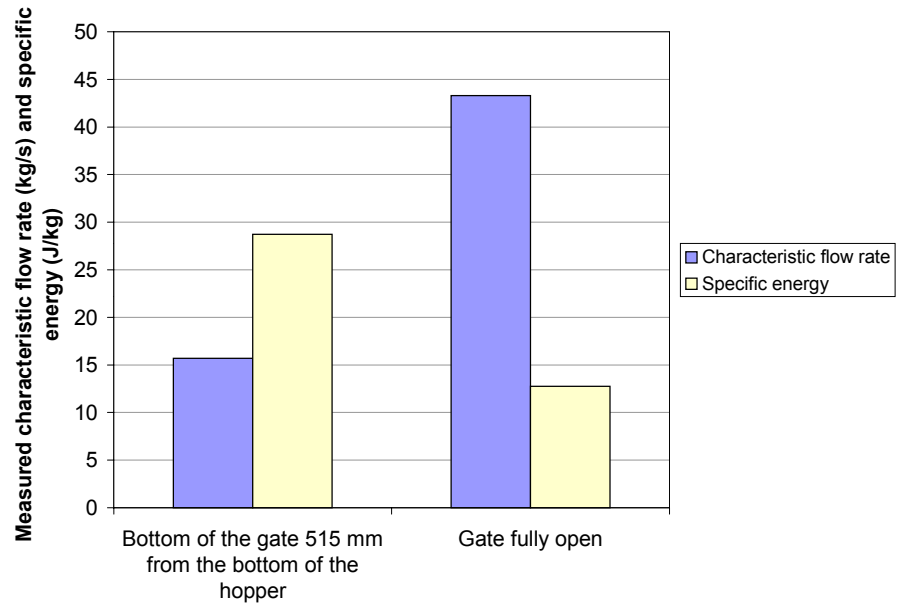
Figure 5.12.   Measured characteristic flow rate and specific energy for compost.
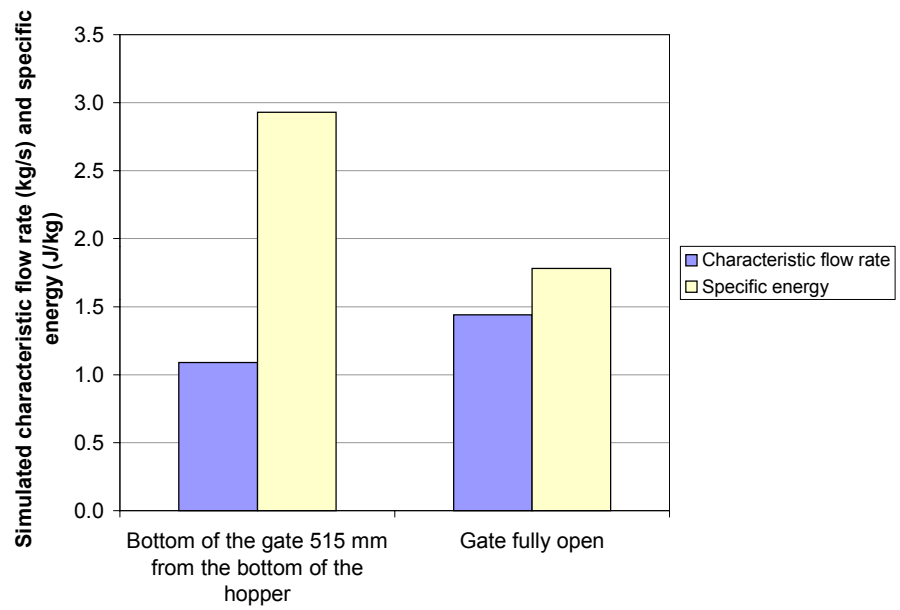
Figure 5.13.   Simulated characteristic flow rate and specific energy for compost.

Figure 5.14 illustrates the use of the DE models to get some insights into the flow of compost in the spreader. It includes an actual picture taken during the unloading test. During the field experiments, it was observed that a fracture plane would consistently appear in the bulk of product. Product crumbling would also consistently occur near the gate and at the back of the spreader. In figure 5.14, it is possible to see that the contact bonds included in the model exhibited a behaviour similar to that of the real compost during the spreading experiments.

Similar fracture patterns
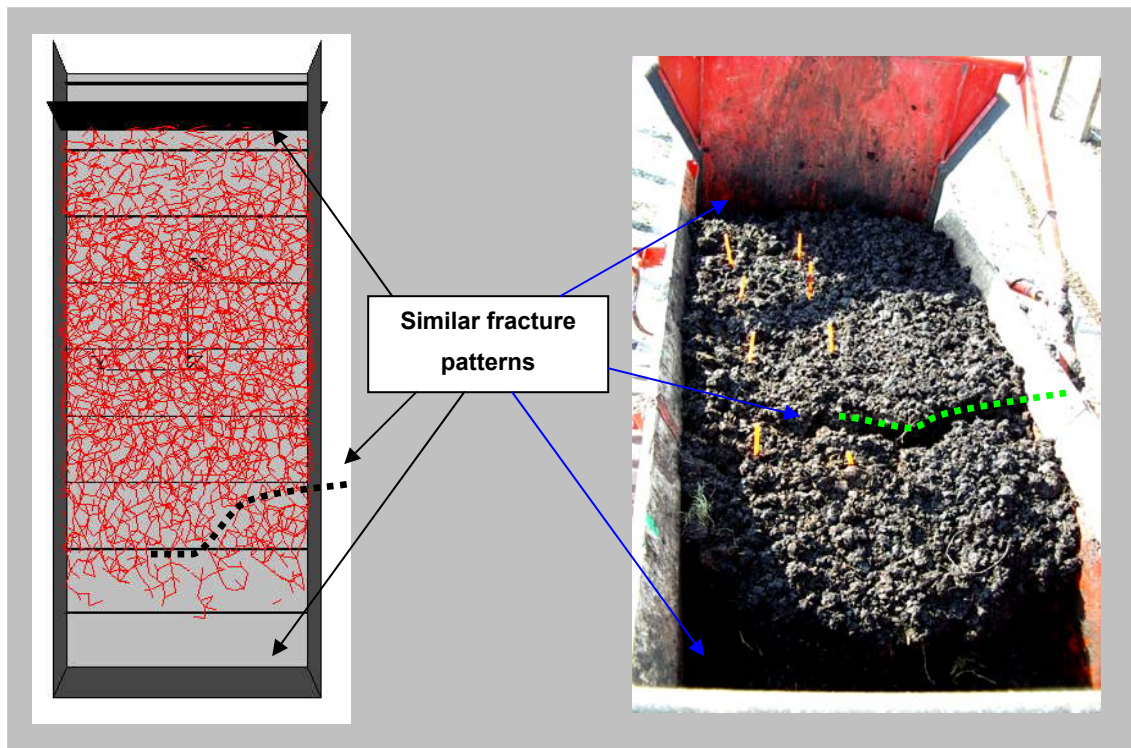
Figure 5.14. Comparison between the modeled and actual compost behaviour. Top view of the modeled (left) and actual (right) spreader and compost (the discharge end is at the top of the figure). The illustration of the modeled spreader includes the contact bonds (represented by the network of short lines) in the top 90 mm of the spreader to allow for a better visualization of the bond breaking patterns.

5.8.2. Sludge spreading & CFD models

The measured flow rate for the Hill 15-2000 spreader showed large variations depending on the physical characteristics of the sludge. The measured and simulated flow rates are presented for fluid and plastic pasty sludge on figures 5.15 and 5.16, respectively. With a fluid pasty sludge, the flow rate decreased regularly during the

entire duration of the spreader emptying process. This continuous decrease implies that the field application rate will be extremely unsteady. At the beginning of the spreading operation, the application rate is very high. A similar decrease in flow rate during the unloading phase of the spreader has been observed for semi-solid manure (Malgeryd and Pettersson, 2001). This phenomenon could be reduced by adjusting the size of the discharge opening as the spreader is being emptied, but a reliable control system would be required for dynamic adjustment. With a viscous material, the discharge rate was highly variable. Large variations of the application rate also occurred with this type of sludge.

The results obtained with CFD simulations were similar (total mass flow through outlets) to those obtained experimentally (discharge rate). Convergence difficulties arose in the case of the plastic pasty sludge. This phenomenon can be considered consistent with the heterogeneous flow observed in practical situations. In this case, the flow is induced by the displacement of large aggregates and cannot be solved by the analysis of the situation in each small cell.
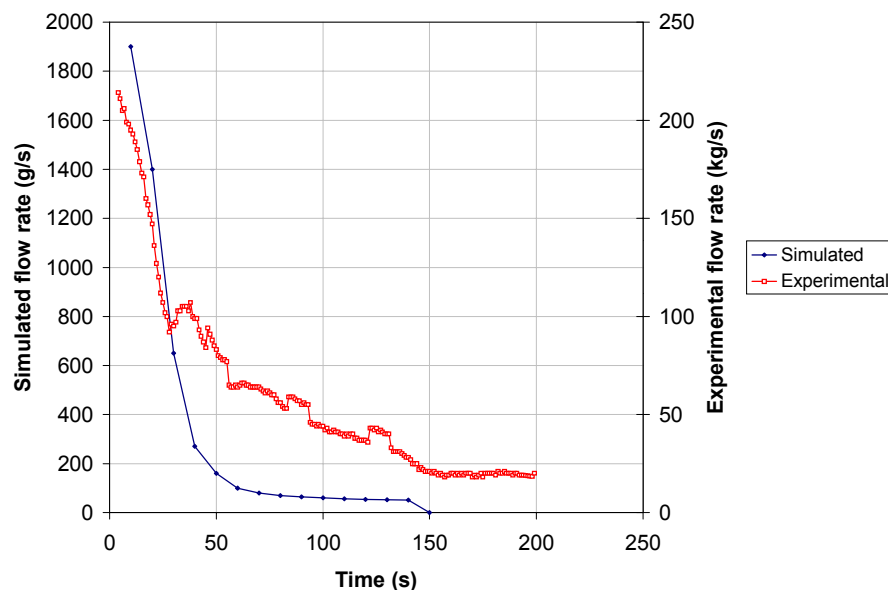
Figure 5.15.   Experimental and simulated flow rate of fluid pasty sludge as a function of time.
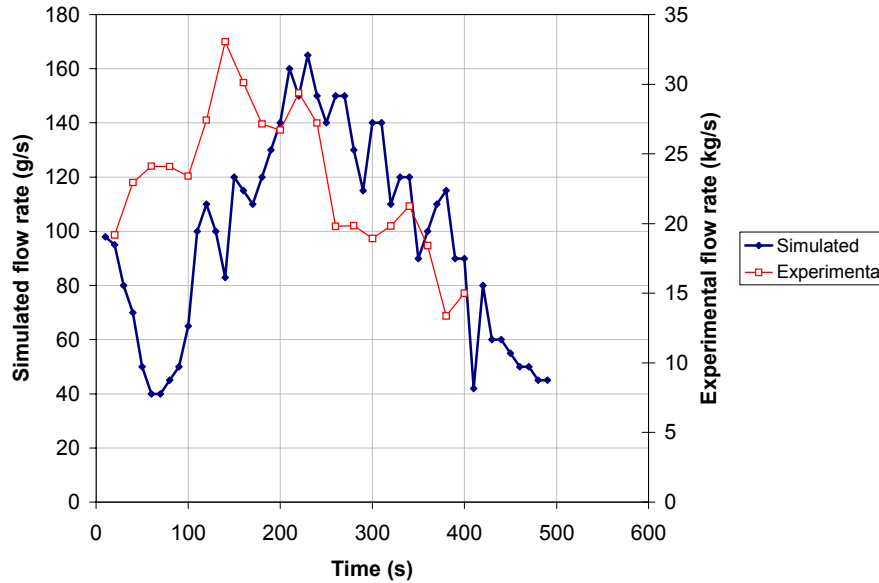
Figure 5.16.   Experimental and simulated flow rate of plastic pasty sludge as a function of time.

Figure 5.17 presents the streamlines inside the holding system of the spreader according to the simplified geometry used in the CFD simulations. With a fluid sludge, it appeared that the flow due to gravity had a high influence on the total flow. Since the flow rate depended on the depth of fluid in the hopper, it decreased rapidly with the discharge time. Under field conditions, it was also possible to observe that the flow rate increased when the machine was traveling uphill. With this type of flow inside the hopper, the sludge level decreased primarily at the discharge end. With a plastic sludge, the sludge level decreased predominantly at the front end of the hopper. Bridging can also occur over the auger and disturb the discharge rate.

(a)   (b)
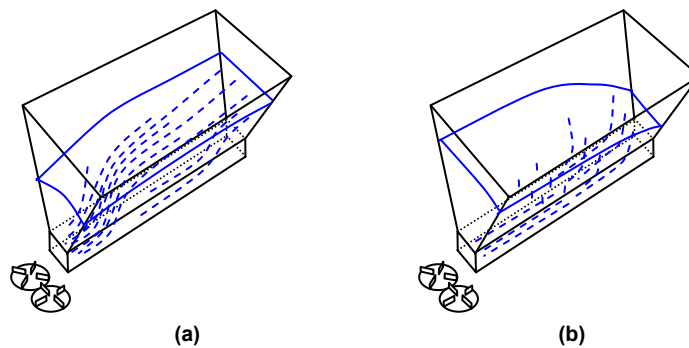
Figure 5.17.   Simulated streamlines inside the spreader tank for (a) fluid pasty sludge and (b) plastic pasty sludge.

Experimental results were also collected during measurements related to the flow of sludge on a spreading disc. High-speed video recordings of the flow showed that the sludge stream, issued from the hopper, was first cut by the vane. A block of sludge was then separated from the main discharge flow. This block flowed along the vane. Upon reaching the tip of the vane, the sludge was divided into fragments and thrown along a trajectory defined by the initial velocity of the sludge when leaving the disc.

Photographs of the flow from the disc showed the particle trajectory every 1/500 second. The length (L) of the trajectory shown by the photograph indicates the velocity (v) of the particle (equation 5.8). The velocity can also be determined from the rotational velocity of the disk. The tangential velocity (v_t) depends on the disc radius (R) and angular velocity (ω) as expressed in equation 5.9. Equation 5.10 relates the radial velocity (v_r) to the tangential velocity (v_t) and throw angle (α) while equation 5.11 gives the velocity (v) as a function of the tangential and radial velocity components. The equations used to calculated the velocity and velocity components were

$$v = 500\,L \qquad (m/s) \quad , \qquad (5.8)$$
$$v_t = R\omega \qquad (m/s) \quad , \qquad (5.9)$$
$$v_r = v_t \tan \alpha \qquad (m/s) \quad \text{and} \quad (5.10)$$
$$v = (v_r^2 + v_t^2)^{0.5} \qquad (m/s) \quad . \qquad (5.11)$$

Figure 5.18 shows a schematic representation of the photographs analysis. The disc radius was 0.20 m. The angular velocity was 83.25 rad/s (795 rpm).
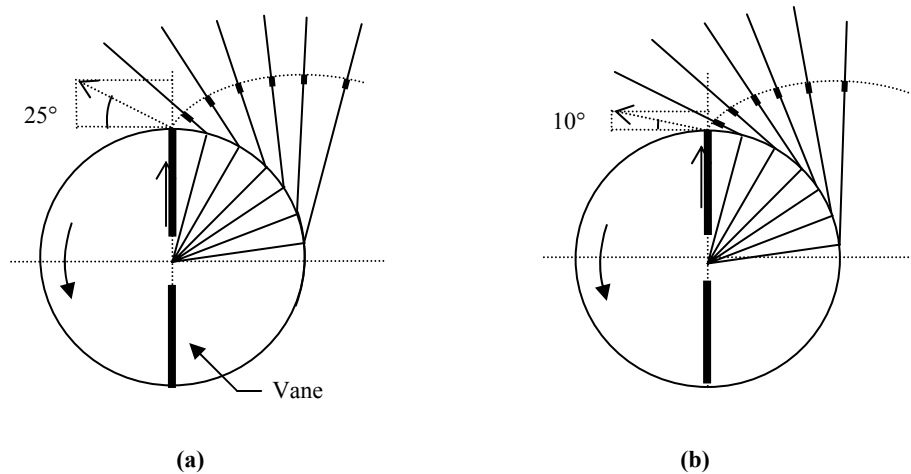
Figure 5.18.   Sludge trajectories from the rotating disc for (a) fluid pasty sludge and (b) plastic pasty sludge.

Knowing that the total velocity is the magnitude of the actual velocity vector and that the tangential velocity can be calculated from the radius and angular velocity of the disc, the radial and total velocities can be determined using the throw angle. Total velocity can be compared to the result calculated from the trajectory length on the photograph (table 5.7).

Table 5.7.   Velocities calculated from the length and angle of the trajectories captured on photographs.

	Fluid pasty sludge	Plastic pasty sludge
Measured throw angle (degrees)	25	10
Tangential velocity from equation 5.9 (m/s)	16.65	16.65
Radial velocity from equation 5.10 (m/s)	7.76	2.94
Total velocity from equation 5.11 (m/s)	18.37	16.91
Total velocity from equation 5.8 (m/s)	24.0	20.0

An increase in sludge viscosity resulted in a decrease in velocity and an increase in residence time along the vane. Consequently, a high viscosity sludge remained on the vane for a longer time and was thrown after a higher angle of rotation. It is then possible to state that the discharge angle, and therefore the repartition of the sludge on the ground, is dependent upon the sludge viscosity, all other machine parameters remaining the same. These results were confirmed by the observation of two spreading patterns on the soil, as shown in figure 5.19. The spreading patterns were visually determined by rating (on a scale of 1 to 10) the amount of sludge in 0.5 m x 0.5 m cells after a static unloading of the spreader.
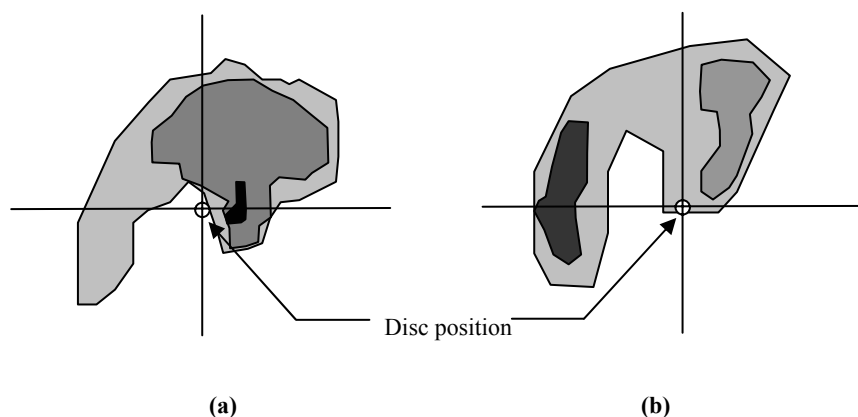
Figure 5.19.   Observed spreading pattern for (a) fluid pasty sludge and (b) plastic pasty sludge (the darker the color, the higher the application rate).

With the fluid sludge, the major part of the disc discharge occurred after a rotation angle of about 100° corresponding to a residence time on the vane of 0.021 s. With the viscous sludge, this rotation angle was about 180° for a residence time on the vane of 0.037 s. With the fluid sludge, the velocity along the vane was high, and the sludge was rapidly thrown away. Most of the sludge was spread in the rear direction, behind the spreader. With the viscous sludge and the same discharge point, the throw was translated laterally.

With CFD simulations, it was possible to calculate the flow of a sludge block swept by a vane. The geometry used for these simulations was the same as the experimental spreader (Hill 15-2000). The discharge point, where the sludge block is cut out from the main stream was located at 80 mm from the center of the disc. The postprocessor showed the displacement of the sludge volume. Simultaneously, the block of sludge was flattened upon the vane surface and flowed towards the tip of the vane. For a fluid pasty sludge, the main flow output duration was 0.035 s, from 0.015 s after the sludge was caught by the vane to 0.050 s. This time interval corresponds to a 160° rotation sector. The same calculation with a plastic pasty sludge yielded a different result. Due to the higher viscosity, the flow velocity was lower with a plastic sludge. The residence time on the vane was increased by the higher viscosity. The projection sector was therefore shifted. Figure 5.20 shows the difference in residence time on the vane for two different types of sludge.

185
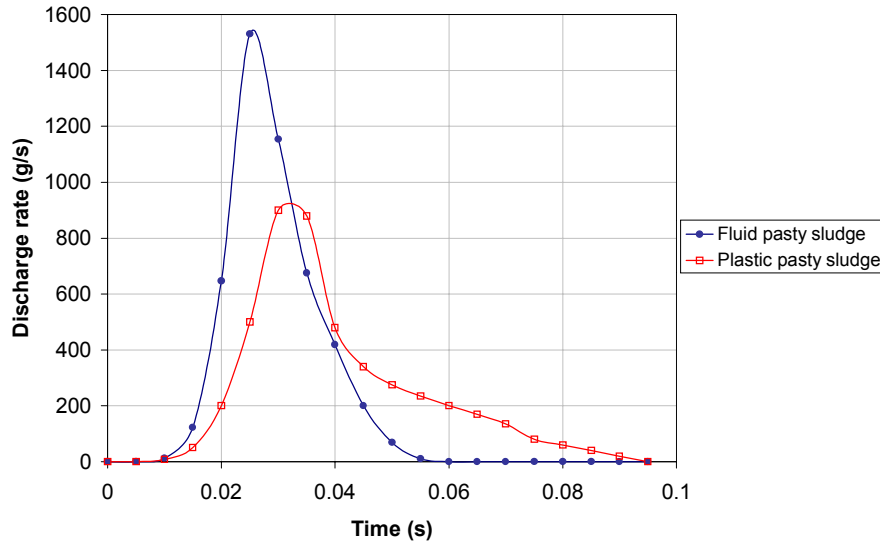
Figure 5.20. Measured residence time for fluid pasty sludge and plastic pasty sludge.

A comparison between the average residence times obtained by CFD simulations and the times measured experimentally is presented in table 5.8. The values of residence time are very close indicating a good ability of the model to represent the flow of sludge on a spreading disc.

Table 5.8. Experimental and simulated residence time on the vane for fluid and plastic pasty sludge.

	Fluid pasty sludge	Plastic pasty sludge
Experiments	0.021 s	0.037 s
CFD simulations	0.025 s	0.033 s

5.9. Conclusions

Numerical modeling was applied to the flow of organic fertilizers in land application equipment. The discrete element method was applied to the flow of two types of composts. A preliminary model of a full-size spreader with dual vertical beaters was capable of realistically predict the ground distribution of the product along with the power requirements of the beaters and discharge conveyor. Scaled numerical models were developed to study the effect of the vertical position of a flow-control gate and the type of compost spread on the discharge flow and energy requirements. The models

186

were validated against experimental results obtained using a full-size manure spreader. For both types of composts, the conveyor was operated at 0.03 m/s and two operational configurations were tested: the gate fully open and the bottom of the gate 515 mm above the bottom of the hopper. An increase in specific power was obtained for both the experimental and simulated results and for both products. The simulated mass efficiency values were in good agreement with the experimental values in the open gate configuration. The reduction in flow rate produced by the lowering of the gate was replicated by the models, but the absolute difference between the flow rate with the gate fully open and the flow rate with the gate lowered was underestimated by the model. As a result, the simulated mass efficiency showed an inverse trend when compared to the experimental results.

Computational fluid dynamics was applied to the flow of sludge in a spreader. The simulated and experimental flow rate curves were in close agreement for both a fluid pasty sludge and a plastic pasty sludge. The simulated streamlines in the hopper were also in good agreement with field observations. The sludge flow on a disc was studied on a scaled experimental spreader. CFD simulations of that flow were also carried out. The CFD models were capable of reproducing sludge flow on a disc with values of residence time well correlated to experimental results.

The two numerical methods applied in this study could be used to successfully model the flow of organic fertilizers in land application equipment. Improvements in the DE models are possible by refining the constitutive models used for the composts. Full-scale models also have the potential of enhancing the accuracy of the simulations as the geometry of the mechanical systems would be implemented with more realism. The CFD models could also be enhanced by improving the representation of the discharge conveyor. The numerical simulations have the potential of revealing valuable information on the flow of these products in land application equipment. It becomes however very challenging to collect experimental data to validate the models. This is greatly illustrated by the analysis of the sludge velocity and residence time on the disc or by the observed fracture patterns in compost during spreading.

5.10. Acknowledgements

5.11. References

Bardet, J.P. 1997. Experimental soil mechanics. Upper Saddle River, NJ : Prentice Hall.

Baudez, J.C. 2001. Rhéologie et phisico-chimie des boues résiduaires pâteuses pour l'étude du stockage et de l'épandage. Unpublished Doctoral Thesis. École national du génie rural, des eaux et des forêts.

Bjerg, B., K. Svidt, G. Zhang, S. Morsing. 2000. The effect of pen partitions and thermal pig simulators on airflow in a livestock test room. Journal of Agricultural Engineering Research, 77(3): 317-326.

Börjesson T. and M. Fahlgren. 2001. Mechanics of fluids in mixing - Bringing mathematical modeling close to reality. Scientific impeller, 6: 55-68.

CEN. 2002. European Standard EN 13080: Agricultural machinery – Manure spreaders – Environmental protection – Requirements and test methods. CEN, European Committee for Standardization.

Chilton, R., R. Stainsby and S. Thompson. 1996. Design of sewage sludge pumping systems. Journal of Hydraulic Research, 34(3): 395-408.

Cleary, P.W. 1998. The filling of dragline buckets. Mathematical Engineering in Industry, 7(1): 1-24.

Courbebaisse, G. and D. Garcia. 2002. Shape analysis and injection molding optimization. Computational Materials Science, 25(4): 547-553.

Cundall, P.A. 1971. A computer model for simulating progressive large scale movements in blocky rock systems. Proceedings of the Symposium of the International Society for Rock Mechanics, Vol. 1, Paper No. II-8.

Cundall, P.A. 1988. Formulation of a three-dimensional distinct element model – Part I. A scheme to detect and represent contacts in a system composed of many polyhedral blocks. International Journal of Rock Mechanics, 25(3): 107-116.

Cundall, P.A. and O.D.L. Strack. 1979. A discrete numerical model for granular assemblies. Geotechnique, 29(1): 47-65.

Djordjevic, N. 2003. Discrete element modeling of the influence of lifters on power draw of tumbling mills. Minerals Engineering, 16: 331-336.

Egrinya, E.A., S. Yamamoto and T. Honna. 2001. Rice growth and nutrient uptake as affected by livestock manure in four Japanese soils. Journal of Plant Nutrition, 24(2): 333-343.

Favier, J.F., M.H. Abbaspour-Fard, M. Kremmer and A.O. Raji. 1999. Shape representation of axi-symmetrical, non-spherical particles in discrete element simulation using multi-element model particles. Engineering Computations, 16(4): 467-480.

Frick, R., J. Heusser and M. Shick. 2001. Technique d'épandage des engrais à base de déchets et de fumier de stabulation libre : Qualité du travail et adéquation de différents systèmes d'épandage. Rapport FAT No. 560.

Hart, R., P.A. Cundall and J. Lemos. 1988. Formulation of a three-dimensional distinct element model – Part II. Mechanical calculations for motion and interaction of a system composed of many polyhedral blocks. International Journal of Rock Mechanics, 25(3): 117-125.

Hirt, C.W. and B.D. Nichols. 1982. Computational method for free surface hydrodynamics. Journal of Pressure Vessel Technology, Transactions of the ASME, 103(2): 136-141.

Hopkins, M.A. and J. Tuhkuri. 1999. Compression of floating ice fields. Journal of Geophysical Research, 104(C7): 15815-15825.

Horner, D.A., J.F. Peters and A. Carillo. 2001. Large scale discrete element modeling of vehicle-soil interaction. Journal of Engineering Mechanics, 127(10): 1027-1032.

Itasca, 1999. PFC3D User's Manual, Version 2.1., Itasca Consulting Group Inc., Minneapolis, Minn.., 55415 USA.

Itasca, 2003. PFC3D User's Manual, Version 3.0.., Itasca Consulting Group Inc., Minneapolis, Minn.., 55415 USA.

Kremmer, M. and J.F. Favier. 2000. Coupling discrete element and rigid body dynamics. ASAE Paper No. 003077, St. Joseph, Mich.: ASAE.

Kremmer, M. and J.F. Favier. 2001a. A method for representing boundaries in discrete element modeling – Part I: Geometry and contact detection. International Journal for Numerical Methods in Engineering, 51: 1407-1421.

Kremmer, M. and J.F. Favier. 2001b. A method for representing boundaries in discrete element modeling – Part II: Kinematics. International Journal for Numerical Methods in Engineering, 51: 1423-1436.

Larney, F.J., H.H. Janzen, B.M. Olson and C.W. Lindwall. 2000. Soil quality and productivity responses to simulated erosion and restorative amendments. Canadian Journal of Soil Science, 80(3): 515-522.

Ma, L., P.J. Ashworth and J.L. Best. 2002. Computational fluid dynamics and the physical modelling of an upland urban river. Geomorphology, 44 (3-4): 375-391.

Maeda, Y., Y. Maruoka, H. Makino and H. Nomura. 2003. Squeeze molding simulation using the distinct element method considering green sand properties. Journal of Materials Processing Technology, 135: 172-178.

Marinari, S., G. Masciandaro, B. Ceccanti and S. Grego. 2000. Influence of organic and mineral fertilizers on soil biological and physical properties. Bioresource Technology, 72(1): 9-17.

Reichrath, S. and T.W. Davies. 2002. Computational fluid dynamics simulations and validation of the pressure distribution on the roof of a commercial multi-span Venlo-type glasshouse. Journal of Wind Engineering and Industrial Aerodynamics, 90(3): 139-149.

Rong, G.H., S.C. Negi and J.C. Jofriet. 1995a. Simulation of flow behavior of bulk solids in bins. Part 1: Model development and validation. Journal of Agricultural Engineering Research, 62: 247-256.

Rong, G.H., S.C. Negi and J.C. Jofriet. 1995b. Simulation of flow behavior of bulk solids in bins. Part 2: Shear bands, flow corrective inserts and velocity profiles. Journal of Agricultural Engineering Research, 62: 257-269.

Silsoe Research Institute (SRI). 1998. Improved precision of manure application. Final Project Report. Silsoe Research Institute, Bedford, UK.

Thirion, F. and C. Chabot. 2003. Épandage des boues résiduaires et effluents organiques: Matériels et pratiques. Cemagref Éditions. Paris, France.

Tsay, J., H.E. Ozkan, D.R. Brazee and R.D. Fox. 2002. CFD simulation of moving spray shields. Transactions of the ASAE, 45(1): 21-26.

Tsay, J., H.E. Ozkan, R.D. Fox and D.R. Brazee. 2002. CFD simulation of mechanical spray shields. Transactions of the ASAE, 45(5): 1271-1280.

Chapter 6

Discrete Element Modeling of Machine-Manure Interactions

6.1. Significance

This chapter relates to objective 5 of the thesis and, as such, it contributes to the ultimate goal of the research work. Chapter 5 clearly demonstrated the potential of numerical methods in simulating the flow of organic fertilizers in handling and land application equipment. In chapter 4, it has been shown how manure products can be modeled using the DEM. Chapter 4 also highlighted that improvements to the manures constitutive models are possible. In this chapter, machine-manure interaction models are developed and the predictions of these models are directly compared to the experimental work that was reported in chapter 3.

Wang (2001) defined virtual prototyping as the construction and testing of a virtual prototype. The virtual prototype, or digital mock-up, was defined as a computer simulation of a physical product that could be presented, analyzed, and tested from various life-cycle aspects such as design/engineering, manufacturing, service, and recycling as if on a real physical model. The definition proposed by Antonio and Zachmann (1998) stated that the idea in virtual prototyping is to replace physical mock-ups by software prototypes. This included all kinds of geometrical and functional simulations, whether or not involving humans. Bearing these definitions in mind, the functional simulations proposed in this thesis could be included as a fundamental part of

a virtual prototyping process for manure handling and land application machinery. This implies that the proposed models not only allow for a better understanding of the machine-product interactions but could be further developed to be integrated to other methods (e.g. computer assisted design (CAD), finite element analysis) to become a powerful engineering tool for the design of manure handling and land application machines.

6.2. Abstract

The discrete element method was applied to the study of the machine-product interactions occurring in manure handling and land application equipment. Two types of conveying systems were modeled along with a hopper and a flow-control gate and the results of the simulations were compared to experimental data. Two simulations were run for the scraper conveying systems. The first one included high strength clustered particles to simulate the clumps contained in the manure used during the field experiments. The results of this first undamped simulation series were in good agreement with the measured data, for a conveyor velocity of 38 mm/s and the bottom of the gate 560 mm above the bottom of the hopper. The simulated characteristic flow rate was overestimated by 40% while the simulated unloading time was 16% lower than the measured value. The specific energy and peak power values predicted by the model were much lower than the measured values. For the operating velocity of 19 mm/s and the gate fully lifted, the predicted results were affected by excessive gravity flow. The characteristic flow rate was however still comparable to the measured value. The simulations allowed for the identification of the effect of the gate on the flow rate and the energy requirements, but this effect was not as clearly highlighted as it was by the experimental results. A second model of the scraper conveying system was developed to include damping as well as breakable clusters. The results of this second series of simulations indicated that the predictions of the model were more closely correlated to the measured data for the high conveyor velocity – low gate setting. The effect of the gate on the energy requirements was replicated by the simulations but to a lesser extent than the experimental results. The 4-auger conveying system was modeled and damped

simulations were carried out with virtual manure including breakable clusters. The predicted characteristic flow rate, unloading time and peak power values were in very good agreement with the experimental results for both the high velocity – low gate and low velocity – high gate configurations. The 4-auger system model was able to predict the effect of the gate on the energy requirements but not on the discharge rate. It is expected that improvements in the manure model would enhance the accuracy of the interactions models. The detailed simulation of a transverse distribution system for banded manure application gave results that were in very good agreement with experimental results obtained with a prototype land applicator. The simulated and experimental transversal coefficients of variation were 4% and 6%, respectively.

6.3.   Introduction

The utilization of computer models and simulations has become an important design tool in numerous industries such as aerospace and automotive. The ever-increasing power of computers combined with the decreasing cost of computing resources and the enhanced sophistication of modeling codes has promoted the expansion of numerical modeling.

The design of agricultural machinery can certainly benefit from numerical modeling. Most modeling efforts have been targeting high revenue agricultural machines for which the cost of developing the models could be justified. Manure land application machines have been much less researched and developed than other agricultural machines due to their low production volume and market value. However, the application of numerical modeling to manure land applicators could significantly impact their design and operation. Moreover, testing and developing manure land application machines based on empirical approaches requires a considerable experimental setup and usually yields limited information on the machine-product interactions that take place in such machines during field operation with variable product properties.

193

6.4. Literature review

Attempts have been made at simulating the action of machinery using the discrete element method. Djordjevic (2003) used the DEM to study the power consumption of a tumbling mill as a function of the height of the lifters. It was found that the power draw of the mill and the mode of energy consumption were significantly affected by the height of the lifters. The proportion of power consumed as friction increased with decreasing lifter height, leaving less power for high intensity comminution caused by impacts.

Djordjevic et al. (2003) studied horizontal and vertical shaft impact crushers using the DEM. The distribution of collision energies obtained via DEM simulations was converted to a product size distribution using impact breakage test data. Experimental results were used to validate the DEM simulation results. An investigation of the effects of the machine design and operational conditions on velocity and energy distributions of collision inside the milling chamber was then carried out. The results indicated that the DEM can be used to model the particle flow behaviour, energy utilisation and product size in the impact crushers.

Horner et al. (2001) reported on the use of large scale discrete element modeling using high-performance DEM codes to simulate vehicle-soil interaction. The approach taken was to use a finite-element grid to model the vehicle component interacting with the soil and developing routines to model the particle-grid interactions. Two examples, one involving the interaction between the landing gear of an aircraft and an unpaved runway, the other dealing with a plough, demonstrated remarkably realistic deformation patterns. In both cases, 10 millions discrete particles were used.

Cleary (1998) used a DE model to simulate the filling process of two different mechanical configurations of dragline buckets. With the bucket motion dynamically responding to the balance of forces applied to it, the simulated fill times, spoil profiles and flows were consistent with available observations. The bucket designs implemented in the model could be compared in terms of filling pattern and drag

coefficient. The motion and stability of the buckets were also found to be dependent upon the size distribution of the particles and their density. Cleary (1998) concluded that such DE models, enabling the prediction of drag coefficient, final spoil volume, surface wear rates and distribution, could become tools to optimize bucket design.

Screw conveyors were modeled by Shimizu and Cundall (2001) in a commercial DEM code (PFC^{3D}, Itasca Consulting Group Inc., Minneapolis, Minnesota, USA). The parametric approach used to model the machine components was presented. Local and global coordinate systems were used for both boundaries representation and contact detection. The simulations results were in good agreement with previous work and empirical equations for both horizontal and vertical screw conveyors.

6.5. Modeling approach

Based on the numerical models developed for manure products presented in chapter 4, the machine-manure interactions taking place in land application equipment were modeled and validated against the experimental results presented in chapter 3. Models of the two conveying systems (scraper and 4-auger systems) were implemented in PFC^{3D} along with the flow-control gate and the physical boundaries of the machine. The focus was on the power requirements of the conveying systems and on the discharge rate produced by each mechanical configuration. The simulation sequence began with the creation of the physical boundaries of the system including the conveying systems. The particles were then created and allowed to come to equilibrium under gravity loading. The gate was then raised to the desired height and the movement of the conveyor was initiated. This section first describes how each mechanical component was modeled in PFC^{3D}. The properties of the virtual products used in each set of simulations are then presented.

6.5.1. Modeling of the spreader hopper

The machine on which the models are based is the prototype land applicator developed at the University of Saskatchewan (Agnew et al., 2004). The hopper is modeled using a number of walls (Itasca, 2003) to represent the physical boundaries (fig. 6.1).

6.5.2. Modeling of the scraper conveyor

The scraper conveyor was modeled as a series of walls representing the slats of the conveying system. The challenge was to develop a code capable of describing the motion of the conveyor where a slat disappearing at the discharge end of the machine is replaced by a new slat at the front end of the hopper. Each slat was made of a pair of walls so the slats would have two active sides (the active side of a wall is the side that recognizes ball contacts). The slat regeneration code monitored the position of the pair of walls (slat) closest to the discharge end of the hopper. When those walls reached the end of the hopper, they were deleted and the code updated the walls that were being monitored for position and generated a new slat at the tractor end of the hopper. The code efficiently mimicked the dynamics of the scraper conveyor.

6.5.3. Modeling of the 4-auger system

General walls were introduced in version 3.0 of PFC^{3D} allowing users to create cylinders and spirals. That feature was used to model the 4-auger system. The motion of the screw conveyors was prescribed as a rotational velocity along the longitudinal axis. Figure 6.1 presents models of the spreader with the two conveying systems.
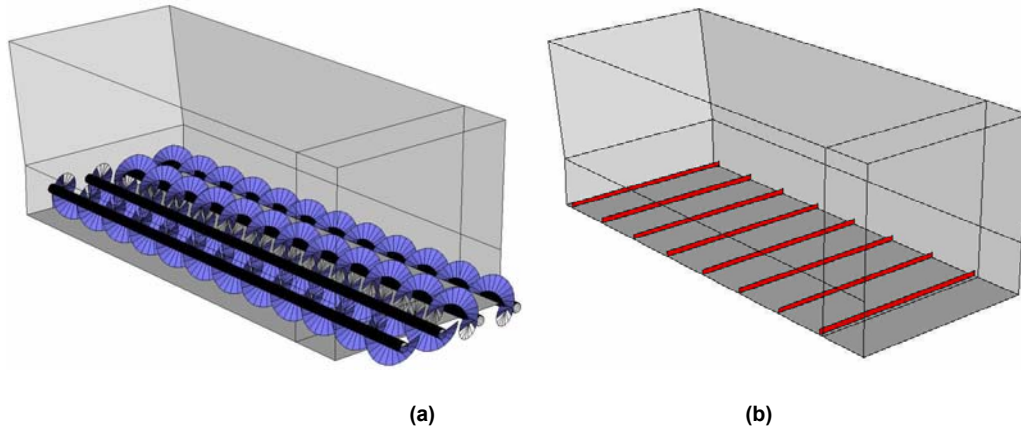
<div align="center">(a)   (b)</div>

Figure 6.1.   Prototype land applicator with (a) 4-auger and (b) scraper conveying systems.

6.5.4. Modeling of the transverse distribution system for surface banded application

The transverse distribution system was developed to allow the machine to perform banded land application (fig. 6.2.). The banding system is made of a tube that houses an auger that is divided into a left-hand flighting auger and a right-hand flighting auger of equal length to promote the flow towards both ends of the tube. The tube features six apertures that can be adjusted in size and moved circumferentially. A transition hopper is located between the main conveying system and the transverse conveyor. PFC^{3D} (version 3.0) can only create general cylinders and does not allow the user to define curved wall segments. A code was developed to model the tube that houses the transverse conveyor using straight wall segments. Using generalized geometric equations, the code can accommodate user-defined apertures sizes and locations. The modeled transverse distribution system is illustrated in figure 6.3.

Figure 6.2. Back view of the prototype land applicator with the transverse distribution system for banded application.
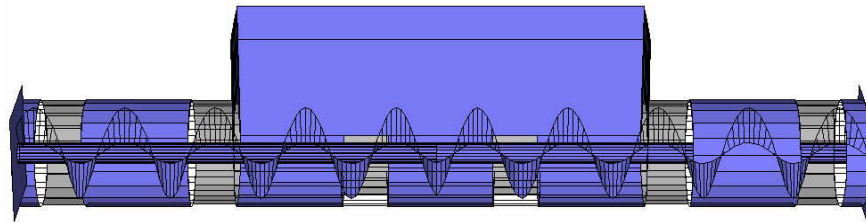

Figure 6.3. PFC^{3D} model of the transverse distribution system (the sections with apertures are highlighted in light grey).
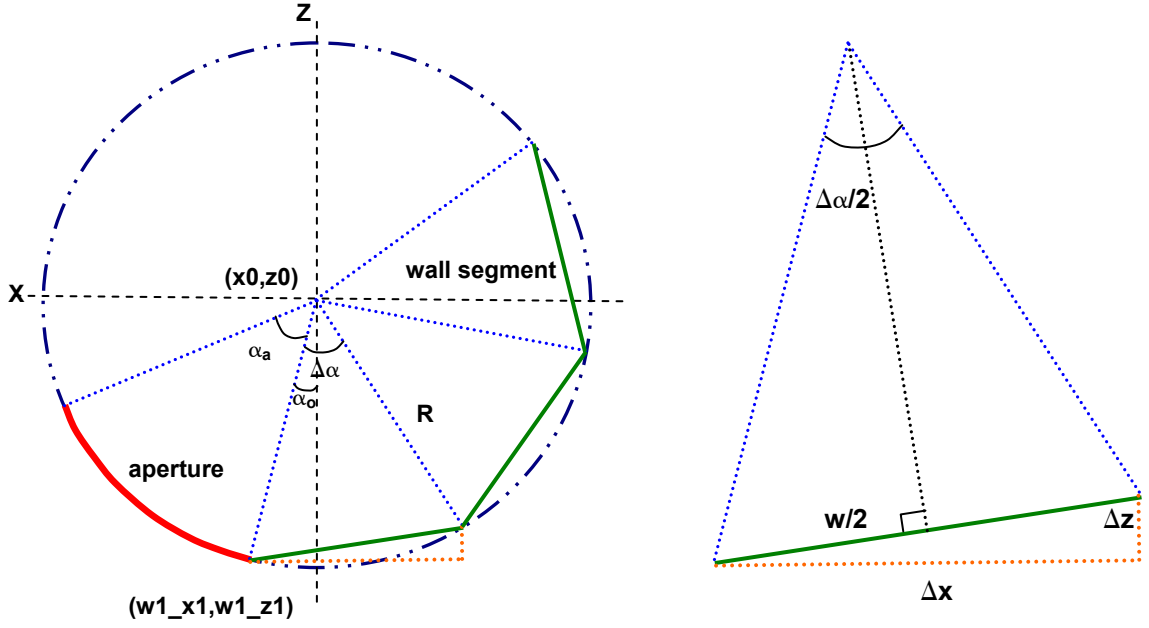
Figure 6.4. Geometry of the transverse tube with apertures (counter-clockwise construction; the discharge end of the machine is on the left-hand side (positive x-axis)).

As illustrated in figure 6.4, the offset was defined as the distance taken around the circumference of the tube from the z-axis to the beginning of the aperture. The equations developed allowed for negative offsets to be defined. The construction of the sections of the tube was done in the counter-clockwise direction. The coordinates of the first point of the first wall segment could be found using equation 6.1 and 6.2:

$$w1\_x1 = x0 + R\sin\alpha_o \qquad \text{and} \qquad (6.1)$$
$$w1\_z1 = z0 - R\cos\alpha_o \qquad . \qquad (6.2)$$

The incremental values Δx and Δz were calculated using equations 6.3, 6.4 and 6.5:

$$w = 2R\sin(\Delta\alpha /2) \qquad , \qquad (6.3)$$
$$\Delta x = w \cos(\Delta\alpha + \Delta\alpha /2 + \alpha_o) \qquad \text{and} \qquad (6.4)$$
$$\Delta z = w \sin(\Delta\alpha + \Delta\alpha /2 + \alpha_o) \qquad . \qquad (6.5)$$

Starting with the user-specified aperture angle (α_a), offset angle (α_o) and number of walls segments (n), the incremental angle ($\Delta\alpha$) could be calculated using 6.6:

199

$$\Delta\alpha = (2\pi - \alpha_a) / n \qquad . \qquad\qquad (6.6)$$

A loop was included to construct the sections of cylinder with apertures (apertures 1, 2, 5, and 6 when starting from the left on figure 6.3):

loop m(1,n)

make wall

(*make wall* is a procedure that includes several lines of code to make the wall at the specified coordinates)

x1 = x2

z1 = z2

$\Delta x = w \cos (m \Delta\alpha + \Delta\alpha./2 - \alpha_o)$

$\Delta z = w \sin (m \Delta\alpha + \Delta\alpha./2 - \alpha_o)$

x2 = x1 - Δx

z2 = z1 + Δz

end loop

The middle section of the transverse tube is cut off in half to accommodate the transition hopper. This required the construction of half cylinders made of wall segments. Defining the starting point at a rotation angle of π radians (counter-clockwise from the positive x-axis), the coordinates of the points of the wall segments for the half cylinders could be calculated using a method similar to the one previously described. When a half-cylinder featured an aperture (apertures 3 and 4 on figure 6.3), the construction was done is two steps. In the first step, the quarter circle with the offset was first created. In the second step, the other quarter circle was generated from an angle of π radians to the end of the aperture.

6.5.5. Modeling of the products used for the simulations

The field testing of the conveying systems was carried out using beef feedlot manure (chapter 3, section 3.6.1). A value of 300 kg/m^3 for the bulk density of that product was

included in the simulations. To replicate the clumps that were present in the manure, 4-particle clusters were implemented. The radii of the 4 particles making up the clusters were taken as 30.0, 45.0, 37.5 and 32.5 mm. The clusters were created according to the procedure described in chapter 4, section 4.5.2.2. The clusters were linked by contact bonds. A high value was given to the bonds strength in both the normal and shear directions, to ensure the clusters would remain intact during the simulations. The remainder of the particles had radii normally distributed between 20 and 40 mm. The Young's modulus of all particles was set to 0.5 MPa and the normal and tangential stiffnesses were calculated according to equations 6.7 and 6.8 for each particle. This virtual product was used in all the simulations presented in section 6.5.1. The equations used to calculate the stiffness values were

$$k_n = 4\,E\,R_p \quad \text{and} \tag{6.7}$$

$$K = \frac{k_s}{k_n} = \frac{\dfrac{(1-v_i)}{G_i} + \dfrac{(1-v_j)}{G_j}}{\dfrac{(1-0.5v_i)}{G_i} + \dfrac{(1-0.5v_j)}{Gj}} \quad , \tag{6.8}$$

where k_n = stiffness in the normal direction,

  E = Young's modulus of the particle,

  R_p = radius of the particle,

  k_s = stiffness in the shear direction,

  v = Poisson's ratio (the indices i and j refer to the two entities in contact) and

  G = Shear modulus (the indices i and j refer to the two entities in contact).

The preliminary simulations of the transverse distribution system (section 6.5.2.1) included a group of 6,210 particles with radii normally distributed between 20 and 30 mm. The density of the particles was taken as 300 kg/m^3 and the normal and tangential stiffnesses were set at 1.0e3 N/m.

For the detailed simulation of the transverse distribution system (section 6.5.2.2), the parameters describing the particles were selected to mimic the dry poultry wastes compost (approximately 60% TS) used during its laboratory testing. The particle density was taken as 1,000 kg/m^3 and the radii of the particles were normally distributed between 7.5 and 20 mm. The Young's modulus was set at 1.0 MPa and the normal and tangential stiffnesses were calculated according to equations 6.7 and 6.8 for each particle.

6.6. Results

From both the simulations and experimental results, it was possible to extract the characteristic flow rate and the specific energy required for the unloading process. The recommendations of European Standard EN 13080 (CEN, 2002) were followed for the data analysis. The characteristic flow rate can be calculated using equation 6.9:

$$s_f = \max_{j=1}^{n-m+1} \left[\frac{1}{m} \sum_{i=j}^{j+m-1} x_i \right] \qquad , \qquad (6.9)$$

where s_f = characteristic flow rate (kg/s),

      n = number of samples during unloading,

      m = number of samples during 30% of the unloading time (m=0.3·n) and

      x_i = flow rate at sample i (kg/s).

This factor is used to assess the amount of material coming out of the spreader as a function of its operating parameters. The characteristic flow rate basically corresponds to the highest average flow rate occurring during 30 percent of the unloading time of the spreader. The other evaluation criterion makes use of the power data to calculate the specific energy required by the conveying systems during the unloading operation. The specific energy is calculated using equation 6.10:

$$E_{unloading} = \frac{\int_{0}^{t_{unloading}} P(t)dt}{M} \qquad , \qquad (6.10)$$

where $E_{unloading}$ = specific energy of the unloading operation (J/kg),

$t_{unloading}$ = unloading time of the spreader (s),

P(t) = power consumption of the floor conveyor as a function of time (W) and

M = mass of product unloaded (kg).

The results section is divided in two sub-sections. The first sub-section presents the results obtained for the models of the scraper and 4-auger conveying systems. The simulation results for the transverse distribution system for banded application are presented next.

6.6.1. Conveying systems

6.6.1.1. Scraper conveying system

Full-scale simulations of the conveying systems studied in chapter 3 were carried out. To highlight the capabilities of the models while optimizing the computational cost of the study, the emphasis was on the extreme cases, i.e. high velocity setting of the conveyors combined with the gate in its lowest position as well as low velocity setting with the gate fully open. The results obtained for the scraper conveyor are presented in table 6.1. The results indicate that the models were capable of predicting the characteristic flow rate with reasonable accuracy. The effect of the gate and that of the velocity of the conveyor on the characteristic flow rate were well replicated with ratios of 0.5 and 0.6 for the simulated and experimental results, respectively. The error on the characteristic flow rate is also consistent from one set of operating parameters to the other with ratios of simulated to measured results of 1.4 and 1.5. The specific energy on the other hand was underestimated by the models. The effect of the change in conveyor velocity and gate opening was also much less obvious in the simulated case. Simulated to experimental ratios in the range of 0.5 to 1.5 are considered good; they

indicate the models are capable of predicting values that are comparable to experimental results.

Table 6.1. Simulated and experimental results for the scraper conveying system (undamped system).

Conveyor type	Conveyor velocity (mm/s)	Gate position[a] (mm)		Simulated	Measured[b]	Simulated to measured ratio
Scraper	38	560	**Characteristic flow rate (kg/s)**	19.0	13.8	1.4
			Specific energy (J/kg)	11.3	107.6	0.1
			Unloading time (s)	149.5	179.0	0.8
			Peak power (kW)	0.3	5.6	0.05
	19	1282	**Characteristic flow rate (kg/s)**	36.2	23.6	1.5
			Specific energy (J/kg)	10.6	47.9	0.2
			Unloading time (s)	284.3	134.5	2.1
			Peak power (kW)	0.2	1.5	0.1
High velocity - low gate to low velocity - open gate ratio			**Characteristic flow rate (kg/s)**	0.5	0.6	
			Specific energy (J/kg)	1.1	2.3	
			Peak power (kW)	2.3	3.8	

[a] Distance between the bottom of the gate and the bottom of the hopper;
[b]Average of the three experimental repetitions.

The unloading time was not predicted well by the model of the scraper conveyor running at 19.4 mm/s with the gate fully open. A comparison between the simulated and experimental unloading times is presented in figures 6.5 and 6.6.
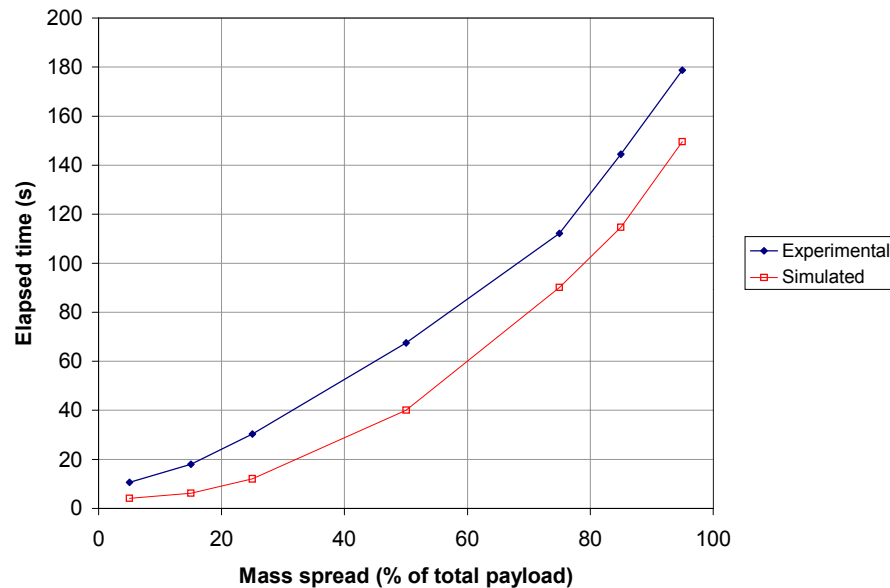

Figure 6.5.   Comparison between the simulated and experimental unloading time for the scraper conveying system operated at 38 mm/s with the bottom of the gate 560 mm above the bottom of the hopper.
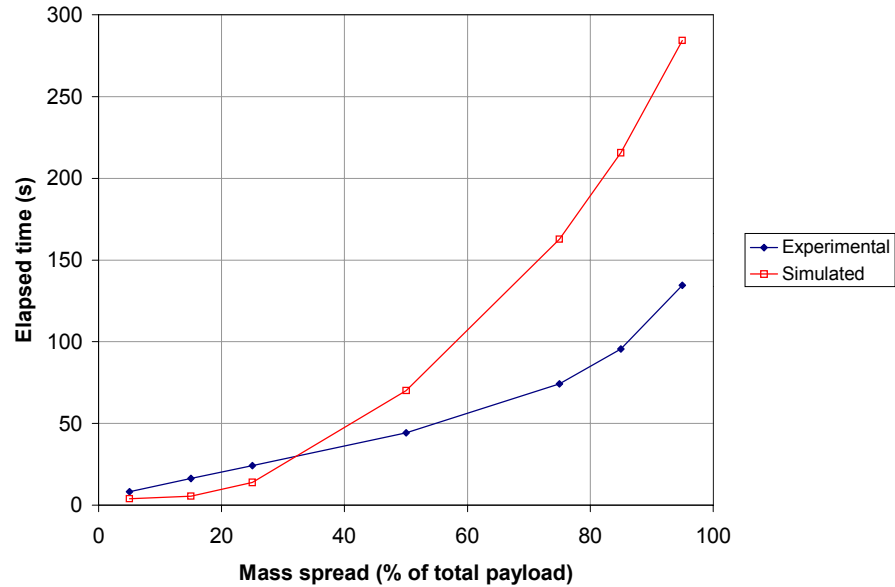
204

Figure 6.6. **Comparison between the simulated and experimental unloading time for the scraper conveying system operated at 19.4 mm/s with the bottom of the gate 1282 mm above the bottom of the hopper.**

Figure 6.5 shows that the simulated unloading times at different stages of the unloading operation closely correlated the experimental times. The results included in figure 6.6 indicate that the flow of manure was not well simulated in the case where the conveyor was operated at the low velocity setting with the gate fully open. It was observed during the simulations that gravity flow would begin as soon as the motion of the conveyor was initiated, meaning the volume of manure would immediately crumble at the discharge end of the spreader. During the field experiments however, the bulk of manure would generally move as a block until it reached the end of the spreader and crumble under gravity. This misrepresentation of the product in the machine-product interaction model is therefore responsible for the time discrepancy. When the same virtual product was spread with the gate lowered, this effect would disappear since the presence of the gate would prevent the occurrence of such early gravity flow. Also, the damping coefficient that is by default applied to the equations of motion in PFC^{3D} was set to zero. This was partially responsible for the slight differences between the times presented in figure 6.5.

With the inconsistencies observed for the unloading time, it is interesting to look at the peak power required by the conveying system. The effect of the change in operating parameters was reproduced by the models with ratios of peak power for the low velocity and open gate setting to peak power required at the high velocity and closed gate configuration of 3.8 and 2.3 for the experimental and simulated cases, respectively. The power requirements predicted by the models were however only 6.1% and 10.3% of the average measured value for the high velocity – closed gate and low velocity – open gate settings, respectively.

Table 6.2 includes the results for the same simulation, but this time with a damping coefficient of 0.35. Also, the clusters normal and shear strength values were set to 10 N. This change in cluster strength was suggested by high values of specific energy obtained with the 4-auger system (section 6.6.1.2.) when using the high-strength clusters proposed initially. Under these new simulating conditions, very good results were obtained for the low gate – high velocity combination with ratios of simulated to measured data of 0.9 and 1.2 for the characteristic flow rate and the unloading time, respectively. The other set of operating parameters however yielded poorer predictions. The characteristic flow rate was underestimated while the predicted unloading time was, as it was the case for a damping coefficient of 0, over 2 times the actual unloading time. It is interesting to note that the ratios of peak power remained approximately the same even with the change in damping coefficient.

Table 6.2. Simulated and experimental results for the scraper conveying system (damping coefficient of 0.35).

Conveyor type	Conveyor velocity (mm/s)	Gate position[a] (mm)		Simulated	Measured[b]	Simulated to measured ratio
Scraper	38	560	Characteristic flow rate (kg/s)	12.9	13.8	0.9
			Specific energy (J/kg)	21.6	107.6	0.2
			Unloading time (s)	208.4	179.0	1.2
			Peak power (kW)	0.5	5.6	0.08
	19	1282	Characteristic flow rate (kg/s)	7.6	23.6	0.3
			Specific energy (J/kg)	17.2	47.9	0.4
			Unloading time (s)	375.7	134.5	2.8
			Peak power (kW)	0.2	1.5	0.1
High velocity - low gate to low velocity - open gate ratio			Characteristic flow rate (kg/s)	1.7	0.6	
			Specific energy (J/kg)	1.3	2.3	
			Peak power (kW)	2.6	3.8	

[a] Distance between the bottom of the gate and the bottom of the hopper;
[b] Average of the three experimental repetitions.

6.6.1.2. Augers conveying system

Figure 6.7 illustrates the simulation of the 4-auger conveying system. Table 6.3 presents the simulation results. The damping coefficient was set to 0.35 and the normal and shear strength of the contact bonds joining the clustered-particles was 10 N. As mentioned in the previous section, the configuration of the 4-auger system created artificially high contact forces when high-strength clusters would get in between two augers. The strength of the clusters was therefore reduced to yield more realistic simulations.
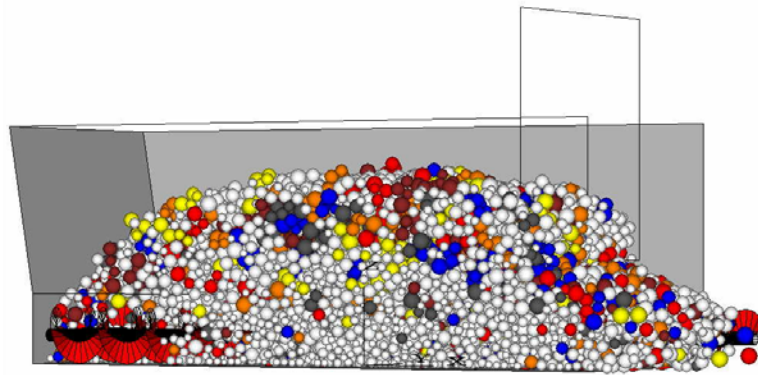

Figure 6.7. Simulation of the 4-auger conveying system.

Table 6.3. Simulated and experimental results for the 4-auger conveying system (damping coefficient of 0.35).

Conveyor type	Conveyor velocity (mm/s)	Gate position[a] (mm)		Simulated	Measured[b]	Simulated to measured ratio
4-auger system	840	560	Characteristic flow rate (kg/s)	48.5	33.7	1.4
			Specific energy (J/kg)	242.3	516.8	0.5
			Unloading time (s)	38.56	42.2	0.9
			Peak power (kW)	19.3	18.8	1.0
	471	1282	Characteristic flow rate (kg/s)	38.0	45.3	0.8
			Specific energy (J/kg)	232.3	185.3	1.3
			Unloading time (s)	55.1	52.4	1.1
			Peak power (kW)	12.6	6.7	1.9
High velocity - low gate to low velocity - open gate ratio			Characteristic flow rate (kg/s)	1.3	0.7	
			Specific energy (J/kg)	1.0	2.8	
			Peak power (kW)	1.5	2.8	

[a] Distance between the bottom of the gate and the bottom of the hopper;
[b] Average of the three experimental repetitions.

As can be observed from the results for the simulation of the scraper conveying system, the case of the gate in its lowest position combined with the high velocity setting of the conveying system was very well replicated by the model. The characteristic flow rate,

unloading time and peak power requirement were all very well correlated by the model with simulated to measured ratios of 1.4, 0.9 and 1.0, respectively. The simulated characteristic flow rate in the open gate – low velocity configuration was underestimated, but still within a reasonable range of the actual value. The simulated unloading time of the second scenario was also in very good agreement with the measured value. The effect of the gate on both the specific energy and the peak power was replicated by the simulations, but with attenuation.

It is now obvious that machine-manure interactions models such as the ones presented in the previous two sections have the potential to be made more accurate by validating them over a wider range of products and machine configurations. However, such-fine tuning is beyond the scope of this thesis. The fact that the unloading time of the machine was well predicted by the models demonstrated that the dynamics of the systems have been correctly implemented. The discrepancies in discharge flow rates and power requirements highlighted the improvements that could be brought to the manure models. There are several parameters to act on to improve the accuracy of the interactions models. One of them is the damping coefficient. With constant velocity boundary conditions and free falling phenomenon, it would be recommended to leave the system undamped (Itasca, 2003). However, the results obtained suggested that a value of 0.35 for the damping coefficient would yield more realistic results in most cases. The usage of clusters seemed to be a valuable means of representing the clumps that were present in the manure. The strength of the bonds linking the clustered particles must be optimized to improve the accuracy of the interactions models.

6.6.2. Transverse distribution system

6.6.2.1. Preliminary simulations of the transverse distribution system
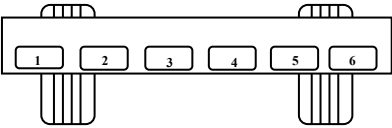
The transverse distribution system was first simulated by vertically extending the transition hopper instead of attaching it at the back of the spreader. All the apertures were 152 mm wide and 146 mm high circumferentially. The offset of the apertures is the circumferential distance between the edge of the aperture that is the closest to the
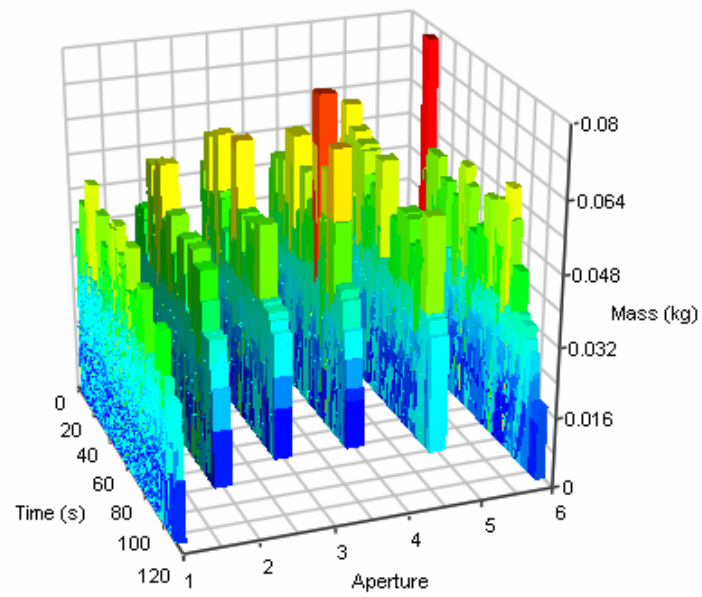
tractor-end of the machine and the vertical axis of the tube. A positive offset indicated that the aperture is towards the discharge end of the machine while a negative offset indicated that part of the aperture is on the tractor-side of the vertical axis of the tube. The values of the offset for each aperture are included in table 6.4.

A first series of simulation was run to investigate the effect of the rotational velocity of the transverse conveyor on the discharge flow of each aperture, the power consumption and the risk of packing at the end caps. Figures 6.8 and 6.9 show the instant mass discharged out of each aperture at 30 rpm and 7.2 rpm for the end and the beginning of the simulations, respectively. Several effects of the velocity of the transverse auger could be observed in figures 6.8 and 6.9. A first observation could be made on the time axis. As expected, when the transverse auger was operated at 7.2 rpm, more time was required to empty the hopper. Also, at the faster velocity of 30 rpm there was a delay of 3.0 seconds between the time when material started flowing out of the middle apertures and the time when the flow began at both ends of the tube. This delay increased to 7.6 seconds at an auger velocity of 7.2 rpm. It could also be seen that the lower auger velocity favoured flow in the middle apertures while the higher velocity promoted increased flow at both ends of the tube. The peak power was approximately 44 W and 536 W for an auger velocity of 7.2 and 30 rpm, respectively (the experimental power requirements at 30 rpm was 350 W). As during the laboratory testing of the transverse distribution system, it was observed that packing at the end caps was an issue. The velocity of the auger was very much a factor in determining the extent of the compaction and both ends of the tube. The simulations indicated that the slower velocity of 7.2 rpm generated much less compaction than the 30 rpm velocity. With 40% of the mass of product left in the machine, the maximum compression force was 20.9 N at 7.2 rpm while it was 28.3 N with as much as 80% of the mass left in the machine in the case of the 30 rpm transverse auger velocity. It was natural to assume that a slower conveyor speed would give more time for the product to flow out of the apertures and create less compaction at the end caps, but the simulations allowed for better observation and quantification of the phenomenon. This is a great example of the usefulness of having models of the system at the design stage to evaluate parameters
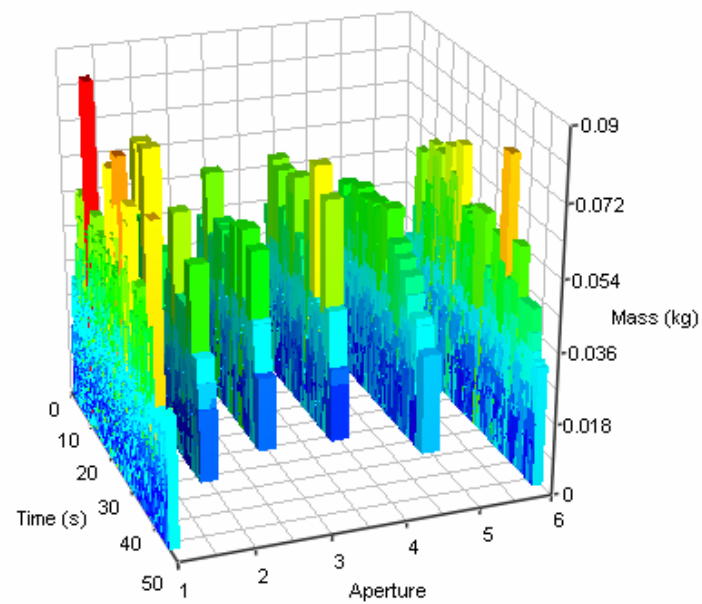
that would be difficult to measure experimentally. As a corrective measure to excessive compaction at the end caps, the flighting of the transverse auger was cut at both ends leaving 152.4 mm of bare shaft before the end caps. The same modification was brought to the model to carry out the detailed numerical simulation of the transverse distribution system.

Table 6.4. Offset values for the apertures on the transverse distribution system.

View from the back of the spreader (not to scale)		

	Offset (mm)	Left view (not to scale)
Aperture 1 and 6	19	
Aperture 2 and 5	6	
Aperture 3 and 4	-57	

(a)

(b)

Figure 6.8. **Instant mass flow from each aperture as a function of time for an auger velocity of (a) 7.2 rpm and (b) 30 rpm; view from the end of the time axis (end of the simulation).**
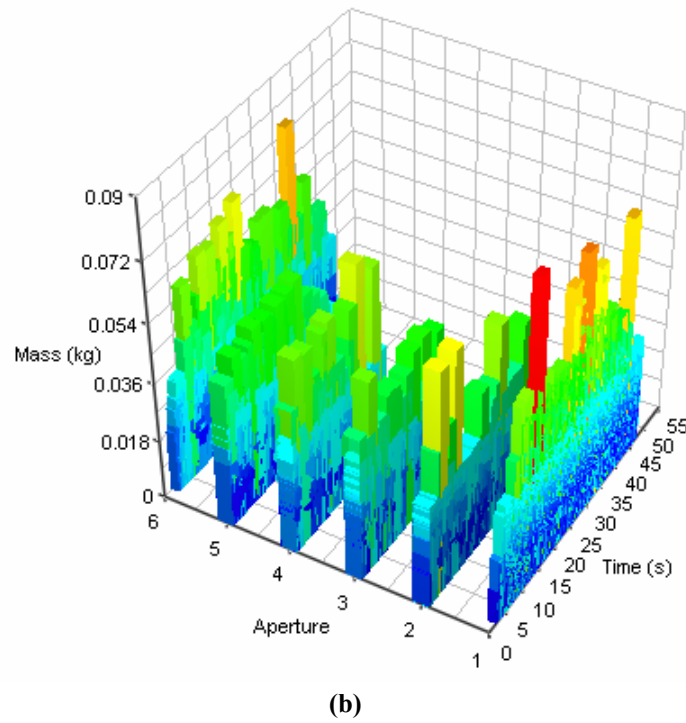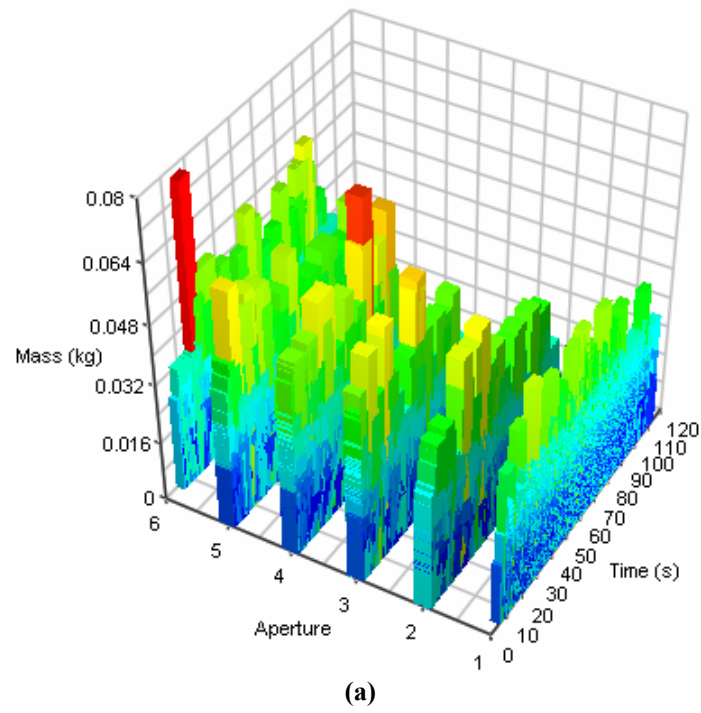
211

Figure 6.9. Instant mass flow from each aperture as a function of time for an auger velocity of (a) 7 rpm and (b) 30 rpm; view from the beginning of the time axis (beginning of the simulation).

6.6.2.2. Detailed simulation of the transverse distribution system

The model of the transverse distribution system was attached to the back of the prototype applicator to replicate the experiments carried out in the laboratory and aiming at measuring the discharge flow at each aperture. Figure 6.10 illustrates the simulation of the prototype land applicator with the transverse distribution system for banded application at three different stages of the unloading operation along with the initial state of the model. The product that was used during the experiments was a fine, dry compost (approximately 60% TS) that was modeled by an assembly of 55,000 particles. The test and simulation parameters are summarized in table 6.5. A sufficient number of particles to replicate the effect of the flow-control gate was used, while avoiding the computational cost of completely filling the hopper. During the laboratory experiments, two rows of containers were placed under the six apertures. When the first series of containers was full, the second series was slid under the apertures. The containers were then weighed to obtain the mass distribution across the transverse distribution system. In post-processing, the same method was applied to the results of the simulation, i.e. the total mass of product discharged at each aperture over a period of 3 seconds was calculated. The results are presented in figure 6.11. The simulated coefficient of variation of the discharged mass across the transverse conveyor was 3.9% while the average coefficient of variation for the three experimental repetitions was 6.0%.

The simulation results for the transverse distribution system illustrated very well the potential of using the models as design tools. With the banded applicator, the discharge flow is a function of the velocity of the 4 main discharge augers, the vertical position of the flow-control gate, the velocity of the transverse conveyor, and the size and position of the 6 apertures. With several parameters influencing the system, one can see the benefits of having models to assist in the design of the implement.
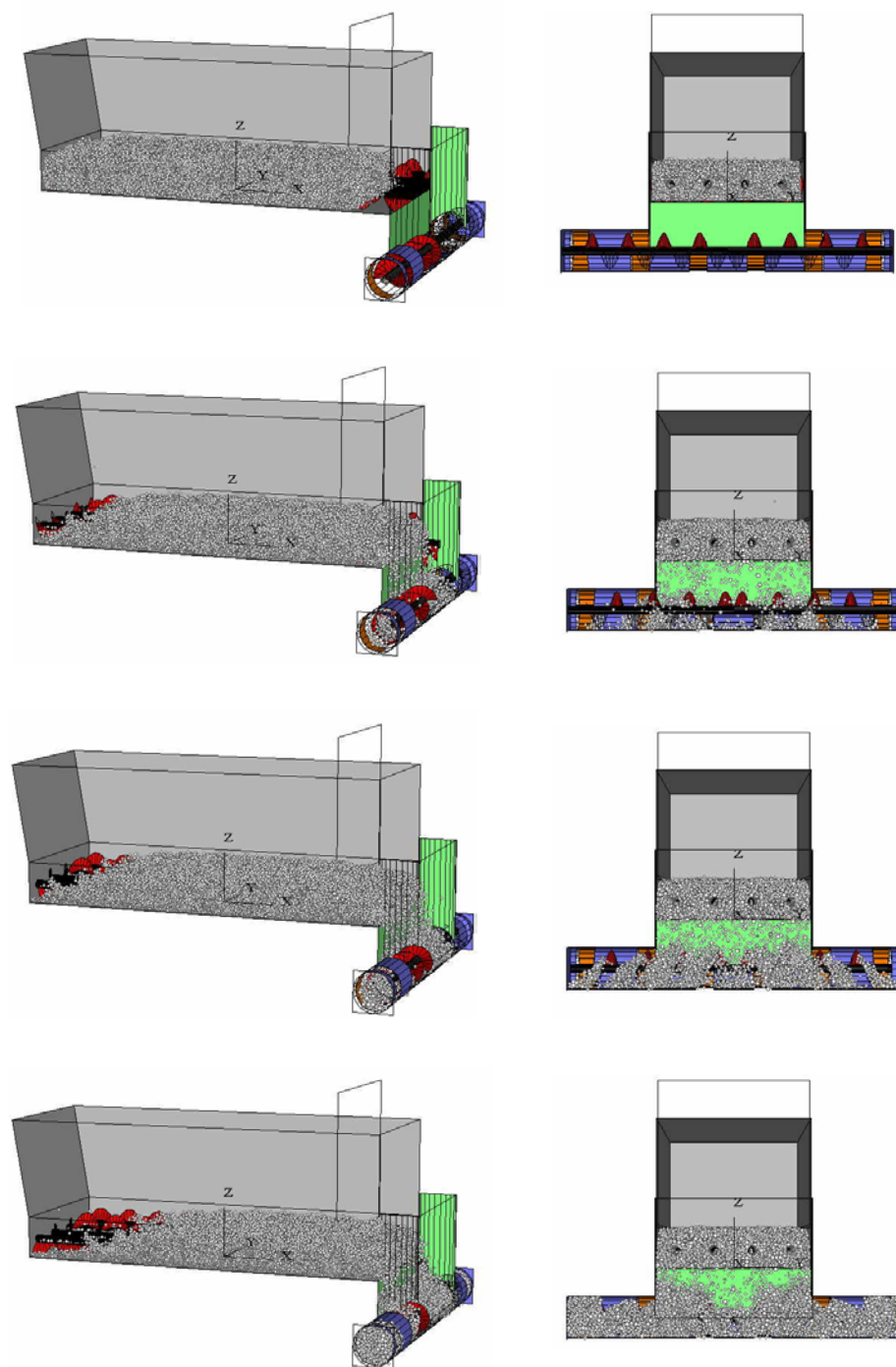
Figure 6.10. Simulation of the prototype land applicator with the transverse distribution system for banded application.

Table 6.5. Parameters used for the simulation of the transverse distribution system for banded application.

Velocity of the main discharge augers (rpm)	30
Velocity of the transverse auger (rpm)	60
Distance from the bottom of the hopper to the bottom of the gate (mm)	356
Virtual compost contact model	Linear
Virtual compost friction coefficient	0.6
Virtual compost particle density (kg/m^3)	1000
Virtual compost particle radii (mm)	7.5 – 20
Virtual compost Young's modulus (MPa)	1
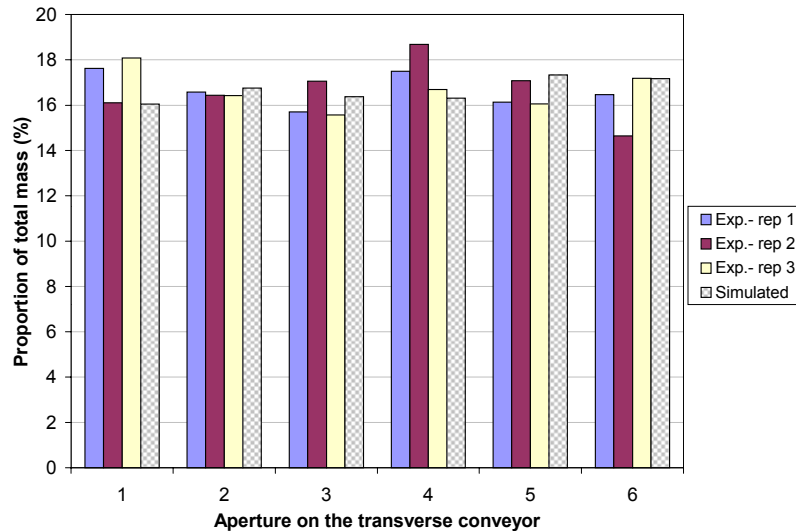
Figure 6.11. Experimental and simulated mass distribution across the transverse distribution system for compost land application.

6.7. Conclusions

Numerical models were developed to simulate the operations of two conveying systems used for manure land application. The results indicated that the models were capable of predicting the discharge rate and the energy requirements with reasonable accuracy. From the results presented, it can be stated that:

- the models of both conveying systems performed better when the gate was in its lowest position. This was due to the attenuation effect of the gate on the gravity flow at the discharge end of the machine. Refinements of the manure model are required in order to improve the predictions of the machine-manure interactions models for the open-gate configurations.

- The effect of the gate on the energy requirements was well replicated by the models. The influence of the gate on the simulated characteristic flow rate was adversely affected by the accuracy of the manure model. It was not possible to correctly replicate the effect of the gate with the manure model utilized.

- The results of the simulations were affected by the clustered particles. The clusters were found to be a good means of mimicking the clumps present in real manure and their effect on the flow. The strength of the bonds linking the clustered particles had an influence on the predictions of the models. Unbreakable clusters, with high strength values, caused artificially high values of contact forces in the case of the 4-auger conveying system. The scraper conveyor was less affected by the strength of the clusters.

- The damping coefficient applied to the equations of motion influenced the simulations results. A value of 0.35 was found to give good results in most situations.

- The experimental mass distribution across the transverse distribution system for banded application was very closely replicated by the numerical model. The simulated coefficient of variation for the mass distribution across the transverse distribution system was 3.9% compared to an average measured coefficient of variation of 6.0%.

The very challenging task of modeling the machine-product interactions taking place in manure handling and land application equipment has been successfully fulfilled. The accuracy of the models has the potential to be greatly enhanced by validating them over a broader range of mechanical systems and manure products as well as refining the manure models.

6.8.   Acknowledgements

6.9.   References

Agnew, J., H. Landry, C. Laguë, M. Roberge and C. Iskra. 2004. Prototype precision applicator for solid and semi-solid livestock manure. ASAE Paper No. 041116, St. Joseph, MI: ASAE.

Antonio, G.S. and G. Zachmann. 1998. Integrating virtual reality of virtual prototyping. Proceedings of the 1998 ASME Design Technical Conference and Computers in Engineering Conference.

CEN. 2002. European Standard EN 13080: Agricultural machinery – Manure spreaders – Environmental protection – Requirements and test methods. CEN, European Committee for Standardization.

Cleary, P.W. 1998. The filling of dragline buckets. Mathematical Engineering in Industry, 7(1): 1-24.

Djordjevic, N. 2003. Discrete element modeling of the influence of lifters on power draw of tumbling mills. Minerals Engineering, 16: 331-336.

Djordjevic, N., F.N. Shi and R.D. Morisson. 2003. Applying discrete element modeling to vertical and horizontal shaft impact crushers. Minerals Engineering, 16: 983-991.

Horner, D.A., J.F. Peters and A. Carillo. 2001. Large scale discrete element modeling of vehicle-soil interaction. Journal of Engineering Mechanics, 127(10): 1027-1032.

Itasca, 2003. PFC3D User's Manual, Version 3.0.., Itasca Consulting Group Inc., Minneapolis, Minn.., 55415 USA.

Shimizu, Y. and P.A. Cundall. 2001. Three-dimensional DEM simulations of bulk handling by screw conveyors. Journal of Engineering Mechanics, 127(9): 864-872.

Wang, G. G. 2001. Definition clarification and review on virtual prototyping. Proceedings of the ASME Design Engineering Technical Conference, 1: 349-357.

Chapter 7

General Discussion and Conclusions

This chapter first regroups the conclusions of chapters 2 through 6 of the thesis. A general discussion and recommendations for future work are then suggested.

7.1. Specific conclusions

Chapter 2 was dedicated to the experiments that were carried out to collect data on the physical and rheological properties of different types of manure. It was found that the density of dairy cattle, poultry and pig manure was in agreement with ASAE D384.1 and other published results. Predictive equations based on total solids concentration were obtained. A method was proposed to calculate a modified value of the geometric mean length obtained by screening. Significantly larger modified geometric mean lengths were observed as the total solids concentration of the products decreased. Static friction coefficients were measured on different surface materials. For design purposes, the observation of similar values for most of the manure products over the majority of the tested surfaces led to a unique equation to predict the static friction coefficient as a function of the total solids concentration. The animal manures studied were found to be non-Newtonian pseudoplastic fluids and the power law could be used to relate shear stress and shear rate. The value of the consistency coefficient was found to increase with the total solids concentration. The apparent viscosity was found to be well correlated to TS for dairy cattle, poultry and pig manure. It was concluded that for the design and analysis of manure handling and land application systems, the ranges of values presented could be used with proper care. Poultry and pig manure generally

exhibited similar behaviours while dairy cattle and sheep manure showed similarities, though not as strong as the former pair due to the straw content of the tested sheep manure. The density values and friction characteristics of manure products were found to be consistent with other published results. The shear stress – shear strain relationships seemed however to be study-specific, but published values still showed similarities.

The experimental work aimed at measuring the performances of conveying systems in land application machines and at studying the effects the geometry of the holding system on the output flow was reported in chapter 3. The conclusions were to the effect that the 4-auger system designed at the University of Saskatchewan required more energy to unload the manure from the hopper, when compared to the scraper conveyor. Also, the specific energy requirements of both the scraper conveyor and the system of 4 augers were significantly affected by the vertical position of the flow-control gate. The characteristic flow rate obtained with the scraper conveyor was significantly affected by the position of the gate, the velocity of the conveyor and the angle of the sidewalls. The characteristic flow rate produced by the 4-auger system was significantly influenced by the position of the gate and the velocity of the augers. There was also a significant effect of the interaction between gate position and conveyor velocity. Similar experiments on a manure spreader of larger capacity featuring a similar scraper conveyor indicated a relation between the vertical position of the gate and the specific energy as well as on the characteristic flow rate for three different products. A relationship was observed between the reduction in the flow section and the decrease of the characteristic flow rate for manure, compost and dry compost. The study of the effects of the geometry of the spreader hopper revealed that the stretch within the tolerance zone, which corresponds to the percentage of the unloading time during which the momentary flow rates lie within plus or minus 15% of the characteristic flow rate, increased with an increase in the length and the width of the hopper. Also, the mass flow rate longitudinal coefficient of variation was observed to decrease when the length of the hopper was increased. The same effect was observed when increasing the width of the hopper and when reducing its height. The physical properties of the product

spread had an influence on the flow curves. Cohesive products generated better values for the stretch within the tolerance zone, the longitudinal coefficient of variation and the unloading time expressed as a percentage of the theoretical unloading time.

Chapter 4 was dedicated to the discrete element representation of manures. In that chapter, methods have been developed to implement manure models in the discrete element code PFC^{3D}. A procedure to create user-defined particle size distributions was presented. This procedure generated very small errors for the number and characteristic dimension of the particles for each size class (average relative error of 0.53% and 0.33%, respectively) for a wide range of particles diameter (0.82 to 30.0 mm). Clustered particles were also introduced to better model the brittle and clumpy nature of organic by-products. The mathematical relations used to generate randomly oriented and located three-sphere clusters were presented. Parameters defining the linear and simplified Hertz-Mindlin constitutive models have been studied. For the linear model, it was shown that the ratio of shear to normal stiffness had a major influence on the angle of internal friction as determined by the virtual direct shear test. To a lesser extent, the Young's modulus was also observed to have an influence on the angle of internal friction. The Young's modulus, friction coefficient, normal and shear strength of the contact bonds as well as normal and shear strength of the contact bonds linking the clustered particles all influenced the apparent cohesion. The shear modulus used in the Hertz-Mindlin model was found to have an influence on both the apparent cohesion and the angle of internal friction. The Poisson's ratio had little effect on those two parameters. The methods presented have the potential to be extended to any type of solid organic by-products.

Chapter 5 was an introductory paper focusing on the utilization of numerical methods in modeling the handling and land application of organic fertilizers. The discrete element method was applied to the flow of two types of composts. A preliminary model of a full-size spreader with dual vertical beaters was capable of realistically predicting the ground distribution of the product along with the power requirements of the beaters and discharge conveyor. Scaled numerical models were developed to study the effect of the

vertical position of a flow-control gate and the type of compost spread on the discharge flow and energy requirements of the conveyor. The models were validated against experimental results obtained using a full-size manure spreader. For both types of composts, the conveyor was operated at 0.03 m/s and two operational configurations were tested: the gate fully open and the bottom of the gate 515 mm above the bottom of the hopper. An increase in specific power was obtained for both the experimental and simulated results and for both products. The simulated mass efficiencies were in good agreement with the measured values in the open gate configuration. The reduction in flow rate produced by the lowering of the gate was replicated by the models, but the absolute difference between the flow rate with the gate fully open and the flow rate with the gate lowered was underestimated by the model. As a result, the simulated mass efficiency showed an inverse trend when compared to the experimental results. Computational fluid dynamics was applied to the flow of sludge in a spreader. The simulated and experimental flow rate curves were in close agreement for both a fluid pasty sludge and a plastic pasty sludge. The simulated streamlines in the hopper were also in good agreement with field observations. The sludge flow on a disc was studied on a scaled experimental spreader. CFD simulations of that flow were also carried out. The CFD models were capable of reproducing sludge flow on a disc with values of residence time well correlated to experimental results. The two numerical methods could be used to successfully model the flow of organic fertilizers in land application equipment. Improvements in the DE models are possible by refining the constitutive models used for the composts. Full-scale models also have the potential of enhancing the accuracy of the simulations as the geometry of the mechanical systems would be implemented with more realism. The CFD models could also be enhanced by improving the representation of the discharge conveyor. It was concluded that the numerical simulations have the potential to reveal valuable information on the flow of these types of products in land application equipment. It becomes however very challenging to collect experimental data to validate the predictions of the models with regard to information on the flow phenomenon occurring in the bulk of product.

In chapter 6, the DEM was applied to model different conveying and land application systems. The results indicated that the models are capable of predicting the discharge rate and the energy requirements with reasonable accuracy. From the results presented, it could be stated that the models of both conveying systems performed better when the gate was in its lowest position. This was due to the attenuation effect of the gate on the gravity flow at the discharge end of the machine. Refinements of the manure model are required in order to improve the predictions of the machine-manure interactions models for the open-gate configurations. The effect of the gate on the energy requirements was well replicated by the models. The influence of the gate on the simulated characteristic flow rate was adversely affected by the accuracy of the manure model. It was not possible to correctly replicate the effect of the gate with the manure model utilized. The results of the simulations were affected by the clustered particles. The clusters were found to be a good means of mimicking the clumps present in real manure and their effect on the flow. The strength of the bonds linking the clustered particles had an influence on the predictions of the models. Unbreakable clusters, with high strength values, caused artificially high values of contact forces in the case of the 4-auger conveying system. The scraper conveyor was less affected by the strength of the clusters. The damping coefficient applied to the equations of motion that are solved for each particle influenced the simulations results. A value of 0.35 was found to give good results in most situations. The experimental mass distribution across the transverse distribution system used for banded application on a prototype precision land applicator was very closely replicated by the numerical model. The simulated coefficient of variation for the mass distribution across the transverse conveyor was 3.9% compared to an average measured coefficient of variation of 6.0%. The very challenging task of modeling the machine-product interactions taking place in manure handling and land application equipment has been successfully fulfilled. The accuracy of the models has the potential to be greatly enhanced by validating them over a broader range of mechanical systems and manure products as well as refining the manure models.

7.2. General discussion and recommendations

The overall goal of this thesis was to develop models of the machine-product interactions taking place in solid and semi-solid manure handling and land application equipment. For that goal to be reached, specific objectives had to be met. Models of manures were required to develop models of the machine-product interactions and the development of those manure models entailed experimental data on the physical and rheological properties of different manure types. Finally, data on the operation of various mechanical systems used in manure handling and land application equipment were required to develop and validate the interactions models. The flow of objectives along with the corresponding chapters of the thesis is illustrated in figure 7.1.
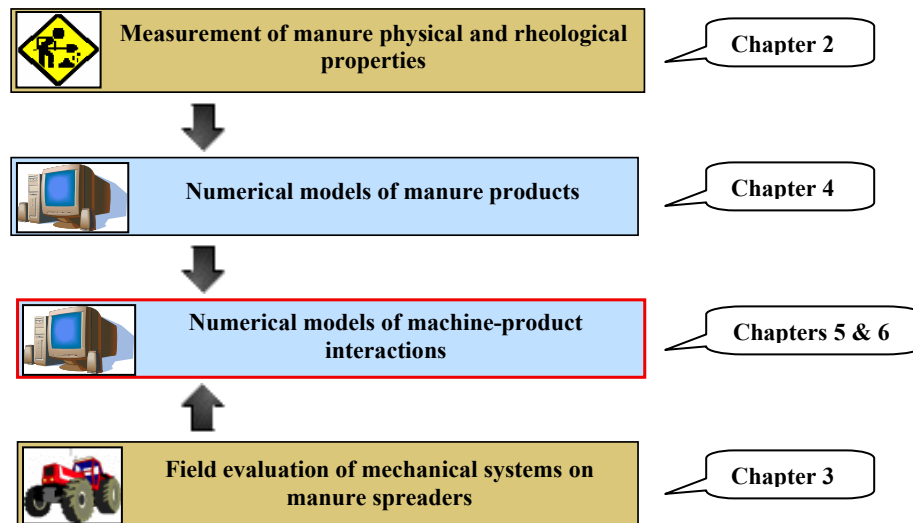
Measurement of manure physical and rheological properties	Chapter 2
Numerical models of manure products	Chapter 4
Numerical models of machine-product interactions	Chapters 5 & 6
Field evaluation of mechanical systems on manure spreaders	Chapter 3

Figure 7.1.   Objectives of the thesis and corresponding chapters.

The initial phase of the research was the quantification of selected physical and rheological properties for animal manures. Several properties were selected based on the influence that they were deemed to have on the performances of handling and land application systems. Several apparatuses were designed and built to allow for the measurement of those properties. The study of the physical and rheological properties of manures has yielded an extensive database of information relevant to the design of manure handling and land application equipment. Relationships were established between the measured properties and the total solids concentration of the manure as

well as its type. However, further work would be required to study in more depth the mechanical properties of the products. It has become evident in chapter 4 that the manure models could benefit from ranges of values for properties such as the Young's modulus or Poisson's ratio. Nevertheless, the basic properties presented in chapter 2 had to be measured as very little information was available in the scientific literature. A deeper study of the semi-solid phase and the liquid – semi-solid and semi-solid – solid transition zones would also be useful. Good relationships for the measured properties could be established at the ends of the total solids concentration spectrum included in the thesis, but it was observed that the behaviour of pasty products (generally between 18% and 30% TS) was difficult to define.

Numerical models of manure products were developed based on the measured properties. The emphasis was put on relating the virtual products to the particle sizing reported in chapter 2, effectively implementing clusters of particles in the models and correlating the results of the direct shear tests. This modeling phase was certainly very challenging. First of all, manure products do exhibit variability in their properties. Also, very little information was available to form a basis for this work. The Discrete Element Method (DEM) used in this research study has been applied to a broad range of engineering applications, but none of them was similar to the task at hand. Chapter 4 presented a sensitivity analysis for several parameters included in the linear and simplified Hertz-Mindlin contact constitutive models. While it has been demonstrated in chapter 4 that it was possible to create a virtual product resembling its physical counterpart, there is still a need to further refine the manure models. A more detailed analysis of the effect of the parameters defining the contact constitutive models should be carried out. The number of parameters that would need to be included in a complete sensitivity analysis is very important. The size of the particles that should be used in the models is also an interesting question. The approach taken in this work was to correlated as much as possible the results of the sieving experiments reported in chapter 2, knowing that the particles are not the elementary elements making up manure. Finer models using smaller particles would be interesting to study, but the computing cost of such an analysis appears very high given the current availability of resources.

224

Field experiments were carried out to evaluate the performances of two conveying systems and to study the effect of the vertical position of the flow-control gate and product properties on the flow of manure. The main parameters were the discharge flow rate and the power consumption of the conveying systems. Standard EN13080 was a determining tool in analyzing the data of all the spreading experiments and allowing for comparisons to be made. The data collected during this phase of the research was of great value in developing and validating the machine-product interactions models. The same type of experimental work was carried out using the prototype precision land applicator developed at the University of Saskatchewan and a full-size commercial manure spreader at Cemagref (France). The amount of engineering data related to the design and operation of land application equipment for solid organic fertilizers is very limited. Research studies focusing on such data have to face very heavy experimental setups (quantities of manure, physical space required for the experiments, required manpower, etc.). It is therefore extremely important to disseminate the research results so the scientific community can build on the acquired knowledge. The results of the research reported in chapter 3 allowed for a better understanding of the flow of organic fertilizers in land application equipment and of the influence of the type of conveying system and geometry of the holding system.

Models of the interactions between organic fertilizers and machinery systems were developed with an emphasis on the conveying system and on the flow-control gate. A model of a full spreader including the spreading devices was also presented in chapter 5. Good correlations could be established between the simulations results and measured or published data. The transverse distribution system for banded manure application was also modeled. The model of the spreader fitted with the banded application system was a great illustration of the power of the developed models as design tools. The discharge flow of the banded applicator is determined by a number of parameters. With several parameters influencing the operation of the equipment and no theoretical or empirical models, the numerical models developed in this thesis become very potent design tools. The correlation between the predictions of the model in terms of transversal product distribution was in close agreement with measured data.

This thesis embraced a broad topic due to the number of objectives that was required to reach the ultimate goal of the research. It has been demonstrated that it is possible to predict engineering data using the machine-product interactions models and that these models have the potential to become powerful engineering tools for the design of improved handling and land application systems for solid and semi-solid manure.

Appendix A   Permission to include published manuscripts in the thesis

Donna M. Hull
Director, Publications
American Society of Agricultural Engineers
2950 Niles Rd.
St. Joseph, MI 49085
hull@asae.org
(269) 428-6326 Fax (269) 429-3852
See the ASAE Online Technical Library at http://asae.frymulti.com

-----Original Message-----
From: Hubert Landry [mailto:Hubert.Landry@asae.org]
Sent: Wednesday, January 19, 2005 2:55 PM
To: vander@asae.org
Subject: Permission to use

Ms. VanderVeen,

I would like to get permission from ASAE to include article PM3094 in my doctorate thesis. My thesis is structured as a series of manuscripts written in a form suitable for publication in scientific journals. Article PM3094 has already been published and another chapter of the thesis has been accepted for publication (PM-05245-2004.R2, accepted for publication 06-12-2004).

Please do not hesitate to contact me should you need further information.

Thank you for your collaboration,
Best regards,

Hubert LANDRY

Graduate Student in Agricultural Engineering
Department of Agricultural and Bioresource Engineering
College of Engineering
University of Saskatchewan
57 Campus Drive, Saskatoon, SK, CANADA S7N 5A9
Room: Eng1A90
Phone: 306.966.5331
Fax: 306.966.5334
Email: Hubert.Landry@asae.org

Appendix B   Chapter 2 in its published format

PHYSICAL AND RHEOLOGICAL PROPERTIES OF MANURE PRODUCTS

H. Landry, C. Laguë, M. Roberge

ABSTRACT. *Selected physical and rheological properties deemed to influence the performances of handling and land application equipment were quantified for different types of manure at different levels of total solids concentration (TS) ranging from 10% to 50% on a wet mass basis. The selected properties included total solids concentration, bulk density, particle size distribution, friction characteristics, and shearing behavior and were measured for dairy cattle, sheep, poultry, and pig manure. The bulk density of all manure products was found to increase with TS and the values for poultry and pig manure were not significantly different at the tested TS levels. The measured density values were in close agreement with ASAE D384. The proposed modified geometric mean length of the particles was found to significantly increase as TS became smaller. The static friction coefficients of all manure types with the exception of pig manure on the different surface materials [plywood, plastic, steel (bare and painted)] did not exhibit large differences and a single linear equation was suggested to predict the static friction coefficient as a function of TS. Animal manures were described as pseudoplastic fluids and the consistency coefficients were found to increase with TS for all manure types. The apparent viscosity of the tested manure products was well correlated to TS. The implications of the property results obtained in this study as well as future research are discussed.*

Keywords. *Handling, Land application, Manure, Physical properties, Rheological properties.*

Proper recycling of animal manure is of paramount importance to increase the sustainability and social acceptance of intensive livestock production. As the environmental and agronomic requirements for ef-fective and safe land application of manure products become more prescriptive, equipment used in manure management systems are subjected to higher performance expectations. Solid and semi−solid manure products represent potential alternatives to reduce some of the environmental and societal problems that may be associated with liquid manure management. Commercial equipment designed to handle and land apply solid and semi−solid manure do exhibit large coefficients of variation for both transversal and longitudinal product distribution (Bisang, 1987; Wilhoit et al., 1993; Frick et al., 2001; Thirion and Chabot, 2003). Appropriate knowledge of the physical and flow properties of the products to be handled is fundamental to the design and operation of efficient systems.

The authors are **Hubert Landry, ASAE Student Member,** Graduate Student, **Claude Laguë, ASAE Member Engineer,** Professor and Dean, **Martin Roberge,** Assistant Professor, Department of Agricultural and Bioresource Engineering, College of Engineering, University of Saskatchewan, Saskatoon, Canada. **Corresponding author:** Hubert Landry, Department of Agricultural and Bioresource Engineering, University of Saskatchewan, 57 Campus Drive, Saskatoon, SK, Canada S7N 5A9; phone: 306−966−5303; fax: 306−966−5334; e−mail: Hubert.Landry@asae.org.

LITERATURE REVIEW

Published research results are readily available in the area of manure chemical properties. Much fewer journal articles have targeted the physical and flow properties of manure products and most of the manure characterization efforts have focused on liquid manure and slurry.

Kumar et al. (1972) studied the flow properties of animal waste slurries. They concluded that the viscosity of dairy cattle slurry decreased with an increase in dilution and an increase in temperature. They also noticed that the flow of slurry is Newtonian at solids contents below 5%. The addition of sawdust up to as much as 10% by weight of the amount of manure decreased the viscosity of a slurry having a total solids content of up to approximately 9%.

Hashimoto and Chen (1976) attempted to identify a parameter that would mathematically describe the rheological properties of aerated and fresh dairy cattle, poultry and swine waste slurries and that could be easily and precisely measured experimentally. They also tried to describe procedures to estimate the effect of rheological properties on pumping, mixing and aerating livestock waste slurries. Their study showed that the rheological consistency coefficient (K) and rheological behavior index (n) of livestock waste slurries can be expressed in terms of the equilibrium sludge volume fraction (Φ_L) as:

$$K = b_1 \phi_L^{b_2} \tag{1}$$

$$n = b_3 + b_4 \ln(\phi_L) \tag{2}$$

where b_1 to b_4 are constants.

Values of these constants were given for the tested animal manures and were found to be dependent on the range of Φ_L. Relationships have also been established to relate mixer power characteristics and pressure head loss in pipeline

transport of slurries to K, n, the effective viscosity, and generalized Reynolds number. A method of determining Φ_L is also presented, but to the authors' knowledge, the equilibrium sludge volume fraction has never been widely used in manure characterization.

Rheological consistency index, flow behavior index, specific heat, and thermal conductivity of beef cattle manure were determined by Chen (1982). Density was also measured for solid contents ranging from 1% to 99%. The results suggested that the density of manure increased as the total solids concentration increased for manure with less than 16% TS. For manure with TS higher than 50%, the bulk density of the manure dropped much below the liquid manure density. The study also included rheological properties for TS ranging from 1% to 14%. Beef cattle slurries were described as non–Newtonian pseudoplastic fluids, the deviation from Newtonian behavior increasing with TS.

Using a constant temperature rotational viscometer, Chen and Shetler (1983) investigated the effect of temperature on the rheological properties of cattle manure having total solids concentrations ranging from 2.5% to 19.3%. The experimented shear rates ranged from 20 to 200 s^{-1} and temperatures varied from 14°C to 64°C. This study confirmed previous findings that beef cattle manure slurry is a non–Newtonian pseudoplastic fluid and a power–law equation could be used in this range of shear rates. The rheological behavior index (n) was found to decrease exponentially with TS, but was not affected by temperature while the rheological consistency index (K), in general, increased as TS increased. The apparent viscosity of the slurry decreased exponentially as temperature increased, and increased as TS increased. An equation relating the apparent viscosity to TS and to the absolute temperature was given.

Chen (1986) later proposed a rheological model for manure slurries and applied this model to experimental data of cattle manure slurry obtained using a rotational viscometer. He found that cattle manure slurry showed negligible yield stress and that the Bingham Plastic, Herschel–Bulkley and Casson models were not applicable. The power law model could be used only for sieved slurries with TS below 4.5%. He also observed a curvilinear relationship of shear stress and shear rate in the logarithmic plot for high TS slurries due to the existence of a limiting viscosity. He proposed the following rheological model for beef cattle manure slurry:

$$\tau = \eta_0 \dot{\gamma} + K'' \dot{\gamma}^{n''} \qquad (3)$$

where τ is the shear stress, $\dot{\gamma}$ is the shear rate, η_0 is the limiting viscosity, and K" and n" are rheological parameters. Nonlinear least square regression was used to fit the proposed model to the experimental rheological data for slurries having TS above 4.5%. The results showed that the proposed model was well correlated to the experimental data. The value of n" for sieved slurries did not vary with TS or temperature, having an average value of 0.307 with a standard deviation of 0.054. Equations expressing η_0 and K" in terms of TS and temperature were also obtained. The values of η_0 and K" were found to increase as TS increased and to decrease as temperature increased.

Achkari–Begdouri and Goodrich (1992) studied the rheological properties of Moroccan dairy cattle manure with total solids concentrations ranging from 2.5% to 12% at temperatures between 20°C and 60°C. Their results showed that in the ranges of total solids and temperature of the study, Moroccan dairy cattle manure behaved as a pseudoplastic fluid. Two equations based on the total solids content and the temperature, one expressing the consistency coefficient and the other to predict the flow behavior index, were proposed.

Solid and semi–solid manures have not been studied as much as liquid manure and slurry in terms of physical properties. A few studies have mentioned the effect of manure properties on the performance of various mechanisms. In their study of spreader distribution patterns for poultry litter, Wilhoit et al. (1993) made observations on the effect of particle size on spreading distances. They concluded that large particles were distributed more evenly and on a larger width when compared to smaller particles that landed closer to the spreader. Wilhoit et al. (1994) also observed the effects of particle size distribution while developing a drop applicator for poultry litter. They concluded that their gravity flow metering system was not appropriate due to the presence of clumps blocking the flow of material from the hopper. Observations were made by Wilhoit and Ling (1996) to the effect that the nature of wood and fly ash caused the spreading uniformity to be inconsistent from trial to trial. In their design of an applicator for side dressing row crops with solid wastes, Glancey and Adams (1996) identified maximum lump size and moisture content as the physical properties presenting potential problems in raw manure conveying.

Glancey and Hoffman (1996) measured physical properties of poultry manure and compost under different management practices. They investigated trends in the measured properties to develop general guidelines for the design and analysis of material handling systems, transportation equipment and spreaders. They concluded that wet bulk density was dependent on moisture content for all the solid wastes evaluated and that knowledge of moisture content was therefore more important than the type or source of material. The static friction characteristics suggested that there was little practical difference between the different products. Another trend identified by the authors indicated that all unscreened waste materials contained large lumps. This presents potential design problems in developing conveying systems to handle unscreened materials.

Agnew et al. (2003) used an air pycnometer to measure the air volume and density of compost. The free air space (FAS) and bulk density of manure compost, municipal solid waste compost, and mixtures of biosolids and amendment materials were measured at various moisture contents and compressive loads. Their results indicated that the FAS decreased with loading and increasing moisture content while the wet bulk density increased with loading and increasing moisture content. A linear relationship was established between FAS and bulk density for all the materials tested under loads.

Malgeryd and Wetterberg (1996) reported the efforts of the Swedish National Machinery Testing Institute and the Swedish Institute of Agricultural Engineering to provide the necessary knowledge of how the physical properties of manures and slurries affect the spreading of different machines. They highlighted the fact that there is a lack of general knowledge about which properties are important in practice and how they should be measured. For manures that can be pumped, four properties were considered significant, namely, fluidity, separation tendency, risk of clogging and dry matter content. For manures that cannot be pumped, five

properties were deemed important: bulk density, stacking ability or consistency, comminuting resistance, heterogeneity and dry matter content. Methods were suggested for measuring those properties. Their results suggested that there is no clear relationship between the active angle of repose and the dry matter content for non–pumpable manures and that bulk density and the active angle of repose are closely related to each other. The active angle of repose could be estimated from the bulk density, which is easier to measure.

Thirion et al. (1998) experienced difficulties in trying to implement the test methods outlined by Malgeryd and Wetterberg (1996). They measured manure properties including normal stress, shear stress, bulk density, friction coefficient, straw content and dry matter content. They included numerous comments on the difficulty of obtaining reliable results and proposed a method for obtaining a numerical value of manure heterogeneity.

Landry and Laguë (1999) studied selected physical properties of papermill residues. They measured bulk density, moisture content, angle of repose, friction coefficient on different materials and particle size distribution. They concluded that while the values of the selected properties were relatively constant among samples that originated from the same papermill, there could also be large variations depending upon the specific origin of the products.

The literature review clearly demonstrates the variability that exists in manure properties and the lack of widely accepted and used methods to measure those physical and rheological properties. More data are required to highlight general trends and to develop design guidelines for manure handling and land application equipment.

OBJECTIVE

The objective of the work reported herein was to measure selected physical and rheological properties of different types of manure products at different levels of total solids concentration with an emphasis on the solid and semi–solid ranges.

MATERIALS AND METHODS

Based on the review of previous work, the properties that were deemed having the most influence on the performances of manure handling and land application equipment were identified as: (a) total solids concentration, (b) bulk density, (c) particle size distribution, (d) friction characteristics, and (e) shearing properties. Four types of manure were investigated: (1) dairy cattle, (2) sheep, (3) poultry, and (4) pig. Manure samples were collected from the facilities on the University of Saskatchewan farm (Saskatoon, Saskatchewan, Canada). The dairy, pig, and poultry (laying hens) barns all featured scrapers to move the manure out of the buildings. The dairy and poultry barns were scraped twice a day and the manure went directly into underground pits. The pig manure was stored in a room at the end of the barn and that room was periodically emptied. Fresh samples were collected after scraping, just before the manure entered the pits. In the case of sheep manure, the samples were collected from outside pens and contained a large proportion of straw. A small amount of chopped straw was used in the free stall barn where the dairy cattle manure samples were collected. No bedding material was used in the pig and poultry barns. With the objective of characterizing the manure products in the state they would be when handled and/or land applied, the samples were not submitted to any treatment (e.g., separation, screening, etc.) prior to testing. Several large samples (approximately 150 L per sample) were collected for each type of manure to avoid using the same material more than once. In order to reach the targeted total solids concentrations, the raw samples were either dried outside or diluted with water. Based on the initial and targeted total solids concentrations, the amount of water to add was estimated by weighing the samples. The TS of the samples was measured daily during the preparation phase. The majority of the tested samples went through one wetting or drying cycle, two wetting phases were sometimes necessary to reach the desired TS level. The samples were stored and handled in 170–L barrels and were tested as soon as the targeted TS level was reached. All property measurements were replicated on four sub–samples.

TOTAL SOLIDS CONCENTRATION

The total solids (TS) concentration of the manure products was determined by drying the samples in an oven overnight at 103°C (*ASAE Standards*, 2002a). TS was the ratio of oven–dry weight to wet weight and was expressed as a percentage.

BULK DENSITY

The bulk density of manure products was measured in an uncompacted state by weighing large containers of known volume filled with manure according to the procedure described by Glancey and Hoffman (1996). A weighing apparatus was designed and built to accommodate large samples (i.e., 170–L barrels). The apparatus was made of a platform supported by two load cells (2224–N capacity; ±1.11 N nonlinearity; ±0.67 N hysteresis; Interface, Scottsdale, Ariz.) and allowed for easy placement of the barrels. The load cells with the data acquisition system were calibrated using a universal testing machine (Model 1011, Instron Corporation, Canton, Mass.). All the test apparatuses that required calibration featured load cells (weighing apparatus, shearbox and large–scale viscometer) and the universal testing machine was used. Observations were made by Thirion et al. (1998) and Frick et al. (2001) to the effect that density values are affected by the measurement method. The chosen method consisted of manually handling the samples to create a consistent state of compaction for the entire test series. Once the barrels were filled to the desired level, opposite sides of the barrels were alternately lifted and dropped twice on the ground from an approximately 300–mm height to compact and level the material.

PARTICLE SIZE DISTRIBUTION

A modified soil sieves shaker and a screen set were used to determine the particle size distribution of the manure samples using a procedure adapted from ASAE S424.1 (*ASAE Standards*, 2002b). The size openings of the screen set used in this study were 25.4, 16.4, 8.7, 5.2, and 1.2 mm. The samples were placed on the top screen (25.4–mm openings), shaken for 90 s, and the screens were finally weighed on a laboratory scale to determine the amount of manure retained on each screen.

FRICTION CHARACTERISTICS

The values of the static friction coefficient of manure products on different surface materials were measured using the inclined plane method (Mohsenin, 1986). Four different surfaces, representative of possible candidate materials for the construction of manure handling and land application equipment, were selected: steel (bare and painted), plastic (PVC), and plywood. An inclined plane apparatus was designed and built to measure the static coefficients of friction of manure products. The apparatus featured an electric motor giving a constant angular inclination velocity of 0.007 rad/s. For the static coefficient of friction experiments, the samples were placed and held in a fiberglass ring having a diameter of 300 mm and a height of 30 mm. The angle of repose of manure products was also measured according to the method described by Henderson et al. (1997) using an apparatus made of a cylinder that could be lifted from a base plane to let the sample flow out of it and form a pile. The radius of the pile was measured at four different locations 90 degrees apart on the base plane. The height of the pile was also measured and the angle of repose was calculated as the arc tangent of the ratio of the height to the average radius. Approximately 10 to 15 L of manure were used for each angle of repose measurement.

SHEARING PROPERTIES

Depending on the total solids concentration of the product that was tested, three different apparatuses were used to characterize the relation between shear stress and shear rate: the shearbox apparatus (Model No. 25301, Wykeham Ferrance Engineering Ltd., Slough, England), a laboratory rotational viscometer (DV–III+ Digital Rheometer, Brookfield, Middleboro, Mass.), and a large–scale rotational viscometer. The large–scale viscometer was designed and built to accommodate the 170–L barrels that were used in the study. It was also introduced to compare the results obtained with small and very large samples (0.5 L–samples were used with the laboratory viscometer compared to approximately 85 L–samples for the large–scale unit). The large–scale viscometer is illustrated in figure 1. The barrel was rotated through the 90–degree gearbox and the torque calculated from the force measured via a load cell located between a fixed back plate and a rigid member attached to the freewheeling spindle shaft. The rotational speeds varied from 0.3 to 100 rpm and 3 to 100 rpm for the laboratory and large–scale viscometer, respectively. The shear rate and shear stress were calculated using equations 4 and 5, respectively.

$$S = \frac{2\omega R_c^2 R_b^2}{R_b^2\left(R_c^2 - R_b^2\right)} \tag{4}$$

$$F' = \frac{M}{2\pi R_b^2 L} \tag{5}$$

where

S = shear rate (s^{-1})
W = angular velocity of spindle (lab) or container (large) (rad/s)
R_c = radius of container (m)
R_b = radius of spindle (m)
F' = shear stress (Pa)

M = torque input by instrument (N–m)
L = effective length of spindle (m)

The appropriate values of R_c, R_b, and L were obtained from the Brookfield documentation in the case of the laboratory viscometer. For the large viscometer, the integration of the apparatus parameters into equation 4 gave a shear rate, in s^{-1}, equal to 0.239 times the rotational velocity of the barrel in revolutions per minute. The immersion depth of the spindle was used as the effective length for the large unit. Four normal loads were used for the direct shear tests (7.0, 22.5, 38.1, and 70.7 kPa) and the rate of shear was constant at 1.2 mm/min. The standard procedure ASTM D3080–98 (ASTM, 1998) was followed.

RESULTS AND DISCUSSION

Table 1 summarizes the results obtained for the total solids concentration of the tested animal manures. It can be seen that some of the tested samples exhibited variability, as assessed by the values of standard deviation. However, the ANOVA performed on the TS results indicated that the measured TS values are similar enough to proceed to comparisons between the different waste products based on the target TS level. The original total solids concentrations of the dairy cattle, sheep, and pig manure samples were around 15%, 30%, and 25%, respectively. For the poultry manure samples, two different initial levels of TS were observed (12% and 18% approximately) depending on the amount of water that got into the manure from leaking drinkers. Samples with a TS level corresponding to a target value were tested as is.

SOLID MANURE PRODUCTS

Solid manure products can be compared on the basis of the properties presented in table 2. As it can be seen from the bulk density results included in table 2, poultry and pig manure are similar products while dairy cattle and sheep manure show significant differences at most TS levels. Using the density
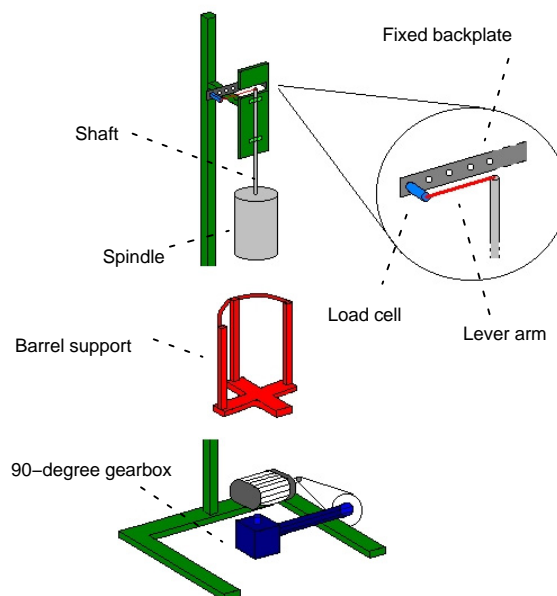

Figure 1. Schematic representation of the large–scale viscometer.

Table 1. Average total solids concentration for the manure products evaluated.

Target TS Level (%)	Measured TS (%)			
	Dairy Cattle	Sheep	Poultry	Pig
50	47.8[a]ab[b] (3.1)[c]	53.0 a (3.1)	47.3 b (1.9)	48.0 ab (1.7)
40	44.4 a (4.7)	41.5 a (4.9)	41.5 a (0.9)	41.7 a (5.2)
30	33.5 a (1.6)	30.7 a (1.9)	34.5 a (0.6)	32.0 a (4.5)
20	23.4 a (1.7)	18.4 a (2.5)	21.2 a (4.2)	22.8 a (0.2)
15	14.2 ab (0.4)	13.8 a (0.1)	14.5 ab (0.6)	14.8 b (0.04)
10	8.9 a (0.2)	10.4 b (0.3)	10.3 b (0.3)	10.7 b (0.6)

[a] Average value.
[b] Values within each TS level row not followed by the same letter are significantly different as determined by Fisher's LSD test at the 1% level.
[c] Standard deviation.

values obtained at the appropriate TS level, the results are very similar to those outlined in ASAE D384.1 (*ASAE Standards*, 2002c). According to the ASAE standard, the density in kg/m^3 of fresh manure is 990 for dairy cattle (14.0%TS), 1000 for sheep (27.5%TS) and for layer (25.0%TS), and 990 for swine (13.1%TS). Using the TS level closest to the ASAE standard, the comparisons (ASAE vs.

current study) of density values in kg/m^3 become dairy cattle (990 vs. 973); sheep (1000 vs. 521); layer (1000 vs. 1028); swine (990 vs. 1026). The only major difference is in sheep manure. This difference was due to the presence of a large proportion of straw in the sheep manure that was used in this study. The densities of all manure products were expected to become stable near the liquid density as TS becomes small.

Relationships between density and total solids concentration were obtained and are presented in figures 2 and 3. The following equations were obtained by polynomial regression analysis, using third order models and forcing the density at 0% TS to be 1000 (the density is in kg/m^3):

Poultry and pig:
$$\text{Density} = -0.02 \text{ TS}^3 + 1.2 \text{ TS}^2 - 11.2 \text{ TS} + 1000;$$
$$R^2 = 0.83 \tag{6}$$

Dairy cattle:
$$\text{Density} = 0.04 \text{ TS}^3 - 2.4 \text{ TS}^2 + 14.6 \text{ TS} + 1000;$$
$$R^2 = 0.93 \tag{7}$$

Sheep:
$$\text{Density} = 0.009 \text{ TS}^3 - 0.9 \text{ TS}^2 + 8.9 \text{ TS} + 1000;$$
$$R^2 = 0.91 \tag{8}$$

Equations 6, 7, and 8 can be used to obtain a reasonable approximation of the bulk density of poultry and pig, dairy cattle and sheep manure respectively. It can be seen on

Table 2. Density, static coefficients of friction, and angle of repose for the solid manure products evaluated.

Target TS Level (%)	Manure Type	Density (kg/m^3)	Static Coefficient of Friction (dimensionless)				Angle of Repose (°)
			Plywood	Plastic	Painted Steel	Bare Steel	
50	Dairy cattle	238.4[a] a[b] (20.1)[c]	0.88 a (0.042)	0.93 a (0.0082)	0.90 a (0.026)	0.80 a (0.0050)	n.a.[d]
	Sheep	332.3 b (20.3)	0.73 b (0.051)	0.79 b (0.048)	0.68 b (0.029)	0.66 b (0.028)	32.2 a (1.3)
	Poultry	607.5 c (75.3)	0.82 a (0.013)	0.88 a (0.022)	0.89 a (0.017)	0.79 a (0.018)	36.1 a (5.3)
	Pig	552.5 c (18.1)	0.83 a (0.029)	0.86 ab (0.052)	0.84 a (0.042)	0.89 c (0.045)	30.1 a (2.2)
40	Dairy cattle	198.6 a (7.9)	0.88 a (0.065)	0.88 a (0.029)	0.82 a (0.031)	0.79 a (0.021)	n.a
	Sheep	556.9 b (52.1)	0.81 a (0.057)	0.86 a (0.056)	0.83 a (0.021)	0.83 a (0.022)	48.0 a (6.8)
	Poultry	884.7 c (117.2)	0.90 a (0.047)	0.83 a (0.051)	0.89 a (0.039)	0.86 a (0.030)	40.3 a (2.9)
	Pig	948.7 c (30)	6.4 b (0.94)	2.3 b (0.43)	2.3 b (0.80)	1.5 b (0.22)	n.a
30	Dairy cattle	267.1 a (6.6)	0.91 a (0.051)	1.0 a (0.052)	1.0 a (0.027)	0.95 a (0.036)	n.a
	Sheep	520.8 b (34.9)	0.92 a (0.088)	0.93 a (0.021)	0.96 a (0.019)	0.91 a (0.055)	33.8 (0.9)
	Poultry	1028.2 c (45.5)	3.4 b (0.38)	0.87 a (0.062)	1.1 a (0.078)	1.0 a (0.20)	n.a.
	Pig	1140.9 c (112.3)	7.8 c (0.49)	0.95 a (0.12)	1.0 a (0.17)	0.80 a (0.080)	n.a
20	Dairy cattle	411.0 a (32.1)	1.0 (0.070)	1.2 (0.030)	1.1 (0.10)	1.1 (0.03)	n.a
	Sheep	1051.2 b (60.2)	These samples were not solid enough to measure the static coefficient of friction, the geometric mean length and the angle of repose.				
	Poultry	1091.8 b (63.9)					
	Pig	1090.0 b (77.3)					

[a] Average value.
[b] Values within each TS level row and property column not followed by the same letter are significantly different as determined by Fisher's LSD test at the 1% level.
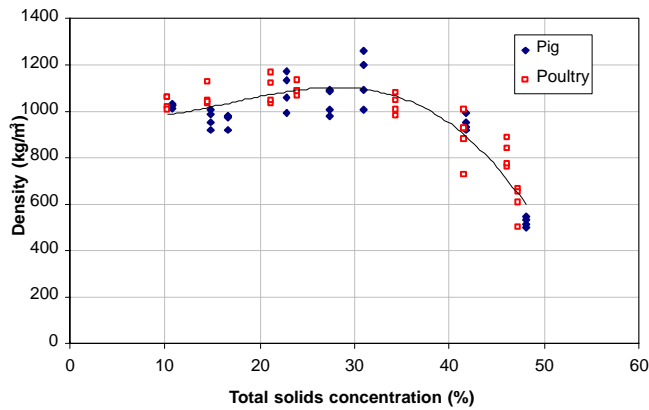[c] Standard deviation.
[d] Data not available.

Vol. 20(3): 277–288

281

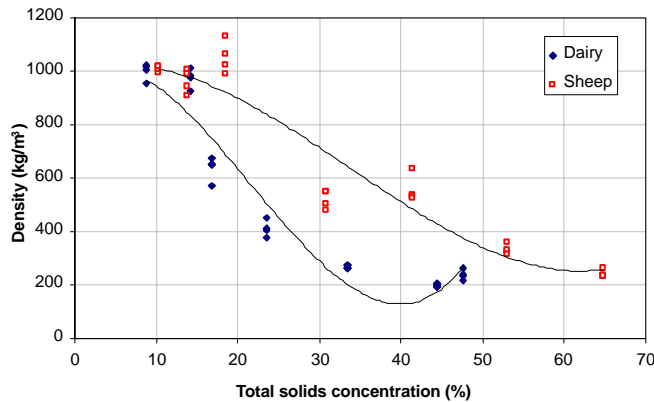**Figure 2. Bulk density values for poultry and pig manure and regression curve.**

Figure 3. Bulk density values for dairy cattle and sheep manure and respective regression curves.

figures 2 and 3 that some density measurements yielded high values, up to 260 kg/m^3 greater than the density of water (1000 kg/m^3). Although density values above 1000 kg/m^3 were also reported by Chen (1982), a bias induced by the initial tension/compression state of the load cells on the weighing apparatus as well as vibration during measurements are potential causes that may have yielded high density results.

Modified geometric mean lengths (Xgm') are presented in table 3. Large lumps were observed on the top screen (25.4–mm openings) yielding an overestimation of the particles' geometric mean length, as calculated according to ASAE S424.1 (*ASAE Standards*, 2002b). The calculations were then adapted using 16.4 mm as the largest size opening to obtain the modified value (Xgm'). Observations were made on the size of the lumps collected on the top screen. Their largest dimension was generally between 30 and 50 mm, but large 100– to 150–mm lumps were also observed, as mentioned by Glancey and Hoffman (1996). These lumps will affect the conveying behavior of the waste products, but it becomes difficult to predict how without prior knowledge of their mechanical strength. The data included in table 3 allow seeing the effect of total solids concentration on the characteristic dimensions of the particles for each manure type. It can be seen that as the total solids concentration decreased, or as the manure products became wetter, the modified geometric mean length became significantly higher. This was due to the increased aggregation ability of the animal wastes as the proportion of water in the manure increased. The data of table 3 also indicate there was no

Table 3. Average modified geometric mean length and standard deviation for dairy cattle, sheep, poultry and pig manure.

	Average TS (%)	Average Xgm'[a] (mm)	Standard Deviation (mm)
Dairy cattle (a[b])	16.8	14.0 a	1.7
	23.4	12.6 ab	0.27
	33.5	11.2 bc	0.46
	44.4	9.6 c	1.3
	47.7	9.5 c	1.1
Sheep (b)	18.4	11.6 a	0.29
	30.7	11.1 a	0.77
	41.5	10.1 b	0.34
	53.0	6.5 c	0.12
	64.8	5.4 d	0.53
Poultry (c)	34.5	18.9 a	0.95
	41.5	14.2 b	0.41
	46.2	13.4 b	0.45
	47.3	10.9 c	0.36
Pig (c)	27.4	18.6 a	1.0
	31.0	19.7 a	0.25
	41.7	12.6 b	0.0
	44.5	11.3 b	0.17
	48.1	12.0 b	0.96

[a] Modified geometric mean length.
[b] Values within each manure type group (rows) and manure type column not followed by the same letter are significantly different as determined by Fisher's LSD test at the 1% level.

significant difference in the overall average modified geometric mean length of poultry and pig manure. Also, the difference between dairy cattle manure and sheep manure in terms of modified geometric mean length was not very important, as suggested by the values of table 3. Predictive equations 9 and 10 for the modified geometric mean length of dairy cattle and sheep manure as well as for poultry and pig manure were obtained (fig. 4).

Dairy cattle and sheep:
$$Xgm' \text{ [mm]} = 16.1 - 0.16 \text{ TS}; \quad R^2 = 0.83 \qquad (9)$$

Poultry and pig:
$$Xgm' \text{ [mm]} = 31.9 - 0.43 \text{ TS}; \quad R^2 = 0.84 \qquad (10)$$

The results obtained for the static friction coefficients indicate that while a fair amount of variability could be observed, similar values of friction coefficient were also present in the database. The large values of static coefficient
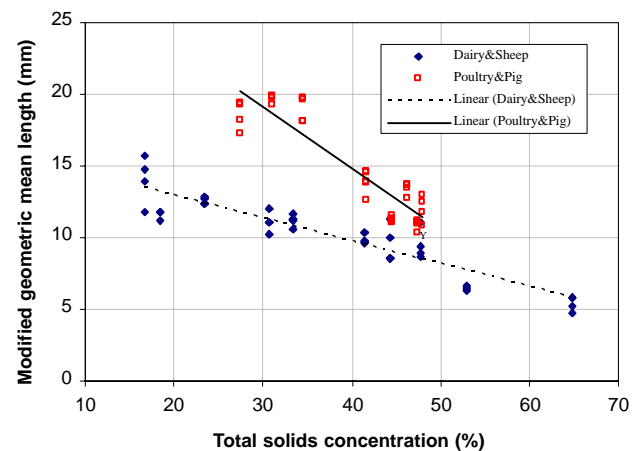

Figure 4. Modified geometric mean length of dairy cattle, sheep, poultry, and pig manure as a function of total solids concentration.

of friction for pig manure could not be explained. More measurements would be required to see if pig manure really exhibits such large friction coefficients or if the values obtained were marginal. When all the coefficient of friction data were analyzed together, no significant differences were found between materials except for plywood, which had significantly higher coefficients of friction. It was observed during the experiments that some products had a different behavior on the inclined plane when they had a paste–like consistency or when seepage occurred. The tested poultry and pig manures exhibited a paste–like consistency at TS between 20% and 30%. It is difficult to define the limits of the solid or liquid states since small TS increments have not been studied in the suspected transition zone. The dairy cattle and sheep manure samples did not seem to have a solid to liquid transition zone as defined as the poultry and pig samples. The coefficient of friction results were further analyzed without the results obtained for these particular cases. The resulting linear regression equation is (fig. 5):

Static friction coefficient [dimensionless] = 1.34 – 0.011 TS;
$\qquad$ $R^2 = 0.71$ $\hspace{3cm}$ (11)

Equation 11 can be used to predict the static friction coefficient of the tested manure products on the selected surface materials. For the design and analysis of handling and land application systems, the choice of appropriate safety factors should compensate for the lack of fit of the equation. More data would be required to deepen the observations made on the friction behavior of pasty products. The coefficients of friction measured in this study are consistent with those reported by Glancey and Hoffman (1996) and with their conclusion that there is little practical difference between the coefficients measured on the various surfaces and for the manure products tested.

The angle of repose results included in table 2 demonstrate that there was no significant difference between the angles measured for all manure types at a given level of total solids concentration. The missing data for this property were due to problems encountered with the apparatus. Some products would also keep the shape of the cylinder they were confined in after it had been lifted from the base plane. However, the results indicate there was little practical difference between

the angles of repose of the tested animal manures. The average of all angle of repose measurements was 38°, which was in agreement with what was presented by Glancey and Hoffman (1996) (average of 37°) and also close to the values reported by Moysey and Hiltz (1985) for commercial fertilizers that had angles of repose between 33° and 36°. The average value of the current study is greater then what was measured by Landry and Laguë (1999) for papermill residues (average of 30°).

The results obtained for the direct shear test were highly variable, as revealed by the large values of standard deviation presented in table 4. General trends could not be observed for the angle of internal friction or the apparent cohesion. The direct shear tests were carried out using a 190.5– × 101.6– × 63.5–mm box and the samples were not screened prior to the experiments. The large aggregates present in most of the tested samples may have been responsible for the inconclusive results, although observations made while testing samples free of large lumps did not show major differences in the recorded data. The direct shear test was difficult to

Table 4. Angle of internal friction and apparent cohesion for the manure products tested.

	Average TS (%)	Angle of Internal Friction (°)		Cohesion (kPa)	
		Average	Standard Deviation	Average	Standard Deviation
Dairy cattle	16.8	36.3 a[a]	3.1	3.0 a	0.7
	23.4	35.6 a	1.1	2.8 a	1.0
	33.5	37.3 ab	1.5	2.1 a	1.4
	44.4	37.6 ab	0.8	3.7 a	0.4
	47.7	40.7 b	1.0	3.1 a	0.9
Sheep	18.4	26.5 a	1.0	7.2 a	1.5
	30.7	23.9 a	0.4	7.4 a	0.9
	41.5	25.9 a	0.8	7.5 a	0.1
	53.0	38.3 b	3.3	1.7 b	1.9
Poultry	34.5	12.4 a	0.2	7.3 a	0.6
	41.5	28.1 b	0.8	11.9 b	0.3
	47.3	22.4 c	3.7	12.0 b	1.2
Pig	31.0	19.2 a	4.0	0.5 a	0.9
	41.7	9.2 b	2.4	9.3 b	0.8
	48.1	24.2 a	1.7	15.6 c	1.4

[a] Values within each manure type row and property column not followed by the same letter are significantly different as determined by Fisher's LSD test at the 1% level.
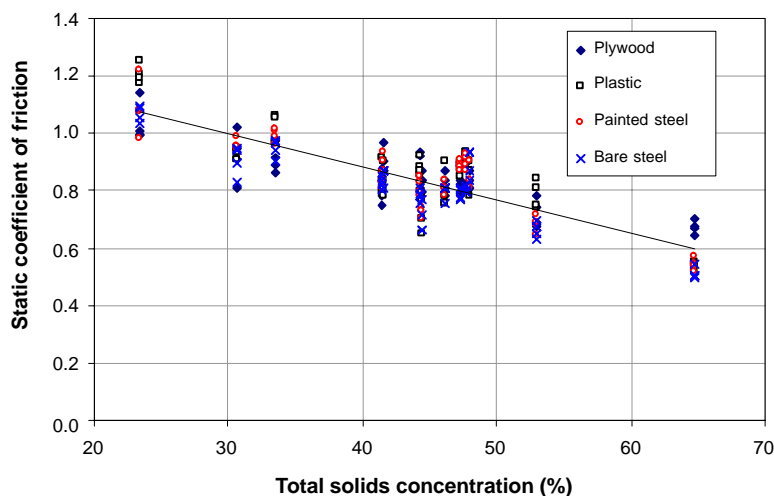

Figure 5. Static coefficient of friction of dairy cattle, sheep, poultry, and pig manure as a function of total solids concentration.

carry out due to the lumpy and heterogeneous nature of manure products. A larger split box could be used to attempt investigating the shearing behavior of manure products with the aggregates. Another option would be to carry out the test on screened samples. Other tests should also be explored, as they may be more suitable to characterize the shear stress – shear rate behavior of organic wastes.

LIQUID AND SEMI-SOLID PRODUCTS

For manure products that could not be tested in the direct shearbox and for which static friction coefficients were irrelevant, the focus was on the density and on the shear stress – shear strain behavior as determined by rotational viscometry. The tested manure products generally displayed a decreasing viscosity with an increasing shear rate, which corresponds to the typical behavior of non–Newtonian pseudoplasic fluids. It was found that the power law $\tau = K\gamma^n$ (where τ is the shear stress, K the consistency coefficient, γ the shear rate, and n the flow behavior index) could be used to describe the relation between shear stress and shear rate for the animal waste products tested. The values of the consistency coefficient K and of the flow behavior index n are presented in table 5 for both the laboratory and the large–scale viscometers. The density results have been previously discussed and included in predictive equations 6, 7, and 8. Comparisons between the results obtained using the large–scale viscometer and the laboratory unit showed there was in most cases no significant difference between the two apparatuses, for both the consistency coefficient K and the

flow behavior index n. The high variability of the results obtained using the large–scale viscometer, with an average coefficient of variation of 20% for all groups of measured data, combined with the rather severe statistical test used, is one factor explaining the similarities between the two viscometers. Results obtained using the laboratory viscometer also exhibited a fair amount of variability, but this could be expected when very small quantities, to fill a 600–mL beaker, are taken from large 150–L samples. To reduce the variability of the results obtained with the large–scale viscometer, two issues must be addressed. The mechanical vibration coming from the motor and the gearbox were substantial and should be damped or reduced to ensure the torque measured is mainly related to the shearing of the fluid. Also, the sensitivity of the torque–measuring load cell should be increased by using a combination of smaller capacity (the load cell used had a capacity of 222 N) and variable lever arm length. More conclusive results might be obtained with an improved large–scale viscometer.

Many similarities between products having the same level of total solids were detected by the statistical analysis. The rather large standard deviations are partly responsible for those conclusions. Figures 6, 7, and 8 allow for a visual appreciation of the shear stress – shear strain relationships for animal waste products. They also illustrate the effect of TS on the consistency coefficient and on the flow behavior index for the various types of manure tested. It should be noted that these charts were plotted using the average experimental values of K and n to calculate the shear stress at the minimum

Table 5. Bulk density, consistency coefficient (K) and flow behavior index (n) for the animal manure products tested.[a]

| Total Solids Concentration (%) | Manure Type | Density (kg/m³) | Measured and Calculated Properties | | | | Shear Rate Range (s⁻¹) | |
| | | | Lab Viscometer | | Large Viscometer | | Viscometer Type | |
			K (Pa·sⁿ)	n (——)	K (Pa·sⁿ)	n (——)	Lab	Large
20	Dairy cattle	411.0[b] a[c] (32.1)[d]	n.a.	n.a.	n.a.	n.a.	n.a.	n.a.
	Sheep	1051.2 b (60.2)	n.a.	n.a.	n.a.	n.a.	n.a.	n.a.
	Poultry	1091.8 b (63.9)	9.9 a (1.4)	0.43 a (0.078)	35.4 a (2.7)	0.29 a (0.083)	[0.07 – 22.10]	[0.64 – 24.14]
	Pig	1090.0 b (77.3)	41.1 b (4.7)	0.34 a (0.018)	56.8 a (14.8)	0.35 a (0.074)	[0.08 – 25.38]	[0.24 – 23.90]
15	Dairy cattle	973.0 a (33.9)	22.9 a (8.3)	0.41 a (0.042)	31.3 a (7.2)	0.30 a (0.12)	[0.07 – 21.61]	[0.61 – 24.37]
	Sheep	961.5 a (44.8)	26.9 a (11.5)	0.36 a (0.076)	19.4 a (8.4)	0.29 a (0.035)	[0.07 – 22.07]	[0.70 – 23.90]
	Poultry	1063.6 b (42.4)	1.7 b (0.06)	0.41 a (0.012)	2.4 b (0.3)	0.38 a (0.018)	[0.07 – 22.00]	[0.80 – 23.90]
	Pig	967.7 a (39.5)	3.4 b (0.2)	0.42 a (0.0058)	2.4 b (0.3)	0.38 a (0.018)	[0.07 – 22.00]	[0.96 – 23.90]
10	Dairy cattle	999.6 a (30.7)	2.6 a (0.3)	0.42 a (0.026)	5.3 a (2.1)	0.11 a (0.10)	[0.07 – 22.00]	[0.90 – 23.90]
	Sheep	1008.3 a (11.1)	3.7 b (0.5)	0.42 a (0.029)	2.7 a (0.9)	0.33 b (0.084)	[0.07 – 22.00]	[0.90 – 23.90]
	Poultry	1036.5 a (26.6)	1.2 c (0.07)	0.37 a (0.022)	8.9 b (2.3)	0.29 ab (0.11)	[0.12 – 30.79]	[0.96 – 24.14]
	Pig	1025.7 a (7.1)	1.0 c (0.04)	0.55 b (0.018)	2.2 a (0.8)	0.21 ab (0.041)	[0.12 – 38.75]	[0.90 – 23.90]

[a] For the viscometry tests, the temperature of the manure samples was between 17ºC and 24ºC.

[b] Average value.

[c] Values within each total solids concentration level row and property column not followed by the same letter are significantly different as determined by Fisher's LSD test at the 1% level (a T–test was used when only two means were available).
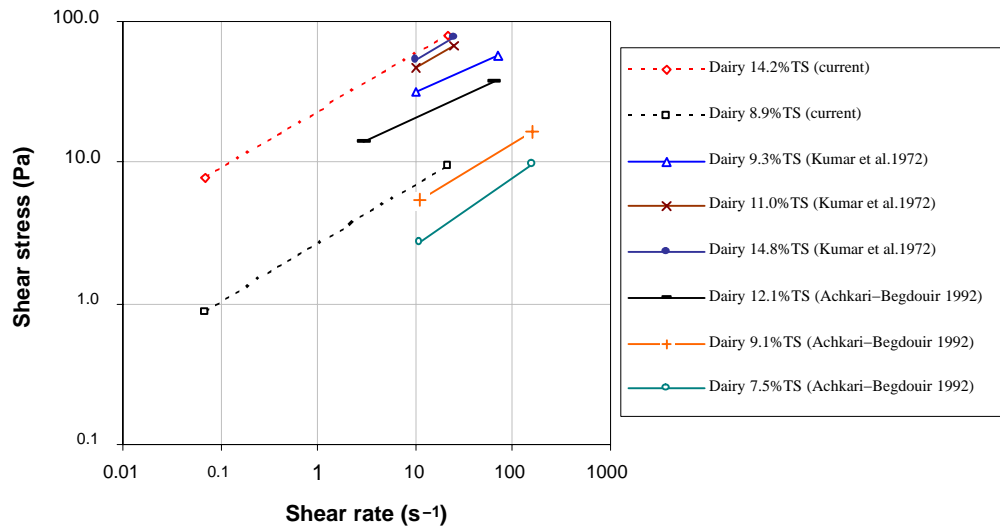
[d] Standard deviation.

Figure 6. Shear stress – shear rate curves for dairy cattle manure (current study and other published results).
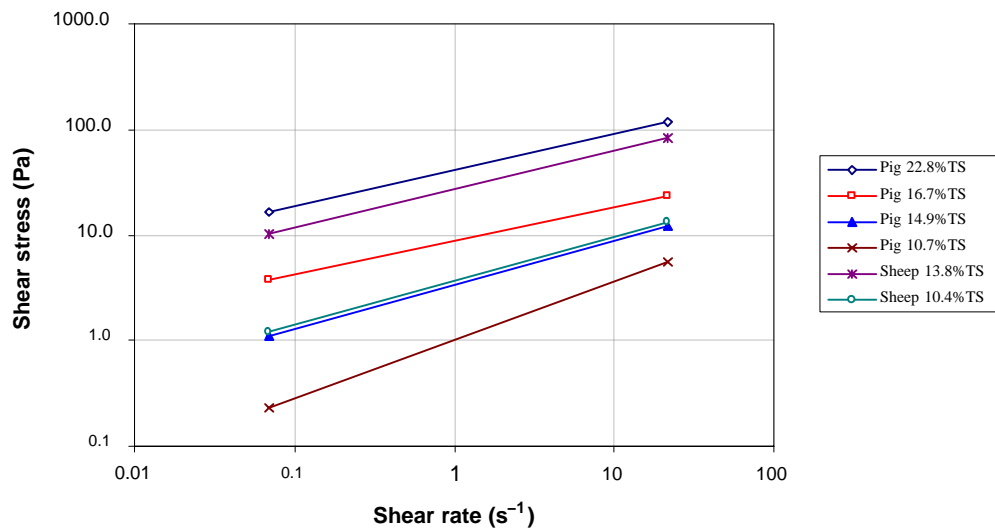

Figure 7. Shear stress – shear rate curves for sheep and pig manure.
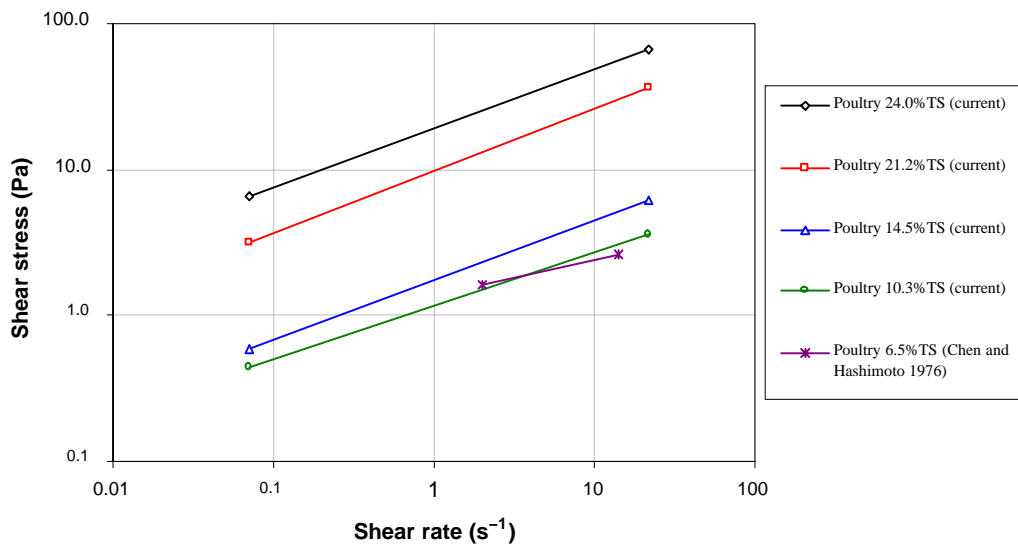

Figure 8. Shear stress – shear rate curves for poultry manure (current study and other published results).

and maximum shear rate values. Results from other studies (Kumar et al., 1972; Chen and Hashimoto, 1976; Achkari–Begdouir and Goodrich, 1992) have been included, using the same plotting method, to illustrate the similarities and

differences among results obtained for manure products originating from very similar sources.

If the viscometry results are further analyzed to evaluate the effect of total solids concentration on the consistency coefficient and flow behavior index using the results obtained with the laboratory viscometer, it can be seen that the value of K became significantly smaller with an increase in TS (table 6). The values of n, however, were not significantly different at various levels of total solids concentration except for pig manure for which the value of the flow behavior index was significantly higher for lower values of TS. This is consistent with the conclusions of Chen and Shetler (1983), but the relationship was not generalized enough to make this observation a conclusion. These observations can also be visualized on figures 6, 7, and 8. Even though a limited number of data were available, a relationship was identified between the consistency coefficient and the total solids concentration for poultry and pig manure. Similar relationships could be established using data obtained by Chen and Shetler (1983). Equations 12 and 13 can be used to predict the consistency coefficient for poultry and pig manure respectively within the ranges of total solids concentration (10% to 25%), temperature (17°C to 24°C), and shear rate (approximately 0.07 to 30 s^{-1}) of this study (where K is in Pa·s^n):

Consistency coefficient for poultry manure:
$$K = 0.14\ TS^2 - 3.52\ TS + 22.93; R^2 = 0.95 \qquad (12)$$

Consistency coefficient for pig manure:
$$K = 0.33\ TS^2 - 7.87\ TS + 46.91; R^2 = 0.98 \qquad (13)$$

To obtain a parameter that may be more useful for design purposes, it was possible to calculate the apparent viscosity (η_{app}) using equation (14) (Chen and Shetler, 1983):

$$\eta_{app} = K\ S^{(n-1)} \qquad (14)$$

Plotting the apparent viscosity at a shear rate of 10 s^{-1} against the total solids concentration on a log–log chart gave predictive equations 15, 16, and 17 (where η_{app} is in Pa·s):

Dairy cattle: $\eta_{app} = 4E{-}05\ TS^{4.4671}$; $R^2 = 0.95$ (15)

Poultry: $\eta_{app} = 6E{-}05\ TS^{3.4721}$; $R^2 = 0.94$ (16)

Pig: $\eta_{app} = 4E{-}06\ TS^{4.6432}$; $R^2 = 0.95$ (17)

The observed relationships between the apparent viscosity and the total solids concentration are in agreement with the relationship obtained by Chen and Shetler (1983). An analysis of the results obtained by several authors (Kumar et al., 1972; Chen and Hashimoto, 1976; Chen, 1982; Chen and Shetler, 1983; Achkari–Begdouir and Goodrich, 1992) have demonstrated the heterogeneity of viscometry results highlighting the fact that the focus should be on determining ranges of acceptable values for manure properties. These results also showed that data obtained at several different times and locations still show similarities. The results of this study also suggested that processing animal manures to produce more homogeneous products in terms of physical and rheological properties may be the only effective way of making handling and land application equipment more efficient in terms of power requirement and uniformity of distribution. With the wide range of animal diets, management practices, and climates that can affect the properties of animal manures combined with differences between animal herds, as well as between individual animals, it is very difficult to design and operate machines with the objective of obtaining optimal performances. However, ranges of values for manure physical and rheological properties, such as the ones obtained in this study, should be the basis of any machinery design or optimization effort. Along with the judgment of the designing engineers, the knowledge base developed in the literature and in this study should allow for improved design and operation of manure handling and land application equipment, within the limits imposed by the inherent variability in the properties of animal manures.

CONCLUSIONS

Physical and flow properties of manure products were measured over a wide range of total solids concentration. Based on the results obtained, the major findings are:
- The density of dairy cattle, poultry, and pig manure was in agreement with ASAE D384.1 and other published results. Predictive equations based on total solids concentration were obtained.
- A method was proposed to calculate a modified value of the geometric mean length obtained by screening. Signifi-

Table 6. Consistency coefficient (K) and flow behavior index (n) obtained using the laboratory viscometer.

	Total Solids Concentration (%)	Laboratory Viscometer	
		K (Pa·s^n)	n (—)
Dairy cattle	14.2	22.9 [a] a [b]	0.41 a
		(8.3) [c]	(0.042)
	8.9	2.6 b	0.42 a
		(0.3)	(0.026)
Sheep	13.8	26.9 a	0.36 a
		(11.5)	(0.076)
	10.4	3.7 b	0.42 a
		(0.5)	(0.029)
Poultry	24.0	19.1 a	0.40 a
		(3.5)	(0.071)
	21.2	9.9 b	0.43 a
		(1.4)	(0.078)
	14.5	1.7 c	0.41 a
		(0.06)	(0.012)
	10.3	1.2 c	0.37 a
		(0.07)	(0.022)
Pig	22.8	41.1 a	0.34 a
		(4.7)	(0.018)
	16.7	8.9 b	0.32 a
		(0.9)	(0.036)
	14.9	3.4 c	0.42 b
		(0.2)	(0.0058)
	10.7	1.0 c	0.55 c
		(0.04)	(0.018)

[a] Average value.
[b] Values within each manure type row and property column not followed by the same letter are significantly different as determined by Fisher's LSD test at the 1% level (a T–test was used when only two means were available).
[c] Standard deviation.

cantly larger modified geometric mean lengths were observed as the total solids concentrations of the products decreased.

- Static friction coefficients were measured on different surface materials. For design purposes, the observation of similar values for most of the manure products over the majority of the tested surfaces led to a unique equation to predict the static friction coefficient as a function of total solids concentration.
- The animal manures studied were non–Newtonian pseudoplastic fluids and the power law could be used to relate shear stress and shear rate. The value of the consistency coefficient increased with the total solids concentration. The apparent viscosity was well correlated to TS for dairy cattle, poultry, and pig manure.
- For the design and analysis of manure handling and land application systems, the ranges of values presented can be used with proper care. Poultry and pig manure generally exhibited similar behaviors while dairy cattle and sheep manure showed similarities, though not as strong as the former due to the straw content of the tested sheep manure. The density values and friction characteristics of manure products were found to be consistent with other published results. The shear stress – shear strain relationships seemed however to be study–specific, but published values still showed similarities.

RECOMMENDATIONS

The lack of standard methods to measure the physical and rheological properties of organic by–products made the characterization of manure products more challenging. Some methods have successfully been used in this study and by other authors. For example, the oven method used to determine total solids concentration of the samples poses no difficulties. The inclined plane method is also a relatively simple means of measuring the static coefficient of friction. Other methods have proven to be more difficult to implement in a manure–testing program. The angle of repose, with a rather simple apparatus, did not give consistent results. The screening method presented in this study gave good results when the calculations were based on the bottom five screens of the six–screen set. It was, however, very labor–intensive to screen adhesive manure products. The results must also be interpreted with care, as the calculated characteristic dimension can become a measure of the aggregation ability of the tested sample. The change in particle size distribution from one TS level to another also includes the effect of the mechanical disturbances induced by the samples preparation. Different screening approaches should be suggested to enhance the potential information that such tests can yield. Innovative tests such as the triaxial test, the slump test, non–rotational viscometry or a test to measure the dynamic coefficient of friction should also be attempted. The pycnometer method used by Agnew et al. (2003) to measure the density of compost gave good results and would certainly be worth trying with other organic fertilizers. These new tests could deepen the knowledge of the engineering properties of manure products, potentially leading to improved ways of handling and land–applying organic by–products.

REFERENCES

ASAE Standards, 2002a. S385.2. Moisture measurement – Forages. St. Joseph, Mich.: ASAE.

ASAE Standards, 2002b. S424.1. Method of determining and expressing particle size of chopped forage materials by screening. St. Joseph, Mich.: ASAE.

ASAE Standards, 2002c. D384.1. Manure production and characteristics. St. Joseph, Mich.: ASAE.

ASTM. 1998. *Annual Book of ASTM Standards*. D3080–98. Standard test method for direct shear test of soils under consolidated drained conditions. West Conshohocken, Penn.: ASTM.

Achkari–Begdouri, A., and P. R. Goodrich. 1992. Rheological properties of Moroccan dairy cattle manure. *Bioresource Technology* 40(2): 149–156.

Agnew, J. M., J. J. Leonard, J. Feddes, and Y. Feng. 2003. A modified air pycnometer for compost air volume and density determination. *Canadian Biosystems Engineering* 45(6): 27–35.

Bisang, M. 1987. Epandeuses de fumier: comparaison de differents dispositifs d'épandage. Technique Agricole, Switzerland. 1987, 49(3), 8 pp.; Rapports FAT No. 300.

Chen, Y. R. 1982. Engineering properties of beef cattle manure. ASAE Paper No. 824085. St. Joseph, Mich.: ASAE.

Chen, Y. R. 1986. Rheological properties of sieved beef–cattle manure slurry: Rheological model and effects of temperature and solids concentration. *Agricultural Wastes* 15(1): 17–33.

Chen, Y. R., and A. G. Hashimoto. 1976. Rheological properties of aerated poultry waste slurries. *Transactions of the ASAE* 19(1): 128–133.

Chen, Y. R., and E. L. Shetler. 1983. Temperature effect on rheological properties of cattle manure slurry. *J. of Testing and Evaluation* 11(6): 360–364.

Frick, R., J. Heusser, and M. Shick. 2001. Technique d'épandage des engrais à base de déchets et de fumier de stabulation libre: Qualité du travail et adéquation de différents systèmes d'épandage. Rapport FAT No. 560.

Glancey, J. L., and R. K. Adams. 1996. Applicator for sidedressing row crops with solid wastes. *Transactions of the ASAE* 39(3): 829–835.

Glancey, J. L., and S. C. Hoffman. 1996. Physical properties of solid waste materials. *Applied Engineering in Agriculture* 12(4): 411–446.

Hashimoto, A. G., and Y. R. Chen. 1976. Rheology of livestock waste slurries. *Transactions of the ASAE* 19(5): 930–934.

Henderson, S. M., R. L. Perry, and J. H. Young. 1997. *Agricultural Process Engineering*. St. Joseph, Mich.: ASAE.

Kumar, M., H. D. Bartlett, and N. N. Mohsenin. 1972. Flow properties of animal waste slurries *Transactions of the ASAE* 15(4): 718–722.

Landry, H., and C. Laguë. 1999. Selected properties of papermill residues. ASAE Paper No. 996058. St. Joseph, Mich.: ASAE.

Ling, Q., and J. H. Wilhoit. 1999. Power requirements of spinner–type spreaders broadcasting poultry litter and wood ash. *Applied Engineering in Agriculture* 15(5): 405–409.

Malgeryd, J., and C. Wetterberg. 1996. Physical properties of solid and liquid manures and their effects on the performance of spreading machines. *J. Agric. Eng. Res.* 64(4): 289–298.

Mohsenin, N. N. 1986. *Physical Properties of Plant and Animal Materials*, 2nd ed. New York: Gordon and Breach.

Moysey, E. B., and S. Hiltz. 1985. Friction properties of fertilizers. *Canadian Agricultural Engineering* 27(2): 79–84.

Reed, W. B., and E. Wacker. 1968. Determination of the distribution pattern of dry fertilizer applicators. ASAE Paper No. 68606. St. Joseph, Mich.: ASAE.

Thirion, F., and C. Chabot. 2003. Épandage des boues résiduaires et effluents organiques: Matériels et pratiques. Cemagref Éditions. Paris, France.

Thirion F., F. Chabot, and D. Andeler. 1998. Determination of physical characteristics of animal manure. *Proceedings of RAMIRAN 98* (8th International Conference on Management Strategies for Organic Waste Use in Agriculture). Rennes, France, 457 –469.

Wilhoit, J. H., and Q. Ling. 1996. Spreader performance evaluation for forest land application of wood and fly ash. *J. of Environmental Quality* 25(5): 945–950.

Wilhoit, J. H., J. S. Bannon, R. R. Duffield, and Q. Ling. 1994. Development and evaluation of a drop applicator for poultry litter. *Applied Engineering in Agriculture* 10(6): 777–782.

Wilhoit, J. H., C. W. Wood, K. H. Yoo, and M. Y. Minkara. 1993. Evaluation of spreader distribution patterns for poultry litter. *Transactions of the ASAE* 9(4): 359–363.

Appendix C   Chapter 3 in its published format

PERFORMANCES OF CONVEYING SYSTEMS FOR MANURE SPREADERS AND EFFECTS OF HOPPER GEOMETRY ON OUTPUT FLOW

H. Landry, E. Piron, J. M. Agnew, C. Laguë, M. Roberge

ABSTRACT. *The objectives of this work were to evaluate the performances of different conveying systems for manure spreaders and to study the effect of the hopper geometry on material flow. Experiments were carried out at the University of Saskatchewan (Canada) and at Cemagref (France). A prototype land applicator was evaluated with both a scraper conveyor and a system of four augers. The specific energy required to unload the machine with the four–auger system was found to be higher than with the scraper conveyor, with average values for all experimental runs of 184 and 73 J/kg, respectively. A three–factor factorial design was used to study the effect of the vertical position of a flow–control gate, velocity of the conveying system, and inclination angle of the sidewalls for both types of conveying systems. The specific energy for both conveying systems was significantly affected by the position of the gate. The characteristic flow rate, as defined in European Standard EN 13080, was influenced by all three factors in the case of the scraper conveyor. The position of the gate, the velocity of the conveyor, and the interaction between these two factors were found to be significantly affecting the characteristic flow rate of the four–auger system. The output flow of three commercial manure spreaders having similar functional units but different hopper geometries was studied. The stretch within the tolerance zone was observed to increase when the length and width of the hopper were increased. The longitudinal coefficient of variation was observed to decrease when the length of the hopper was increased. The same effect was observed when increasing the width of the hopper and when reducing its depth. The physical properties of the products spread were deemed to have an influence on the response of the evaluation criteria to changes in hopper geometry. Cohesive products were observed to improve the discharge flow in terms of the stretch within the tolerance zone, the longitudinal coefficient of variation, and the actual to theoretical unloading time ratio.*

Keywords. Manure spreaders, Conveyor, Specific energy, Characteristic flow rate, Hopper geometry.

Optimal design of the manure holding and conveying systems on land application equipment constitutes a critical step in controlling material discharge and thus application rate. These systems need to be designed or selected on the basis of the physical and flow properties of the materials to be handled. Sludge spreaders are typically equipped with one or several discharge augers while solid manure spreaders generally feature scraper conveyors. The geometry of the manure holding system, or hopper, is defined by the required machine capacity and other design constraints. To improve the performances of solid and semi–solid manure land application equipment, an enhanced understanding of material flow within such machines is required. The role of the conveying system must therefore be examined in greater detail in terms of power requirements as well as the qualitative and quantitative characteristics of the induced flow. The effect of the machine geometry on the output flow must also be investigated in more depth.

OBJECTIVES

The general objective of the research work reported herein was to investigate the effects of different holding and conveying systems for solid and semi–solid manure spreaders on material discharge rate and energy requirements. The specific objectives were:

- to investigate the performances of two types of conveying systems in terms of specific energy and discharge rate as affected by the velocity at which these conveying systems are operated, the position of a vertical flow–control gate and the inclination of the sidewalls of the manure holding system,
- to examine the effect of the position of a flow–control gate on the specific energy and discharge rate for different types of organic fertilizers, and

The authors are **Hubert Landry, ASAE Member,** Graduate Student, Department of Agricultural and Bioresource Engineering, University of Saskatchewan, Saskatoon, Saskatchewan, Canada; **Emmanuel Piron,** Research Engineer, Department of Agricultural and Food Engineering, Technologies, Information Support Systems and Processes for Agriculture and Food Industry Research Unit, Cemagref, France; **Joy M. Agnew, ASAE Member Engineer,** Research Engineer, **Claude Laguë, ASAE Member Engineer,** Professor and Dean, and **Martin Roberge,** Assistant Professor, Department of Agricultural and Bioresource Engineering, University of Saskatchewan, Saskatoon, Saskatchewan, Canada. **Corresponding author:** Hubert Landry, 57 Campus Drive, Saskatoon, SK S7N 5A9, Canada; phone: 306–966–5331; fax: 306–966–5334; e–mail: Hubert.Landry@asae.org.

- to study the longitudinal uniformity of product distribution obtainable with commercial manure spreaders having different hopper geometries and used to spread organic fertilizers exhibiting various physical properties.

LITERATURE REVIEW

Bulinski and Klonowski (1998) studied the effect of floor conveyor velocity and hopper loading on the overall power requirements of a solid manure spreader. They measured power ranging from 2.03 to 25.67 kW for manure loads and conveyor velocities ranging from 0 to 60.35 kN and 5 to 33 mm/s, respectively. They concluded that both the velocity of the floor conveyor and the amount of manure in the hopper significantly affected the power requirements.

Ling and Wilhoit (1999) investigated the power requirements of spinner–type spreaders broadcasting poultry litter and wood ash. Their results showed that the power consumption of the hydraulically operated spinner system when spreading poultry litter increased as the spinner speed and flow rate increased. There was no significant difference in the power consumption for poultry litter and wood ash spreading. The maximum power consumption for both products was about 10 kW. The power consumption of the conveyor system, from the proposed analytical equation, was found to change with the depth of product inside the hopper, length of the hopper, gate height and width, hopper angle, product specific weight, conveyor velocity, internal friction of the product, and its friction coefficient in the hopper. From a sensitivity analysis, the factors most affecting power consumption were found to be material depth, hopper length, and gate opening width while the least sensitive factors included gate height and hopper angle. The power consumption of the conveyor was smaller than that of the spinners. The conveyor power requirements increased as material flow rate increased. The total power requirements for poultry litter and wood ash spreading were very similar (maximum total power requirement of 18.72 and 18.11 kW, respectively) at the same flow rate and spinner speed because the density of the materials and friction coefficients were very close.

Ling et al. (1996) also investigated the influence of the height of the flow–metering gate and of the velocity of the floor conveyor on the performance of a spinner–type spreader broadcasting poultry manure. They obtained longitudinal distributions with coefficients of variation between 9% and 41%. Ling et al. (1996) concluded that there were no significant effects of gate opening and conveyor velocity on the longitudinal uniformity of application of the material.

Weil and Higgins (1975) conducted tests on helicoid and ribbon screw conveyors to determine which sewage sludge physical properties and which screw conveyor operational variables were most closely correlated to the total power requirements and the mass flow rate for the conveyors. The sludge samples were submitted to the slump test as well as viscometry and density measurements. The results indicated that solids content and viscosity were highly correlated with slump and could therefore be substituted in the predictive equations for power and mass flow rate. Weil and Higgins (1975) concluded that the screw conveyor rotational velocity and one sludge physical property were sufficient to adequately describe the power requirements of the conveyors. The proposed mathematical model for the mass flow rate required the inclination angle of the conveyor in addition to its rotational velocity and one property of the sludge.

MATERIALS AND METHODS

Experimental work associated with the first specific objective was completed at the University of Saskatchewan (Canada). Experiments to meet the second and third specific objectives were carried out at the Montoldre station of Cemagref (France).

CONVEYING SYSTEMS

A prototype land applicator built from a commercial manure spreader (New Idea, model 362) was used in the part of the study completed at the University of Saskatchewan. Two different conveyor types could be fitted in the prototype: a scraper conveyor and a system of four augers. A hydraulically actuated vertical gate was added at the discharge end of the spreader to better control the flow. The sidewalls of the spreader were extended vertically to increase the volume of the hopper and were mounted on hinges that allowed control of their inclination for the study of the effects of hopper geometry. The prototype featured four load cells placed between the hopper and the main frame for continuous mass measurement of the machine and determination of the mass flow rate. The torque at the power take–off (PTO) was measured using a torque transducer and a magnetic velocity sensor was used to measure the rotational velocity of the PTO shaft. Table 1 presents the characteristics of the prototype land applicator.

Experiments were carried out with two types of conveying systems (scraper and four–auger systems) to evaluate the effect of the discharge conveyor linear velocity (19 and 38 mm/s for the scraper conveyor; 471 and 840 mm/s for the four–auger system), gate vertical opening (bottom of the gate 0.56 and 1.28 m from the bottom of the hopper), and angle of the sidewalls (0 and 10° from vertical) on power requirements and mass flow rate.

The experiments were carried out using beef feedlot manure that had been stored in swaths for about five months and that had an average total solids concentration (TS) of 57.0% ± 2.8% on a wet mass basis. The manure contained straw and presented large clumps. Enough material was available to run three replications of all treatments combinations in a complete factorial design for each of the conveying systems.

Table 1. Characteristics of the prototype land applicator and of the two conveying systems.

Length at the bottom of the hopper (m)	3.31
Length at maximum height (m)	3.67
Maximum width at the bottom of the hopper (m)	1.31
Width at maximum height (m)	1.31
Depth (m)	1.33
Volume (m^3)	6.04
Cross–section (m^2)	1.74
Floor area (m^2)	4.34
Slat interval (mm)	413
Slat height (mm)	38
Augers diameter (mm)	305
Augers spacing (mm)	324

Table 2. Products used to study the effect of the vertical position of the flow–control gate on the discharge rate and power consumption of the scraper conveying system at Cemagref.

Product Description	Total Solids Concentration (%) Avg.	St. Dev.	Bulk Density (kg/m^3) Avg.	St. Dev.
(1) Feedlot manure with straw stored in the field for approx. 1 year	28.1	11.0	720.9	44.2
(2) Compost of product (1)	29.3	1.0	810.7	23.4
(3) Product (2) after several passes into the spreader and an outside drying period of approx. 3 weeks; designated as dry compost	59.0	0.6	612.0	6.9

An additional series of experiments was carried out at Cemagref to study the effects of the vertical position of the flow–control gate on the discharge rate and power consumption of the scraper conveying system for different organic fertilizers. The vertical beaters of a commercial manure spreader (corresponding to the machine featuring a narrow, short hopper in the geometry experiments, summarized in table 3) were removed, and stationary unloading trials were run. The mass of the tractor–spreader system was continuously recorded by six truck–type scales. The power requirements of the hydraulically driven floor conveyor were measured by means of a flow meter and a pressure transducer. Three different products were used for these experiments and are presented in table 2.

HOPPER GEOMETRY

Three commercial manure spreaders were used in this part of the study. The machines were selected according to the similarity of their spreading system (dual vertical beaters), floor conveyor (hydraulically driven scraper conveyor) and the differences in the geometry of their hopper. Table 3 summarizes the characteristics of the machines. Static spreading tests were carried out and the mass of the tractor–spreader system was continuously recorded by truck–type scales. Three different products were used in the hopper geometry experiments and are presented in table 4. The first two products (manure and compost) were the same as in the study of the effect of the position of the gate (table 2). A more substantial analysis of the products properties was performed for this part of the study. However, no replications of the properties measurements could be performed due to the limited amounts of products available.

The global homogeneity was evaluated using an automatic penetrometry method developed at Cemagref (Piron,

2003). The method was developed as a non–destructive means of measuring the consistency and homogeneity of organic fertilizers stored in swaths. It consists of taking a number of penetrometer readings side–by–side in the swaths to produce a spatial representation of the measured pressures. The results can then be analyzed graphically or statistically. Using a data set, the average pressure and its standard deviation can be calculated and used to determine a consistency index as well as a homogeneity index. Those indices allow for objective comparisons to be made among different products. The measured homogeneity increased from manure to compost and then to co–compost. The calculated heterogeneity indices were 1.11, 0.92 and 0.70 for manure, compost and co–compost, respectively. The feedlot manure was characterized by large clumps structured by intermeshing straw and these clumps were compacted to various degrees, creating a heterogeneous product. At the other end of the spectrum, the co–compost had a fairly well defined and constant particle size and had less internal structure.

DATA ANALYSIS

The basis for the analysis of all series of experiments was European Standard EN 13080 (CEN, 2002). A representative plot used for the analysis of the longitudinal distribution obtained with a manure spreader according to Standard EN 13080 is presented in figure 1. Several parameters can be calculated from the flow curve. The first parameter used to compare the conveying systems was the characteristic flow rate as outlined in European Standard EN 13080 (CEN,

Table 3. Characteristics of the three spreaders used to study the effect of the hopper geometry.

	Narrow Hopper Short Hopper	Long Hopper	Wide Hopper Long Hopper
Length (m)	3.57	5.85	4.45
Width at the bottom of the hopper (m)	1.43	1.42	1.94
Width at maximum height (m)	1.63	1.97	1.94
Depth (m)	1.30	1.30	1.15
Volume (m^3)	6.15	10.00	9.50
Cross–section (m^2)	1.74	2.14	2.22
Floor area (m^2)	3.70	7.83	8.61
Angle of the beaters (vs. floor) (deg)	75	75	75
Gate	Yes	Yes	No
Slat interval (mm)	425	453	490
Beaters diameter (mm)	690	860	980
Beaters velocity (rpm)	360	380	353

Table 4. Products used to study the effect of the geometry of the spreader hopper on the longitudinal uniformity of product distribution and energy requirements.

Product Description	Total Solids Concentration (%)	Bulk Density (kg/m^3)	Static Friction Coefficient on Steel[a]	Angle of Internal Friction[b] (deg)	Apparent Cohesion[b] (kPa)
(1) Feedlot manure with straw	28.1	720.9	0.73	19.3	23.0
(2) Compost of product (1)	29.3	810.7	0.63	17.1	7.8
(3) Co–compost of green wastes mixed with fermentable domestic wastes	66.5	1085.0	0.65	42.0	8.8

[a] Measured by the inclined plane method (Mohsenin, 1986).
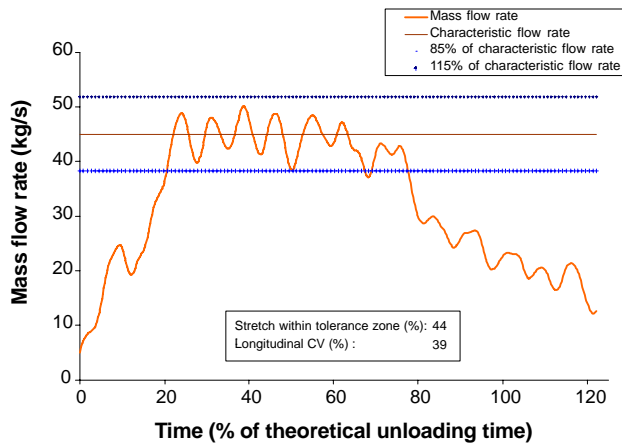[b] Determined by the direct shear test.

Figure 1. Longitudinal distribution curve (static spreading trial carried out at Cemagref with the machine having a narrow and long hopper; with product 2 in table 2; total unloading time is 342 s).

2002). This parameter is used to assess the amount of material coming out of the spreader as a function of its operating parameters. The characteristic flow rate basically corresponds to the highest average flow rate occurring during 30% of the unloading time of the spreader. From the characteristic flow rate, it is possible to define the tolerance zone, which corresponds to the range of flow rates between –15% and +15% of the characteristic flow rate (fig. 1). It is also possible to calculate the stretch within the tolerance zone, corresponding to the percentage of the unloading time during which the momentary flow rates lie within the tolerance zone. The longitudinal coefficient of variation (CV) is calculated based

on the average flow rate and its standard deviation. It is used to evaluate the variability of the flow rate during the unloading of the machine. Another comparison criterion makes use of the power data to calculate the specific energy required by the conveying systems during the unloading operation. The curve of power as a function of time is integrated to calculate the energy and that value is divided by the mass of product spread to obtain the specific energy.

RESULTS AND DISCUSSION

CONVEYING SYSTEMS

Effects of Gate Position and Sidewalls Inclination (Scraper and Auger Conveying Systems)

Figure 2 summarizes the results obtained for the power requirements of the conveying systems as well as their characteristic flow rate, for the experiments carried out at the University of Saskatchewan with beef feedlot manure. The experimental results for both the specific energy and characteristic flow rate were analyzed to highlight the effect of the factors included in the experiment. The results of the statistical analysis indicated a significant effect of the gate on the specific energy for both conveying systems at the 5% level. The characteristic flow rate of the scraper conveyor was significantly affected by the gate, the velocity of the conveyor, and the inclination angle of the sidewalls. In the case of the characteristic flow rate of the four–auger system, the significant factors were the gate, the velocity of the conveyor, and the interaction between these two parameters. The four–auger system required significantly more energy to move the mass of manure out of the spreader when compared
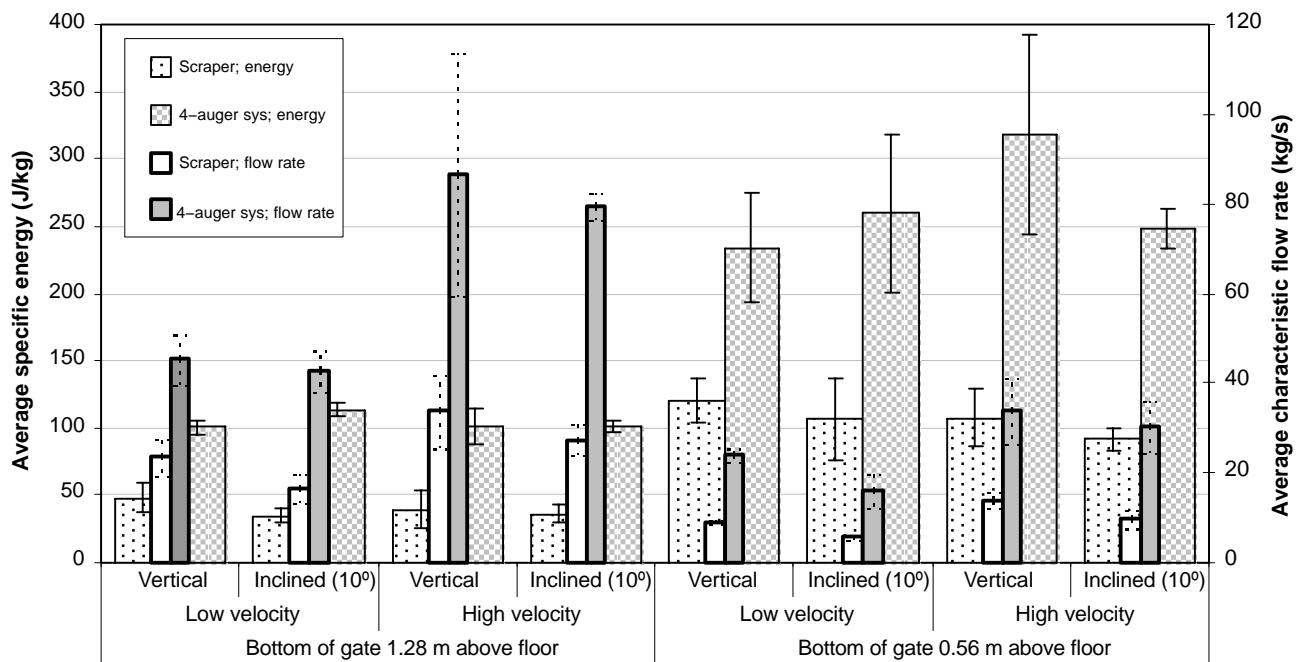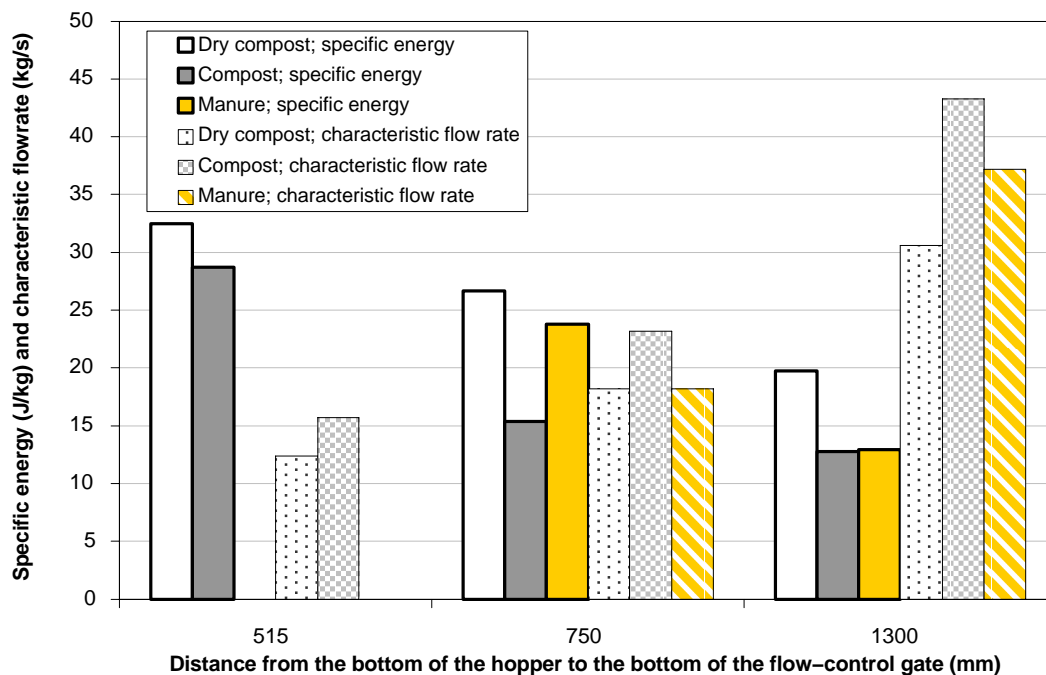

Figure 2. Specific energy required by the conveying systems for the unloading of the spreader and characteristic flow rate obtained as a function of the operating parameters (the error bars correspond to the standard deviation; vertical and inclined at 10° refer to the sidewalls; the low velocity corresponds to 19 and 471 mm/s for the scraper conveyor and the system of four augers, respectively; the high velocity corresponds to 38 and 840 mm/s for the scraper conveyor and the system of four augers, respectively.).

to the scraper conveyor. As expected, the usage of a flow−control gate had a significant effect on the power required to unload the spreader, as reflected by the values of specific energy. The effect of the gate was significant for both conveying systems.

The analysis of the characteristic flow rate is more complex. It should be understood that European Standard EN 13080 (CEN, 2002) is intended for the analysis of the results of spreading tests, as defined by the standard. This study targeted the evaluation of conveying systems and hopper geometries and, as a result, did not correspond entirely to the tests and conditions described in the standard. Nevertheless, the machines produced flows that were dependent upon their operational parameters, and these flows can be characterized using the criteria included in European Standard EN 13080 (CEN, 2002). The statistical analysis suggested that the gate vertical position, the velocity of the conveyor, and the angle of the sidewalls all influenced the characteristic flow rate obtained when the scraper conveyor was used. As expected, the characteristic flow rate was higher when the gate was at its higher position and when the conveyor was operated at the high velocity setting. For the angle of the sidewalls, the reduction of the flow section resulting from the inclination of the sidewalls caused the characteristic flow rate to become significantly smaller when compared to the results obtained with vertical sidewalls. The cross−section of the opening when the bottom of the gate was at 0.56 m above the bottom of the hopper and the sidewalls were vertical, including the cross section of the conveyors themselves, was 0.73 m². When the bottom of the gate was at 1.28 m above the bottom of the hopper, this cross−section increased to 1.68 m². With the sidewalls inclined 10° from vertical and the bottom of the gate 0.56 m above the bottom of the hopper, the cross−section of the opening was 0.53 and 0.54 m² for the scraper conveyor and the four−auger system, respectively. Raising the bottom of the gate to 1.28 m above the bottom of the hopper increased

the flow section to 1.37 and 1.38 m² for the scraper and four−auger conveying system, respectively. The results obtained with the four−auger system indicated significant effects of the gate vertical position and conveyor velocity. The statistical analysis also highlighted the interaction of conveyor velocity and gate opening. At the high velocity setting, the effect of the vertical position of the gate on the characteristic flow rate became more important. The four−auger system featured two augers with left−hand flighting next to two right−hand augers. This promoted the flow of product towards the center of the spreader, making the effect of the angle of the sidewalls less significant, as indicated by the results of the statistical analysis.

Effects of Gate Position and Products Properties (Scraper Conveying System)

Figure 3 summarizes the results obtained at Cemagref for the specific energy and characteristic flow rate as a function of the vertical position of the flow−control gate for different organic fertilizers. The experiments were not performed with manure at the lowest gate height due to magnitude of the force that would be transmitted to the gate. Also, the available amounts of products did not allow for replications of the experiments to be carried out. The results obtained confirmed the effect of the flow−control gate measured during the first experimental phase presented in the previous section. As the gate was lowered, the energy required to unload the spreader increased and the characteristic flow rate decreased for all products. When further analyzing the values of the characteristic flow rate, one can observe that a reduction of approximately 42% of the flow section (the gate was moved down from 1300 to 750 mm) induced a reduction of 51%, 46%, and 41% in the characteristic flow rate of manure, compost, and dry compost, respectively. When the flow section was further reduced by approximately 31% (the

Figure 3. Specific energy required by the scraper conveyor to unload the spreader and characteristic flow rate obtained as a function of the vertical position of the flow−metering gate for three different products.

gate was further lowered from 750 to 515 mm), the characteristic flow rate decreased by 32% for both compost and dry compost.

HOPPER GEOMETRY

Three phases can be identified on the discharge flow curves (fig 1): (1) a phase of increasing flow rate, associated to the "loading" of the spreading devices, having a length proportional to the distance between the spreading devices and the gate; (2) an intermediate "constant" flow rate phase; (3) a phase of decreasing flow rate that lasts until the end of the unloading of the spreader. A visual analysis of the flow rate curves revealed that a product with less internal structure, indicated by a small value of cohesion, produced a shorter constant flow rate phase, and a longer phase of decreasing flow rate. This observation was independent of the hopper geometry. Also, the more heterogeneous the product, the noisier the flow rate curve was. Figure 4 summarizes the results obtained for the hopper geometry experiments. The amount of compost available did not allow for the experiments with the machine featuring a wide and long hopper to be carried out. Therefore no data could be collected for that machine–product combination. Some effects of the hopper geometry on the evaluation criteria, namely stretch within the tolerance zone, longitudinal coefficient of variation, and unloading time, can be observed from the values presented in figure 4.

An increase in hopper length translated in higher values of stretch within the tolerance zone, resulting in less variation of the application rate in the field. The same effect was observed with an increase in hopper width. The longitudinal coefficient of variation decreased as the hopper went from narrow and short to narrow and long. It was further reduced when using a wide and long hopper. The actual unloading time, expressed as a percentage of the theoretical unloading time, consistently decreased when going from a short to a long hopper, with the exception of the product having the smallest cohesion (co–compost). With the hopper depth being equivalent, the crumbling of the mass of product at the

beater–end of the machine happened over an equivalent longitudinal distance, regardless of the width of the machine. Also, the longer the unloading time, which increased with the hopper length, the smaller the ratio was of the time required to evacuate the crumbled product to the total unloading time. This attenuation of the effect of the crumbling events on the total unloading time made it closer to the theoretical unloading time. This explains the lower ratios of actual to theoretical unloading time observed when using a longer machine. The absence of a gate is a mechanical parameter inherent to the spreader that can explain the improvement in the evaluation criteria for the wider machine. The type of gate featured on the tested machines is generally used only during loading and transportation. As a result, a more even loading of the spreading system (beaters) was observed for the spreader not fitted with a gate, favoring the even flow rate phase of the longitudinal distribution curve, which in turn benefited the stretch within the tolerance zone and the longitudinal coefficient of variation. Since the depth of the machines tested did not vary significantly, the effect of that parameter was studied by conducting spreading trials with the narrow and short hopper half–full. The results were very much affected by the depth of the hopper with values of stretch within the tolerance zone twice as large on average as the values obtained with the hopper full. The longitudinal coefficient of variation also decreased with the hopper depth. Crumbling events of lesser importance at both ends of the spreader, associated with an inferior depth of product in the machine, contributed to improve the duration of the even flow rate phase. With the total unloading time only slightly affected by the reduction in hopper depth, this effect translated into better results in terms of stretch within the tolerance zone and longitudinal coefficient of variation. Those observations can be related to the utilization of a flow–control gate.

The effects of the hopper geometry on the flow coming out of the machines are not independent from the characteristics of the products spread. Highly cohesive products allowed for higher values of stretch within the tolerance zone when
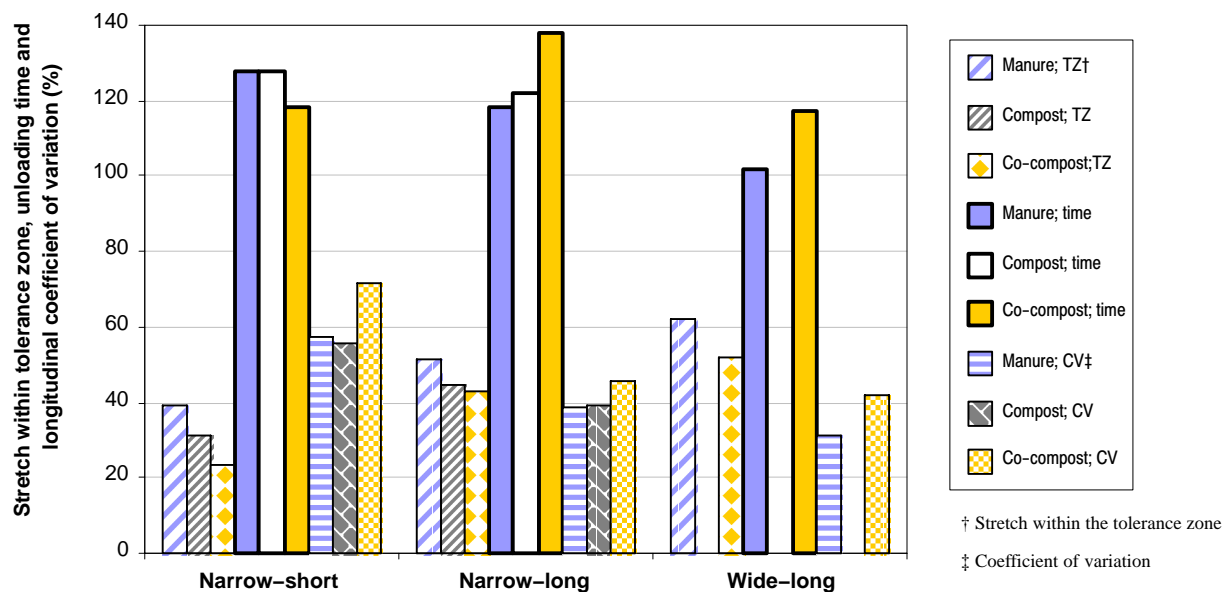
Figure 4. Effect of hopper geometry and product type on the stretch within the tolerance zone, the unloading time expressed as a percentage of the theoretical unloading time, and the longitudinal coefficient of variation.

compared to non–cohesive products (fig. 4). The greater duration of the decreasing flow rate phase at the end of the unloading process in the case of products with low cohesion values was detrimental to this criterion. Non–cohesive products crumbled, regularly or by intermittent crumbling events, while more cohesive products moved as a mass. As a result, the durations of the increasing and decreasing flow rate phases were inferior for cohesive products. This translated into less variation in the flow rate and better values of stretch within the tolerance zone. The longitudinal coefficient of variation and unloading time, expressed as a proportion of the theoretical unloading time, were always greater when spreading non–cohesive products as compared to more cohesive products. The non–cohesive products exhibited a more homogenous particle size distribution, resulting in less instantaneous variations of the flow rate. When comparing the results obtained from the experiments aimed at evaluating the performance of conveying systems to those from the hopper geometry tests, it was observed that the spreading devices had a regulating effect on the flow. The values of the coefficient of variation were somewhat higher when the spreading devices were removed. The values of stretch within the tolerance zone were low since the crumbling events were not attenuated by the spreading devices. The four–auger system seemed to perform better than the scraper conveyor, with an average value of longitudinal CV of 58% compared to 75% for all the experimental runs. This can be related to the shearing and processing action of the augers on the product. Using the data collected for the second specific objective, the coefficient of variation of the longitudinal distribution can be studied and related to the results obtained from the hopper geometry experiments. The results obtained at Cemagref highlighted an effect of the gate on the longitudinal coefficient of variation (table 5). The longitudinal CV obtained when unloading dry compost with fine homogeneous particles was the most affected by the vertical position of the gate. This is consistent with the observation made on the behavior of cohesive and non–cohesive products, and on the smoothing effect of the gate on the flow curves.

CONCLUSIONS

Experiments were carried out to gain an enhanced understanding of the flow of organic fertilizers in land application equipment. The focus was on the conveying and holding systems. The performances of two types of conveying systems for manure spreaders have been investigated. The results indicated that:
- The four–auger system designed at the University of Saskatchewan required more energy to unload manure out of the spreader, when compared to the scraper conveyor.
- The specific energy requirements of both the scraper conveyor and the four–auger system were significantly affected by the vertical position of the flow–control gate.
- The characteristic flow rate obtained with the scraper conveyor was significantly affected by the position of the gate, the velocity of the conveyor and the angle of the sidewalls.

Table 5. Longitudinal coefficient of variation as a function of the vertical position of the gate and of the product spread.[a]

Distance (mm)[b]	Longitudinal Coefficient of Variation (%)		
	Manure	Compost	Dry Compost
1300	70.5	82.1	60.8
750	51.1	43.6	35.6
515	n.a.[c]	41.8	24.0

[a] Experiments carried out at Cemagref with the spreader featuring a narrow and short hopper, without beaters.
[b] From the bottom of the hopper to the bottom of the gate.
[c] Data not available.

- The characteristic flow rate produced by the four–auger system was significantly influenced by the position of the gate and the velocity of the augers. There was also a significant effect of the interaction between gate position and conveyor velocity.

OBSERVATIONS

Experiments similar to those carried out to study conveying systems were performed using a manure spreader of larger capacity featuring a similar scraper conveyor. The results from single runs indicated a relation between the vertical position of the gate and the specific energy as well as between the position of the gate and the characteristic flow rate, for three different products. A relationship was also observed between the reduction in the flow section and the reduction of the characteristic flow rate for manure, compost, and dry compost.

The effect of the geometry of the holding system was studied. The main observations were:
- The stretch within the tolerance zone, which corresponds to the percentage of the unloading time during which the momentary flow rates lie within ±15% of the characteristic flow rate, was observed to increase with an increase in the length and the width of the hopper.
- The mass flow rate longitudinal coefficient of variation was observed to decrease when the length of the hopper increased. The same effect was observed when increasing the width of the hopper and when reducing its depth.
- The physical properties of the product spread had an influence on the flow curves. Cohesive products generated better values for the stretch within the tolerance zone, the longitudinal coefficient of variation and the unloading time expressed as a percentage of the theoretical unloading time.

The amount of engineering data related to the design and operation of land application equipment for solid organic fertilizers is very limited. Research studies focusing on such data have to deal with very heavy experimental setups. It is therefore extremely important to disseminate the research results so the scientific community can build on the acquired knowledge. The results of the research reported herein allowed for a better understanding of the flow of organic fertilizers in land application equipment and of the roles of the conveying and holding systems.

REFERENCES

Bulinski, J., and J. Klonowski. 1998. Analysis of power requirement for manure spreader working units. Annals of Warsaw Agricultural University, No. 33, 27–32. Warsaw, Poland.

CEN. 2002. European Standard EN 13080. Agricultural machinery – Manure spreaders – Environmental protection – Requirements and test methods. CEN, European Committee for Standardization. Brussels, Belgium.

Ling, Q., and J. H. Wilhoit. 1999. Power requirements of spinner–type spreaders broadcasting poultry litter and wood ash. *Applied Engineering in Agriculture* 15(5): 405–409.

Ling, Q., J. H. Wilhoit, and L. J. Kutz. 1996. Effect of material metering on the performance of a spinner–type spreader broadcasting poultry litter. *New Trends in Farm Machinery Development and Agriculture*, 41–49. Warrendale, Pa.: SAE.

Mohsenin, N. N. 1986. *Physical Properties of Plant and Animal Materials*, 2nd ed. New York: Gordon and Breach.

Piron, E. 2003. Tester l'homogénéité du compost, une nouvelle technique. *Matériel Agricole* 72: 58.

Weil, M., and A. Higgins. 1975. Performance of screw conveyors for unloading sludges from field transports. *Managing Livestock Wastes, Proc. of the 3rd International Symposium on Livestock Wastes*, 441–443. St. Joseph, Mich.: ASAE.

Appendix D　　Electronic files used in the thesis

Appendix D includes the files that were used at various stages of the research work presented in this thesis. It consists of files from the data acquisition systems, MS Excel files and the source code used for the PFC^{3D} simulations along with saved files of the simulations. The files are stored on three discs:

- Chapter 2　*CD 1*
  - Properties data files
    - Dairy Cow
    - Direct shear test
    - Large Viscometer Results
    - Pig
    - Poultry
    - Sheep
    - Small Viscometer Results
    - Statistical Analysis
    - Summary files and other files
    - Testing equipment files (calibration)

- Chapter 3　*CD 1*
  - Field testing - scraper conveyor
  - Field testing - screw conveyors
  - Statistical Analysis
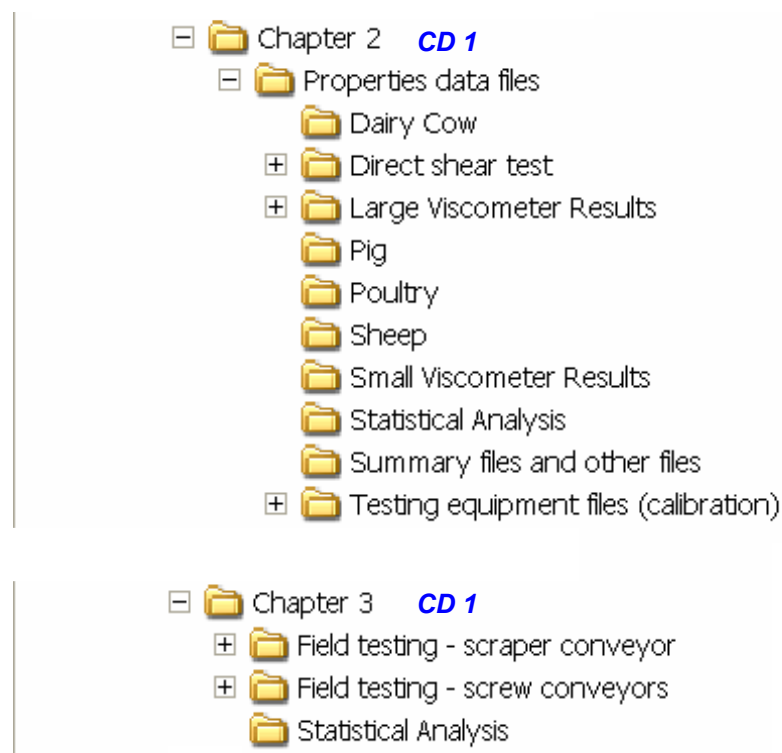
- Chapter 4   *CD 2 & CD 3*
  - PFC DAT files   *CD 2*
    - Cluster generation code
    - Example for Hertz model
    - Example for linear model
    - Particle size distribution
  - PFC SAV files   *CD 2*
    - Hertz model
      - Poisson ratio sensitivity
      - Shear modulus sensitivity
    - Linear model   *CD 3*
      - Contact bonds in clusters sensitivity
      - Contact bonds sensitivity
      - Friction coefficient sensitivity
      - Stiffness ratio sensitivity
      - Young modulus sensitivity

- Chapter 5   *CD 1*
  - Sims of Cemagref spreader with compost
  - Sims of Cemagref spreader with dry compost
  - Sims of spreader with dual vertical beaters
    - Moving machine
    - Stationary machine

- Chapter 6   *CD 2*
  - Augers conveying system sims
  - Detailed sim of transverse distribution system
  - Preliminary sims of transverse distribution system
  - Scraper conveyor sims